ERDC/GSL TR-20-38

Geotechnical and Structures Laboratory

US Army Corps
of Engineers®
Engineer Research and
Development Center

ERDC
ENGINEER RESEARCH & DEVELOPMENT CENTER

Evaluation of Thin Flexible Pavements under Simulated Aircraft Traffic

W. Jeremy Robinson

December 2020

The U.S. Army Engineer Research and Development Center (ERDC) solves the nation's toughest engineering and environmental challenges. ERDC develops innovative solutions in civil and military engineering, geospatial sciences, water resources, and environmental sciences for the Army, the Department of Defense, civilian agencies, and our nation's public good. Find out more at www.erdc.usace.army.mil.

To search for other technical reports published by ERDC, visit the ERDC online library at https://erdclibrary.on.worldcat.org/discovery.

ERDC/GSL TR-20-38
December 2020

Evaluation of Thin Flexible Pavements under Simulated Aircraft Traffic

W. Jeremy Robinson

Geotechnical and Structures Laboratory
U.S. Army Engineer Research and Development Center
3909 Halls Ferry Road
Vicksburg, MS 39180-6199

Final report

Prepared for Headquarters, Air Force Civil Engineer Center
Tyndall Air Force Base, FL 32403-5319

Under Work Unit 473719

Abstract

A full-scale airfield pavement test section was constructed and trafficked by the U.S. Army Engineer Research and Development Center (ERDC) to evaluate the performance of relatively thin airfield pavement structures. The test section consisted of 16 test items that included three asphalt pavement thicknesses and two different aggregate base courses. The test items were subjected to simulated aircraft traffic to evaluate their response and performance to realistic aircraft loads and to evaluate the effect of reductions in tire pressure on thin asphalt pavement. Rutting behavior, pavement cracking, instrumentation response, and falling weight deflectometer response were monitored at selected traffic intervals. The results of this study were used to extend existing Department of Defense pavement design and evaluation techniques to include the evaluation of airfield pavement sections that do not meet the current criteria for aggregate base quality and minimum asphalt concrete surface thickness. These performance data were used to develop new aggregate base failure design curves using existing stress-based design methodology.

Contents

Figures and Tables

Figures

Tables

Preface

This study was conducted for the U.S. Air Force Civil Engineer Pavement Technical Support Program under Work Unit 473719 sponsored by Headquarters, U.S. Air Force Civil Engineer Center (AFCEC) located at Tyndall Air Force Base, FL. Dr. Craig Rutland, AFCEC, provided technical guidance and review during the project. Mr. Jeb S. Tingle was the ERDC program manager.

The work was performed by the Airfields and Pavements Branch (GMA) of the Engineering Systems Division (GM), U.S. Army Engineer Research and Development Center, Geotechnical and Structures Laboratory (ERDC-GSL). At the time of publication, Ms. Anna M. Jordan was Chief, GMA; Mr. Justin S. Strickler was Chief, GM; and Ms. Pamela G. Kinnebrew, GZT, was the Technical Director for Military Engineering. The Deputy Director of ERDC-GSL was Mr. Charles W. Ertle II, and the Director was Mr. Bartley P. Durst.

COL Teresa A. Schlosser was the Commander of ERDC, and Dr. David Pittman was the Director.

1 Introduction

1.1 Background

The U.S. Air Force (USAF) Airfield Pavement Evaluation (APE) team routinely evaluates airfield pavement systems around the world to support USAF missions. Its mission requires that the team evaluate nontraditional pavement structures to assess the number of operations they can support prior to requiring extensive maintenance or repairs. Many of these pavements have been constructed with alternative paving materials not meeting current U.S. construction standards. In many cases, the flexible pavement surface thickness is below minimum standard thickness requirements, complicating pavement evaluation. New performance models are required to add pavement performance data points for thin flexible pavements at the lower end of the traffic curve.

1.2 Literature review

Webster (1993) constructed and trafficked a full-scale, flexible airfield pavement test section that included eight individual test items to evaluate the potential benefit of reinforcing the aggregate base with different geogrid products. The test section included five unreinforced test items that are relevant to the current study. The entire test section was surfaced with 2.2 to 2.6 in. of a Federal Aviation Administration (FAA) specified P-401 hot mix asphalt concrete, and the five unreinforced test items had high quality crushed limestone base course thicknesses of 6.0, 10.0, 12.0, 14.0, and 18.0 in. with California Bearing Ratio (CBR) of 100. The subgrade consisted of a high-plasticity clay (CH) material constructed at a CBR of 7.1 for the 6.0- and 10-in. base items and a CBR of 2.8 for the 12.0-, 14.0-, and 18.0- in. base items. Traffic was applied by using a single-wheel load cart with an aircraft wheel loaded to 30,000 lb with a tire pressure of 68 psi. The traffic results showed that the 6.0-in.-thick base course supported only 670 passes prior to failure (1.0-in. rut depth), while the 10.0-in.-thick base course supported more than 15,000 passes over the 7.1 CBR subgrade. For the weaker 2.8 CBR subgrade test items, the 12.0-in.-thick base item supported only 90 passes, the 14.0-in.-thick base supported 106 passes, and the 18.0-in.-thick base item supported 1,131 passes. Thus, the performance of the unreinforced flexible airfield pavement test items was more sensitive to subgrade strength than the thickness of the aggregate base course.

Bell and Mason (2008) constructed and trafficked a full-scale flexible airfield pavement test section that included six individual test items to investigate the effect of reduced asphalt thickness on pavement performance and validate the Department of Defense (DoD) minimum asphalt thickness criteria. The test items had asphalt thicknesses ranging from 2.5 to 5.0 in., base thicknesses ranging from 6.0 to 7.7 in., and subbase thicknesses ranging from 12.0 to 17.0 in. The subbase material for all test items was a gravelly sand mixture with a CBR ranging from 42 to 55. Four test items included a crushed gravel base course with a CBR ranging from 38 to 54, while two of the test items included a high-quality crushed limestone base course with a CBR ranging from 95 to 100. All test items were constructed over a high-plasticity clay (CH) subgrade with a CBR ranging from 9.1 to 9.9. A Heavy Vehicle Simulator (HVS) with single-wheel C-17 and F-15E gear configurations was used to apply simulated aircraft traffic. It was concluded that the DoD minimum asphalt thickness criteria (4.0 in. for a 100-CBR base and 5.0 in. for an 80-CBR base) were reasonable and that a pavement's design life could be reduced by half if the minimum required asphalt thickness was not adhered to. Further, it was found that a 1.0-in. increase in asphalt thickness resulted in three times the passes to failure. It was noted that the exact failure location (i.e., base, subbase, or subgrade) could not be identified, and that multiple layers contributed to the total permanent deformation in each item.

Bianchini and Gonzalez (2015) developed a CBR-Beta procedure for the design and evaluation of unsurfaced airfield pavements. Numerous historical research efforts (Thompson and Burns 1960; Ladd and Ulery 1967; Burns and McCall 1968; Hammitt 1970; Ladd 1970) were queried to gather a database of performance data related to unsurfaced airfield pavements that encompassed a range of subgrade CBR values from about 2 to 50 and included both single-wheel and multi-wheel gear assemblies. It was noted that failure in an unsurfaced pavement section was defined as a 3-in. rut depth, whereas a 1.0-in. rut depth was considered failure in an asphalt surfaced pavement section. A mechanistic-empirical approach was utilized to derive an unsurfaced pavement model similar in form to the existing surfaced Beta model. The equation was fitted through the assembled dataset; and the a, b, and c coefficients were determined. It was found that the design curve represented a reasonable fit of the data and that the adoption of the Beta parameter for unsurfaced airfield thickness design was recommended.

The results of the literature review indicate that little research has focused on flexible pavements constructed below the minimum specified layer thicknesses, particularly in terms of existing pavement design methodologies. The work completed by Gonzalez (2015; described in detail in Chapter 9) represents the development of the CBR-Beta criterion with a focus on subgrade failure, and no documented updates to the original derivation have been published to date. The Beta-criterion was expanded to predict performance in unsurfaced pavement applications (Bianchini and Gonzalez 2015), suggesting that the general form of the model was applicable to other pavement types. Thus, a focused study on the behavior of the existing model targeting base course failure in thin-asphalt pavement represents an expansion of the current state of knowledge.

1.3 Objective

The objective of this effort was to evaluate the performance of relatively thin flexible pavements to develop improved pavement design and evaluation methodology.

1.4 Scope

The scope of this project included the construction and trafficking of 16 different test items to evaluate structural performance of nonstandard flexible pavement designs. The test items were constructed by the U.S. Army Engineer Research and Development Center (ERDC) in the Hangar 2 Pavement Test Facility. The test items were fully instrumented to gather pavement response data of the nonstandard pavements under aircraft loading conditions. Simulated traffic was applied by using a single-wheel C-130 and a single-wheel C-17 aircraft tire. Pavement performance data (to include surface deformation, instrumentation response, and structural deterioration) were monitored at selected traffic intervals. Data were used to extend current DoD design methodologies, particularly for the failure of base course constructed over relatively thin asphalt pavement layers. These data can be used as a tool to evaluate nonstandard airfield pavement cross sections and project anticipated operations to failure.

2 Test Plan and Layout

A large, full-scale pavement test section was constructed under cover in Hangar 2 at ERDC to evaluate the performance of relatively thin, flexible pavement structures subjected to simulated aircraft traffic. Construction under cover minimized the influence of soil moisture changes due to inclement weather for the duration of the test.

The full-scale test section included 12 individual test items to evaluate the performance of thin flexible pavements using traditional high-quality base course materials and four test items to evaluate the performance of thin flexible pavement using nonstandard (and consequently weaker) base course materials. Each test item was 12.5 ft wide by 30 ft long. The test items were constructed with a nominal 36-in.-thick high-plasticity (CH) clay subgrade placed to achieve a target California Bearing Ratio (CBR) value of 10%. The 12-in.-thick base course consisted of a high-quality crushed limestone and a lower quality crushed gravel. Asphalt surface thicknesses ranged from 1.0 to 2.5 in. The full-scale test section was subjected to two types of aircraft traffic: simulated single-wheel C-130 and single-wheel C-17. Traffic testing was conducted at normal operating wheel loads and tire pressures as well as at reduced tire pressures to evaluate the effect of reducing tire pressure on pavement performance. Thus, the following comparisons can be made from this study:

1. Effect of asphalt thickness
2. Effect of base course strength
3. Effect of aircraft type
4. Effect of reduced aircraft tire pressure.

Figure 1 shows a plan view of the full-scale test section, including the 16 individual test items and the paved buffer zones. Each test item is labeled with the design asphalt thickness, base course type, and a unique identifier that will be referenced throughout this report. The identifier is of the following form (example C17RTP1 shown):

C17	RTP	1
Aircraft type (C17 or C130)	Tire Pressure Designation (RTP = reduced tire pressure) (NTP = normal tire pressure)	Item number in the test series

The test items contained a suite of instrumentation consisting of asphalt strain gauges, earth pressure cells, single-depth deflectometers, moisture probes, pore-water pressure transducers, and temperature probes.

Simulated aircraft traffic was applied by using a single-wheel C-130 tire configuration and a single-wheel C-17 tire configuration. The respective wheel configurations were mounted to a steel frame capable of housing a series of cast lead weights to achieve each targeted gross load. The steel frame was mobilized via a front-end loader outfitted with a custom fabricated connection apparatus to the steel frame. The single-wheel C-130 tire configuration was outfitted with a 35,000-lb total load, and the single-wheel C-17 tire configuration was outfitted with a 45,000-lb total load. Tire pressures for the C-130 tire configuration were 100 psi (normal tire pressure) and 80 psi (reduced tire pressure). Tire pressures for the C-17 tire configurations were 142 psi (normal tire pressure) and 115 psi (reduced tire pressure).

Figure 1. Test section plan view.

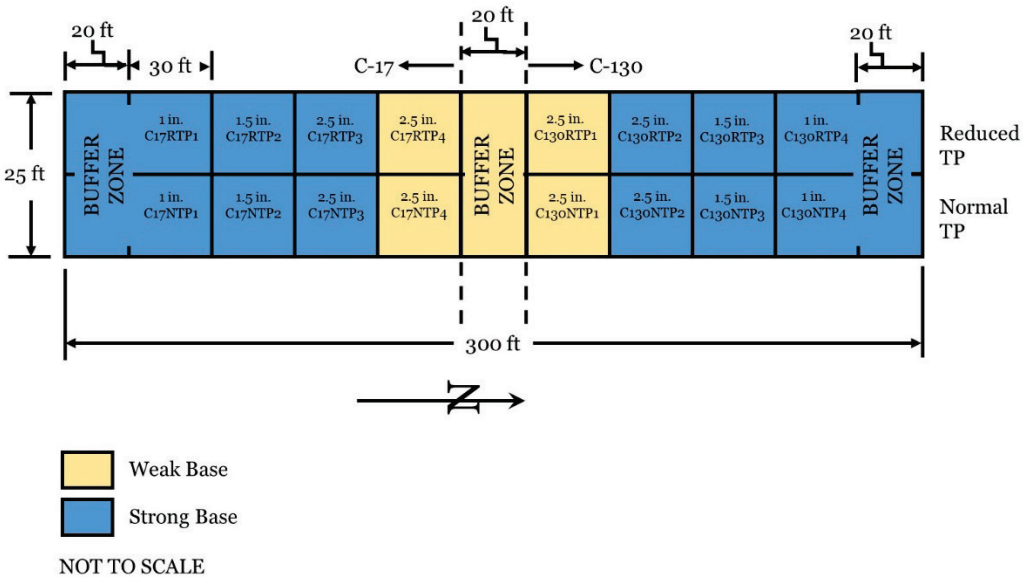

3 Materials

Laboratory tests were performed to characterize each component layer material as well as underlying subgrade soils. Material characterization test results are presented in the following paragraphs.

3.1 Subgrade

In-situ subgrade soils encountered at the bottom of the excavation consisted of a low-plasticity clay. A No. 200 wash test indicated that the material consisted of 7.1% sand and 92.9% fines. The soil had a liquid limit (LL) of 41%, a plastic limit (PL) of 22%, and a plasticity index (PI) of 19%. Modified Proctor compaction tests (ASTM D1557) indicated maximum dry density was 116.3 pcf at an optimum moisture content of 13.5% (Figure 2) (ASTM 2012).

Figure 2. In-situ subgrade moisture/density relationship.

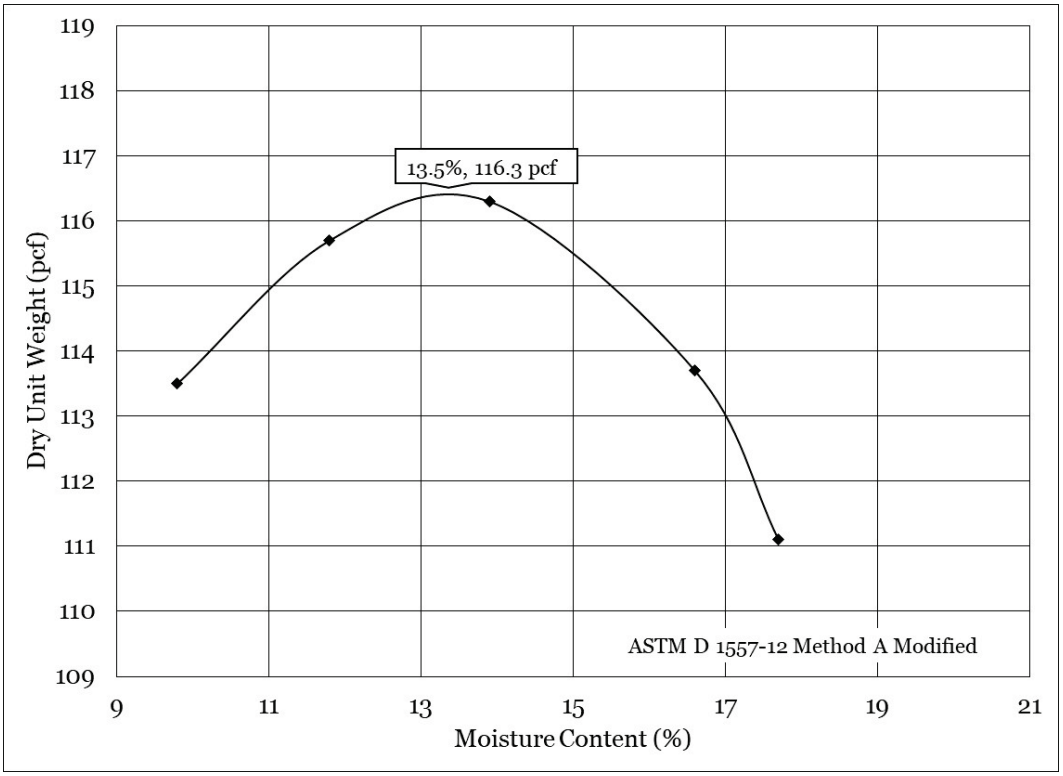

Design subgrade soils consisted of a locally sourced high-plasticity clay, commonly referred to as Vicksburg Buckshot. This material has been used extensively in test-section construction, namely for its ability to maintain moisture content (and consequently design strength) over an

extended time period. A particle size analysis indicated the material consisted of 96.8% fines passing the No. 200 sieve. The soil had a LL of 85%, a PL of 29%, and a PI of 56%, as determined by American Society for Testing and Materials (ASTM) D4318 (2017c). According to the Unified Soil Classification System (USCS; ASTM 2017a), the soil was classified as a high-plasticity clay (CH) and an A-7-6 according to the American Association of State and Highway Transportation Officials (AASHTO) classification system (2012).

Modified Proctor compaction tests (ASTM D1557) were performed to determine the relationship between moisture content and dry density. Maximum dry density was found to be 104.2 pcf at an optimum moisture content of 19.7% (ASTM 2012). Graphical results of the moisture-density relationship test are shown in Figure 3.

Figure 3. Clay subgrade moisture/density relationship.

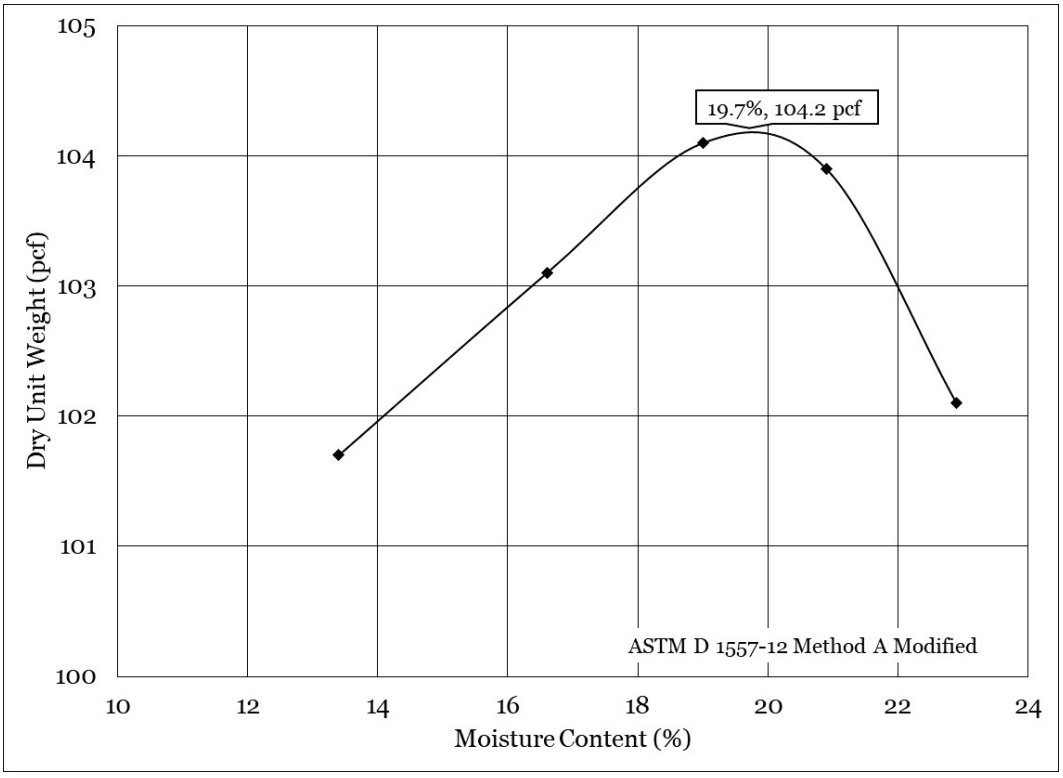

To determine an in-place moisture content at the targeted 10 CBR, a suite of laboratory CBR tests (ASTM D1883) was performed (ASTM 2016). These tests were conducted at moisture contents ranging from approximately 20% to approximately 40%. A target in-place moisture content of 29% was selected based on the relationship between

moisture content and CBR. The relationship between CBR and moisture content is presented graphically in Figure 4.

Figure 4. Clay subgrade CBR/moisture content relationship.

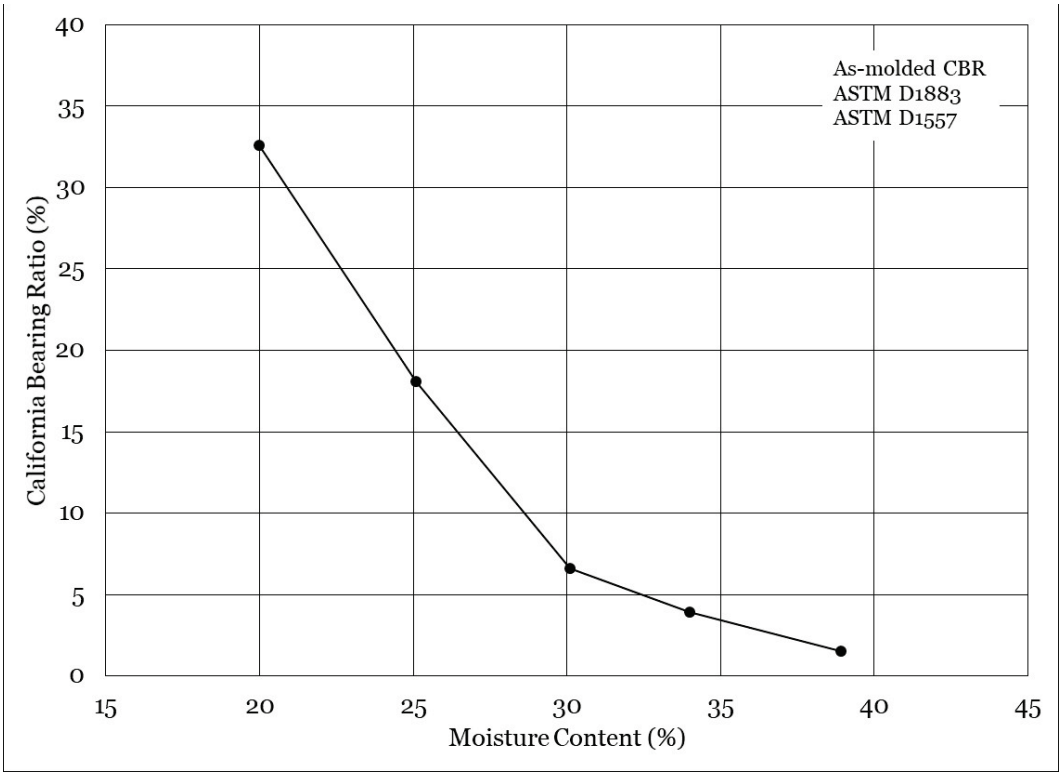

3.2 Base course

Crushed limestone (LMS) and crushed gravel (GR) (Figure 5) were used to construct the flexible aggregate base course. Crushed limestone was selected to represent a strong base (historically this material yields an in-situ CBR of 100+), and the crushed gravel was selected to represent a base material that may be substantially weaker yet representative of materials that could be encountered under much thinner pavement sections. Material characterization results are summarized in the following sections.

Crushed limestone

The gradation for the crushed limestone base is shown in Figure 6. ASTM procedure D2487 was used to determine that the base course was comprised of 66.9% gravel, 26.5% sand, and 6.6% nonplastic fines passing the No. 200 sieve (ASTM 2017a). The coefficient of curvature (Cc) was calculated as 3.17, and the coefficient of uniformity (Cu) was 31.46. The crushed limestone aggregate base was classified as a poorly graded gravel

with silt and sand (GP-GM) according to the USCS (ASTM 2017a) and an A-1-a according to the AASHTO procedure (2012). Modified Proctor compaction tests (Figure 7) were performed in accordance with ASTM D1557 Method C Modified (2012). The maximum dry density was 146.6 pcf at an optimum moisture content of 5.4%.

Figure 5. Base course aggregate.

(a) Crushed limestone base (b) Crushed gravel base

Figure 6. Crushed limestone base particle-size analysis.

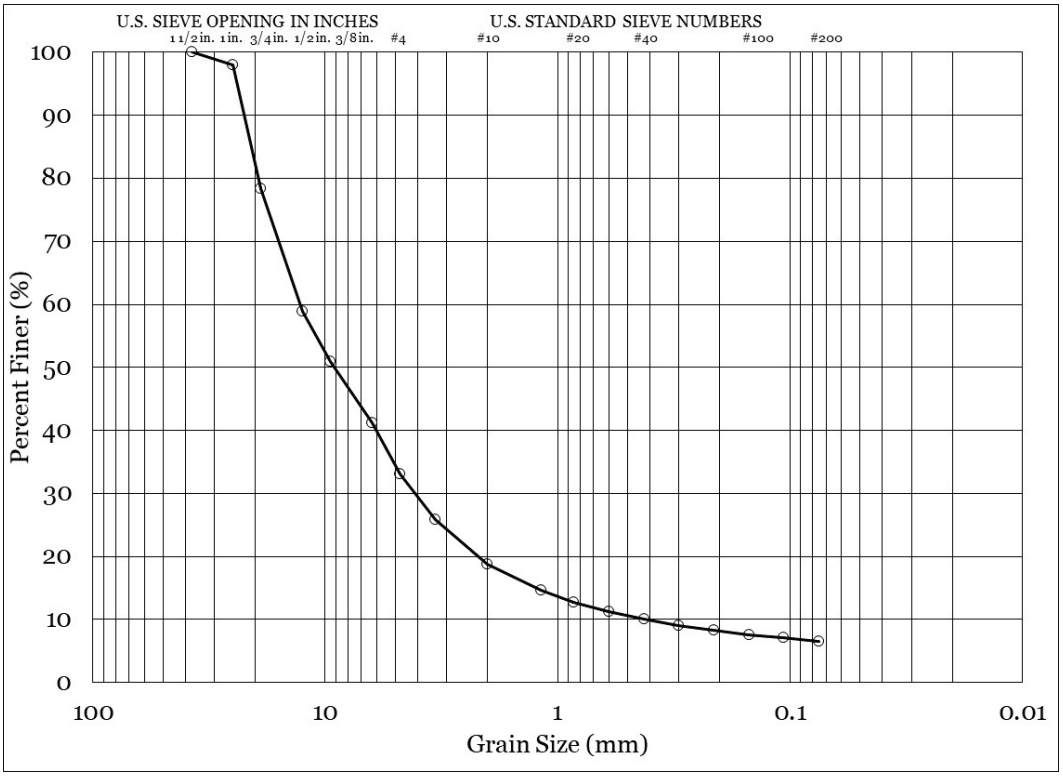

Figure 7. Crushed limestone base moisture/density relationship.

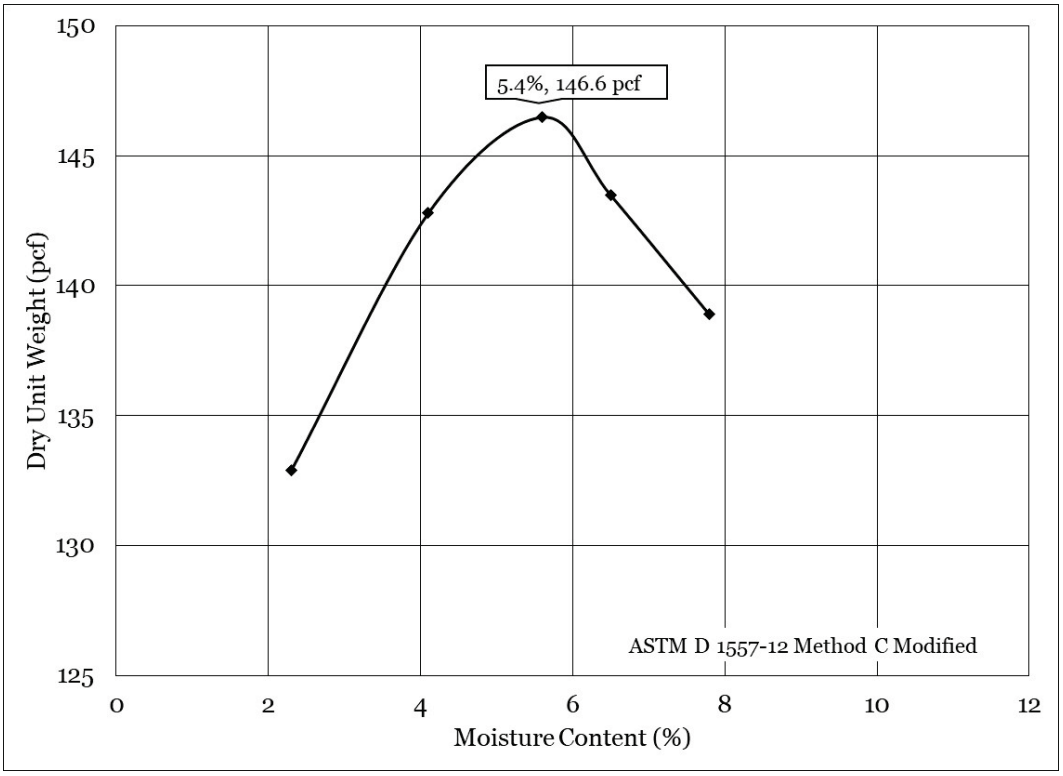

Crushed gravel

The gradation for the crushed gravel is shown in Figure 8. The crushed gravel base course was comprised of 77% gravel, 21.6% sand, and 1.4% nonplastic fines passing the No. 200 sieve. The Cc was calculated as 1.88, and the Cu was 5.93. The crushed gravel aggregate base was classified as a well-graded gravel with sand (GW) according to the USCS (ASTM 2017a) and an A-1-a according to the AASHTO procedure (2012). Modified Proctor compaction tests (Figure 9) were performed in accordance with ASTM D1557 Method C Modified (2012). The maximum dry density was 124.7 pcf at an optimum moisture content of 7.6%.

Figure 8. Crushed gravel base particle-size analysis.

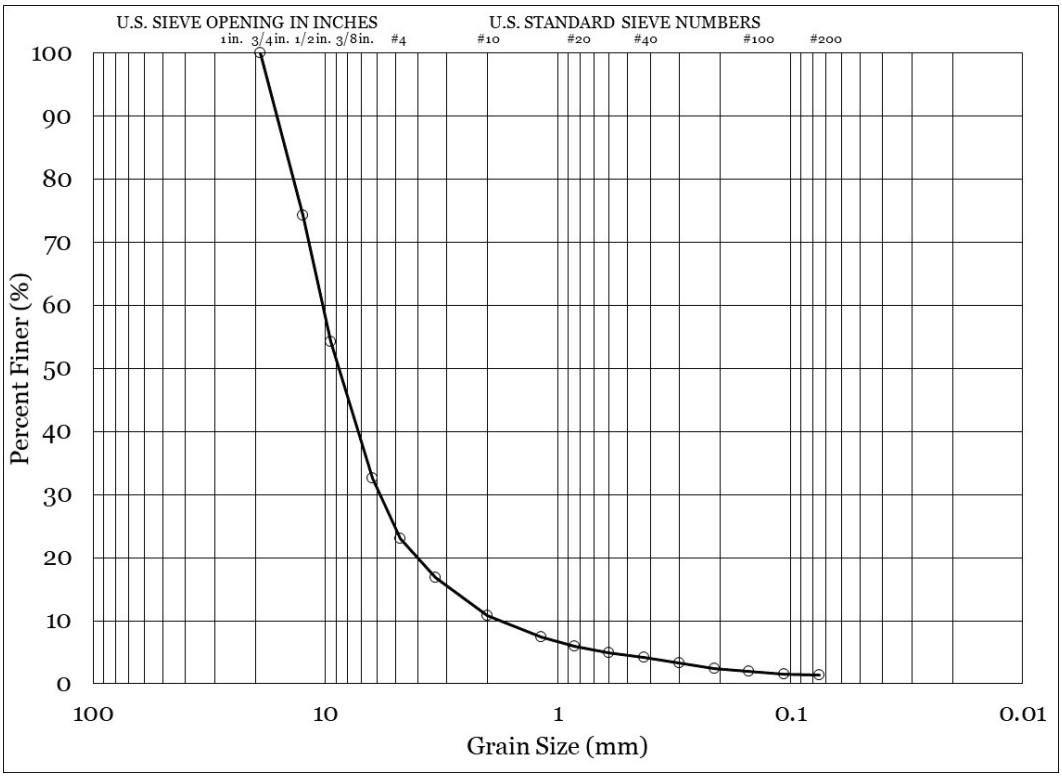

Figure 9. Crushed gravel base moisture/density relationship.

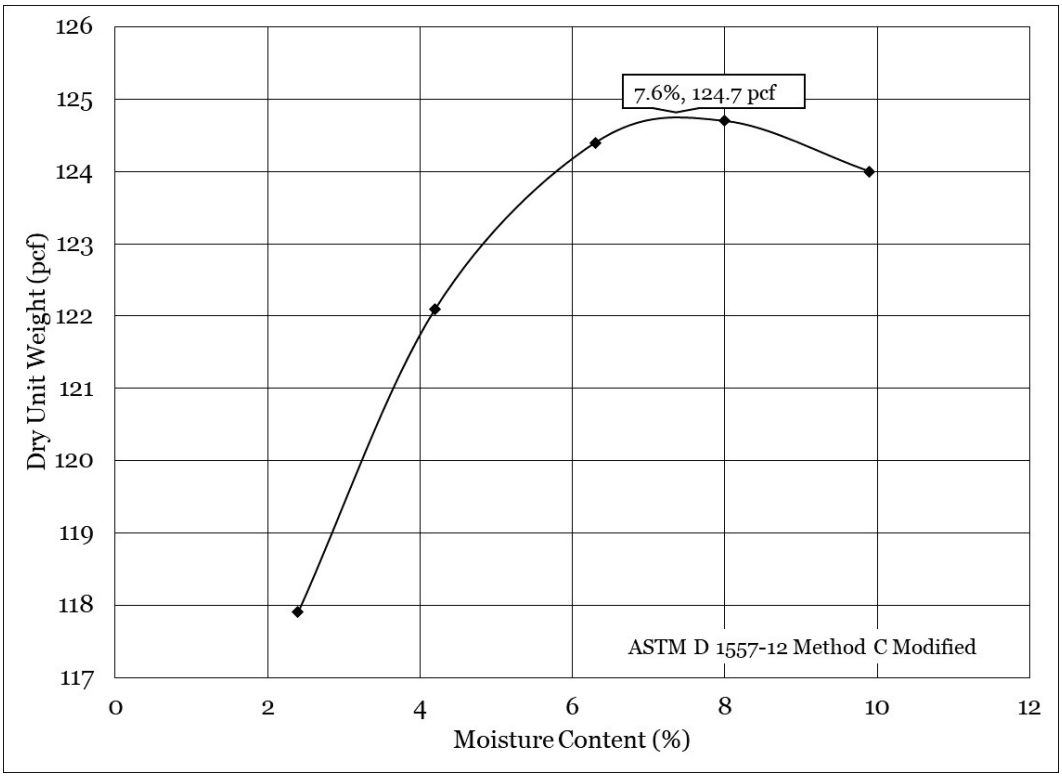

3.3 Asphalt

A 9.5-mm nominal maximum aggregate size (NMAS) hot-mix asphalt (HMA) surface mixture was selected for placement of the wearing surface of all test items. The asphalt mixture was one that is representative of a typical airfield mix and consisted of 40% limestone aggregate, 59% gravel/sand, and 1% hydrated lime. Recycled asphalt pavement (RAP) was not allowed, and natural sand was limited to 15% of the total aggregate blend. Pertinent mixture properties are summarized in Table 1.

Table 1. Hot-mix asphalt design properties.

Test Property		Design Value
N_{design}		75
Binder Grade		PG 67-22
Mixing Temp (°F)		310
Compaction Temp (°F)		300
Percent Passing (%)	1.0 in. (25.0 mm)	100
	3/4 in. (19.0 mm)	100
	1/2 in. (12.5 mm)	100
	3/8 in. (9.5 mm)	99
	#4 (4.75 mm)	74
	#8 (2.36 mm)	48
	#16 (1.18 mm)	33
	#30 (0.60 mm)	22
	#50 (0.30 mm)	11
	#100 (0.15 mm)	7
	#200 (0.075 mm)	5.3
Aggregate specific gravity (G_{sb})		2.590
Percent binder by total mass (P_b (%))		5.7
Theoretical maximum specific gravity (G_{mm})		2.410
Voids in Mineral Aggregate (%)		15.8
Voids Filled with Asphalt (%)		74.7
P_{200}/P_{be}		1.01

4 Instrumentation

Instrumentation was installed in the subgrade, base course, and HMA surface course to monitor pavement response during test section trafficking. Sensors used to capture the pavement response included earth pressure cells (EPCs), single-depth deflectometers (SDDs), and asphalt strain gauges (ASGs). Pore-water pressure, temperature sensors, and moisture sensors were installed to monitor environmental parameters. Figures 10 and 11 show the plan and profile view of the typical instrumentation layout for a test item, respectively.

Figure 10. Instrumentation plan view.

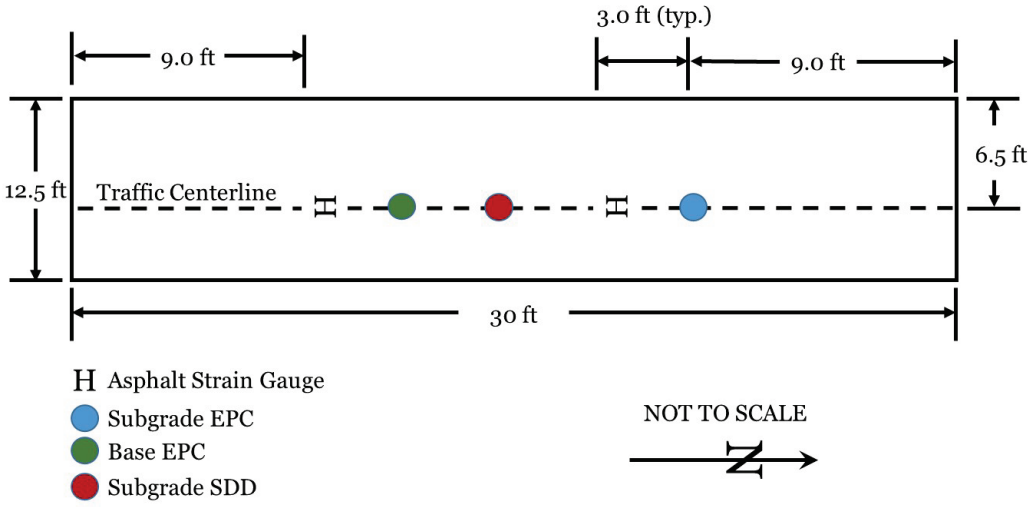

Figure 11. Instrumentation profile view.

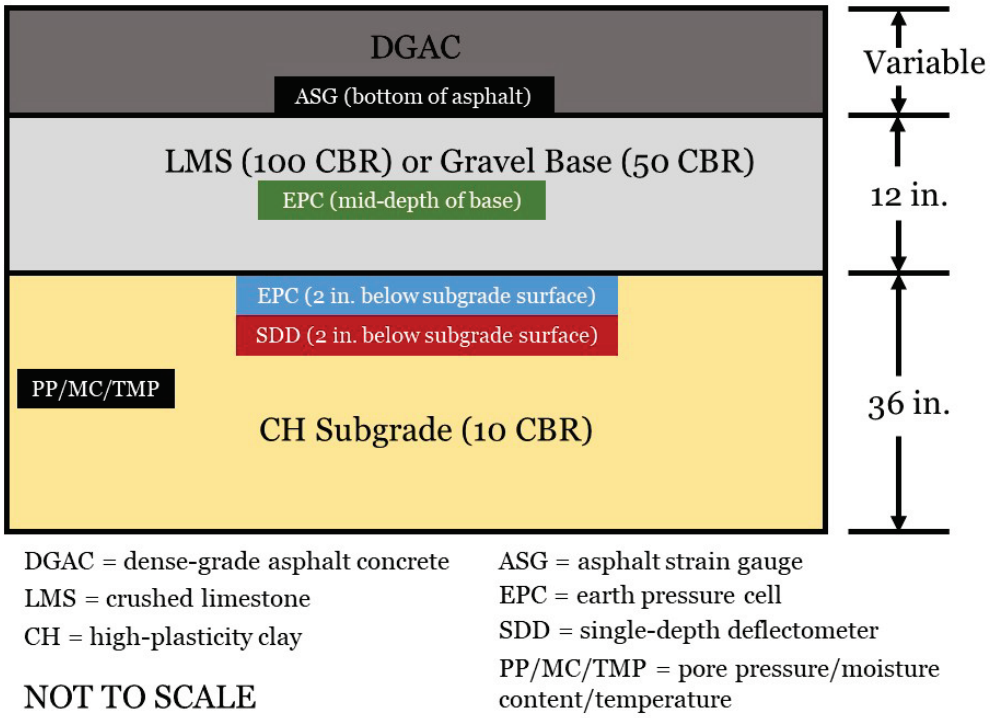

4.1 Earth pressure cells

Vertical stresses in the base course and subgrade were measured by using 9-in.-diam Geokon EPCs. EPCs provide a quantitative measurement of the vertical distribution of the stresses within each traffic lane during testing. Cells with a maximum pressure range up to 145 psi were installed in the subgrade, and 325-psi EPCs were installed in the base course. The EPCs in the base course were located 6 in. below the top of the base, while the EPCs placed in the subgrade were located 2 in. below the top of the subgrade. Figure 12 shows an EPC being installed 2 in. below the surface of the subgrade at the interface with the base course.

Installation commenced by locating each EPC at the pre-planned station within each test item and carefully outlining the excavation area to minimize disturbance to adjacent soils. Measurements were made by using a rod and level to determine pre-excavation elevation and to benchmark proper placement depth. The EPC area was excavated to the target depth, the bottom of the excavation was carefully leveled, and a thin layer of clean sand was evenly spread to ensure the gauge maintained full contact with the underlying subgrade soils. Shallow trenches (approximately 1 in. deep) were excavated to the edge of each test item for

wire placement and protection from subsequent construction activities. After excavation was complete, an EPC was placed in the excavation, and alignment was verified. Design subgrade soils were placed around each EPC and were compacted with a pneumatic hammer in an attempt to minimize density variations in the disturbed area.

Figure 12. EPC installation technique.

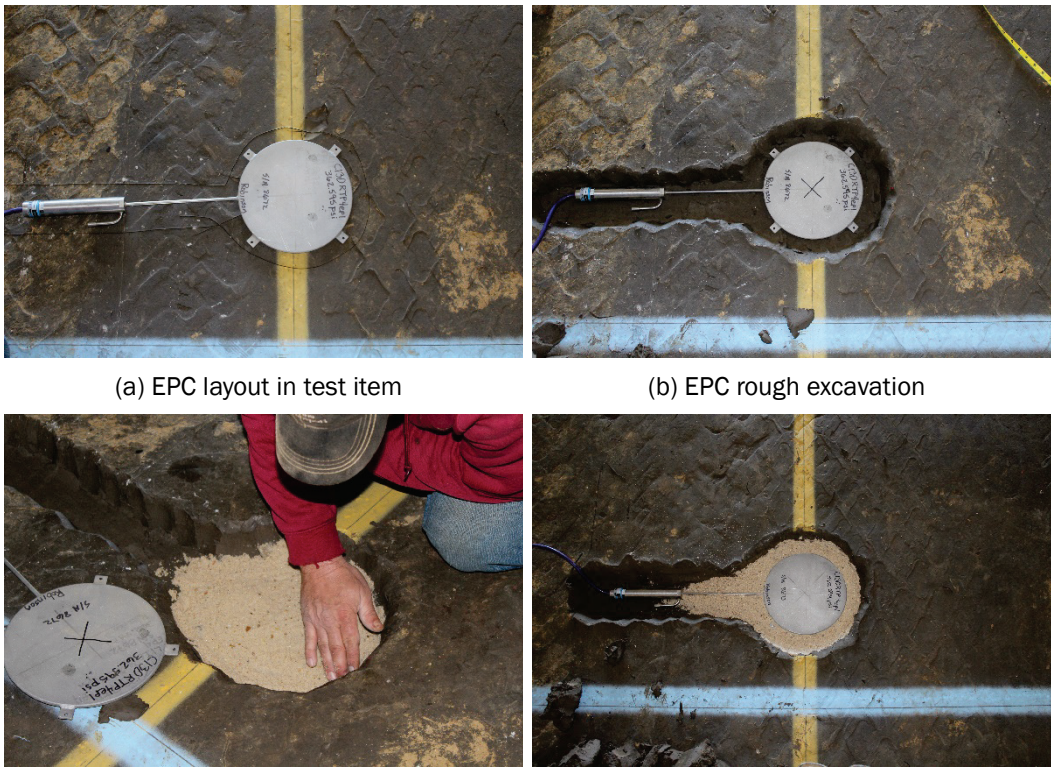

(a) EPC layout in test item

(b) EPC rough excavation

(c) Spreading thin sand layer

(d) Placement completed

4.2 Single-depth deflectometer

Vertical deflections in the subgrade were measured using single-depth deflectometers (SDDs) that were assembled by ERDC. One SDD was placed in the middle of each test item along the centerline of traffic. The SDD was placed such that the shaft was anchored at a depth of 8 ft from the top of the subgrade. A linear velocity displacement transducer (LVDT) with a range of ±1 in. was placed in the housing such that it was in contact with both the anchor rod and the surface plate, as shown in Figure 13. Thus, the LVDT measured movement of the plate 2 in. below the base-subgrade interface relative to the control point located at a depth of 8 ft.

Similar to EPC installation, each SDD was placed at a pre-planned location and excavated such that the top of the removable access plate was 2 in. below the existing subgrade elevation. A borehole was advanced at the center of the plate location to a depth of approximately 8 ft by using earth auger drilling techniques. Rapid-setting concrete was placed in the borehole, and the instrument assembly was lowered to the target depth. After the concrete had sufficiently cured, the LVDT was installed through a removable access plate such that the tip of the LVDT was in contact with the fixed anchor rod. Subgrade soils were then compacted over the surface of the SDD assembly. Photographs summarizing SDD installation are shown in Figure 14.

Figure 13. Single-depth deflectometer schematic.

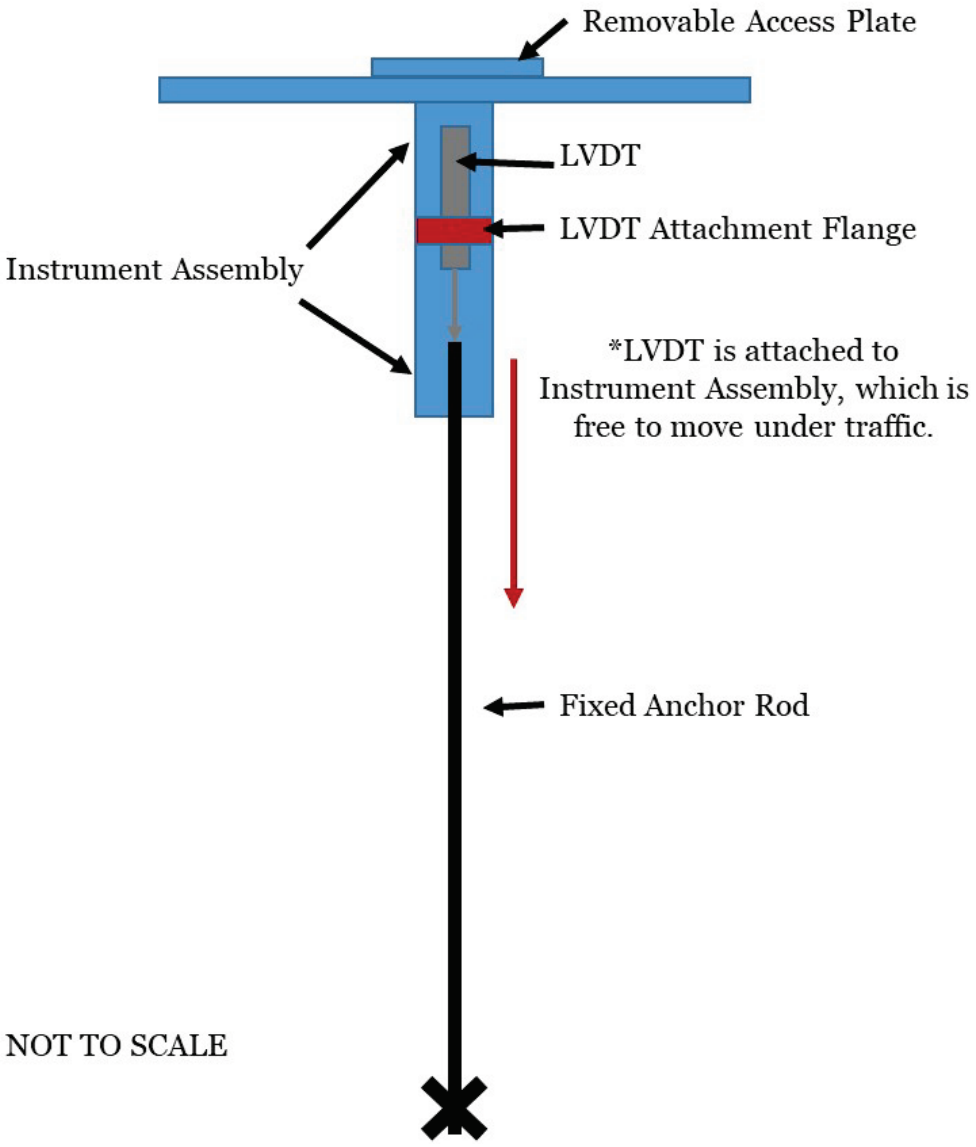

Figure 14. Single-depth deflectometer installation.

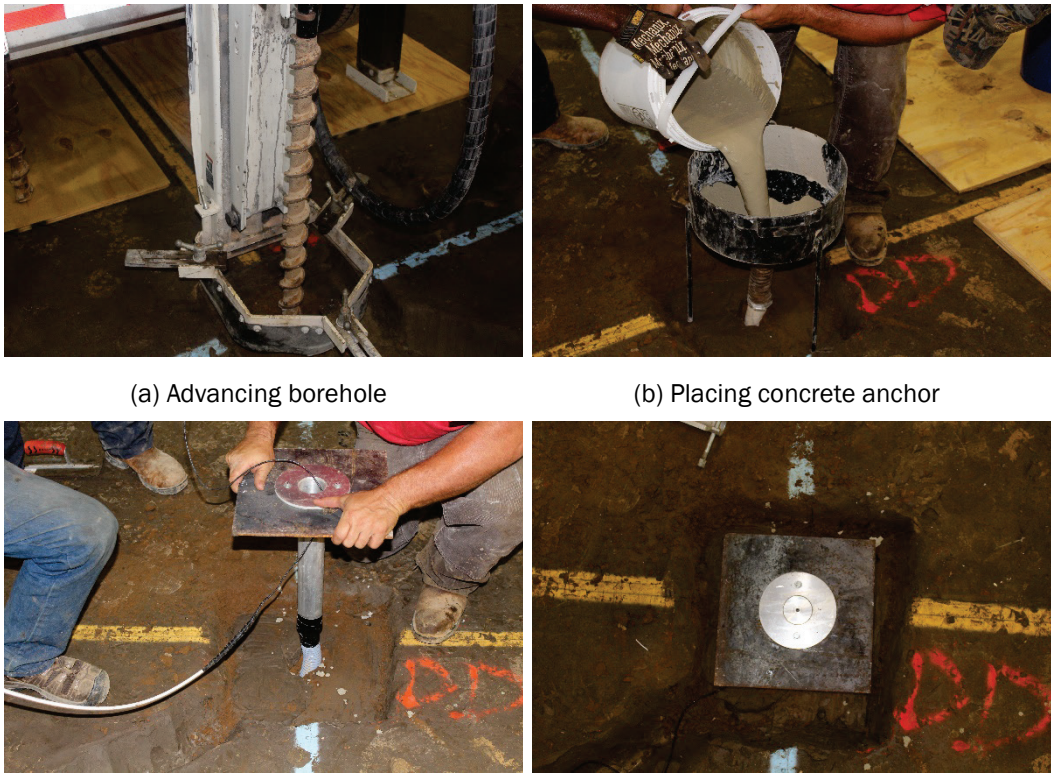

(a) Advancing borehole (b) Placing concrete anchor

(c) Setting gauge assembly (d) Completed installation

4.3 Asphalt strain gauges

Tensile strain at the bottom of an HMA layer provides a quantitative measure of the pavement response during trafficking. The tensile strain at the bottom of the asphalt is a key response parameter linked to fatigue damage in the HMA layer. For this study, strain at the bottom of the HMA surface was measured by using dynamic asphalt strain gauges (ASGs) in the longitudinal (i.e. with traffic) direction. The ASGs were manufactured by Tokyo Sokki and were capable of measuring a range of ±5,000 microstrain. The gauges were adhered to the surface of the base course with a heated asphalt binder, and HMA from the asphalt paver was placed as cover over each of the gauges immediately prior to paving the entire test section. This process is shown in Figure 15.

Figure 15. Asphalt strain gauge installation.

(a) Trenching for wire

(b) Adhered to surface

(c) Covering with HMA

(d) Compacted prior to paving

5 Pavement Characterization

5.1 As-built properties

Quality control tests were performed during construction of each material lift to ensure target values were achieved and to monitor material consistency. Dry density and moisture content were measured by using a nuclear moisture density device in accordance with ASTM D6938 (2017b) to verify the uniformity of each material lift. Field in-place CBR tests were performed in general accordance with ASTM D4429 (2009) on each compacted lift to ensure target values were achieved. To further characterize the strength of the completed base and subgrade layers, Dynamic Cone Penetrometer (DCP) tests were performed in accordance with ASTM D6951 (2018). Asphalt cores were obtained from each test item, and core densities were determined in accordance with AASHTO T166 (2016). As-built properties are summarized in Table 2 for the C-130 traffic lanes and Table 3 for the C-17 traffic lanes.

5.2 Dynamic cone penetrometer

A series of DCP tests was performed to characterize the strength of the unbound gravel pavement layers. DCP tests were performed after completion of asphalt placement, following the procedures described by ASTM D 6951 (2018). Measured values of the DCP index (millimeters of penetration per hammer blow) were converted to CBR strength by using the relationship developed by Webster et al. (1992) and Webster et al. (1994). As-built DCP results can be found in Appendix A.

5.3 Falling weight deflectometer

Falling weight deflectometer (FWD) tests were performed on the surface of the test items after construction and prior to trafficking. The measured impulse stiffness modulus (ISM) was used to evaluate the stiffness of the constructed pavement section and to provide a baseline for subsequent comparison under traffic. The ISM is the ratio of the applied load to the measured plate deflection with higher values representing a stiffer pavement structure. ISM results are discussed in Chapter 7.

Table 2. C-130 traffic lane as–built properties.

Property	C130RTP1	C130RTP2	C130RTP3	C130RTP4	C130NTP1	C130NTP2	C130NTP3	C130NTP4
CH Subgrade (104.2 pcf @ 19.7%)[1]								
Wet Density (pcf)	119.3 ± 1.4	117.7 ± 2.3	116.8 ± 2.4	118.0 ± 3.6	119.1 ± 1.5	118.3 ± 2.0	118.1 ±2.3	117.7 ± 3.1
Dry Density (pcf)	93.2 ± 1.5	91.6 ± 2.6	90.2 ± 2.6	91.8 ± 3.7	92.4 ± 1.1	91.6 ± 2.4	92.0 ± 2.7	91.5 ± 2.8
Nuclear Moisture Content (%)	27.5 ± 1.1	27.7 ± 1.6	28.2 ± 2.2	27.7 ± 2.1	28.7 ± 1.6	28.2 ± 1.7	27.6 ± 1.7	27.7 ± 1.9
Compaction (%)	89.4	87.9	86.6	88.1	88.7	87.9	88.3	87.8
Oven-Dried Moisture (%)	29.9 ± 1.2	29.8 ± 1.2	30.1 ± 1.5	29.4 ± 1.0	29.7 ± 1.7	30.5 ± 0.6	29.5 ± 1.0	29.8 ± 1.3
In-Place CBR (%)	9.8 ± 0.5	9.6 ± 0.7	9.4 ± 0.4	9.9 ± 0.7	9.8 ± 0.4	9.8 ± 0.6	10.1 ± 0.6	9.5 ± 0.5
Base Course (146.7 pcf @ 5.9%; 124.7 pcf @ 7.6%)[1]								
Material Type	GR	LMS	LMS	LMS	GR	LMS	LMS	LMS
Wet Density (pcf)	124.0 ± 1.5	148.5 ± 3.8	147.7 ± 4.8	145.7 ± 4.8	123.8 ±1.2	150.0 ±0.9	147.2 ± 2.0	146.1 ±0.6
Dry Density (pcf)	118.0 ± 0.8	142.9 ± 4.6	142.1 ± 4.6	140.4 ± 3.7	118.1 ± 0.4	143.2 ± 1.9	141.6 ±1.8	140.8 ±0.9
Nuclear Moisture Content (%)	5.2 ± 1.3	4.0 ± 0.7	3.9 ± 0.1	3.7 ± 0.7	4.6 ± 0.9	4.8 ± 0.9	4.0 ± 1.0	4.1 ± 1.0
Compaction (%)	94.6	97.5	96.9	95.8	94.7	97.7	96.6	96.0
Oven-Dried Moisture (%)	1.4 ± 0.2	2.2 ± 0.3	2.5 ± 0.2	3.0 ± 0.3	1.4 ± 0.2	2.2 ± 0.3	2.5 ± 0.2	3.0 ± 0.3
In-Place CBR (%)	42	100+	100+	100+	47	100+	100+	100+
Thickness (in.)	12.1 ± 0.3	12.2 ± 0.2	12.2 ± 0.3	12.0 ± 0.3	12.2 ± 0.3	11.9 ± 0.2	11.9 ± 0.2	11.8 ± 0.2
Asphalt								
Compaction (%)	90.0	90.0	90.2	89.5	92.9	90.0	91.1	87.9
Thickness (in.)	2.5 ± 0.2	2.5 ± 0.2	1.5 ± 0.2	1.0 ± 0.2	2.6 ± 0.2	2.7 ± 0.2	1.5 ± 0.2	1.1 ± 0.2

[1]Maximum dry density and optimum moisture content as determined from ASTM D1557; GR = gravel; LMS = limestone

Table 3. C-17 traffic lane as-built properties.

Property	C17RTP1	C17RTP2	C17RTP3	C17RTP4	C17NTP1	C17NTP2	C17NTP3	C17NTP4
CH Subgrade (104.2 pcf @ 19.7%)[1]								
Wet Density (pcf)	118.3 ± 2.7	118.1 ± 2.1	116.4 ± 2.7	116.4 ± 2.4	119.1 ± 1.2	118.2 ± 2.1	117.2 ± 2.8	117.9 ± 1.9
Dry Density (pcf)	93.1 ± 2.1	92.2 ± 2.2	90.5 ± 2.6	90.4 ± 2.6	92.9 ± 0.8	91.5 ± 2.1	91.2 ± 3.0	91.0 ± 1.5
Nuclear Moisture Content (%)	27.3 ± 1.7	27.5 ± 1.2	27.9 ± 2.3	27.7 ± 2.1	27.9 ± 1.2	28.4 ± 1.8	27.5 ± 2.2	27.7 ± 1.6
Compaction (%)	89.3	88.5	86.9	86.8	89.2	87.8	87.5	87.3
Oven-Dried Moisture (%)	29.4 ± 0.6	28.9 ± 1.3	30.5 ± 0.7	29.0 ± 1.2	29.2 ± 0.6	29.7 ± 0.6	29.6 ± 1.0	30.4 ± 1.3
In-Place CBR (%)	9.7 ± 0.4	10.0 ± 0.7	9.6 ± 0.6	9.9 ± 0.7	9.5 ± 0.4	9.6 ± 0.6	9.5 ± 0.5	9.4 ± 0.6
Base Course (146.7 pcf @ 5.9%; 124.7 pcf @ 7.6%)[1]								
Material Type	LMS	LMS	LMS	GR	LMS	LMS	LMS	GR
Wet Density (pcf)	149.2 ± 0.7	152.0 ±2.0	151.1 ± 2.7	125.0 ±3.4	151.0 ± 2.5	149.9 ±2.6	146.7 ±0.5	125.5 ±1.7
Dry Density (pcf)	142.4 ± 0.6	145.2 ± 1.8	144.3 ± 2.3	120.0 ±2.3	144.0 ±2.7	143.1 ± 2.5	139.9 ±0.4	120.5 ±1.3
Nuclear Moisture Content (%)	4.8 ± 0.3	4.7 ± 0.1	4.8 ± 0.4	4.1 ± 0.9	4.9 ± 0.4	4.7 ± 0.1	4.8 ± 0.2	4.1 ± 0.6
Compaction (%)	97.1	99.0	98.4	96.2	98.2	97.6	95.4	96.6
Oven-Dried Moisture (%)	2.8 ± 0.2	2.6 ± 0.3	2.6 ± 0.1	1.4 ± 0.3	2.8 ± 0.2	2.6 ± 0.3	2.6 ± 0.1	1.4 ± 0.3
In-Place CBR (%)	100+	100+	100+	47	100+	100+	100+	46
Thickness (in.)	11.9 ± 0.2	12.1 ± 0.3	11.8 ± 0.2	12.2 ± 0.2	12.0 ± 0.3	11.8 ± 0.2	11.9 ± 0.2	12.1 ± 0.3
Asphalt								
Compaction (%)	89.6	90.4	90.8	91.0	89.8	90.3	91.3	91.2
Thickness (in.)	1.0 ± 0.2	1.5 ± 0.2	2.5 ± 0.2	2.5 ± 0.3	1.0 ± 0.1	1.6 ± 0.2	2.7 ± 0.2	2.5 ± 0.2

[1]Maximum dry density and optimum moisture content as determined from ASTM D1557; GR = gravel; LMS = limestone

6 Traffic Testing

Simulated aircraft traffic was applied by using a single-wheel tire configuration mounted to a steel frame that was capable of being loaded with a series of lead weights to achieve the targeted single-wheel load. The loaded steel frame was mobilized via a front-end loader and was attached to the loader with an in-house fabricated quick-attach connector plate. The connector plate was fabricated such that the steel frame was allowed to rotate transverse to the traffic direction to account for subtle changes in pavement surface elevation. It is noted that the connection was fixed in the traffic direction and that front-to-back levelness of the steel frame was visually verified both prior to and during traffic application. The steel-frame was outfitted with outrigger tires on each side, near the midspan of the load frame, as a means of stabilizing the frame and preventing overturn. During traffic application, one outrigger remained in contact with the pavement to ensure overall stability. The opposite outrigger was elevated such that it was not in contact with the pavement surface but was near the surface in case of an overturn condition. Figure 16 shows the load cart frame and the primary mover.

Figure 16. Load cart frame and primary mover.

6.1 C-130 tire configuration

A single-wheel C-130 tire was mounted to the steel frame and was loaded with lead weights to target a total load of approximately 35,000 lb. Lead weights were evenly distributed both front-to-back and side-to-side on the steel frame, and the target total load was verified by using a calibrated mobile aircraft scale. The aircraft scales indicated that a total load of 34,875 lb was achieved, representing 99.6% of the target load.

Tire pressure for the normal tire pressure test series was 100 psi, and tire pressure for the reduced tire pressure test series was 80 psi. The C-130 tire was inflated with compressed nitrogen, and tire pressure was verified (and adjusted when necessary) twice daily -- typically before traffic began in the morning and after traffic was paused during lunch break. Prior to initial traffic application for each tire pressure series, tire-area imprints were obtained to investigate changes in measured tire-contact area with changes in tire pressure. These imprints were made by affixing a thick construction-paper outline on the pavement surface and rolling the loaded test tire onto the paper outline. The tire outline was painted by using marking paint and was allowed time to dry such that, when the tire was reversed off the paper outline, a distinguishable paint halo was preserved. Each tire outline (Figure 17) was photographed and uploaded to a computer-aided drawing program.

By digitizing the tire imprint, accurate contact-area determinations could be made and compared to a common assumption that contact area can be approximated by dividing the total load by the tire-inflation pressure. Contact-area measurements were made to determine total area (i.e., simply the area inside the perimeter of the tire and the contact area, which excluded the tread pattern). For the C-130 tire, it was found that the assumed contact area (based on the measured wheel load and inflation pressure) overestimated contact area in both cases. A summary of measured C-130 tire characteristics is shown in Table 4.

Table 4. C-130 tire physical characteristics.

Condition	Inflation Pressure (psi)	Load (lb)	Length (in.)	Width (in.)	Total Area (in.^{2})	Contact Area (in.^{2})	Assumed Contact Area (in.^{2})	Actual Contact Pressure (psi)
Normal	100	34,875	26.2	17.4	382.8	306.3	348.7	113.9
Reduced	80	34,875	27.5	17.9	408.3	341.3	435.9	102.2

Figure 17. C-130 tire print at normal and reduced tire pressure.

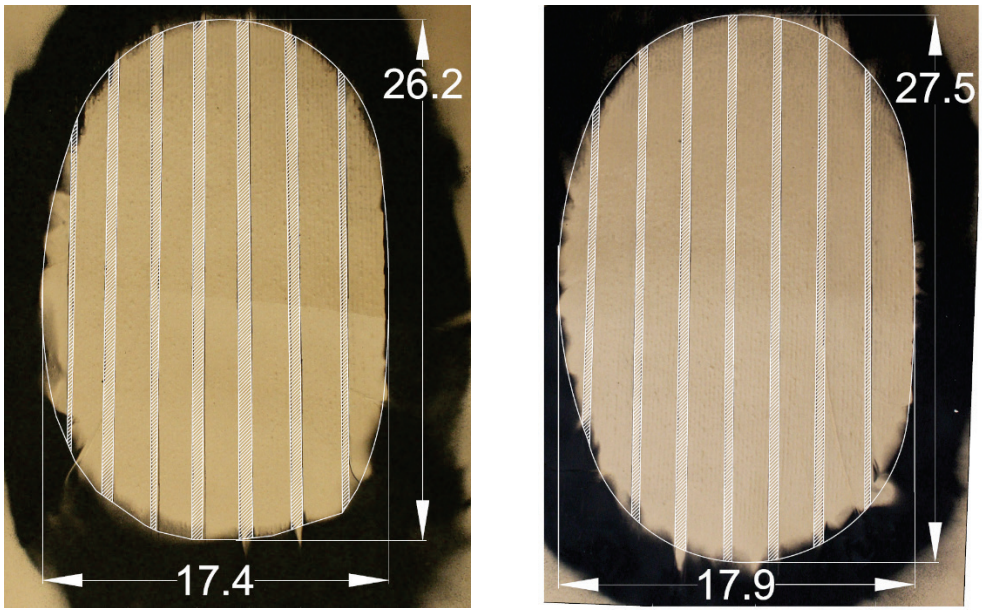

a) C-130 Normal Tire Pressure Print

b) C-130 Reduced Tire Pressure Print

6.2 C-17 tire configuration

A single-wheel C-17 tire was mounted to the steel frame and was loaded with lead weights to target a total load of 45,000 lb. The calibrated mobile aircraft scales indicated that a total load of 46,100 lb was achieved, representing 102.4% of the target load.

Tire pressure for the normal tire pressure test series was 142 psi, and tire pressure for the reduced tire pressure test series was 115 psi. Tire imprints for the C-17 at both normal and reduced tire pressures are shown in Figure 18. It was found that the assumed and the actual contact area agreed reasonably well (see Table 5), which was in contrast to observations for the C-130. It is hypothesized that the observed differences could be due to sidewall stiffness differences in the two test tires. Further, it is noted that the C-130 tire was a new tire that was purchased from a local distributor and the C-17 tire was a used tire that had been decommissioned from flight operations. The higher sidewall stiffness of a new C-130 tire could explain the observed lower actual contact area (i.e., the new tire would deform less under loading).

Table 5. C-17 tire physical characteristics.

Condition	Inflation Pressure (psi)	Load (lb)	Length (in.)	Width (in.)	Total Area (in.²)	Contact Area (in.²)	Assumed Contact Area (in.²)	Actual Contact Pressure (psi)
Normal	142	46,100	22.9	17.3	346.1	321.0	324.6	144
Reduced	115	46,100	25.2	19.5	432.8	406.1	400.9	114

Figure 18. C-17 tire print at normal and reduced tire pressure.

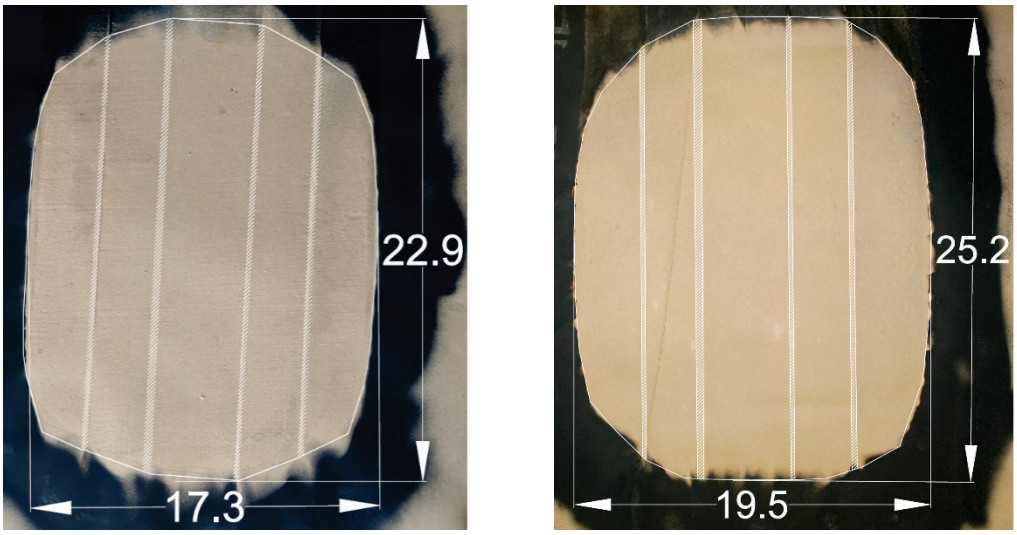

a) C-17 Normal Tire Pressure Print

b) C-17 Reduced Tire Pressure Print

6.3 Traffic pattern

A normally distributed traffic pattern (Figure 19) with a total wander width of 54 in. was used to apply test traffic to each test item. Traffic was applied bi-directionally, where one pass was advanced forward in the selected position and the return pass was applied in the same selected position. Tire position was maneuvered in the buffer-zone areas to minimize effects from side shifting the load frame within a test area.

An 18-in.-wheel-path width was estimated from previous experiments for both the C-130 and C-17 tire and was used for marking the traffic pattern on the test lane. As noted previously, the actual tire width was less in some cases but more in others. However, the minor deviations observed were considered reasonable given the inherent variability in applying traffic with a driver.

Traffic was applied such that 12 total passes constituted a full pattern to the test area. When the test item centerline was considered, the applied

traffic pattern resulted in six coverages, yielding a pass/coverage ratio = 12 passes/6 coverages = 2.0.

Figure 19. Normally distributed wander pattern.

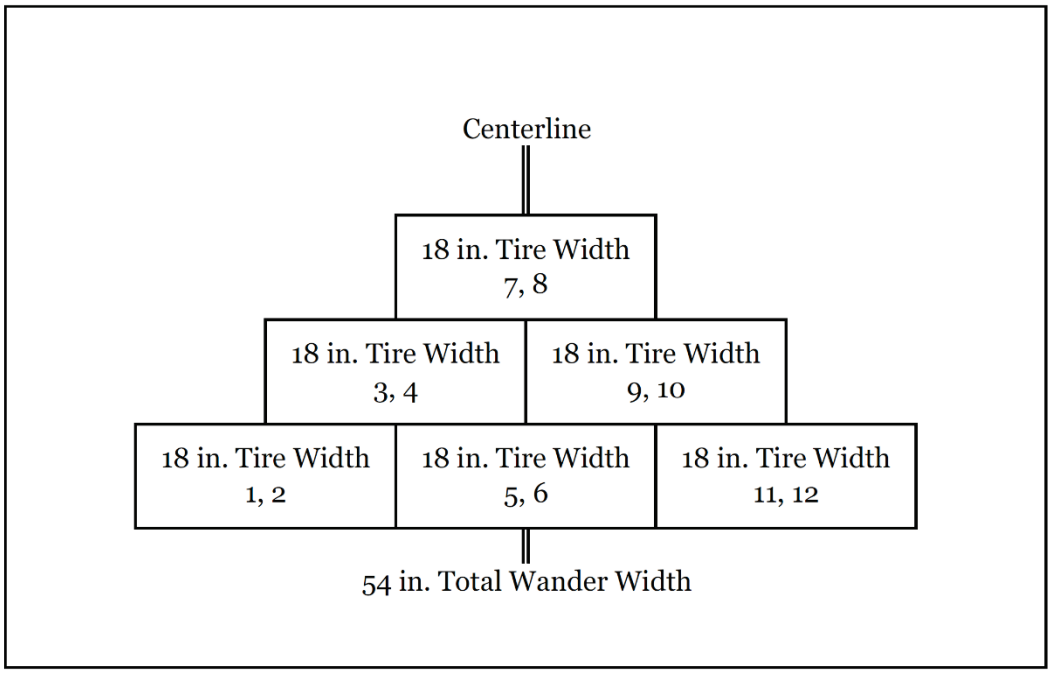

7 Results

Failure of the flexible pavement test items was defined as 1 in. of rutting, where rutting included permanent surface deformation in the wheel path and upheaval outside the wheel path. After achieving 1 in. of rutting, traffic was continued to target 3 in. of rutting, which is typical unsurfaced pavement failure criteria. Further, 1 in. of upheaval was also targeted, which is the typical test section failure criteria targeted by the FAA. Thus, it was desired to achieve several failure thresholds in order to extend the usefulness of the test data.

7.1 C-130 traffic results

C-130 rutting

Rut depth progression for the normal tire pressure test series is presented in Figure 20. Rapid rutting was observed in C130NTP1, which was expected due to the weaker gravel base material. The limestone base course items experienced a much slower rutting development when compared to the gravel base course item, and rut depth progression was logical relative to asphalt thickness. This highlights the importance of a competent aggregate base course, particularly in thin asphalt-surfaced pavements. C130NTP2 displayed the best rutting performance and had the thickest asphalt layer. Notably, C130NTP3 and C130NTP4 had similar rut depth development, and C130NTP3 performed only slightly better than C130NTP4. This suggests that increasing asphalt thickness by 0.5 in. had little effect on rut depth formation. However, the improvement observed by increasing asphalt thickness 1.0 in. (C130NTP3 vs. C130NTP4) resulted in a meaningful performance difference.

A paired t-test was performed to determine whether the observed differences in performance were statistically significant. Simply, the t-test was used to evaluate the difference in rut depth at each traffic level and to determine whether the average difference between datasets was equal to zero. A summary of pertinent statistics is presented in Table 6. It should be noted that the paired t-test indicated the difference between C130NTP3 and C130NTP4 was statistically significant at $\alpha = 0.05$; however, as noted previously, the differences were not considered practically meaningful.

Figure 20. C-130 normal tire pressure rut depth.

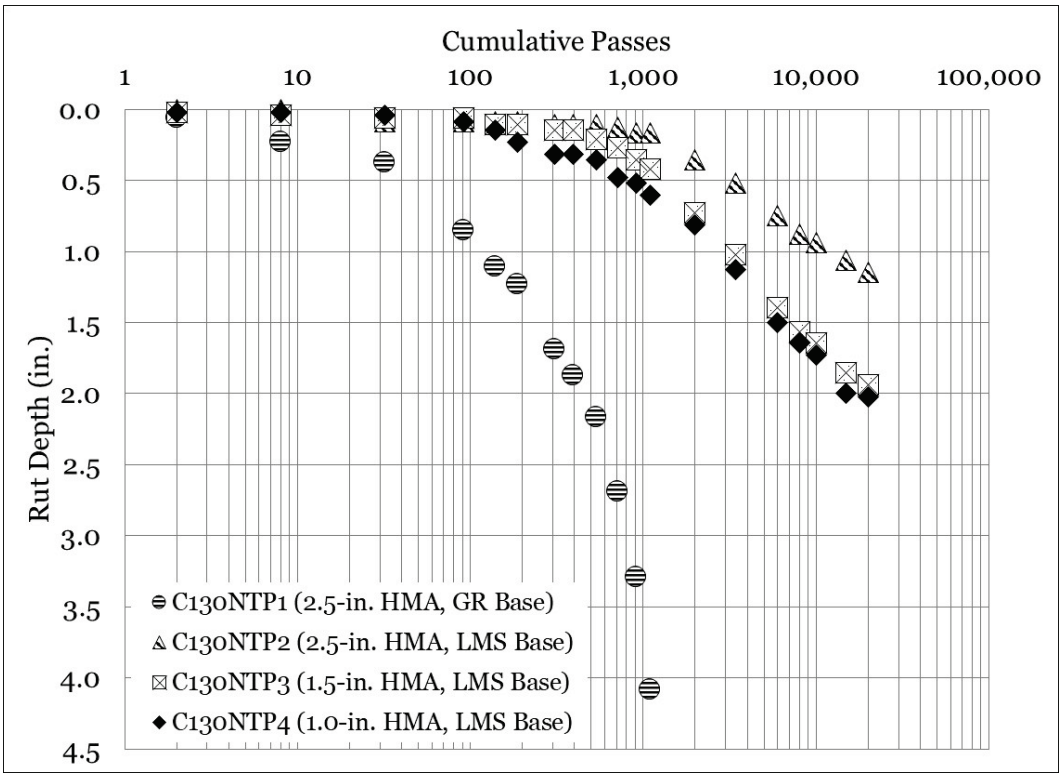

Table 6. Statistical analysis – C-130 normal tire pressure rut depth.

Interaction	n	p-value	Significant	Better Performer
C130NTP1 vs. C130NTP2	13	0.001	Yes	C130NTP2
C130NTP1 vs. C130NTP3	13	0.001	Yes	C130NTP3
C130NTP1 vs. C130NTP4	13	0.001	Yes	C130NTP4
C130NTP2 vs. C130NTP3	20	0.001	Yes	C130NTP2
C130NTP2 vs. C130NTP4	20	<0.001	Yes	C130NTP2
C130NTP3 vs. C130NTP4	20	<0.001	Yes	C130NTP3

Rut depth progression for the reduced tire pressure test series is presented in Figure 21. Similar to the normal tire pressure test series, C130RTP1 (weaker gravel base) deteriorated rapidly under traffic. This suggests that on weak base materials, tire pressure has little effect on overall performance; rather, total load controls pavement performance. Meaningful differences were observed between the limestone base sections, and performance followed expected trends with increased asphalt thickness. A statistical analysis (Table 7) indicated that performance differences in all items were statistically significant.

Figure 21. C-130 reduced tire pressure rut depth.

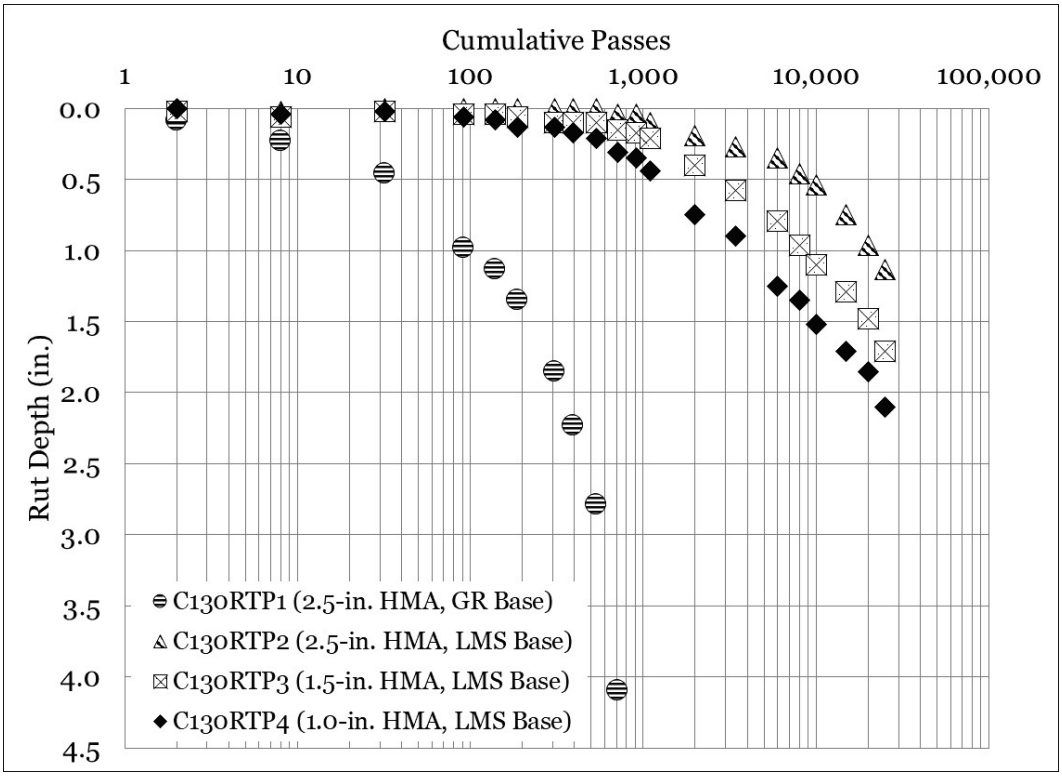

Table 7. Statistical analysis – C-130 reduced tire pressure rut depth.

Interaction	n	p-value	Significant	Better Performer
C130RTP1 vs. C130RTP2	11	0.005	Yes	C130RTP2
C130RTP1 vs. C130RTP3	11	0.005	Yes	C130RTP3
C130RTP1 vs. C130RTP4	11	0.005	Yes	C130RTP4
C130RTP2 vs. C130RTP3	21	<0.001	Yes	C130RTP2
C130RTP2 vs. C130RTP4	21	<0.001	Yes	C130RTP2
C130RTP3 vs. C130RTP4	21	<0.001	Yes	C130RTP3

Rut depth performance for each item was plotted in a series of equality plots shown in Figures 22 to 25. Reduced tire pressure rut depths were plotted on the y-axis, and normal tire pressure rut depths were plotted on the x-axis. A line of equality (LOE) (shown as a solid dark line on each graph) was plotted, and a best-fit linear trend line was plotted through each dataset. Linear equations (with y-intercept = 0) and R^2 values are presented, allowing for interpretation of overall performance differences.

The equality plots indicated that performance of the gravel base reduced tire pressure item was approximately 29% worse than the normal tire pressure item. This was not expected; however, it is noted

that the performance diverges from the equality plot at high rut levels (e.g., 2.0+ in.) and that the performance is generally equivalent at more reasonable rut levels (<= 1.0 in.). Performance improvement for the limestone base items was 15% in the 1.0-in. HMA test item, 34% in the 1.5-in. HMA test item, and 36% in the 2.5-in. HMA test item.

A statistical analysis (Table 8) indicated that average rutting in C130NTP1 and C130RTP1 was not statistically different (p-value = 0.064). Comparisons between companion limestone base test items were all statistically significant, and it was observed that average rutting was less in those items trafficked under reduced tire pressures.

Photographs showing rutting observed in the C-130 normal and reduced tire test items are presented in Figure 26.

Figure 22. Equality plot – C-130 rut depth (2.5-in. HMA, GR base).

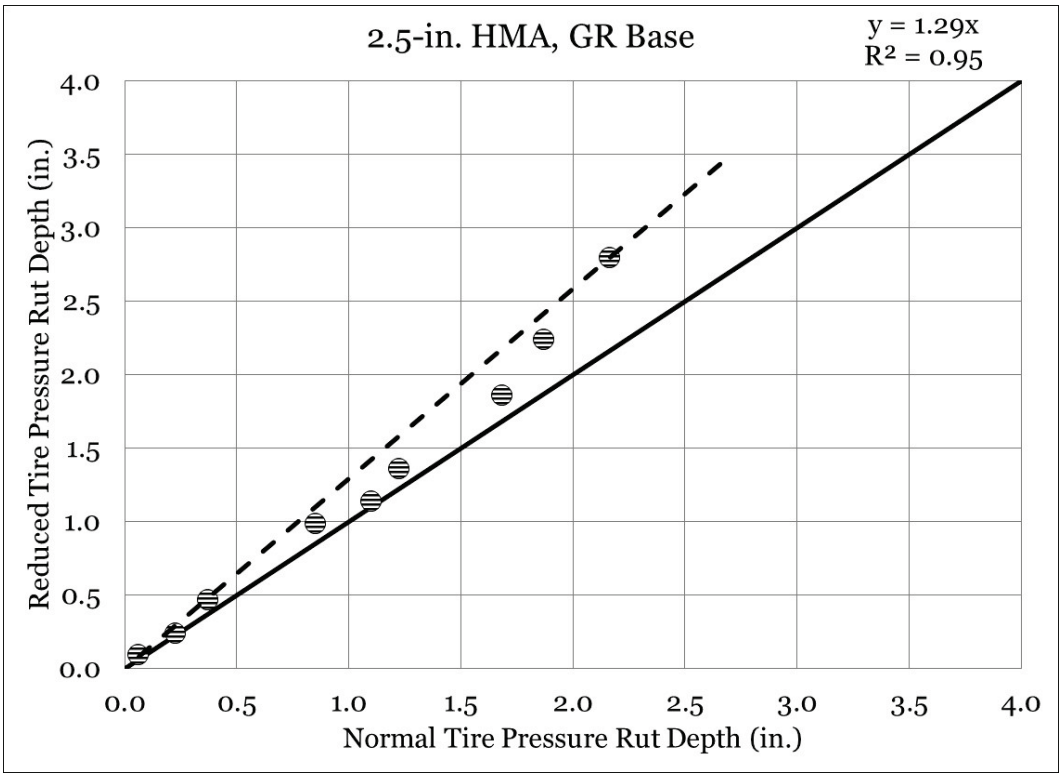

Figure 23. Equality plot – C-130 rut depth (2.5-in. HMA, LMS base).

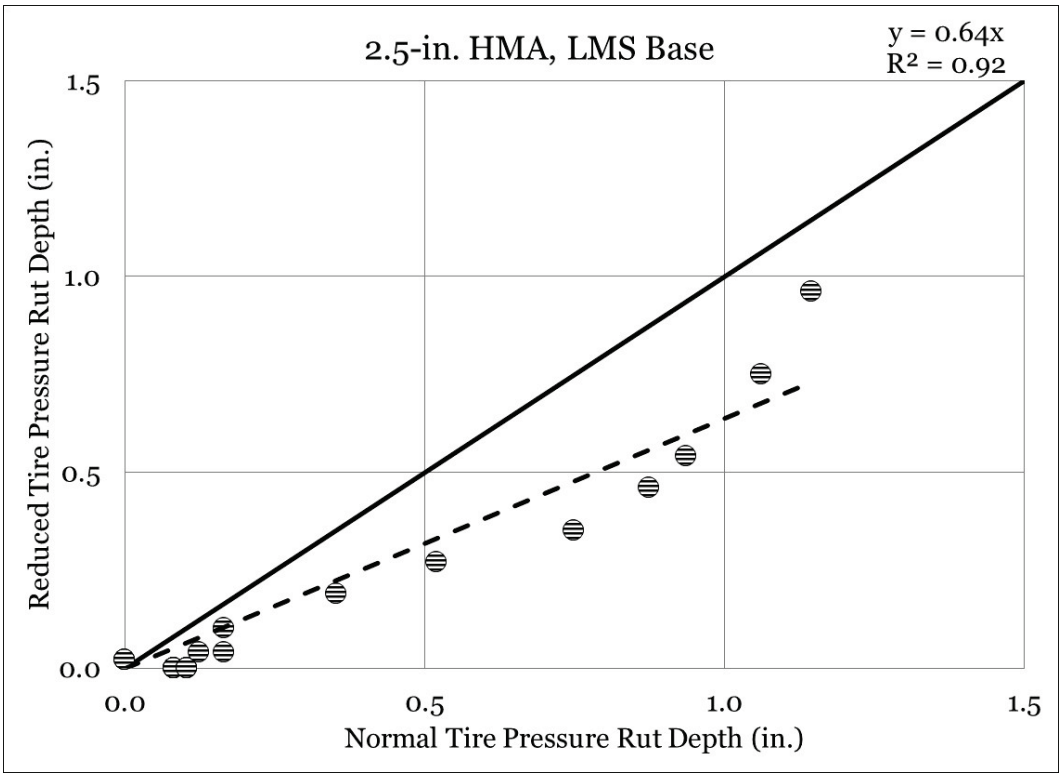

Figure 24. Equality plot – C-130 rut depth (1.5-in. HMA, LMS base).

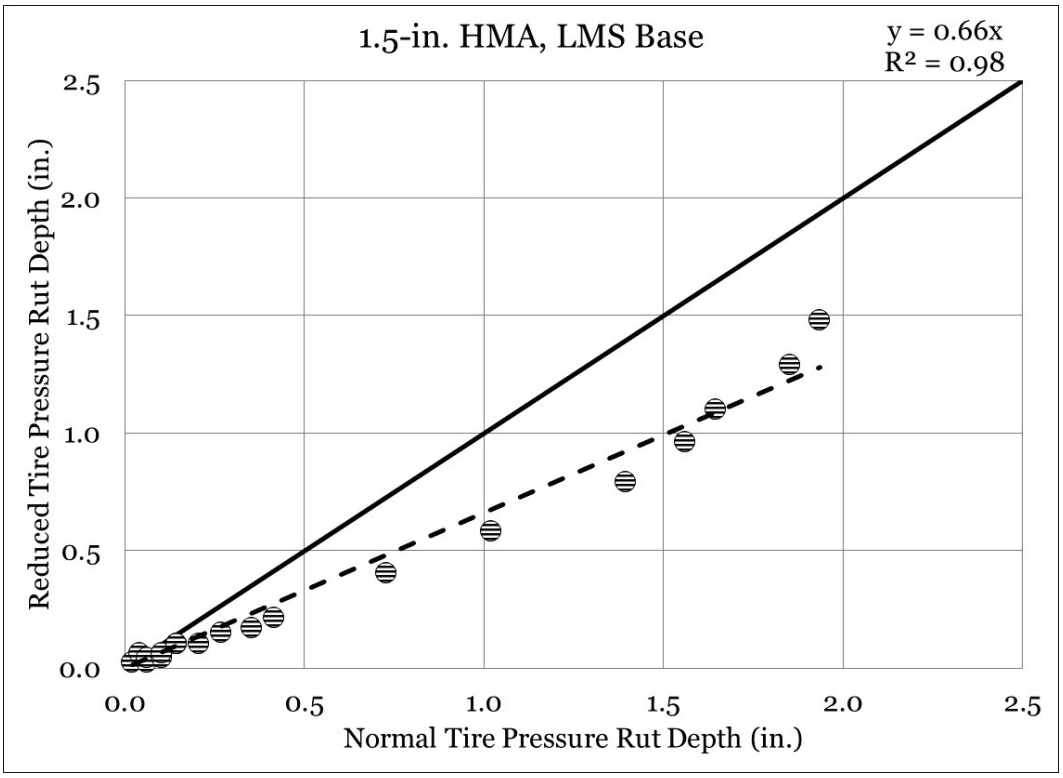

Figure 25. Equality plot – C-130 rut depth (1.0-in. HMA, LMS base).

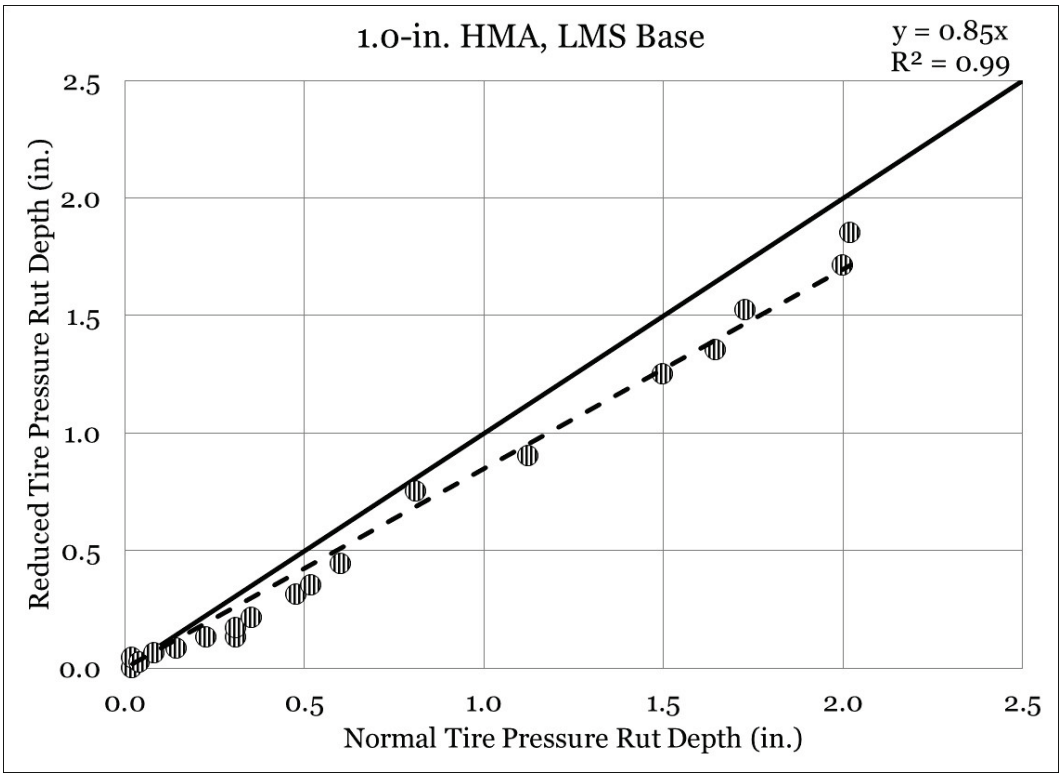

Table 8. Statistical analysis – C-130 rut depth and tire pressure.

Interaction	n	p-value	Significant	Better Performer
C130NTP1 vs. C130RTP1	11	0.064	No	Same
C130NTP2 vs. C130RTP2	20	<0.001	Yes	C130RTP2
C130NTP3 vs. C130RTP3	20	<0.001	Yes	C130RTP3
C130NTP4 vs. C130RTP4	20	<0.001	Yes	C130RTP4

Figure 26. Photographs of rutting in C-130 test items.

(a) C130NTP1 (Pass 1,100)

(b) C130RTP1 (Pass 716)

(c) C130NTP2 (Pass 20,004)

(b) C130RTP2 (Pass 25,008)

(e) C130NTP3 (Pass 20,004)

(b) C130RTP3 (Pass 25,008)

(f) C130NTP4 (Pass 20,004)

(b) C130RTP4 (Pass 25,008)

C-130 Cracking

At each traffic interval, a visual inspection of each test item was performed to inspect for surface cracking. It was hypothesized that the relatively thin asphalt pavement would behave simply as a membrane layer and would be susceptible to surface cracking. Total cracking was measured by using a rolling wheel and recorded in total linear feet. A summary of measured cracking (total length in linear feet) for the normal tire pressure test series is presented in Figure 27. It should be noted that no measurable cracking was detected in C130NTP2 (2.5-in. HMA, LMS base).

Observed cracking followed generally expected trends. The weakest test item (C130NTP1) was the first item to display measurable surface cracking (at 716 passes) that progressed rapidly with increasing traffic. Cracking initiated in C130NTP4 at 908 passes and trended upward thereafter. Foreign object debris (FOD) development was observed at 2,000 passes in C130NTP4. Cracking in C130NTP3 was first observed at 2,000 passes.

Crack development in the reduced tire pressure test series is presented in Figure 28. It was observed that the general increasing trend observed in the reduced tire pressure series was similar to that observed in the normal tire pressure test series. Cracking was observed in C130RTP1 first, followed by C130RTP4 and C130RTP3. It is noted that significant FOD was observed in C130NTP4 at the 6,000-pass inspection.

Equality plots for observed cracking are presented in Figures 29 to 31. It was hypothesized that reducing the tire pressure would reduce surface stresses, resulting in either a reduction or a delay in surface cracking. The 2.5-in. HMA, GR base test items did not follow this expected trend, and it was observed that cracking progressed more rapidly in the reduced tire pressure test item than in the normal tire pressure test item. However, when it is considered that the reduced tire pressure rutting performance was approximately 29% worse (on average) than the normal tire pressure rutting, the increase in surface deformation could justify the increase in cracking.

A review of the 1.0-in. HMA, LMS equality plot (Figure 30) indicated that cracking in these items was generally equivalent, and it was observed that the data plotted slightly above the LOE in some cases and slightly below in other. The linear trend line indicated that cracking in the reduced tire pressure item was 9% greater than that observed in the normal tire pressure item.

The 1.5-in.-HMA, LMS equality plot (Figure 31) revealed a more substantial improvement in cracking performance with a reduction in tire pressure. Cracking in the reduced tire pressure test item was found to be approximately 73% of that observed in the normal tire pressure test item, and it was observed that all data plotted below the LOE, indicating that reduced tire pressure improved cracking performance at all traffic levels.

Note cracking was not observed in C130NTP2 or C130RTP2; thus, no equality plot is presented for these test items. Examples of observed cracking are presented in Figure 32.

Figure 27. Visual cracking progression – C-130 normal tire pressure.

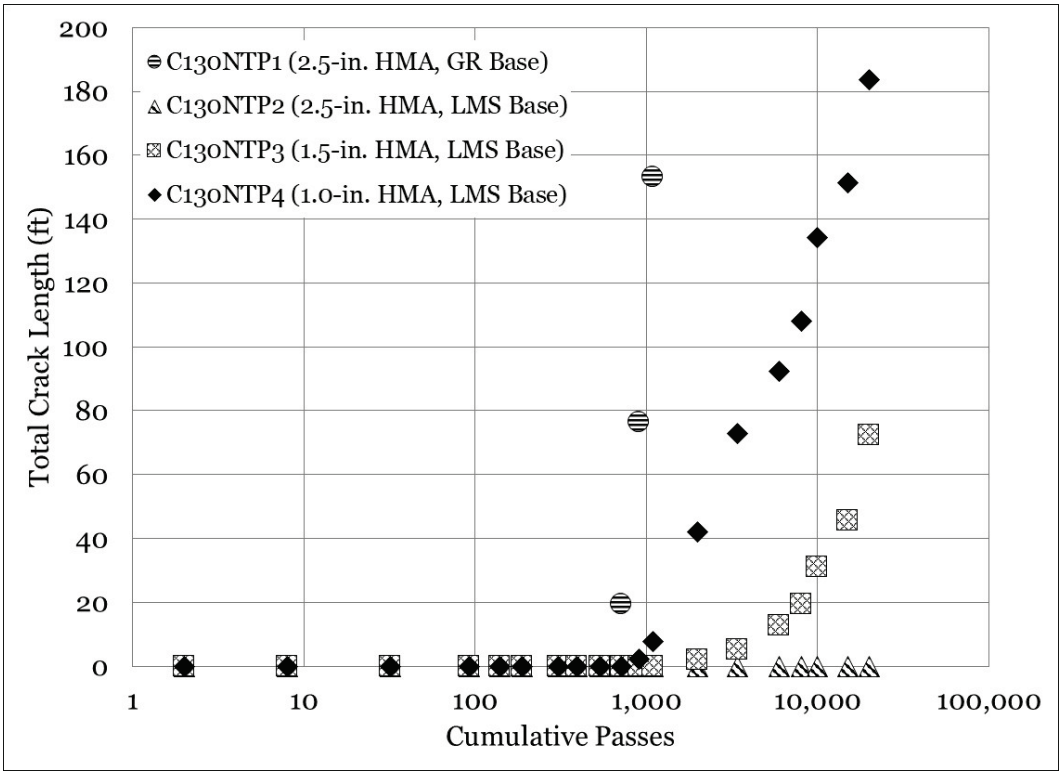

Figure 28. Visual cracking progression – C-130 reduced tire pressure.

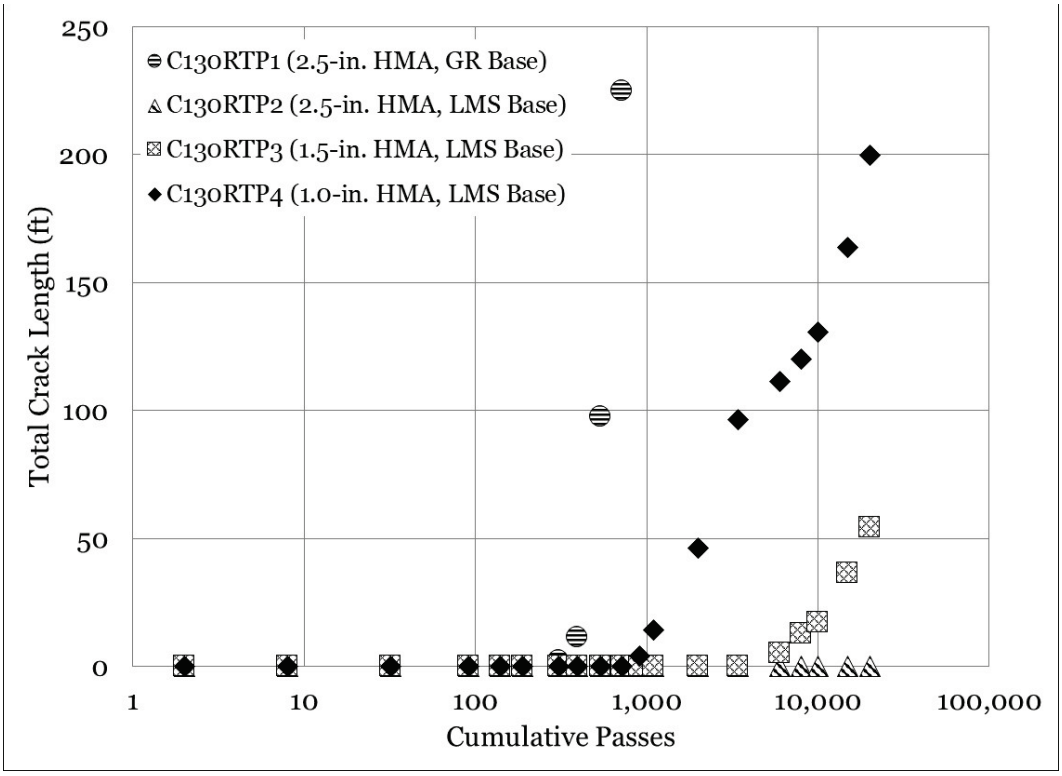

Figure 29. Equality plot - C-130 cracking (2.5-in. HMA, GR base).

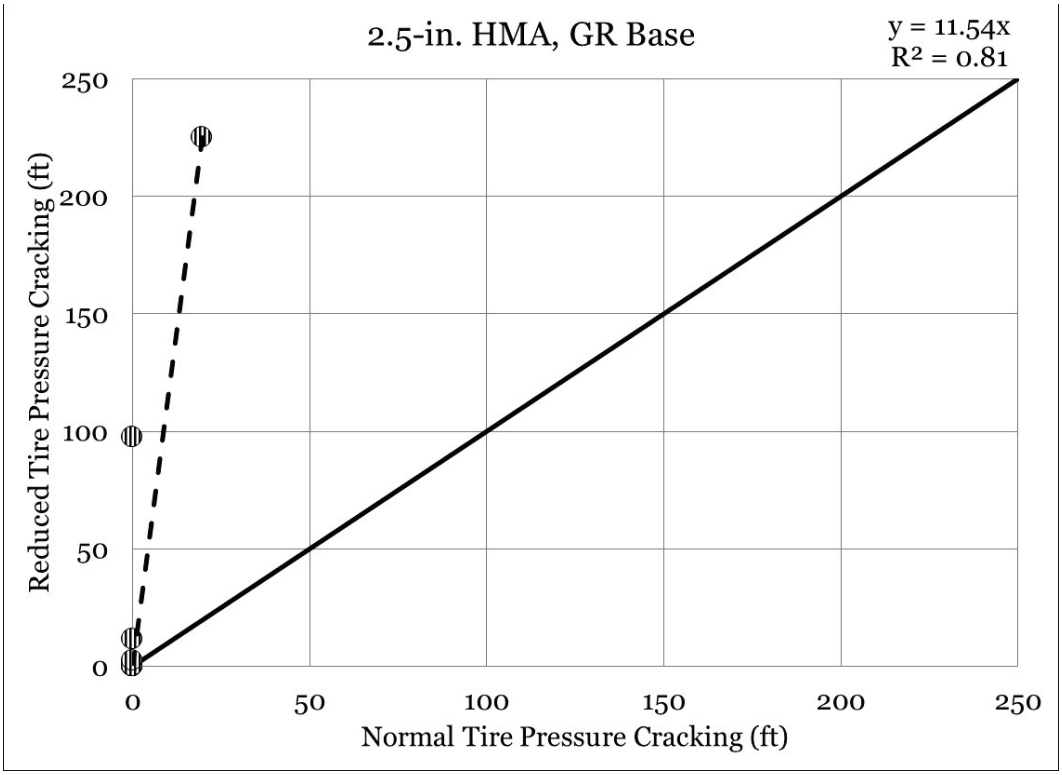

Figure 30. Equality plot - C-130 cracking (1.0-in. HMA, LMS base).

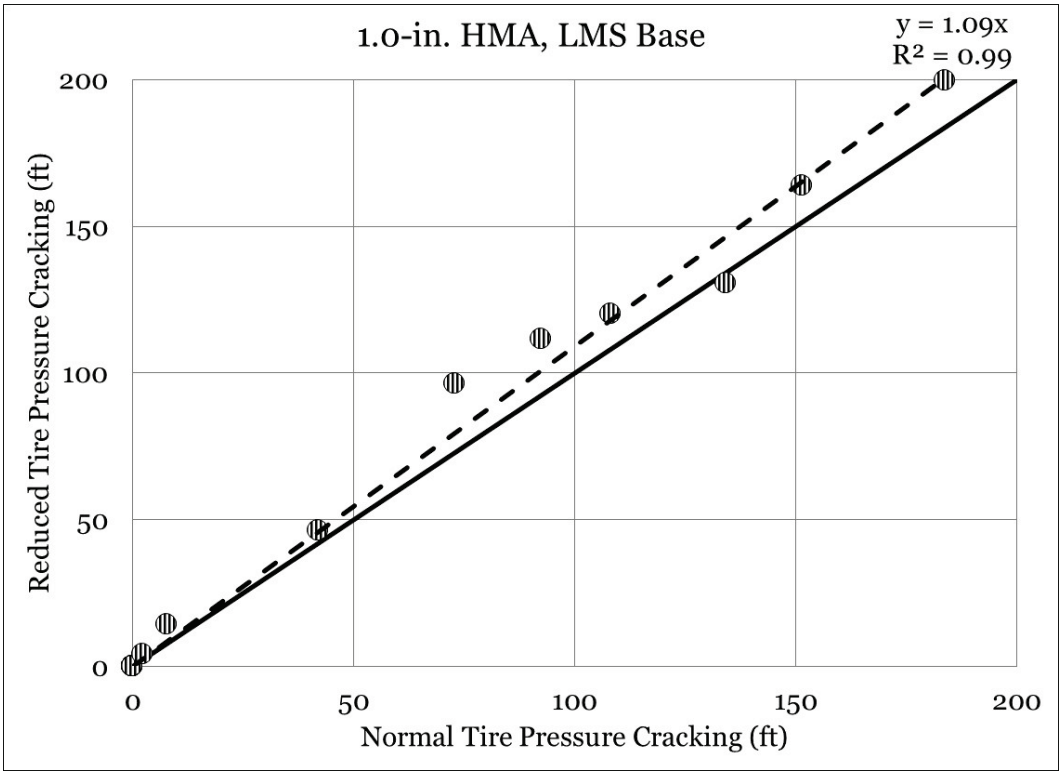

Figure 31. Equality plot - C-130 cracking (1.5-in. HMA, LMS base).

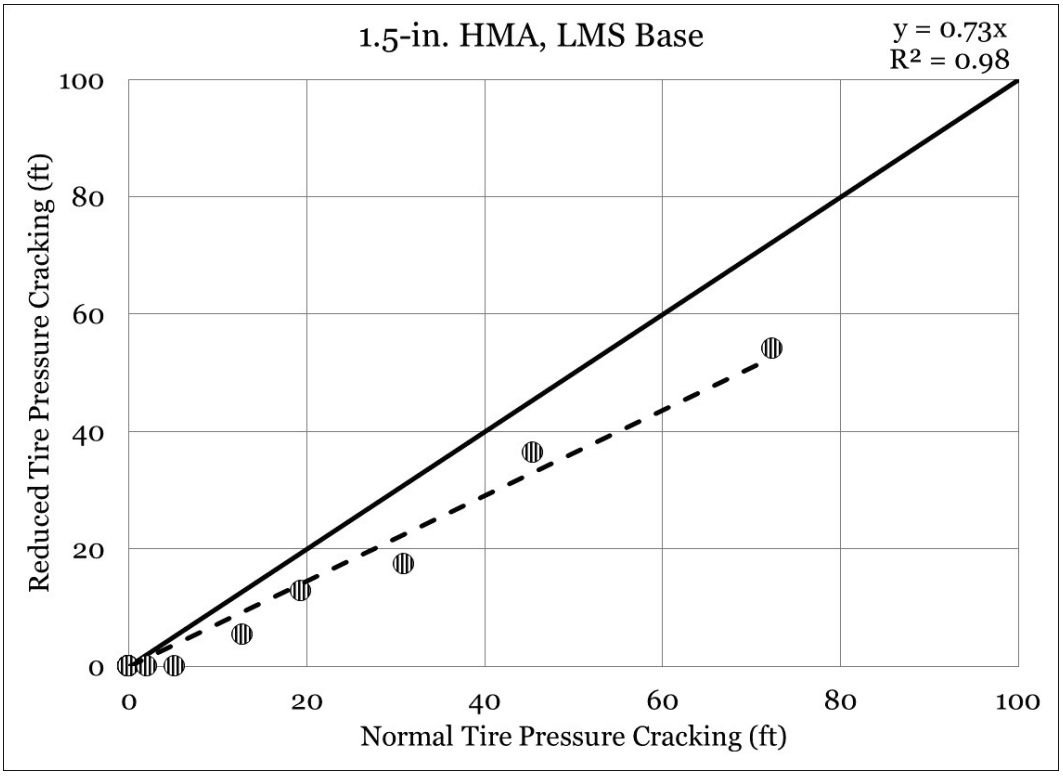

Figure 32. Photographs of cracking in C-130 test items.

(a) C130NTP1 overall cracking

(b) C130NTP1 cracking close-up

(c) C130NTP3 overall cracking

(d) C130NTP3 cracking close-up

(e) C130NTP4 overall cracking

(f) C130NTP4 cracking close-up

C-130 passes to rut depth

Summaries of C-130 passes to various rut depths are presented in Figures 33 through 36. Rut depths were selected to match those currently defined as threshold values for varying levels of pavement condition determination: low (0.25 in. to 0.5), medium (0.5 in. to 1.0 in.), and high (>1.0 in.). After 1.0 in. of rutting, data were selected in 0.5-in. intervals to monitor performance at excessive rutting levels.

A review of passes to specified rut depth for 2.5-in -HMA, GR base (Figure 33) indicated that generally equivalent passes were observed at most levels of rutting. At lower levels of rutting (i.e., 1.0 in. or less), it was observed that passes to failure were practically equivalent with respect to tire pressure. This suggests that total load, rather than tire pressure, was the primary performance driver in weaker base course pavements. As rutting level increased beyond 1.0-in. rutting, more meaningful differences were observed. Differences ranged from approximately 30% at 2.0-in. rutting up to 44% at 3.0-in. rutting (normal tire pressure had higher passes to rut). This could be attributed to the inherent variability in the weak gravel base and variations in shear flow at high levels of deformation.

Passes to specified rut depth for the 2.5-in. HMA, LMS base (Figure 34) displayed a reasonable trend (reduced tire pressure sustained more passes than normal tire pressure). Differences in performance were more prevalent, and it was observed that the differences remained mostly consistent with rut depth development. Improvement attributed to reducing tire pressure was on the order of 50%, and improvement tended to increase with an increase in rut depth. It is noted that 1.5-in. rutting could not be achieved in a reasonable number of traffic applications for these items.

The reduced tire pressure item in the 1.5-in. HMA, LMS base test (Figure 35) performed better than the companion normal tire pressure item at all rutting levels. At low rutting levels (0.25 in.), improvement was approximately 50%, and improvement increased to over 60% at high rutting levels (1.5 in.). It is noted that 2.0-in. rutting could not be achieved in a reasonable number of traffic applications for these items.

Similar observations can be made in the 1.0-in. HMA, LMS base test items (Figure 36). Reducing tire pressure improved passes to specified rutting from 65% at low rutting (0.25 in.) to 30% at high rutting (1.0 in.).

Figure 33. C-130 passes to various rut depths (2.5-in. HMA, GR base).

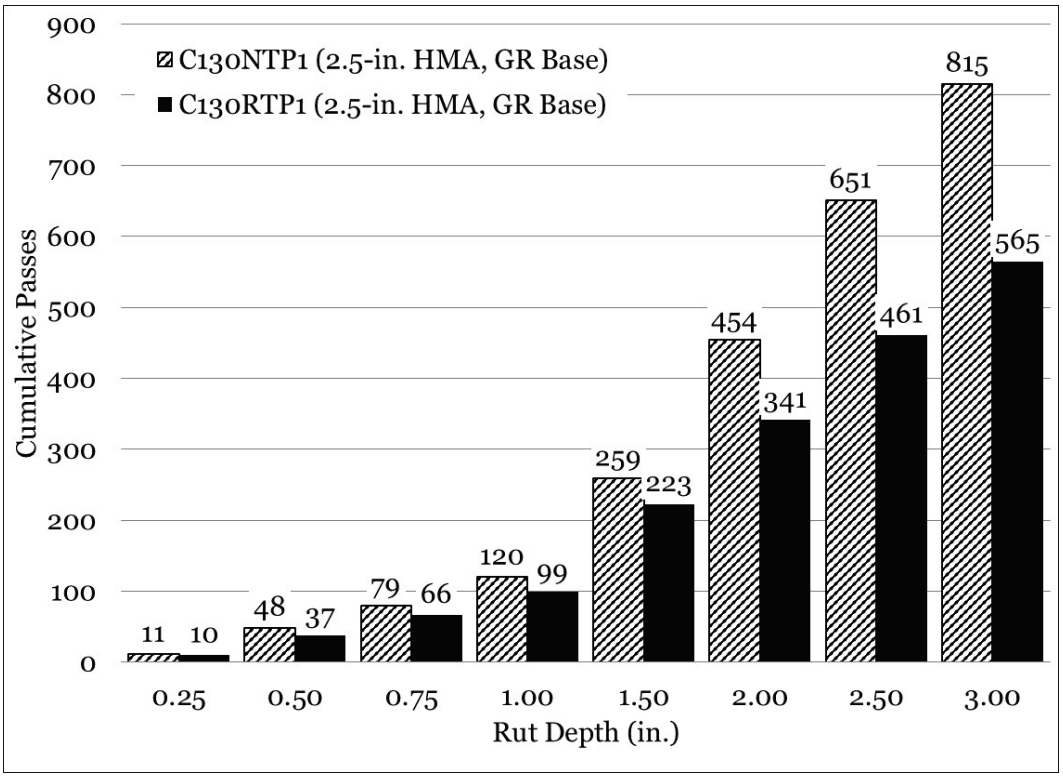

Figure 34. C-130 passes to various rut depths (2.5-in. HMA, LMS base).

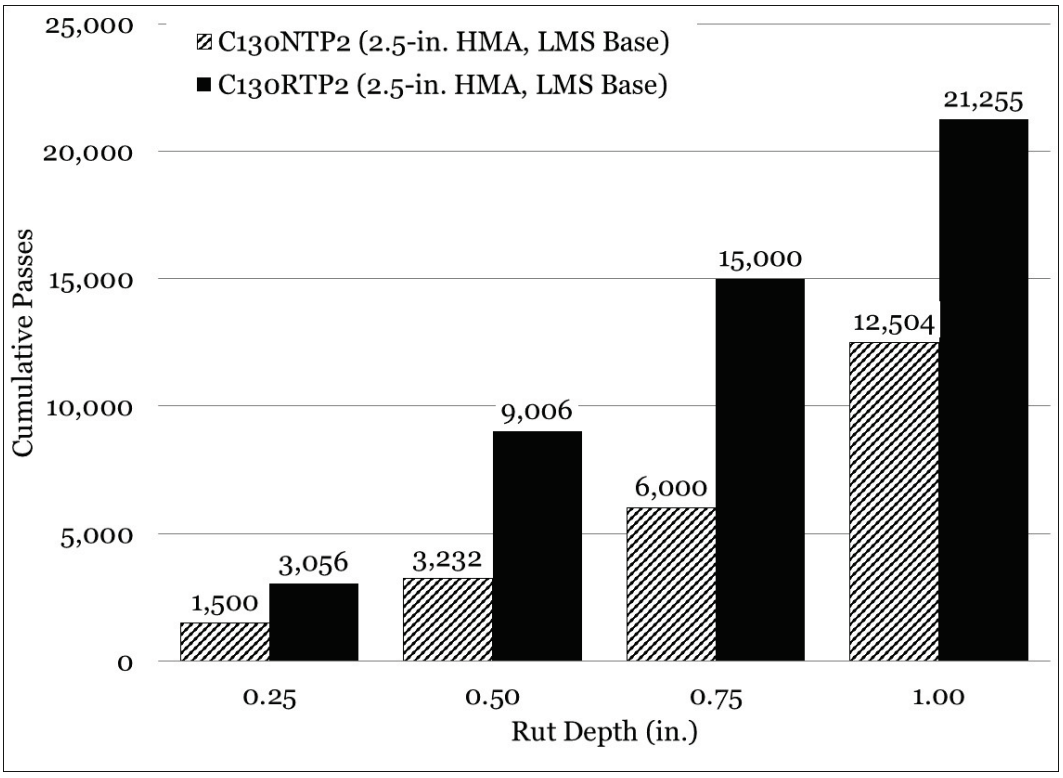

Figure 35. C-130 passes to various rut depths (1.5-in. HMA, LMS base).

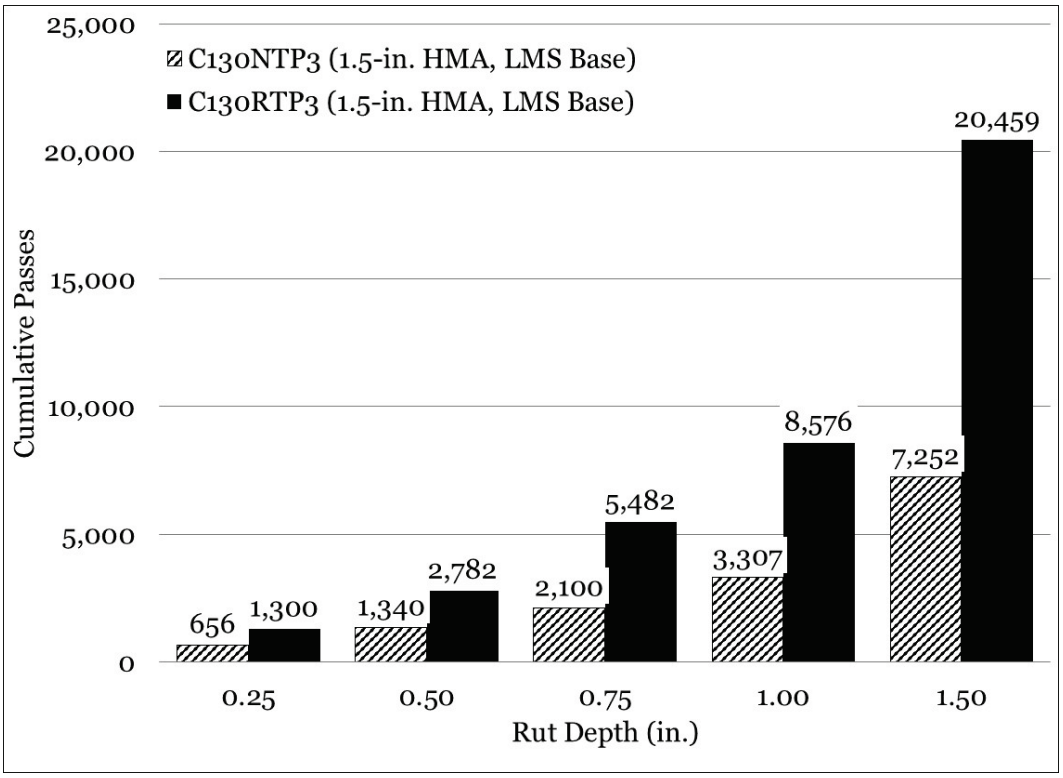

Figure 36. C-130 passes to various rut depths (1.0-in. HMA, LMS base).

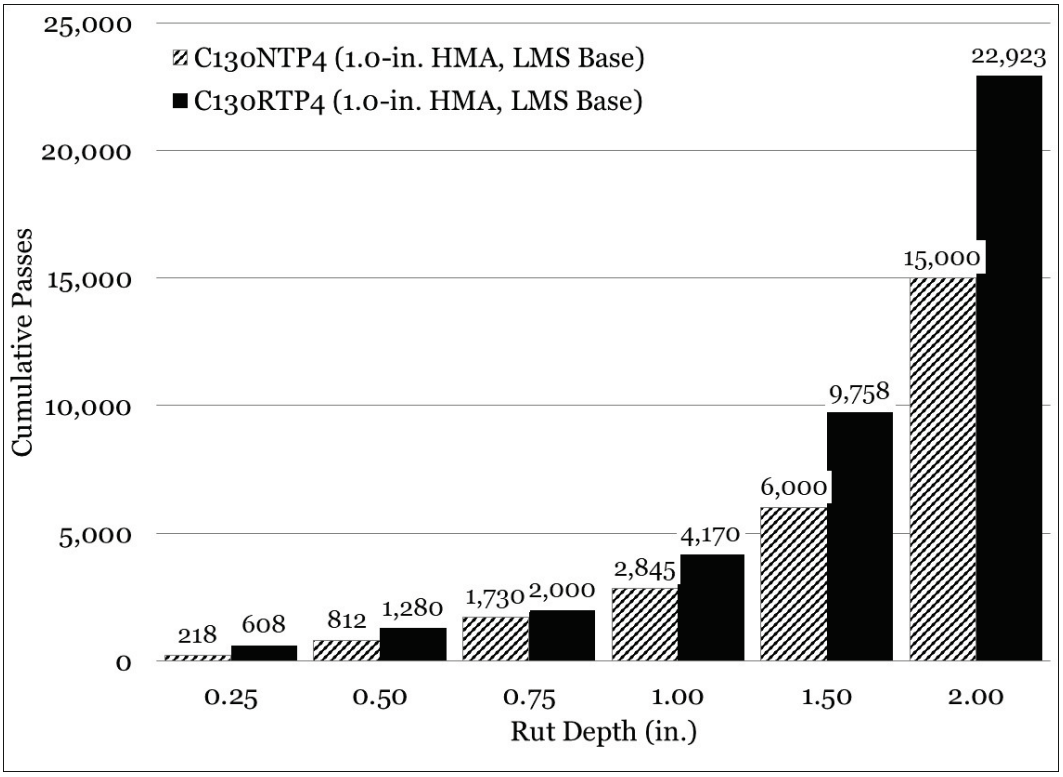

C-130 impulse stiffness

Falling weight deflectometer (FWD) data were collected to monitor overall structural deterioration with increasing traffic levels. The Impulse Stiffness Modulus (ISM), which is the applied load divided by the measured plate deflection, was used as the basis for comparison. In each test item, FWD data were collected at the five locations of installed instrumentation. Thus, pavement stiffness and instrumentation response were collected at each FWD test location. Average ISM values for each test item at each traffic interval were calculated and used for analysis. Average ISM values for the normal tire pressure test series are presented in Figure 37.

Initial ISM values followed a logical progression of increasing asphalt thickness for the limestone base test items: thicker asphalt resulted in higher ISM. It was observed that C130NTP1 had the highest initial ISM value and that a change in base course CBR from 100 (C130NTP1) to 47 (C130NTP4) resulted in an approximate 49% reduction in initial ISM. Differences in C130NTP3 (1.5-in. HMA) and C130NTP3 (1.0-in. HMA) were unremarkable, suggesting that the FWD was not capable of detecting the 0.5-in. asphalt thickness difference. This is in general agreement with rut depth observations.

Average ISM values trended lower with increases in applied traffic and deterioration, which was expected. It was observed that declines in average ISM were generally equivalent for all test items.

A statistical analysis (Table 9) confirmed that average ISM values in C130NTP1 were statistically different from the other test items. C130NTP3 and C130NTP4 were not statistically different from each other (p-value = 0.100).

Figure 37. C-130 normal tire pressure ISM.

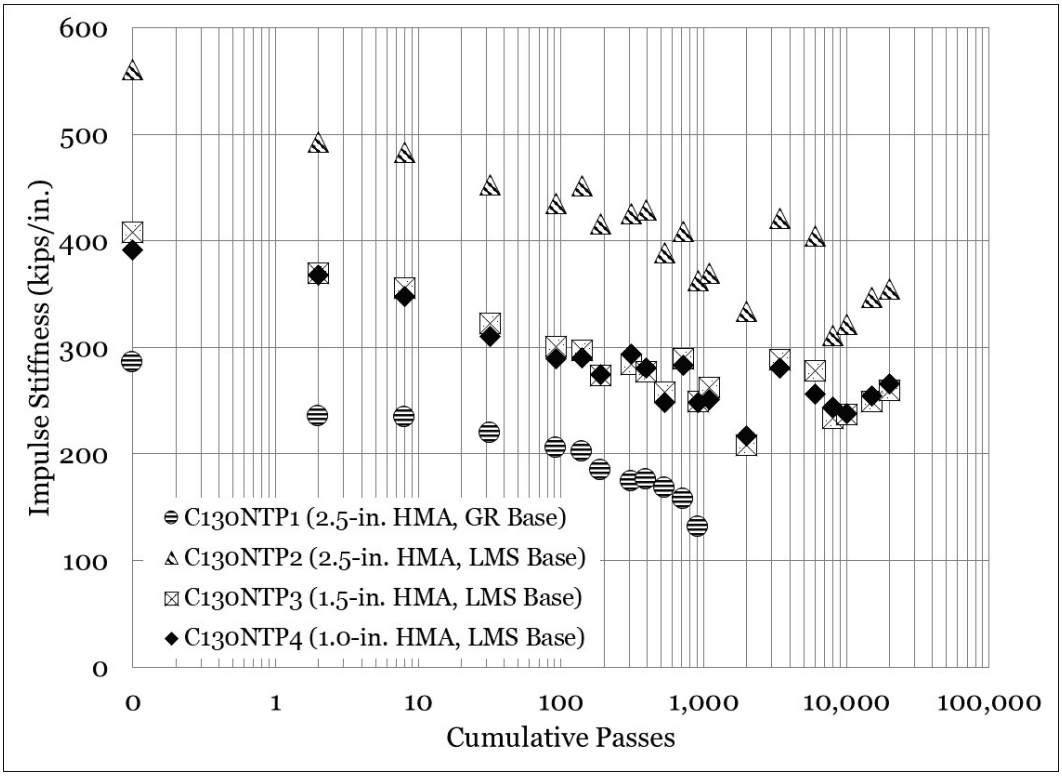

Table 9. Statistical analysis – C-130 normal tire pressure ISM.

Interaction	n	p-value	Significant	Better Performer
C130NTP1 vs. C130NTP2	12	<0.001	Yes	C130NTP2
C130NTP1 vs. C130NTP3	12	<0.001	Yes	C130NTP3
C130NTP1 vs. C130NTP4	12	<0.001	Yes	C130NTP4
C130NTP2 vs. C130NTP3	20	<0.001	Yes	C130NTP2
C130NTP2 vs. C130NTP4	20	<0.001	Yes	C130NTP2
C130NTP3 vs. C130NTP4	20	0.100	No	Same

Average ISM values for the reduced tire pressure test series are presented in Figure 38. Initial ISM values for the reduced tire pressure series were found to follow a logical increase in asphalt thickness. Initial difference in C130RTP3 (1.5-in. HMA) and C130RTP4 (1.0-in. HMA) was approximately 9%; however, the difference was considered small in a practical sense. Changing base course from a 100 CBR (C130RTP2) to a 42 CBR (C130RTP1) resulted in a 61% decrease in initial ISM. Similar to the normal tire pressure series, ISM values trended downward with an increase in traffic level and deterioration. ISM declines were observed to

be equivalent for all test items. A statistical analysis (Table 10) indicated that all test comparisons were statistically significant.

Figure 38. C-130 reduced tire pressure ISM.

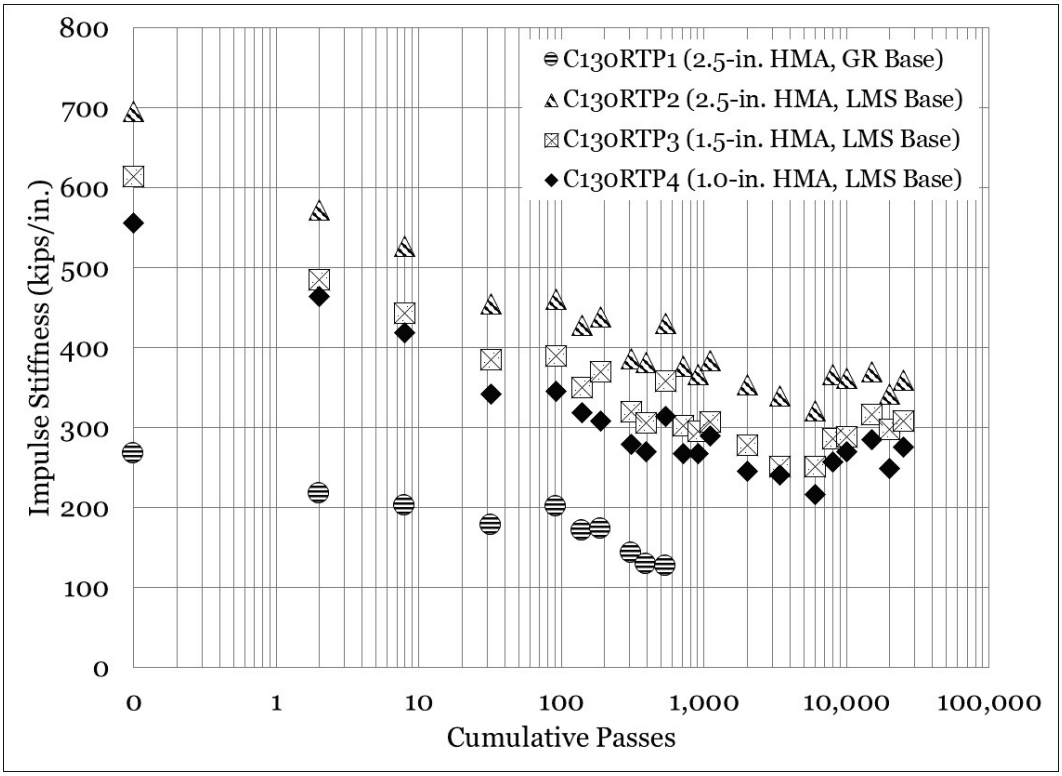

Table 10. Statistical analysis - C-130 reduced tire pressure ISM.

Interaction	n	p-value	Significant	Better Performer
C130RTP1 vs. C130RTP2	10	<0.001	Yes	C130RTP2
C130RTP1 vs. C130RTP3	10	<0.001	Yes	C130RTP3
C130RTP1 vs. C130RTP4	10	<0.001	Yes	C130RTP4
C130RTP2 vs. C130RTP3	21	<0.001	Yes	C130RTP2
C130RTP2 vs. C130RTP4	21	<0.001	Yes	C130RTP2
C130RTP3 vs. C130RTP4	21	<0.001	Yes	C130RTP3

Equality plots for ISM are presented in Figures 39 through 42. It was anticipated that ISM for the reduced tire pressure series would be greater than that for the normal tire pressure series, assuming the rate of structural deterioration would be reduced with a reduction in tire pressure. In that case, it would be expected that the data would plot above the LOE. In the case of 2.5-in. HMA with gravel base (Figure 39), it was observed that the trend was below the LOE, indicating that C130NTP1

deteriorated more slowly (approximately 13%) than C130RTP1. This observation, although not expected, further suggests that total load rather than tire pressure is driving performance in weaker base courses.

The 2.5-in. HMA, LMS base items (Figure 40) were found to have about equivalent ISM performance, and C130RTP2 was found to have approximately 3% better performance than C130NTP2.

Larger differences were observed in the 1.5-in. HMA (Figure 41) and 1.0-in. HMA (Figure 42) test items. The reduced tire pressure item having 1.5-in. HMA was found to possess 22% better ISM performance than the companion normal tire pressure test item, and the 1.0-in. HMA was found to have 11% better performance.

A paired t-test (Table 11) indicated that average ISM in the 2.5-in. HMA, LMS base test items was not statistically different (p-value = 0.454). Statistically significant differences were observed in all other test items. In the 2.5-in. HMA, GR base test items, the normal tire pressure item had a higher average ISM than the reduced tire pressure item. The 1.5-in. HMA and 1.0-in. HMA (both over LMS base) items had higher average ISM in the reduced tire pressure series.

Figure 39. Equality plot – C-130 ISM (2.5-in. HMA, GR base).

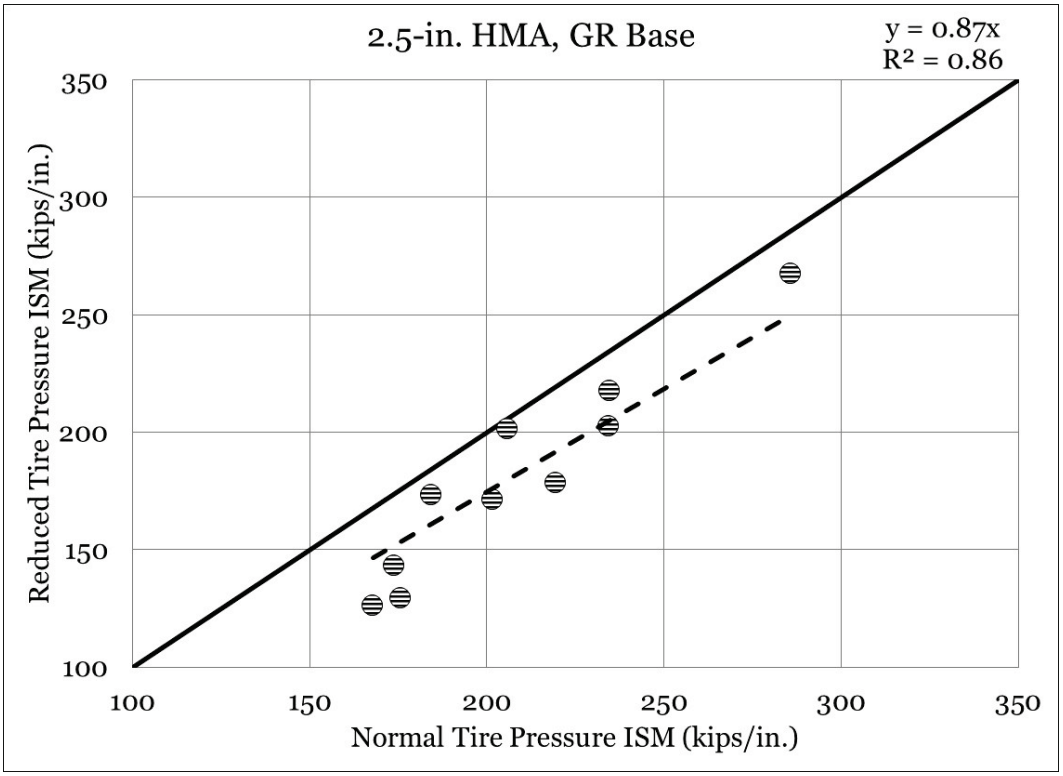

Figure 40. Equality plot – C-130 ISM (2.5-in. HMA, LMS base).

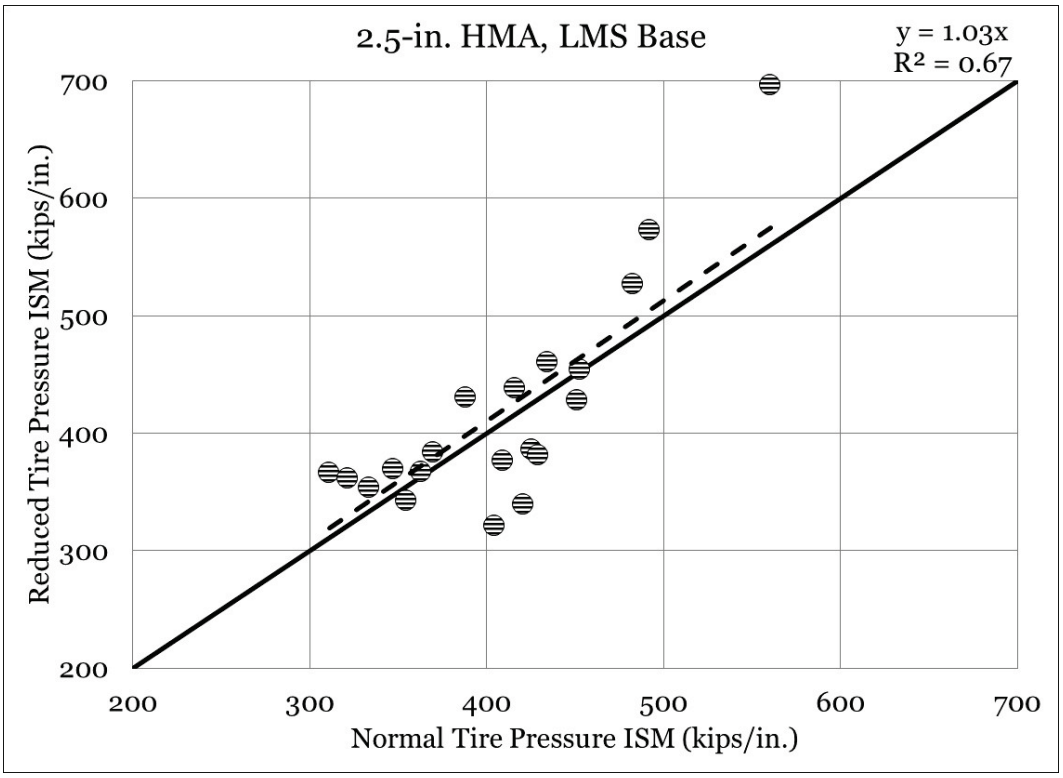

Figure 41. Equality plot – C-130 ISM (1.5-in. HMA, LMS base).

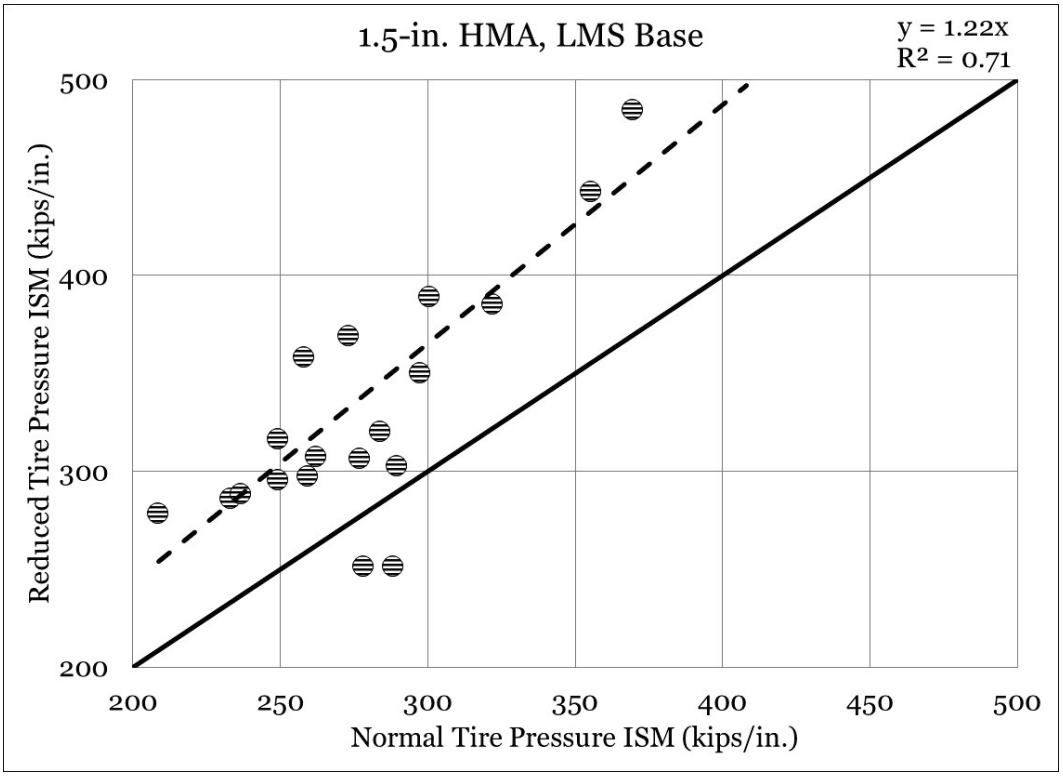

Figure 42. Equality plot – C-130 ISM (1.0-in. HMA, LMS base).

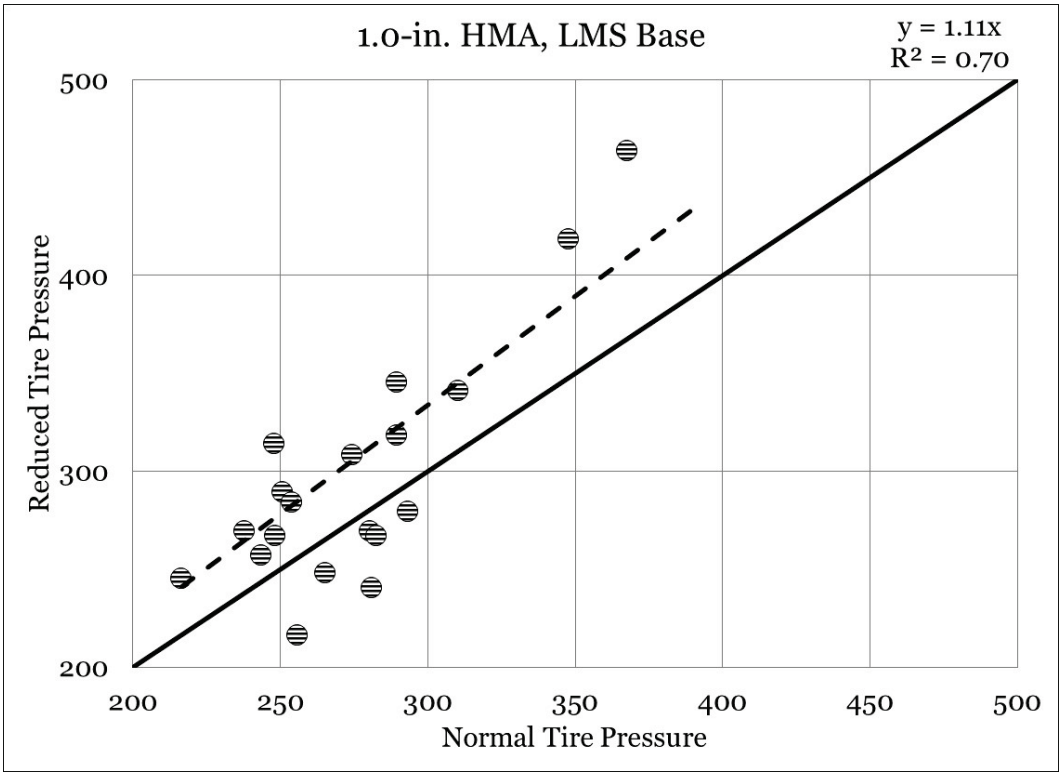

Table 11. Statistical analysis – C-130 ISM and tire pressure.

Interaction	n	p-value	Significant	Better Performer
C130NTP1 vs. C130RTP1	10	<0.001	Yes	C130NTP1
C130NTP2 vs. C130RTP2	20	0.454	No	Same
C130NTP3 vs. C130RTP3	20	<0.001	Yes	C130RTP3
C130NTP4 vs. C130RTP4	20	0.017	Yes	C130RTP4

C-130 subgrade pressure response

Subgrade vertical pressure response data for the normal tire pressure test series are presented in Figure 43. Subgrade vertical pressures were found to increase with increasing traffic, and subgrade vertical pressure was found to be consistently higher in C130NTP1 (2.5-in. HMA, GR base), which was anticipated due to the weaker base aggregate. Further, it was observed that a rather steep increase in subgrade vertical pressure occurred near the end of traffic in C130NTP1, while the LMS base test items appeared to have generally level pressures at higher traffic levels. This suggests that at high levels of rutting, substantial shear flow occurred in the gravel base layer. Initial subgrade vertical pressure was lowest in C130NTP4 (1.0-in. HMA, LMS base), and initial pressures were approximately equivalent in C130NTP2 and C130NTP3. This was not expected, as C130NTP4 had the thinnest cross section; however, a review of the data indicated that, after approximately 200 passes, the subgrade vertical pressures transitioned to a logical order: thinner sections have higher subgrade pressure. These initial differences in the LMS base test items could be attributed to aggregate shakedown or initial densification of the LMS layer.

A summary of a statistical analysis for subgrade vertical pressure is presented in Table 12. C130NTP1 (2.5-in. HMA, GR base) was found to be statistically different from the other test items, and it was observed that C130NTP1 had higher average subgrade pressure than all other test items. C130NTP2 (2.5-in. HMA, LMS base) was found to be statistically different from C130NTP3 (p-value < 0.001) and C130NTP4 (p-value = 0.022), and C130NTP2 was found to have lower average subgrade pressure than these test items. Average subgrade pressure responses in C130NTP3 and C130NTP4 were not found to be statistically different (p-value = 0.177), suggesting that the addition of 0.5-in. HMA was not effective in significantly reducing subgrade pressure.

Figure 43. C-130 normal tire pressure subgrade pressure response.

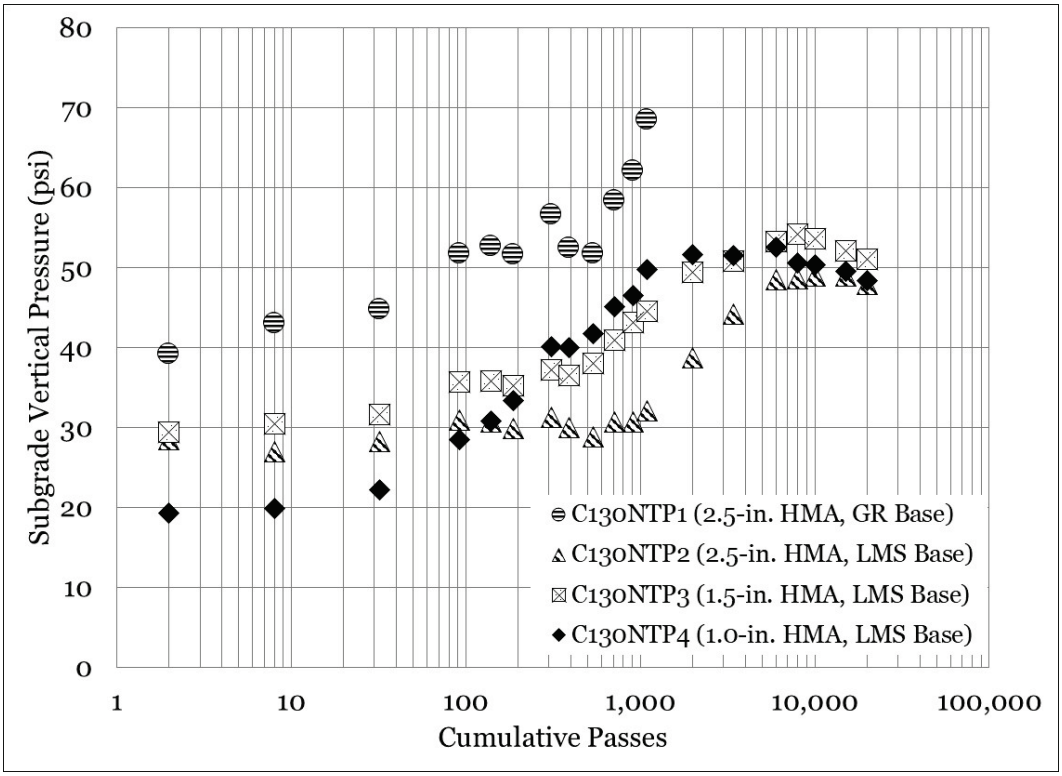

Table 12. Statistical analysis – C-130 normal tire pressure subgrade pressure.

Interaction	n	p-value	Significant	Better Performer
C130NTP1 vs. C130NTP2	12	<0.001	Yes	C130NTP2
C130NTP1 vs. C130NTP3	12	<0.001	Yes	C130NTP3
C130NTP1 vs. C130NTP4	12	<0.001	Yes	C130NTP4
C130NTP2 vs. C130NTP3	19	<0.001	Yes	C130NTP2
C130NTP2 vs. C130NTP4	19	0.022	Yes	C130NTP2
C130NTP3 vs. C130NTP4	19	0.177	No	Same

Subgrade pressure response for the reduced tire test series is shown in Figure 44. Similar to the normal tire pressure test series, the highest subgrade pressures were observed in C130RTP1 (2.5-in. HMA, GR base) for the duration of traffic application. Initial subgrade pressures were generally equivalent in the LMS base test items; and after approximately 100 passes, differences in subgrade pressure became evident, with C130RTP4 (1.0-in. HMA) having higher pressures than the other LMS test items. Comparable to the normal tire pressure test, the GR base test item displayed a steep increase in subgrade pressure

late in traffic, indicating that a reduction in tire pressure garners little change in the observed failure mechanism.

Results of a statistical analysis for subgrade vertical pressure in the reduced tire pressure test series are presented in Table 13. Comparisons between C130RTP1 (2.5-in. HMA, GR base) and the LMS base test items were found to be statistically significant, and C130RTP1 was observed to have higher average subgrade pressures than all other test items. C130RTP2 (2.5-in. HMA, LMS base) was statistically different from the other LMS test items and had lower average subgrade pressure, which was expected due to the additional asphalt layer thickness. Comparison of C130RTP3 and C130RTP4 was not found to be statistically significant, indicating that, at reduced tire pressures, an additional 0.5-in. HMA did not improve average subgrade pressure. Recall, a similar observation was made in the normal tire pressure test series.

Figure 44. C-130 reduced tire pressure subgrade pressure response.

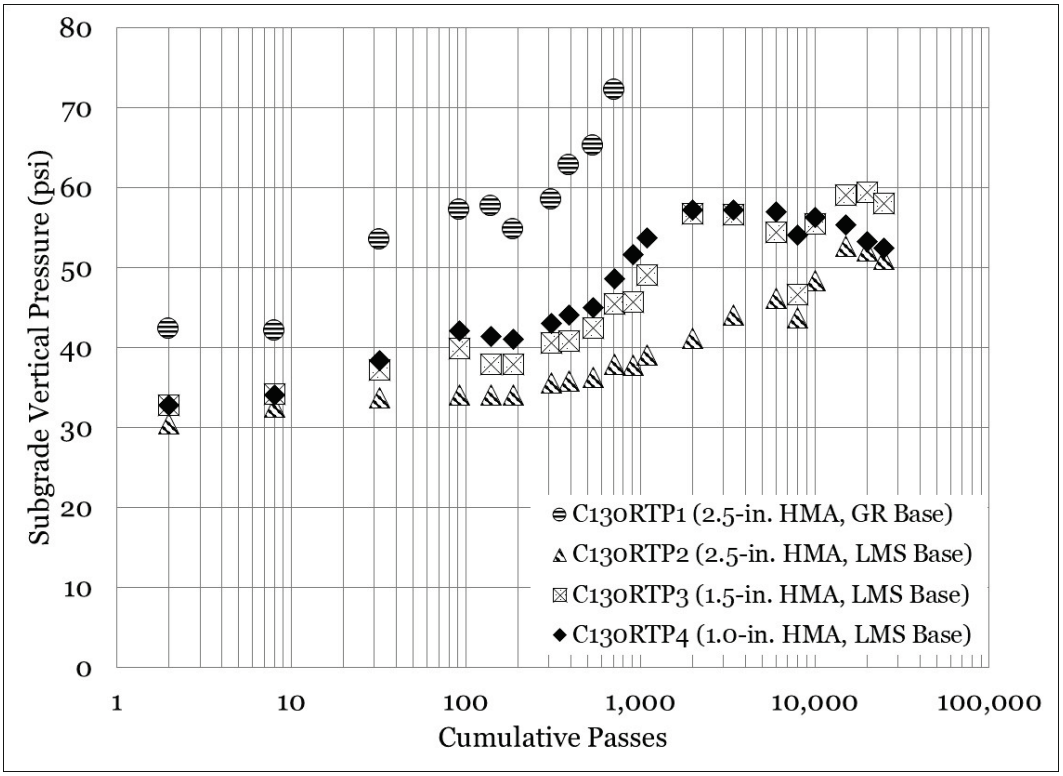

Table 13. Statistical analysis – C-130 reduced tire pressure subgrade pressure.

Interaction	n	p-value	Significant	Better Performer
C130RTP1 vs. C130RTP2	10	<0.001	Yes	C130RTP2
C130RTP1 vs. C130RTP3	10	<0.001	Yes	C130RTP3
C130RTP1 vs. C130RTP4	10	<0.001	Yes	C130RTP4
C130RTP2 vs. C130RTP3	20	<0.001	Yes	C130RTP2
C130RTP2 vs. C130RTP4	20	<0.001	Yes	C130RTP2
C130RTP3 vs. C130RTP4	20	0.083	No	Same

Equality plots for normal and reduced tire pressure subgrade pressure response are presented in Figures 45 through 48. Subgrade pressure response for the reduced tire pressure test was plotted on the y-axis, and subgrade pressure response for the normal tire pressure was plotted on the x-axis. The LOE is represented by a solid line, and a best-fit linear trend (with y-intercept = 0) is represented by a dashed line. Data plotted below the LOE indicates better performance (i.e., comparatively lower subgrade pressures).

A review of the 2.5-in. HMA, GR base plot (Figure 45) showed a majority of the data plotted above the LOE, indicating that subgrade pressures were consistently higher in the reduced tire pressure test item. The fitted trend line suggested that subgrade pressures in the reduced tire pressure item were generally 13% higher than the normal tire pressure test item, indicating that a reduction in tire pressure was not successful in reducing vertical pressure at the subgrade.

In the 2.5-in. HMA, LMS base plot (Figure 46), it was observed that most of the data plotted above the LOE, and that some data plotted below the LOE at higher pressure levels. The fitted trend line suggested subgrade pressure in the reduced tire pressure test item was approximately 8% higher than that of the normal tire pressure test series.

Similar observations were made in the 1.5-in. HMA, LMS plot (Figure 47), in which reduced tire pressure subgrade pressure was approximately 8% higher than that of the normal tire pressure test series. Almost all data plotted above the LOE, and a relatively good trend line fit was noted ($R^2 = 0.84$).

A review of the 1.0-in. HMA, LMS plot (Figure 48) revealed the linear trend line was a relatively poor fit to the data ($R^2 = 0.47$). It is noted that

all the data plotted above the LOE and that the reduced tire pressure subgrade pressure was approximately 14% higher than the normal tire pressure subgrade pressure.

A statistical comparison of subgrade pressure response with changes in tire pressure is summarized in Table 14. It was observed that all comparisons were found to be statistically significant. The results of the statistical analysis indicated that average subgrade pressure was lower in the normal tire pressure test series than in the reduced tire pressure test series.

Figure 45. Equality plot – C-130 subgrade pressure response (2.5-in. HMA, GR base).

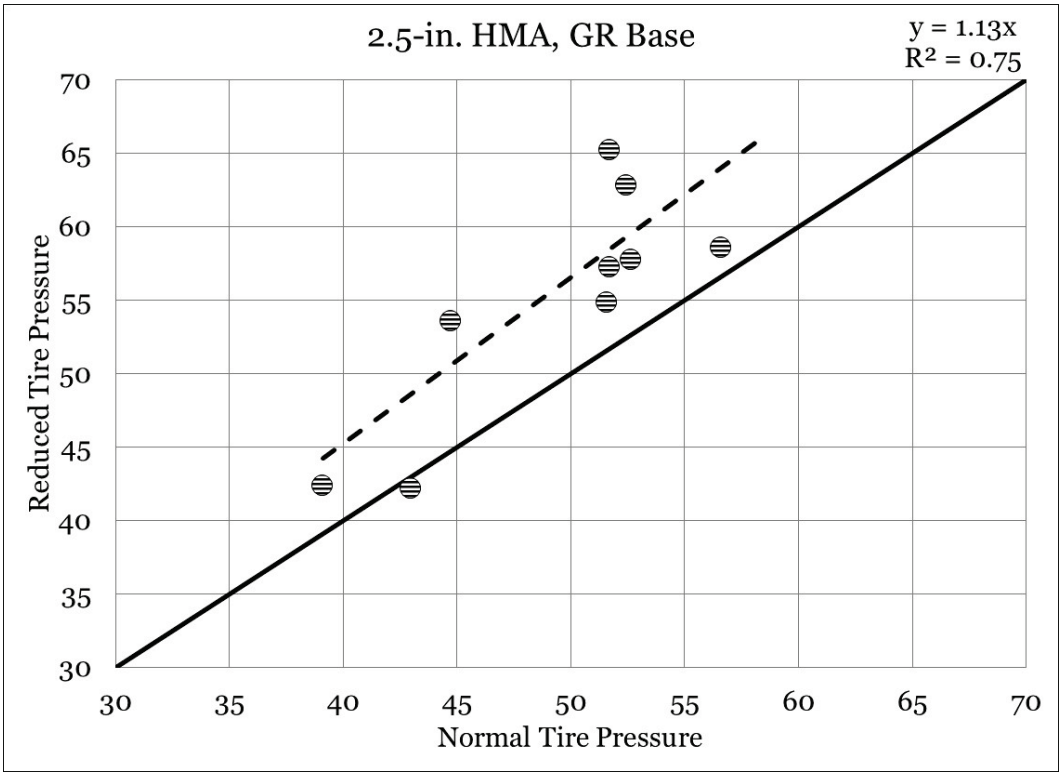

Figure 46. Equality plot – C-130 subgrade pressure response (2.5-in. HMA, LMS base).

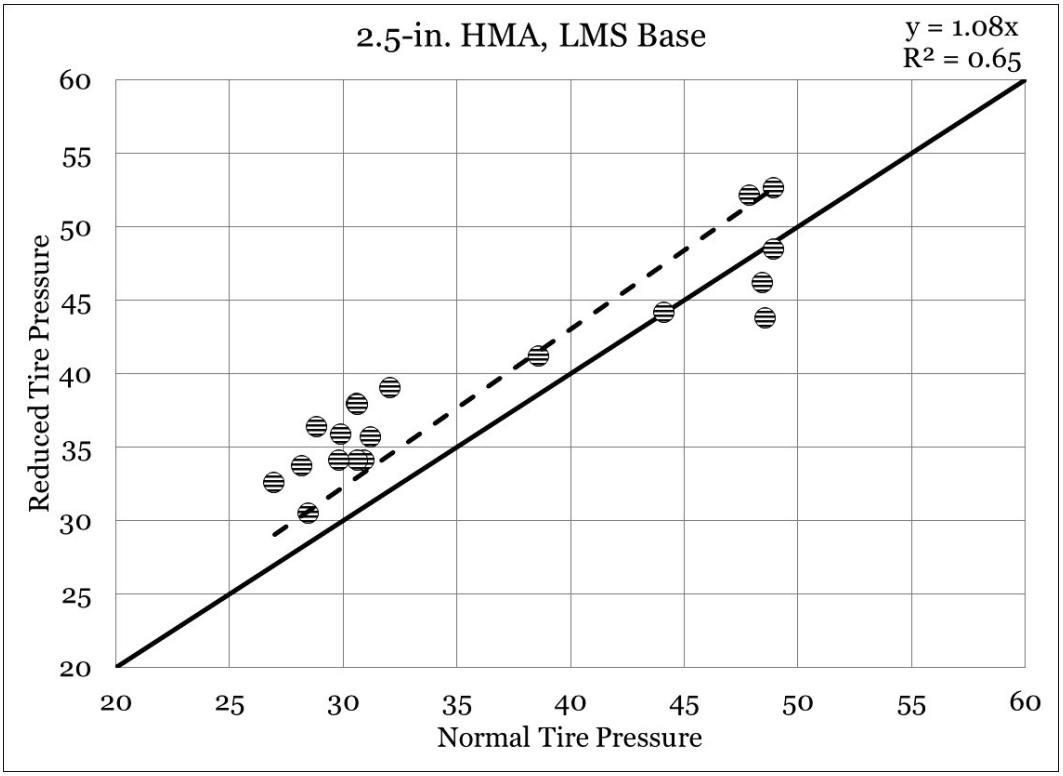

Figure 47. Equality plot – C-130 subgrade pressure response (1.5-in. HMA, LMS base).

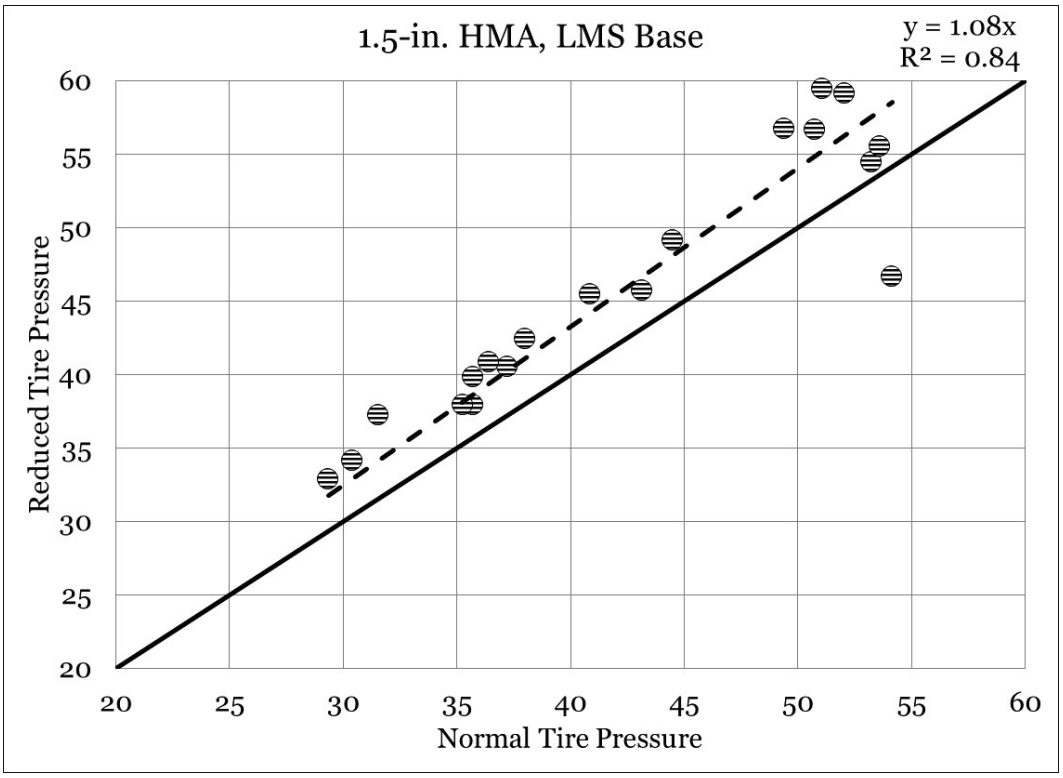

Figure 48. Equality plot – C-130 subgrade pressure response (1.0-in. HMA, LMS base).

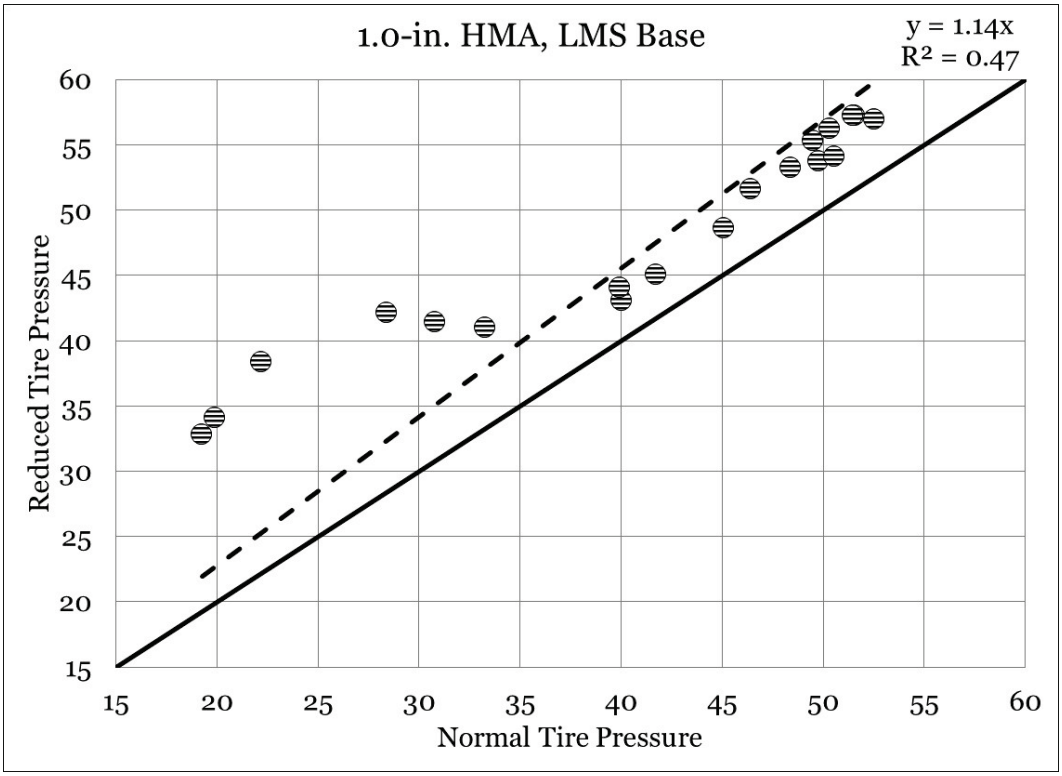

Table 14. Statistical analysis – C-130 subgrade pressure and tire pressure.

Interaction	n	p-value	Significant	Better Performer
C130NTP1 vs. C130RTP1	10	0.003	Yes	C130NTP1
C130NTP2 vs. C130RTP2	19	<0.001	Yes	C130NTP2
C130NTP3 vs. C130RTP3	19	<0.001	Yes	C130NTP3
C130NTP4 vs. C130RTP4	19	<0.001	Yes	C130NTP4

C-130 base pressure response

Base pressure response for the normal tire pressure test series is presented in Figure 49. The lowest initial base pressure was observed in C130NTP2, which was expected; however, the next lowest initial pressure was observed in C130NTP1, which does not agree with observations from the subgrade pressure response. However, this could suggest that the weak base was not effective in supporting the applied load and that more of the load was directly transferred to the subgrade. Around 100 passes, it was observed that base pressure appeared to transition to a more logical order; however, the differences observed were relatively small, and confident trends were difficult to detect.

A summary of a statistical analysis for base vertical pressure is displayed in Table 15. C130NTP1 (2.5-in. HMA, GR base) was found to be statistically different from the other test items except C130NTP3 (p-value = 0.648). C130NTP2 was found to be statistically different from the other test items and was found to be the better performer (lower pressure) in all cases. Notably, C130NTP1 had a statistically significant lower base pressure than C130NTP4, suggesting that an additional 1.5 in. of asphalt was capable of overcoming the reduced CBR of the gravel base layer. It should be noted, however, that the interaction was mildly significant (p-value = 0.038).

Figure 49. C-130 normal tire pressure base pressure response.

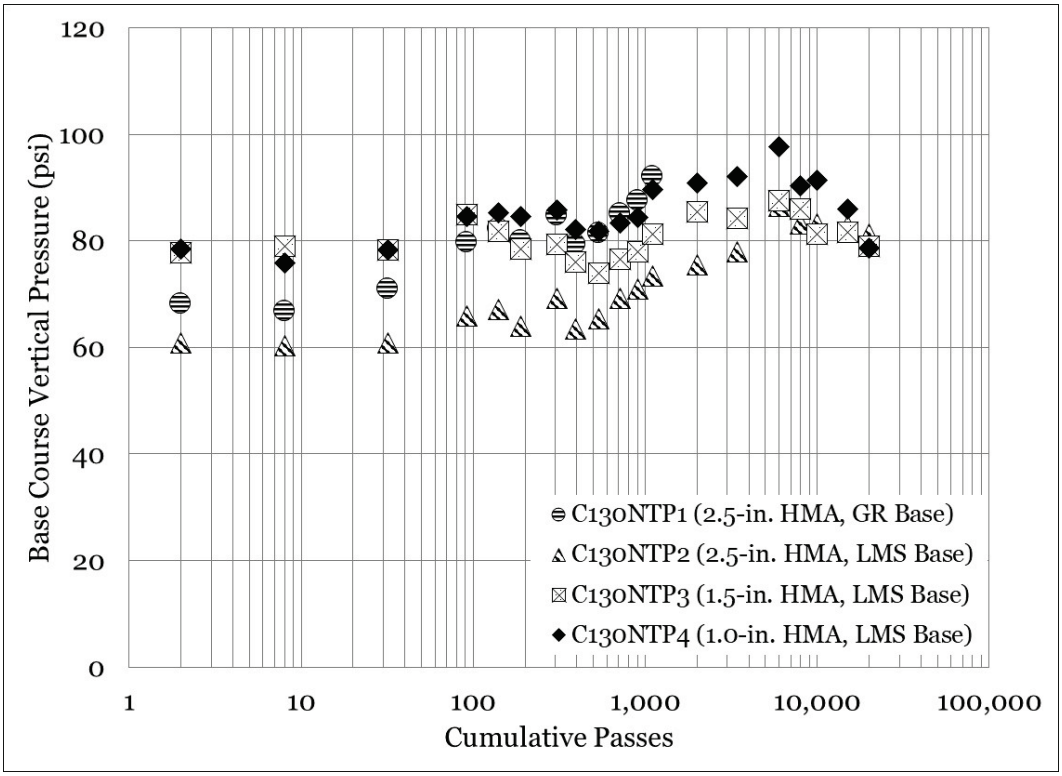

Table 15. Statistical analysis – C-130 normal tire pressure base pressure.

Interaction	n	p-value	Significant	Better Performer
C130NTP1 vs. C130NTP2	12	<0.001	Yes	C130NTP2
C130NTP1 vs. C130NTP3	12	0.648	No	Same
C130NTP1 vs. C130NTP4	12	0.038	Yes	C130NTP1
C130NTP2 vs. C130NTP3	19	<0.001	Yes	C130NTP2
C130NTP2 vs. C130NTP4	19	<0.001	Yes	C130NTP2
C130NTP3 vs. C130NTP4	19	<0.001	Yes	C130NTP3

Base pressure response for the reduced tire pressure test series is shown in Figure 50. C130RTP2 had the lowest base pressure over the duration of trafficking; and, similar to the normal tire pressure test series, definite trends in the pressure data were difficult to perceive. C130RTP4 (1.0-in. HMA, LMS Base) generally had the highest base pressure, although later in traffic, C130RTP1 transitioned to having a higher base pressure, comparatively.

Figure 50. C-130 reduced tire pressure base pressure response.

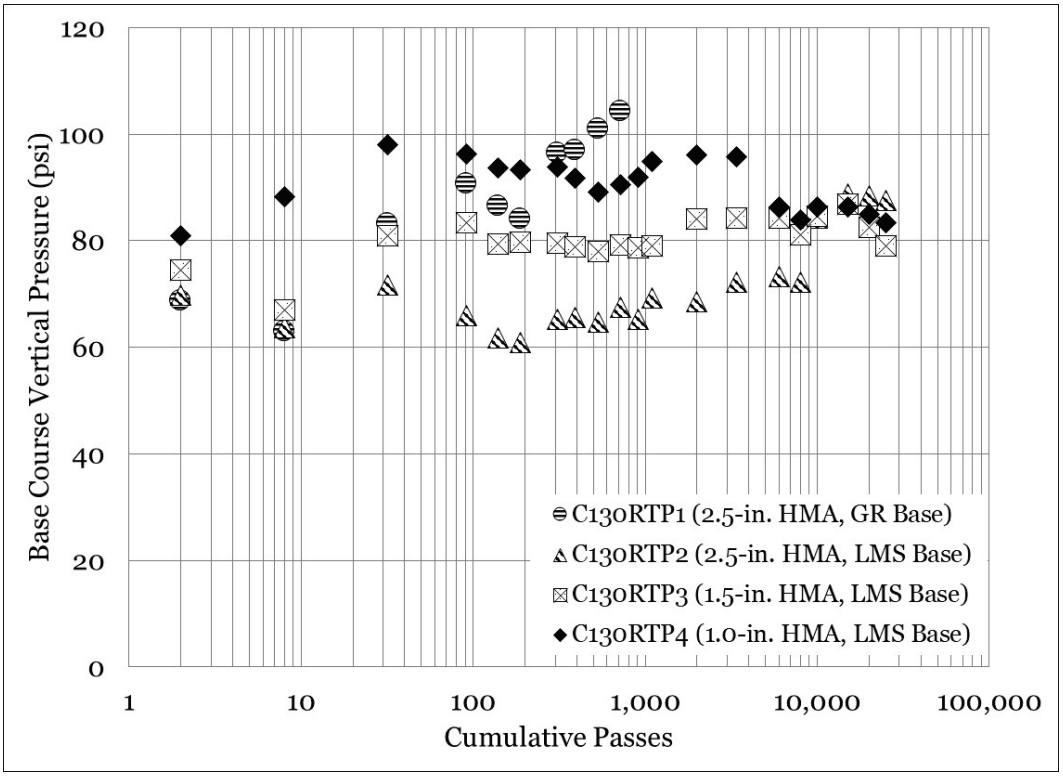

A statistical analysis (Table 16) indicated that C130RTP1 and C130RTP4 were not statistically different (p-value = 0.324), suggesting that an additional 1.5 in. of asphalt was structurally equivalent to the higher CBR base. All other comparisons were found to be statistically significant, and it was observed that the determined better performers were logical.

Table 16. Statistical analysis – C-130 reduced tire pressure base pressure.

Interaction	n	p-value	Significant	Better Performer
C130RTP1 vs. C130RTP2	10	0.001	Yes	C130RTP2
C130RTP1 vs. C130RTP3	10	0.022	Yes	C130RTP3
C130RTP1 vs. C130RTP4	10	0.324	No	Same
C130RTP2 vs. C130RTP3	20	<0.001	Yes	C130RTP2
C130RTP2 vs. C130RTP4	20	<0.001	Yes	C130RTP2
C130RTP3 vs. C130RTP4	20	<0.001	Yes	C130RTP3

Equality plots for normal and reduced tire pressure base pressure are shown in Figures 51 through 54. Base pressure response for the reduced tire pressure test item was plotted on the y-axis, and base pressure response for the normal tire pressure test item was plotted on the x-axis. The LOE is represented by a solid line, and a best-fit linear trend (with y-intercept = 0) is represented by a dashed line. Data plotted below the LOE indicate lower base pressure for the reduced tire pressure test item.

A review of the 2.5-in. HMA, GR base data (Figure 51) showed that a majority of the data plotted above the LOE, indicating that base pressure was consistently higher in the reduced tire pressure test series. The fitted trend line indicated that base pressure in the reduced tire pressure test series was on the order of 13% higher than the normal tire pressure test series. This suggests that a reduction in tire pressure was not successful in reducing vertical pressure in the base course.

A slight reduction (approximately 2%) in vertical base course pressure was observed in the 2.5-in. HMA, LMS base test items (Figure 52). It is noted that the trend line poorly fits the observed data ($R^2 = 0.39$) and that a practical review of the data indicated that the pressures were generally equivalent.

A review of the 1.5-in. HMA, LMS base equality plot (Figure 53) indicated that vertical pressures were generally equivalent (1% reduction in the reduced tire pressure item) and that the linear trend line explained a small portion of the variability in the data ($R^2 = 0.15$). It is noted that the data plotted both above and below the LOE, suggesting that there were not meaningful differences in base pressure.

A review of the relationship for the 1.0-in. HMA, LMS base test items (Figure 54) revealed that there was essentially no relationship between the

observed data. Note $R^2 = -1.32$ for the fitted trend line, which indicated that the fitted trend was worse than that of a horizontal line. It should be noted that a negative R^2 is possible, given that that fitted equation was forced to have a y-intercept = 0. This simply indicates there is no linear correlation between the reduced and normal tire pressure data when subjected to the previously mentioned constraint.

Figure 51. Equality plot – C-130 base pressure response (2.5-in. HMA, GR base).

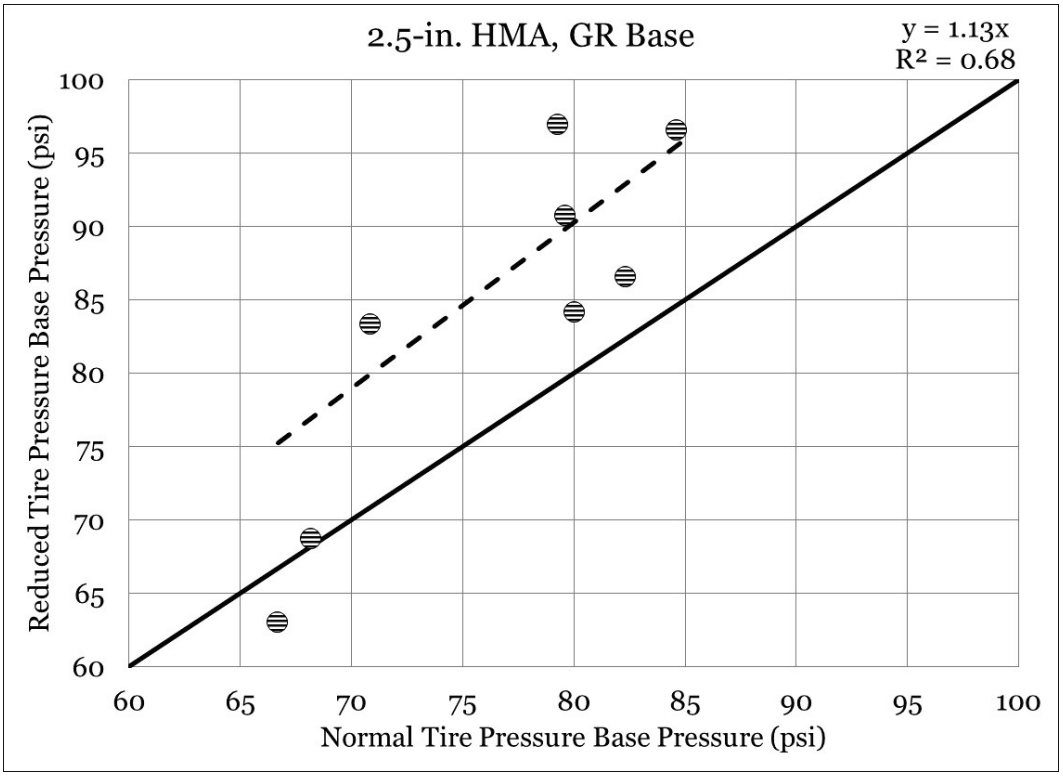

Figure 52. Equality plot – C-130 base pressure response (2.5-in. HMA, LMS base).

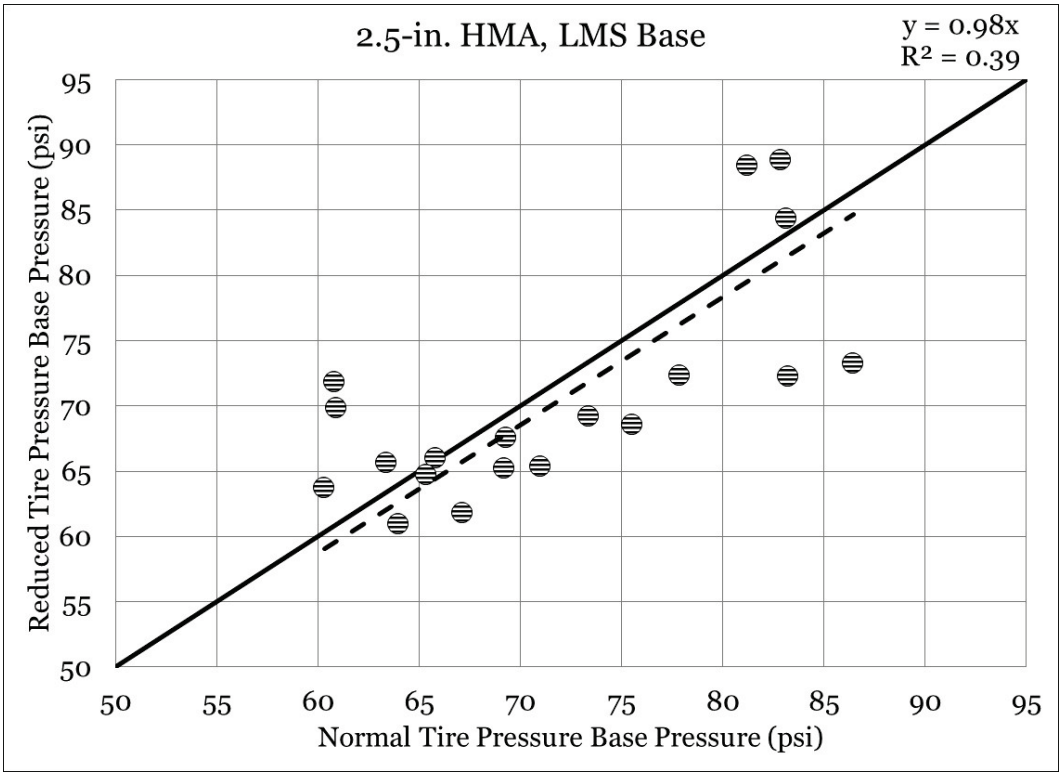

Figure 53. Equality plot – C-130 base pressure response (1.5-in. HMA, LMS base).

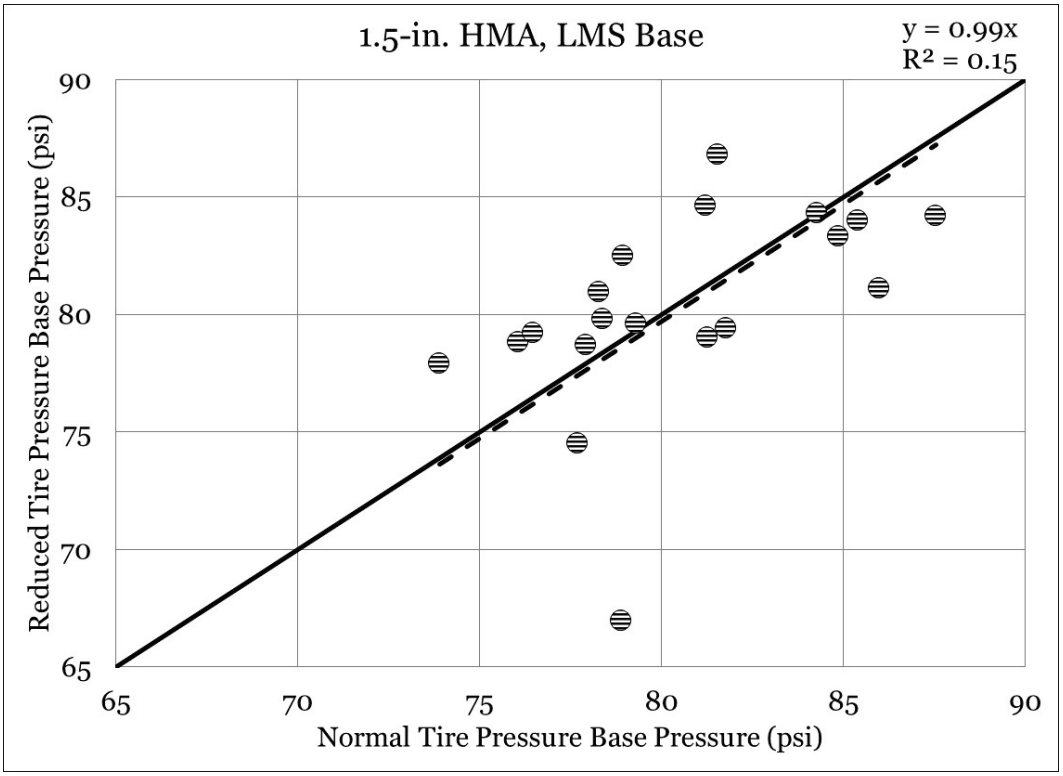

Figure 54. Equality plot – C-130 base pressure response (1.0-in. HMA, LMS base).

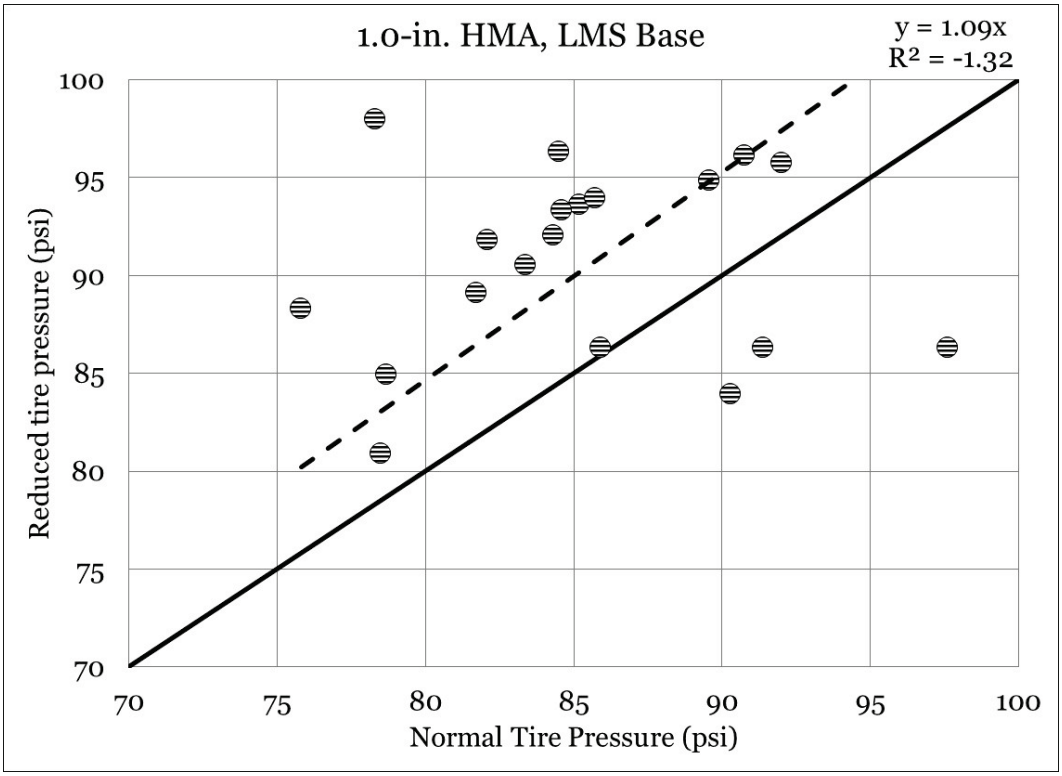

A summary of the statistical comparison for base pressure response with a change in tire pressure is presented in Table 17. A comparison of base vertical pressure in the 2.5-in. HMA, GR base test items was found to be statistically significant (p-value = 0.004), and average base pressure was found to be lower in the normal tire pressure test item. Comparisons made between the 2.5-in. HMA, LMS base and the 1.5-in. HMA, LMS base test items were not found to be statistically significant. Base pressure in the 1.0-in. HMA, LMS base items was found to be statistically significant (p-value = 0.004), and it was observed that the normal tire pressure item had lower average base pressure.

Table 17. Statistical analysis – C-130 base pressure and tire pressure.

Interaction	n	p-value	Significant	Better Performer
C130NTP1 vs. C130RTP1	10	0.004	Yes	C130NTP1
C130NTP2 vs. C130RTP2	19	0.454	No	Same
C130NTP3 vs. C130RTP3	19	0.814	No	Same
C130NTP4 vs. C130RTP4	19	0.004	Yes	C130NTP4

C-130 single-depth deflectometer response

The results obtained from an SDD for the normal tire pressure test series are presented in Figure 55. Values plotted for each SDD represent total deflection; thus, each value is comprised of both accumulated (i.e., permanent) and dynamic (i.e., recoverable) deflection. It was observed that total subgrade deflection increased from the onset of traffic in C130NTP1 (2.5-in. HMA, GR base), suggesting that the weak gravel base layer was not capable of providing sufficient protection of the subgrade and was not capable of efficiently reducing load on the subgrade. A smaller increase in initial total deflection was observed in the LMS base test items, and a growth in total deflection was observed beginning around 100 passes. This is generally consistent with observations made in both subgrade and base pressure response and supports the hypothesis of an initial period of densification or shakedown in the LMS aggregate layer. Total subgrade deformation followed logical trends, with the GR base item having the highest and most rapid measured subgrade deflection, followed by the LMS base items in order of decreasing asphalt thickness.

Figure 55. C-130 normal tire pressure total subgrade deflection.

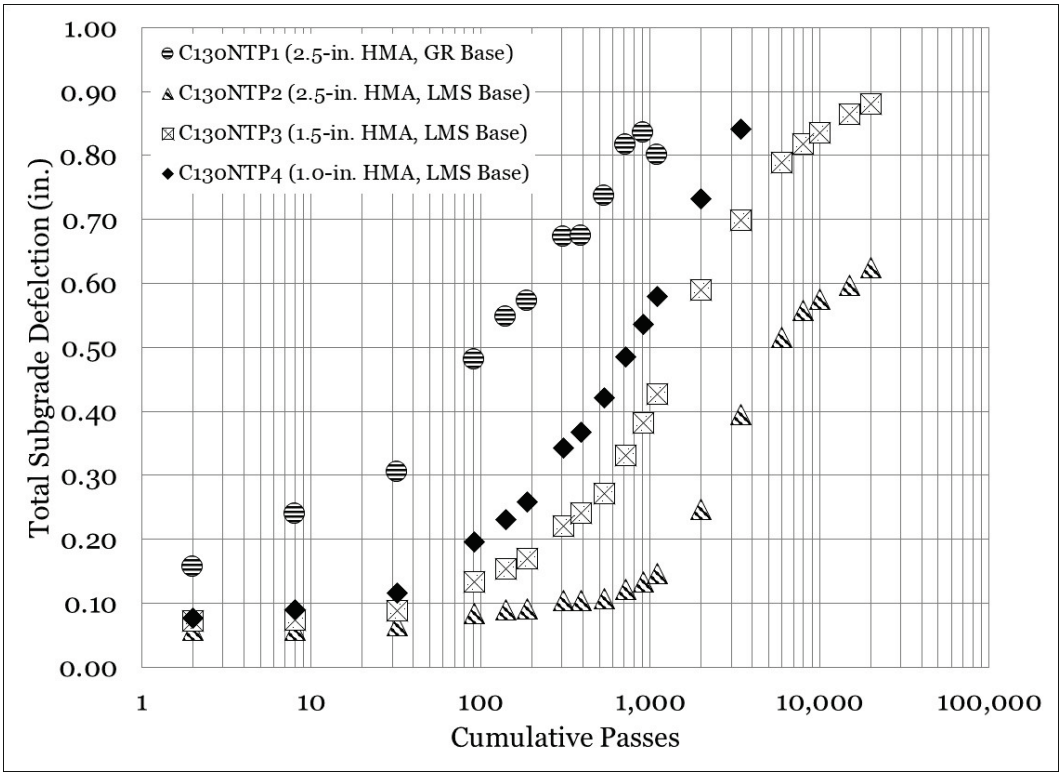

A statistical analysis (Table 18) indicated that all comparisons were statistically significant (p-value < 0.001 for all comparisons). C130NTP2

was found to have the best average total deflection performance in the LMS base test items, followed by C130NTP3 and C130NTP2.

Table 18. Statistical analysis – C-130 normal tire pressure subgrade deflection.

Interaction	n	p-value	Significant	Better Performer
C130NTP1 vs. C130NTP2	12	<0.001	Yes	C130NTP2
C130NTP1 vs. C130NTP3	12	<0.001	Yes	C130NTP3
C130NTP1 vs. C130NTP4	12	<0.001	Yes	C130NTP4
C130NTP2 vs. C130NTP3	19	<0.001	Yes	C130NTP2
C130NTP2 vs. C130NTP4	14	<0.001	Yes	C130NTP2
C130NTP3 vs. C130NTP4	14	<0.001	Yes	C130NTP3

Total deflection data for the reduced tire pressure test series are presented in Figure 56. Similar trends to the normal tire pressure test series were observed in the reduced tire pressure test series. An increase in total deflection was observed in C130RTP1 (2.5-in. HMA, GR base) from the onset of traffic, and deflections were observed to be the highest in this item at all traffic levels. At approximately 100 passes, it was observed that C130RTP4 (1.0-HMA, LMS base) began to separate from the other LMS test items, which is consistent with observations made in the normal tire pressure test series. Conversely, total deflection differences up to 100 passes in C130RTP2 and C130RPT3 were unremarkable, and observable differences did not manifest until nearly 1,000 passes. This suggests that reducing tire pressure may impact total deflection progression in the thicker asphalt test items. The order of performance followed logical expectations, similar to the normal tire pressure test series.

A statistical comparison (Table 19) indicated that all comparisons were statistically significant (p-value < 0.001 for all comparisons). C130RTP2 had the best (i.e., lowest) total subgrade deflection among the LMS base test items, followed by C130NTP3 and C130NTP2.

Figure 56. C-130 reduced tire pressure total subgrade deflection.

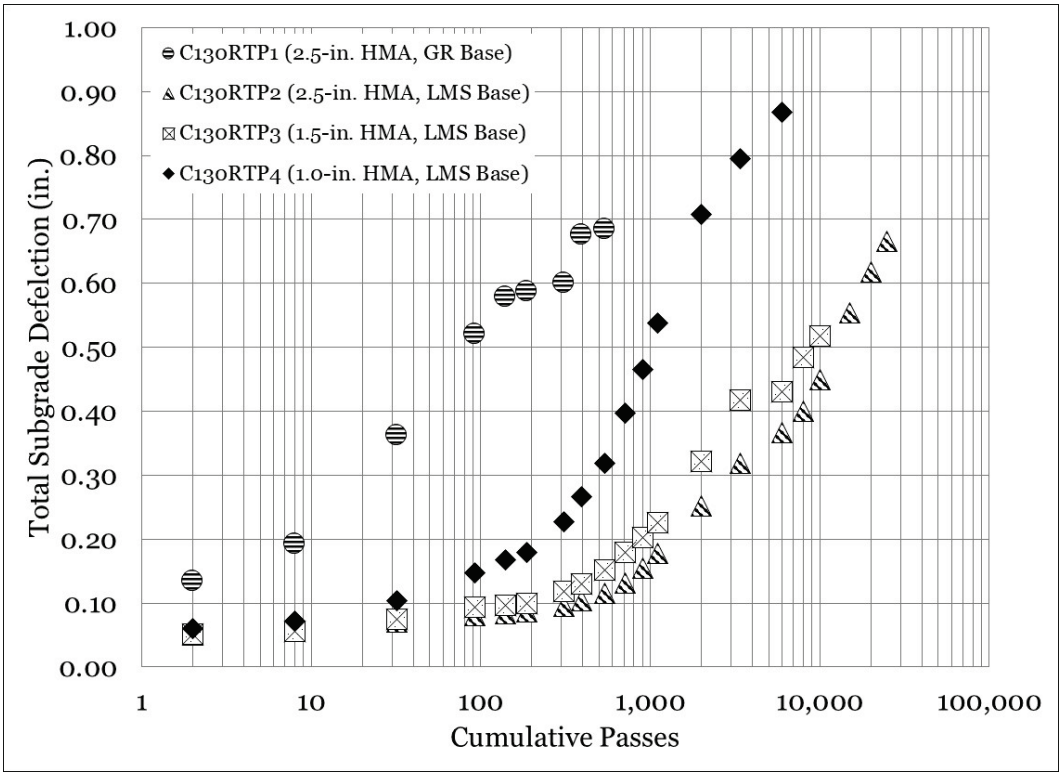

Table 19. Statistical analysis – C-130 reduced tire pressure subgrade deflection.

Interaction	n	p-value	Significant	Better Performer
C130RTP1 vs. C130RTP2	9	<0.001	Yes	C130RTP2
C130RTP1 vs. C130RTP3	9	<0.001	Yes	C130RTP3
C130RTP1 vs. C130RTP4	9	<0.001	Yes	C130RTP4
C130RTP2 vs. C130RTP3	17	<0.001	Yes	C130RTP2
C130RTP2 vs. C130RTP4	15	<0.001	Yes	C130RTP2
C130RTP3 vs. C130RTP4	15	<0.001	Yes	C130RTP3

Equality plots for normal and reduced tire pressure total subgrade deflection are presented in Figures 57 through 60. Total subgrade deflection for the reduced tire pressure item was plotted on the y-axis, and total subgrade deflection for the normal tire pressure item was plotted on the x-axis. The solid line represents the LOE, and the dashed line represents the best-fit linear trend line through the data, where the y-intercept was set equal to zero. Data plotted below the LOE indicate lower subgrade deflection (i.e., improved performance from reduced tire pressure).

A review of the 2.5-in. HMA, GR base equality plot (Figure 57) showed that the data generally follow the LOE, indicating that generally equivalent performance was observed between the reduced and the normal tire pressures. The linear trend line displayed a good fit ($R^2 = 0.95$), and the regression equation suggested that the reduced tire pressure test item had 2% less total deflection than the normal tire pressure test item.

A greater improvement was observed between the reduced tire pressure and the normal tire pressure in the 2.5-in. HMA, LMS base (Figure 58) test item (14%). It was observed that improvement appeared to be greater as deflection increased (evidenced by a departure from the LOE at +0.40-in. deflection).

The 1.5-in. HMA, LMS base test item (Figure 59) showed the greatest improvement as a function of tire pressure for all the test items, having an approximate 42% improvement. It is noted that all data points plotted below the LOE, and the linear trend line had a very good fit to the measured data ($R^2 = 0.99$)

General improvement was observed in the 1.0-in. HMA, LMS base test item (Figure 60) and was found to be on the order of 12%. All data were found to plot at or below the LOE, and the regression equation was found to describe approximately 97% of the data variability.

A statistical comparison of total subgrade deflection as a function of tire pressure is shown in Table 20. Comparison of the 2.5-in. HMA, GR base test items was not statistically significant (p-value = 0.738), suggesting that reducing tire pressure did not change the average subgrade deflection. Similarly, the 2.5-in. HMA, LMS base comparison was not found to be statistically significant (p-value = 0.057); however, it should be noted that the interaction would be significant at less than a 95% level of significance. Differences in 1.5 HMA, LMS and 1.0 HMA, LMS were both found to be statistically significant ($p < 0.001$), and it was found that average deflection was less in the reduced tire pressure series for both test items.

Figure 57. Equality plot – C-130 subgrade deflection (2.5-in. HMA, GR base).

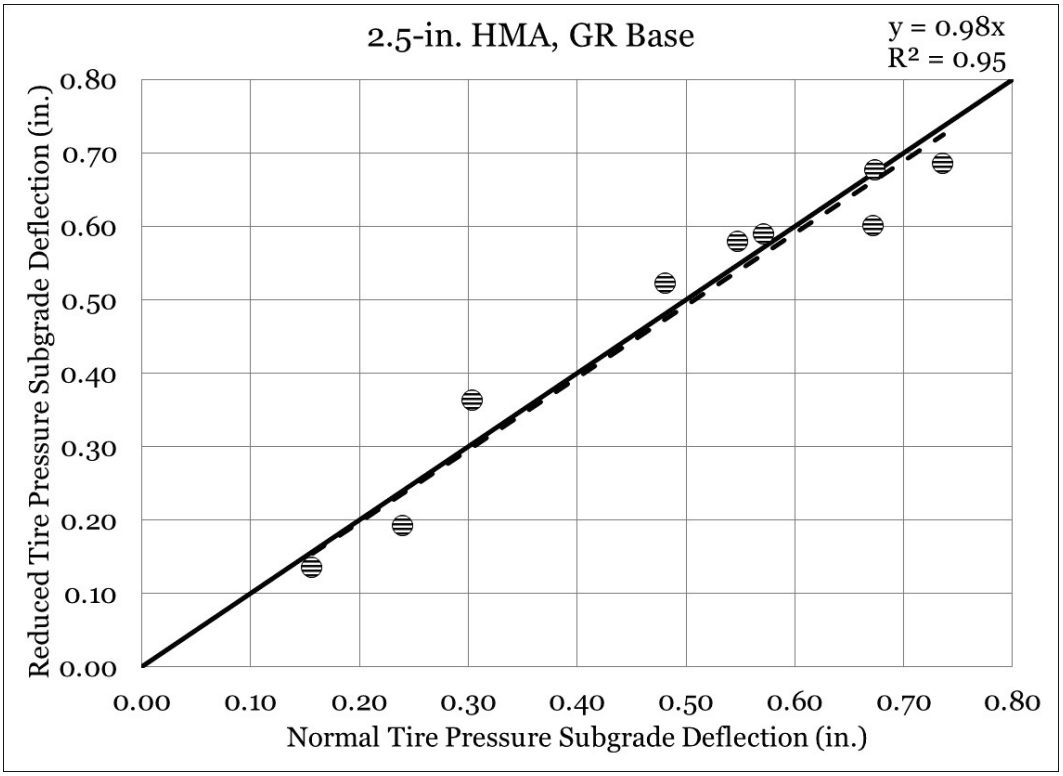

Figure 58. Equality plot – C-130 subgrade deflection (2.5-in. HMA, LMS base).

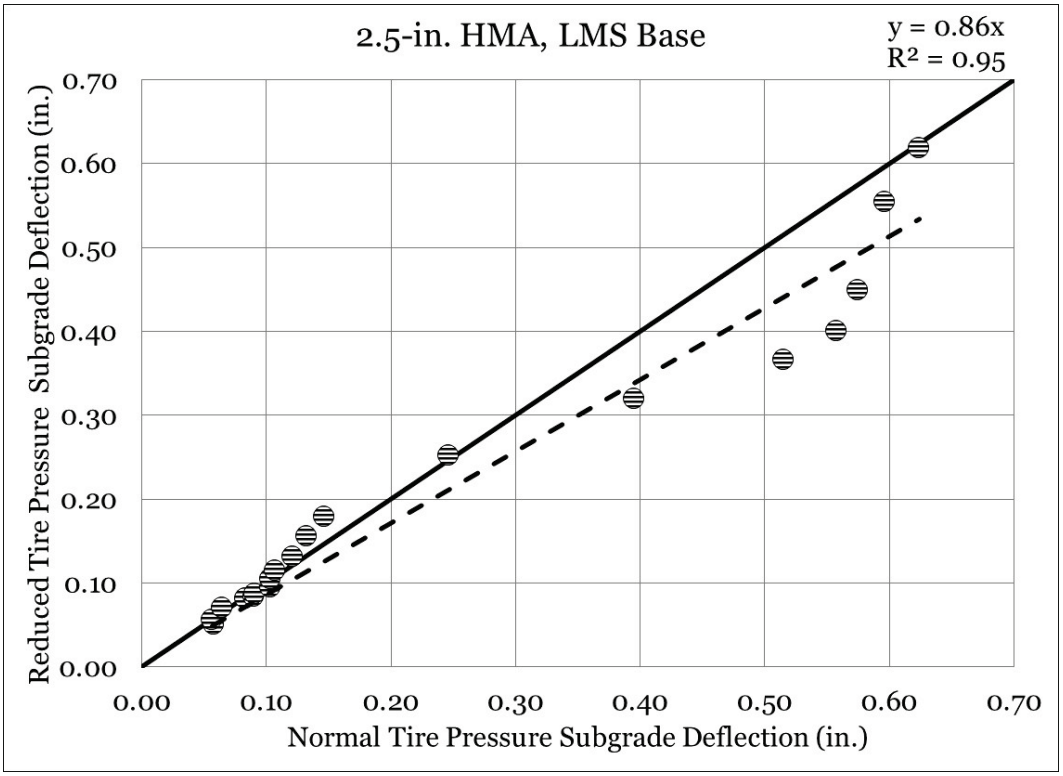

Figure 59. Equality plot – C-130 subgrade deflection (1.5-in. HMA, LMS base).

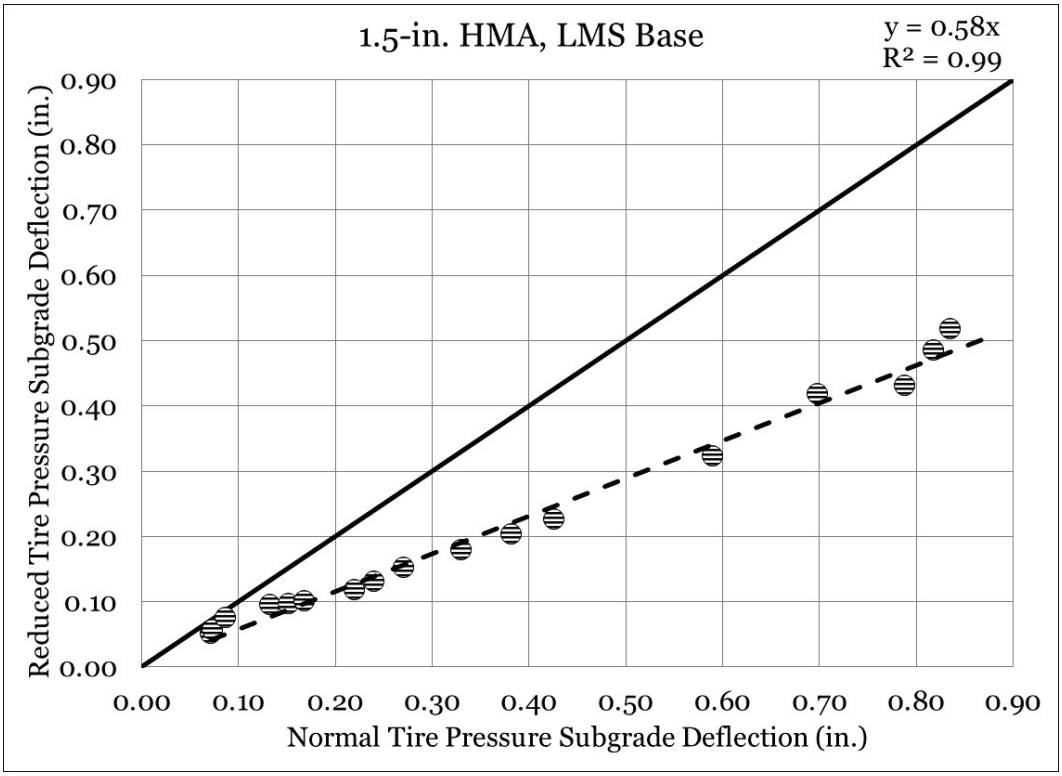

Figure 60. Equality plot – C-130 subgrade deflection (1.0-in. HMA, LMS base).

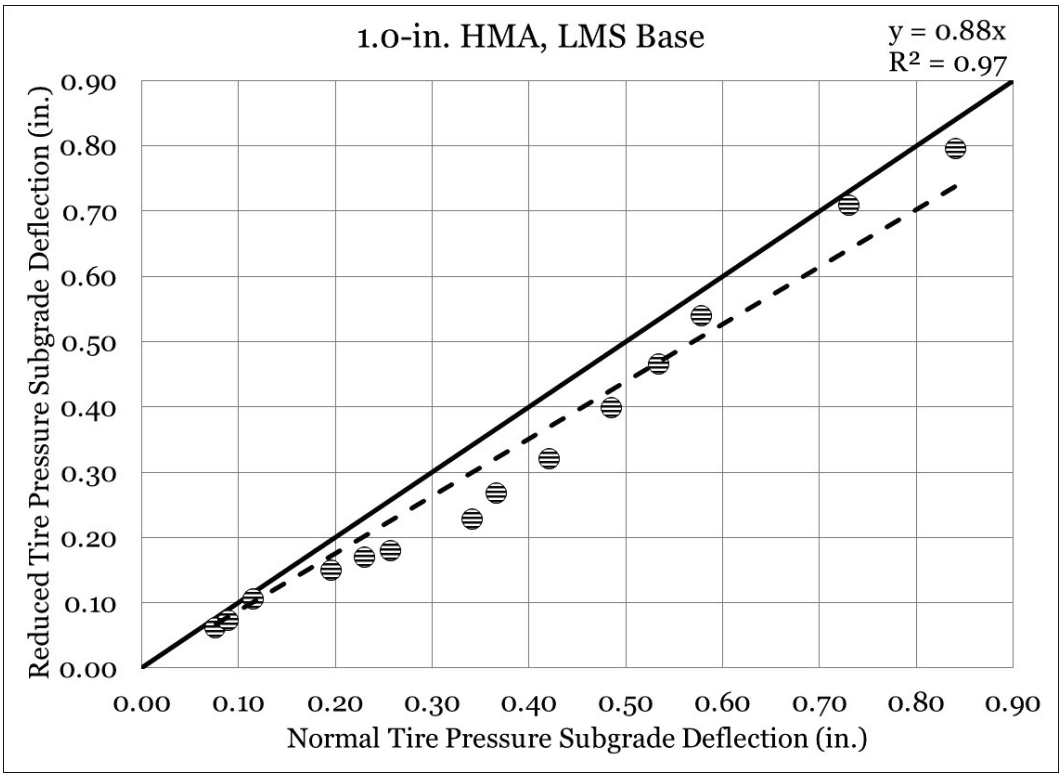

Table 20. Statistical analysis – C-130 subgrade deflection and tire pressure.

Interaction	n	p-value	Significant	Better Performer
C130NTP1 vs. C130RTP1	9	0.738	No	Same
C130NTP2 vs. C130RTP2	19	0.057	No	Same
C130NTP3 vs. C130RTP3	17	<0.001	Yes	C130RTP3
C130NTP4 vs. C130RTP4	15	<0.001	Yes	C130RTP4

C-130 asphalt strain gauge response

Asphalt strain gauge response for the normal tire pressure test series is shown in Figure 61. Asphalt strain gauge values represent total strain response, which consists of a compression component and a tension component. Thus, the response values shown are the difference of minimum values and maximum values (i.e., peak to trough). This provides a simplified means for comparing total response between test items.

The highest total strain values were observed in C130NTP1, which was logical considering the rapid deformation that occurred in this test item. Total strain values were much lower in the LMS base test items, which was expected; and it was observed that total strain remained generally consistent with slower increases observed for the duration of trafficking. Similar to other instrumentation response values, there appeared to be an initial period of settlement in each section before meaningful differences in response could be observed. Near 30 passes, differences in asphalt strain response began to become evident. It was observed that total strain values followed an expected sequence: thinner asphalt had progressively higher strain values.

Statistical comparisons of asphalt strain response are summarized in Table 21. It was observed that all comparisons were statistically significant ($p < 0.001$). All LMS base test items were found to have lower average total strain than the GR base test item, as expected. C130NTP2 had lower average total strain than all other LMS base test items.

Figure 61. C-130 normal tire pressure total asphalt strain.

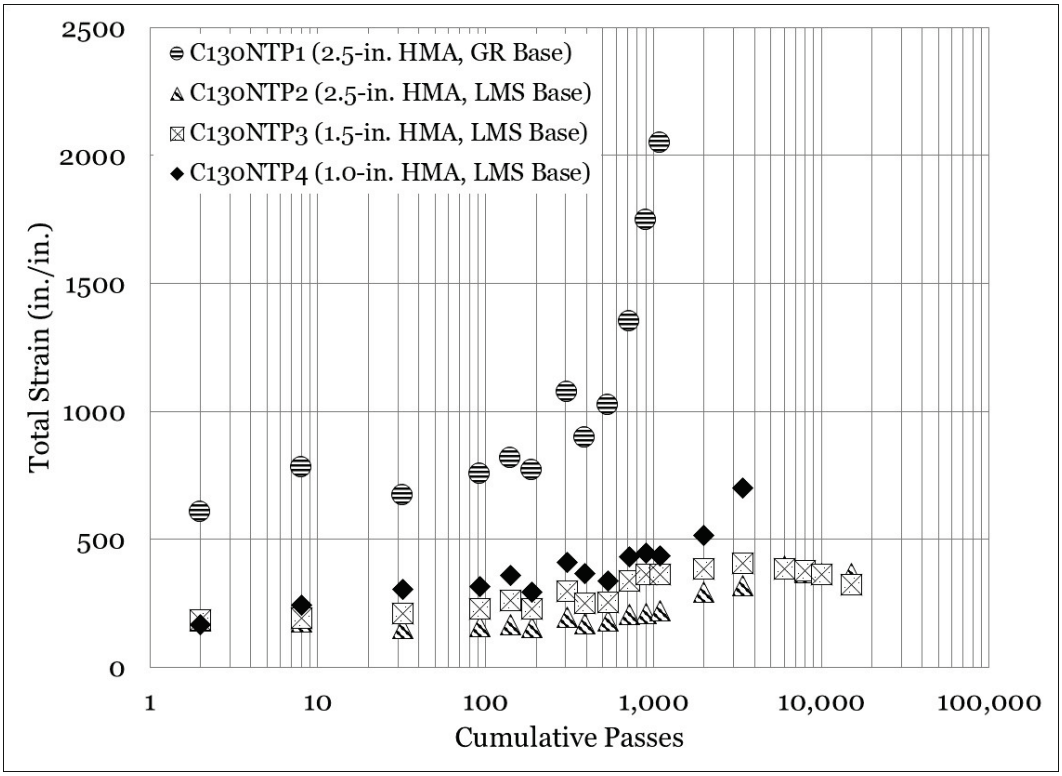

Table 21. Statistical analysis – C-130 normal tire pressure asphalt strain response.

Interaction	n	p-value	Significant	Better Performer
C130NTP1 vs. C130NTP2	12	<0.001	Yes	C130NTP2
C130NTP1 vs. C130NTP3	12	<0.001	Yes	C130NTP3
C130NTP1 vs. C130NTP4	12	<0.001	Yes	C130NTP4
C130NTP2 vs. C130NTP3	18	<0.001	Yes	C130NTP2
C130NTP2 vs. C130NTP4	18	<0.001	Yes	C130NTP2
C130NTP3 vs. C130NTP4	14	<0.001	Yes	C130NTP3

Total asphalt strain for the reduced tire pressure test series is presented in Figure 62. Unlike the normal tire pressure test series, C130RTP4 (1.0-in. HMA, LMS base) was found to have the highest initial total strain. However, as additional traffic was applied, it was observed that C130RTP1 (2.5-in. HMA, GR base) overtook C130RTP4. This could be attributed to minor differences in asphalt density at the gauge location, particularly since the other responses fall in the expected order. After about 30 passes (similar to the normal tire pressure response), expected performance followed expected trends. The LMS base test items were observed to have generally consistent strain response throughout traffic duration, and increases were observed near the end of traffic in C130RTP4.

Statistical comparisons for total asphalt strain for the reduced tire pressure test series are presented in Table 22. C130RTP1 was found to be statistically different from C130RTP2 (p-value = 0.003) and C130RPT3 (p-value = 0.006), and C130RTP1 was found to have higher average total strain than these test items. Comparison of C130RTP1 and C130RTP4 was not found to be statistically significant (p-value = 0.077), although a review of the data suggested that meaningful differences were observed. C130RTP2 was statistically different from the other LMS base test items, and it was observed that C130RTP2 had lower average total strain than the other LMS base test items.

Figure 62. C-130 reduced tire pressure total asphalt strain.

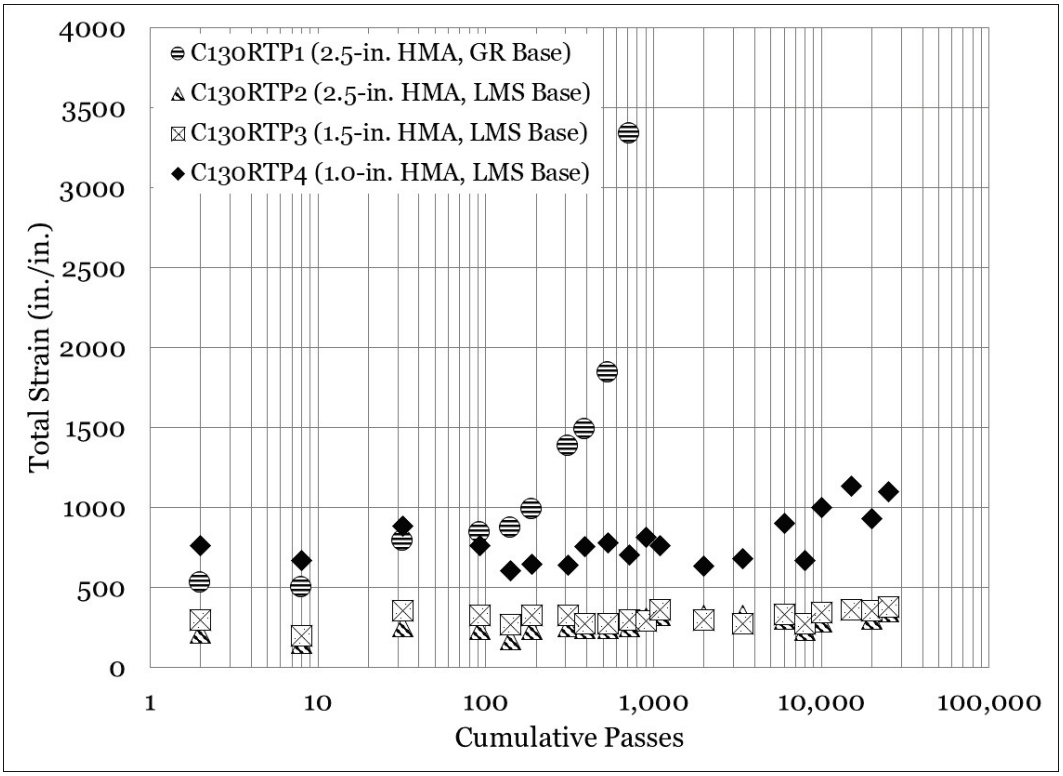

Table 22. Statistical analysis – C-130 reduced tire pressure asphalt strain response.

Interaction	n	p-value	Significant	Better Performer
C130RTP1 vs. C130RTP2	10	0.003	Yes	C130RTP2
C130RTP1 vs. C130RTP3	10	0.006	Yes	C130RTP3
C130RTP1 vs. C130RTP4	10	0.077	No	Same
C130RTP2 vs. C130RTP3	20	<0.001	Yes	C130RTP2
C130RTP2 vs. C130RTP4	20	<0.001	Yes	C130RTP2
C130RTP3 vs. C130RTP4	20	<0.001	Yes	C130RTP3

Equality plots for total asphalt strain are presented in Figures 63 through 66. Total asphalt strain for the reduced tire pressure test item was plotted on the y-axis, and total asphalt strain for the normal tire pressure test item was plotted on the x-axis. The LOE is represented by a solid line, and the best-fit linear trend line is represented by a dashed line. Data plotted below the LOE indicate lower total asphalt strain.

A review of the 2.5-in. HMA, GR base equality plot (Figure 63) indicated that measured total strain was higher (55%) in the reduced tire pressure item when compared to the normal tire pressure item. The linear regression had a poor fit, with an $R^2 = 0.58$.

When the other total strain equality plots are considered (Figures 64 through 66), it was observed that all R^2 values are negative, indicating the linear model was a worse fit than a horizontal line. Thus, it could be concluded that there was no correlation between total strain for the reduced tire pressure and the normal tire pressure test series, when a linear model subject to the constraint y-intercept=0 was considered. Further, based on the poor fit in the 2.5-in. HMA, GR test item and the lack of fit in the LMS test items, it could be concluded that reducing tire pressure in relatively thin asphalt sections had little effect on measured asphalt strain. It is hypothesized that subtle differences in asphalt properties (namely compaction) influence measured total strain values in thin asphalt pavements.

A statistical comparison of total strain values with tire pressure (Table 23) indicated that only 1.0-in. HMA, LMS base was statistically significant (p-value <0.001); however, based on previous observations, the robustness of the statistical measure should be interpreted with caution.

Figure 63. Equality plot – C-130 asphalt strain (2.5-in. HMA, GR base).

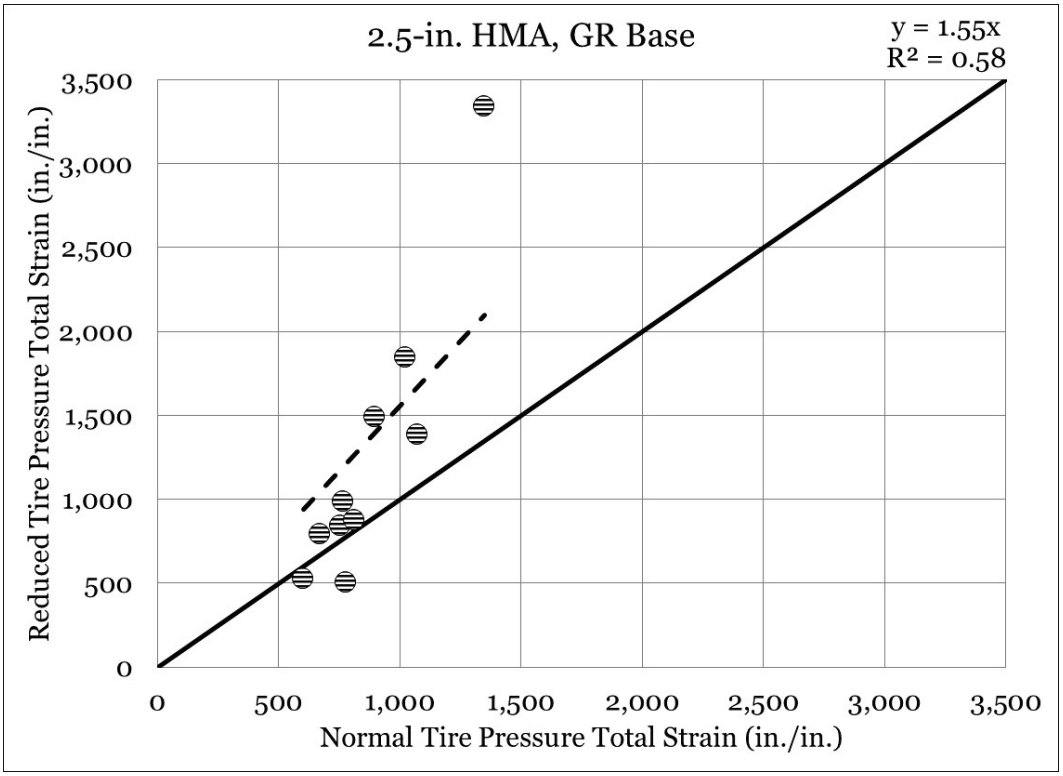

Figure 64. Equality plot – C-130 asphalt strain (2.5-in. HMA, LMS base).

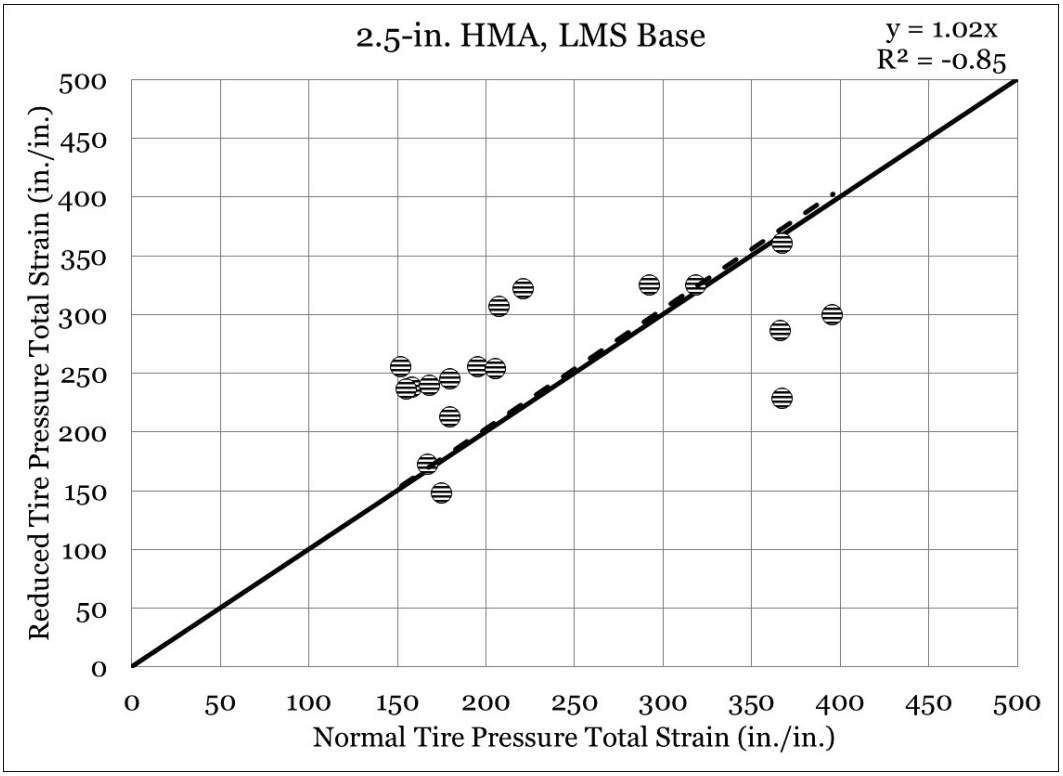

Figure 65. Equality plot – C-130 asphalt strain (1.5-in. HMA, LMS base).

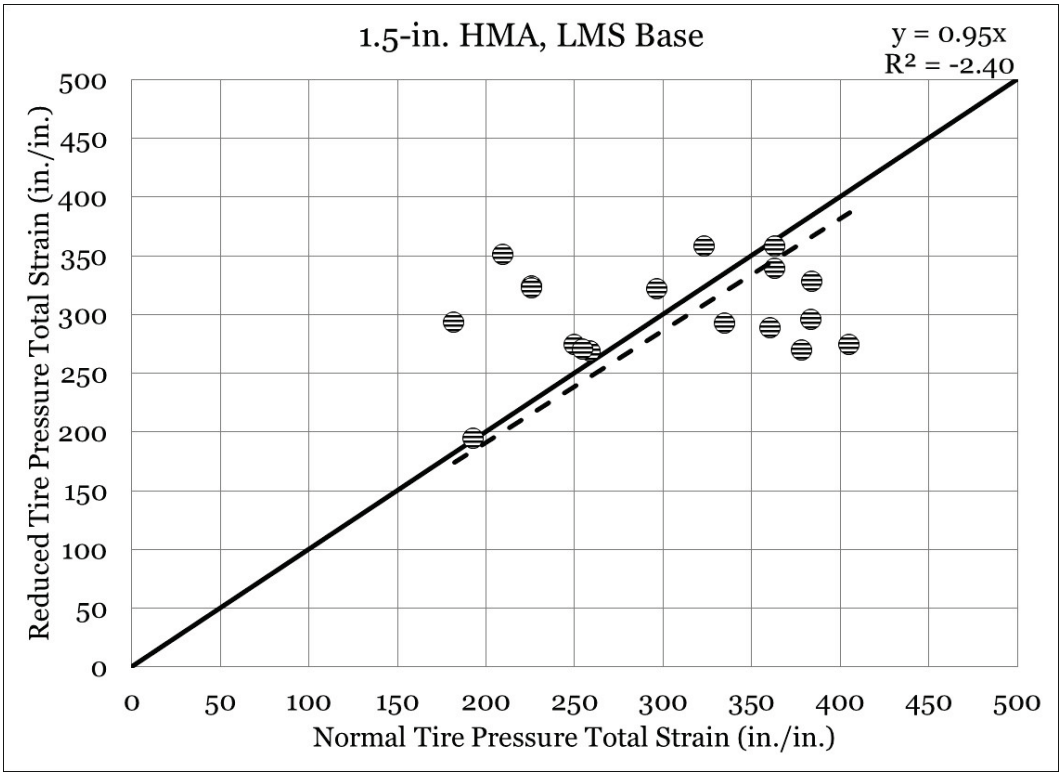

Figure 66. Equality plot – C-130 asphalt strain (1.0-in. HMA, LMS base).

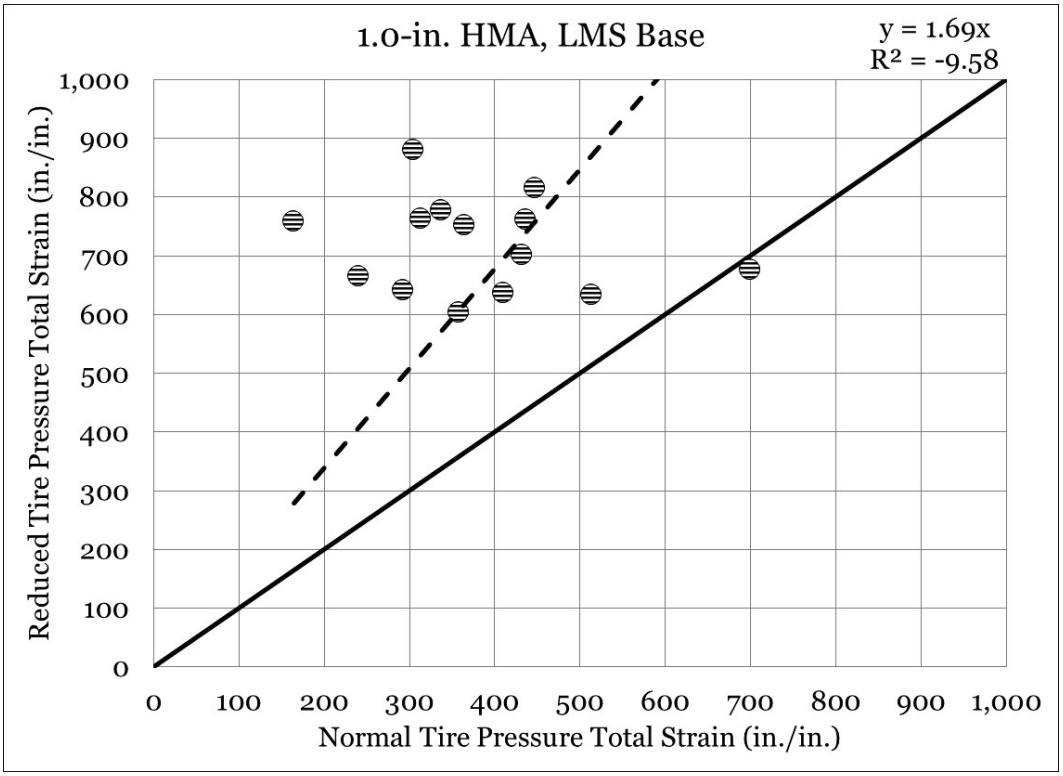

Table 23. Statistical analysis – C-130 total asphalt strain and tire pressure.

Interaction	n	p-value	Significant	Better Performer
C130NTP1 vs. C130RTP1	10	0.094	No	Same
C130NTP2 vs. C130RTP2	18	0.180	No	Same
C130NTP3 vs. C130RTP3	18	0.959	No	Same
C130NTP4 vs. C130RTP4	14	<0.001	Yes	C130NTP4

7.2 C-17 traffic results

C-17 rutting

Rut depth progression for the normal tire pressure test series is shown in Figure 67. C17NTP4 rutted rapidly, and it was observed that 1 in. of rutting occurred at approximately 30 passes. Rutting was observed to progress in excess of 4.0 in. after 90 total passes. Total rutting was slower in the limestone base sections, and the 2.5-in. HMA item was found to be the best performer. Minor differences were observed in the 1.0-in. and 1.5-in. HMA items, indicating that increasing the asphalt thickness by 0.5 in. had little impact on rut depth progression.

The results of a statistical analysis are presented in Table 24. It was observed that C17NTP1 (1.0-in. HMA, LMS base) and C17NTP2 (1.5-in. HMA, LMS base) were not statistically different (p-value = 0.063). C17NTP3 was observed to be statistically different from all other test items, which was consistent with visual observation. Surprisingly, C17NTP4 (2.5-in. HMA, GR base) was not statistically different from the other test items. However, a review of the statistical analysis showed that comparisons made to C17NTP4 were limited to only five observations, due to the rapid rut development. Thus, the results of a paired t-test for C17NTP4 were statistically weak, and the reduced number of observations increased the probability of a type II statistical error (i.e., incorrectly accepting the null hypothesis that the means are equal, when it is in fact false).

Rut depth progression for the C-17 reduced tire pressure test series is shown in Figure 68. Similar to the normal tire pressure test series, C17RTP4 deformed rapidly under traffic, reaching 1.0 in. of rutting at approximately 30 passes. Rutting performance in the limestone base test items was observed to be equivalent early in traffic, and some differences became more evident with an increase in traffic application.

Figure 67. C-17 normal tire pressure rut depth.

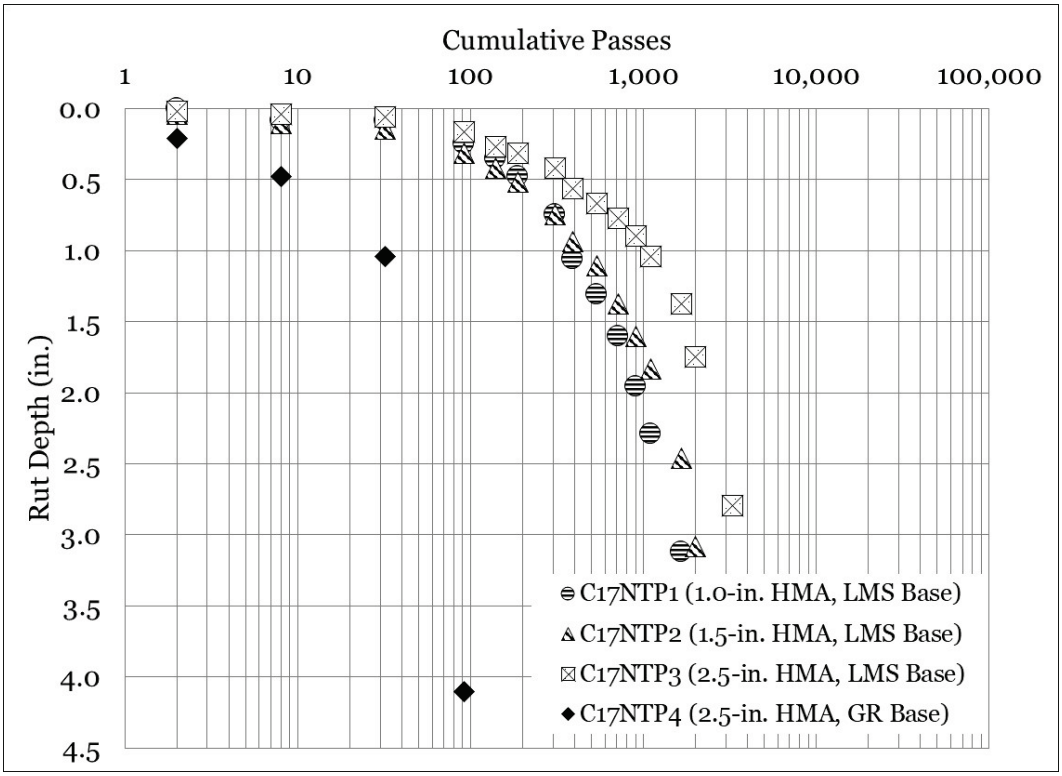

Table 24. Statistical analysis – C-17 normal tire pressure rut depth.

Interaction	n	p-value	Significant	Better Performer
C17NTP1 vs. C17NTP2	14	0.063	No	Same
C17NTP1 vs. C17NTP3	14	0.006	Yes	C17NTP3
C17NTP1 vs. C17NTP4	5	0.202	No	Same
C17NTP2 vs. C17NTP3	15	0.001	Yes	C17NTP3
C17NTP2 vs. C17NTP4	5	0.211	No	Same
C17NTP3 vs. C17NTP4	5	0.202	No	Same

C17RTP1 (1.0-in. HMA, LMS base) was found to be the worst performer at increasing traffic levels. Notably, C17RTP2 (1.5-in. HMA, LMS base) and C17RTP3 (2.5-in. HMA, LMS base) displayed similar rutting behavior; and C17RTP2 performed slightly better, which was not expected due to the 1.0-in. difference in asphalt thickness. A review of as-built properties did not reveal a meaningful difference in material characteristics that could explain this behavior; however, it was hypothesized that subtle differences in asphalt properties could have influenced performance, particularly at higher loads.

A statistical analysis (Table 25) confirmed that average rutting in C17RTP2 and C17RTP3 was statistically equivalent (p-value = 0.057). Also, it was found that average rutting in C17RTP1 and C17RTP3 was not statistically different (p-value = 0.185). All other comparisons were found to be statistically significant, and it was observed that C17RTP4 was the worst performer, as expected.

Figure 68. C-17 reduced tire pressure rut depth.

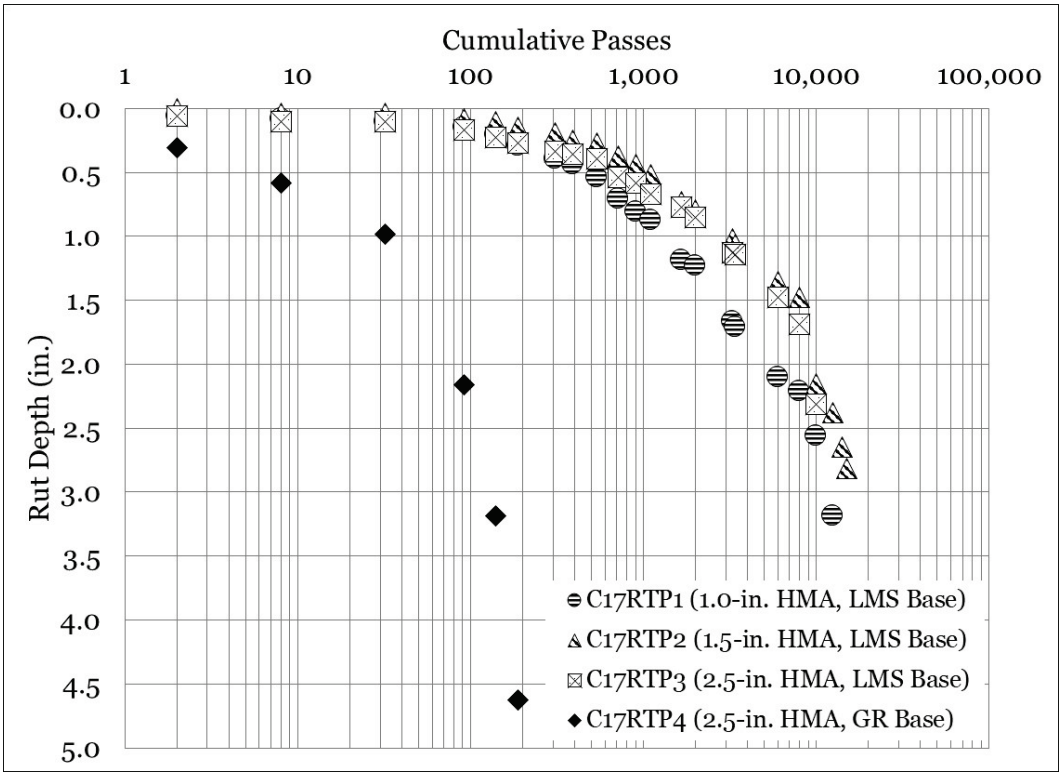

Table 25. Statistical analysis – C-17 reduced tire pressure rut depth.

Interaction	n	p-value	Significant	Better Performer
C17RTP1 vs. C17RTP2	22	<0.001	Yes	C17RTP2
C17RTP1 vs. C17RTP3	21	0.185	No	Same
C17RTP1 vs. C17RTP4	7	0.038	Yes	C17RTP1
C17RTP2 vs. C17RTP3	21	0.057	No	Same
C17RTP2 vs. C17RTP4	7	0.036	Yes	C17RTP2
C17RTP3 vs. C17RTP4	7	0.039	Yes	C17RTP3

Equality plots, presented in Figures 69 through 72, indicated that a reduction in tire pressure resulted in a meaningful improvement in rutting performance. Reduced tire pressure rut depths were plotted on

the y-axis, and normal tire pressure rut depths were plotted on the x-axis. Data plotted below the LOE indicated an improvement in rutting performance with a reduction in tire pressure.

A review of the 1.0-in. HMA, LMS base equality plot (Figure 69) indicated that a reduction in tire pressure resulted in an approximate 60% improvement in rutting performance. A reduction in tire pressure resulted in a 73% improvement in rutting performance in the 1.5-in. HMA, LMS base (Figure 70), and it was observed that a slightly less (although meaningful) improvement of 50% was identified in the 2.5-in. HMA, LMS base (Figure 71). It was noted that the equality plot for the 2.5-in. HMA, GR base (Figure 72) indicated that a 44% improvement was realized with a reduction in tire pressure; however, the data were found to plot on the LOE at rut depths up to 1.0 in. and diverged from the LOE at higher rut depths.

A summary of a statistical comparison for C-17 traffic rut depth as a function of tire pressure is presented in Table 26. It was observed that all comparisons for the limestone base test items were statistically significant, indicating that changes in tire pressure resulted in meaningful differences in rut depth performance. It was found that, in the case of the limestone base course test items, the reduced tire pressure test items were found to have lower average rut depths than the normal tire pressure counterparts. The statistical comparison for the 2.5-in. HMA, GR base test items was not found to be statistically significant (p-value = 0.415). This suggested that total load rather than tire pressure was controlling rutting performance in the weaker gravel base course pavement test item.

Photographs of rutting in the C-17 test items are shown in Figure 73.

Figure 69. Equality plot – C-17 rut depth (1.0-in. HMA, LMS base).

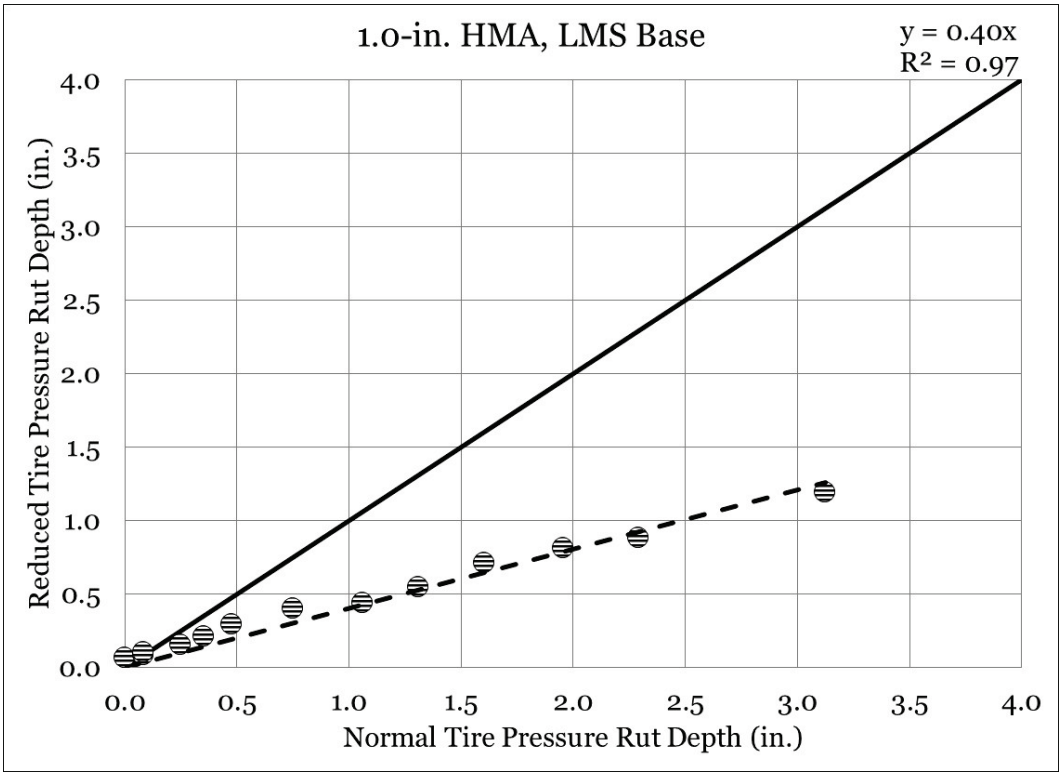

Figure 70. Equality plot – C-17 rut depth (1.5-in. HMA, LMS base).

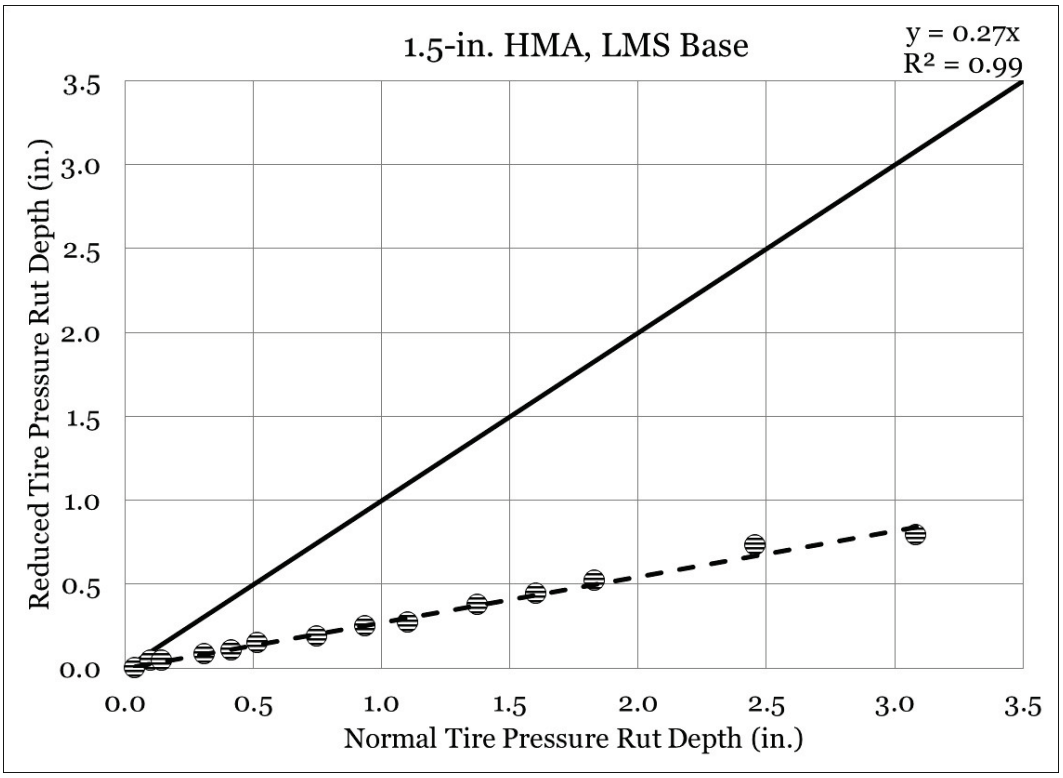

Figure 71. Equality plot – C-17 rut depth (2.5-in. HMA LMS base).

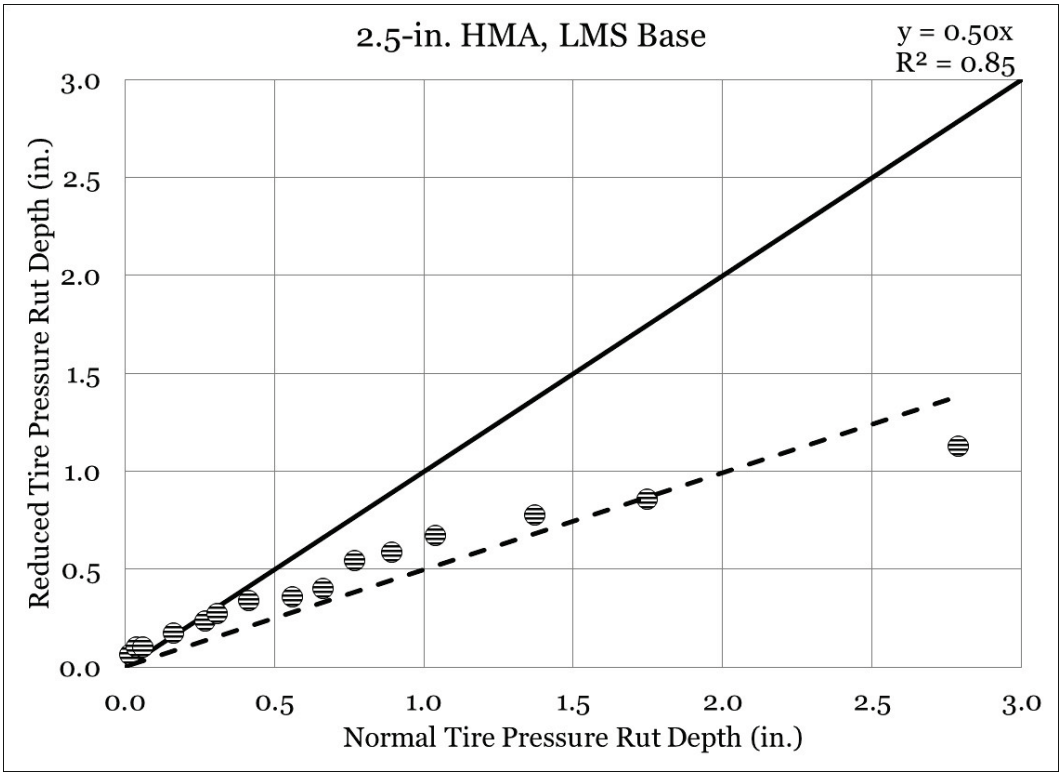

Figure 72. Equality plot – C-17 rut depth (2.5-in. HMA, GR base).

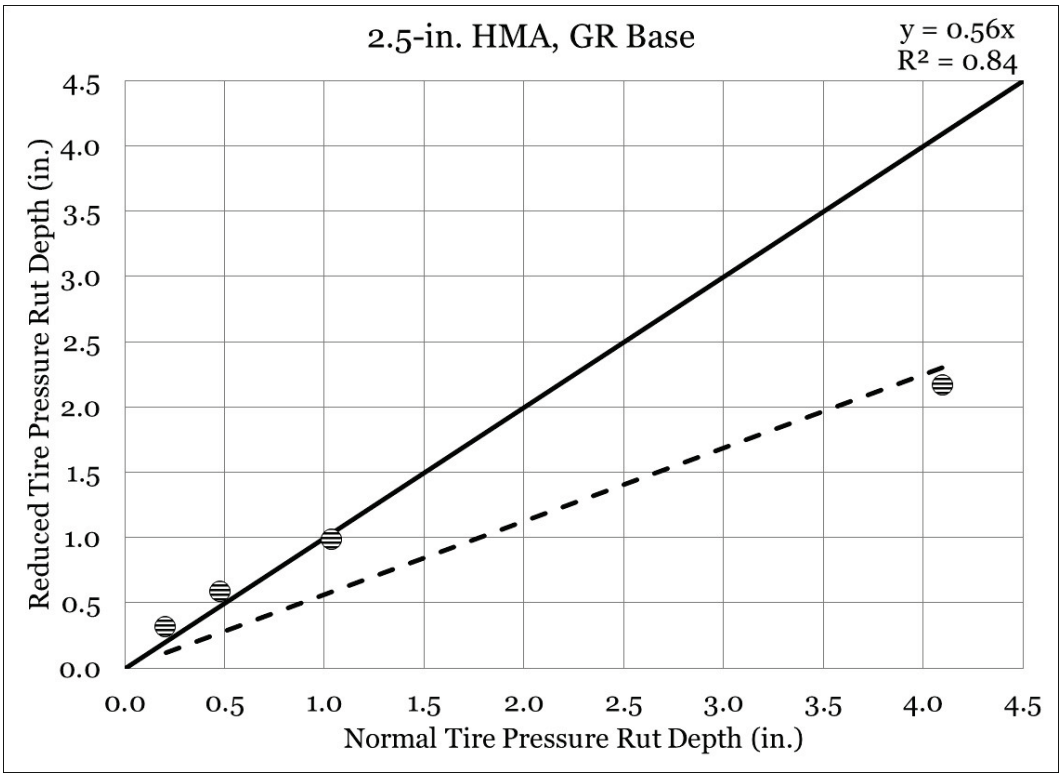

Table 26. Statistical analysis – C-17 rut depth and tire pressure.

Interaction	n	p-value	Significant	Better Performer
C17NTP1 vs. C17RTP1	14	0.006	Yes	C17RTP1
C17NTP2 vs. C17RTP2	15	0.001	Yes	C17RTP2
C17NTP3 vs. C17RTP3	16	0.022	Yes	C17RTP3
C17NTP4 vs. C17RTP4	5	0.415	No	Same

C-17 cracking

A visual inspection of each test item was performed to measure surface cracking at selected traffic intervals. Total cracking was measured by using a rolling wheel and recorded in total linear feet. Total cracking with increasing aircraft passes for the normal tire pressure test series is presented in Figure 74.

C17NTP4 (the weakest test item) was the first item to display surface cracking at approximately 92 passes, which was the last data collection point for that test item (note rutting was 4.1 in. at this data point). It is noted that no cracking was observed at the prior data collection point (32 passes); thus, the addition of 60 passes resulted in both a large increase in rutting and a meaningful cracking development. C17NTP1 began cracking at 308 passes (0.75-in. rut depth), followed by C17NTP2 at 716 passes (1.4-in. rut depth). C17NTP3 (2.5-in. HMA, LMS base) was the last item to show surface cracking, which was observed at 3,260 passes (2.8-in. rut depth). It was observed that as asphalt pavements became thinner, cracking was observed earlier in traffic application and at a lower rut depth.

Total cracking for the reduced tire pressure test items is shown in Figure 75. C17RTP4 displayed the first visual cracking, as expected. The limestone base test items developed cracking in a logical order (i.e., thinner asphalt to progressively thicker asphalt layer). When compared to the normal tire pressure test items, it was observed that cracking generally occurred later in traffic application in the reduced tire pressure series. Equality plots (Figure 76 and Figure 77) revealed that a 20% improvement in cracking was observed in the 1.0-in. HMA, LMS base, and a 74% improvement in cracking was observed in the 1.5-in. HMA, LMS base items. Insufficient data were available to present equality plots for the 2.5-in. HMA, LMS base and 2.5-in. HMA, GR base items, although it should be noted that crack progression was less in the reduced tire pressure test items. Examples of observed cracking are presented in Figure 78.

Figure 73. Photographs of rutting in C-17 test items.

(a) C17NPT1 (Pass 1,652)

(b) C17RTP1 (Pass 14,052)

(c) C17NPT2 (Pass 2,000)

(d) C17RTP2 (Pass 15,000)

(e) C17NPT3 (Pass 3,260)

(f) C17RTP3 (Pass 12,504)

(g) C17NTP4 (Pass 92)

(h) C17RTP4 (Pass 188)

Figure 74. Visual cracking progression – C-17 normal tire pressure.

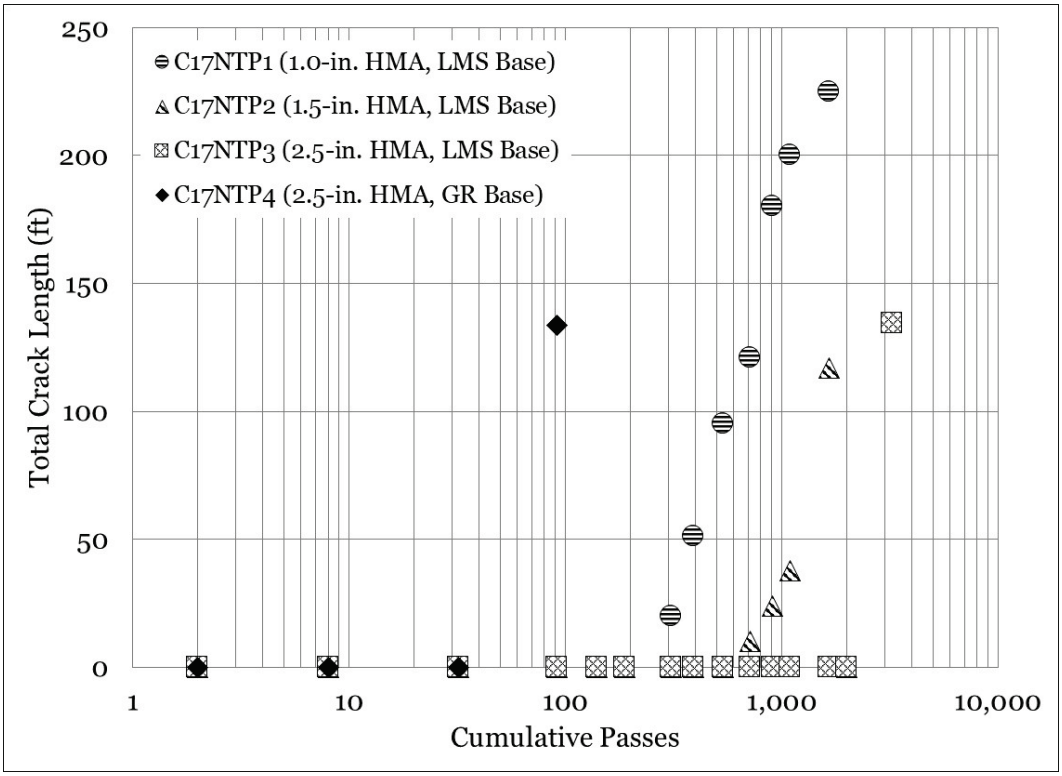

Figure 75. Visual cracking progression – C-17 reduced tire pressure.

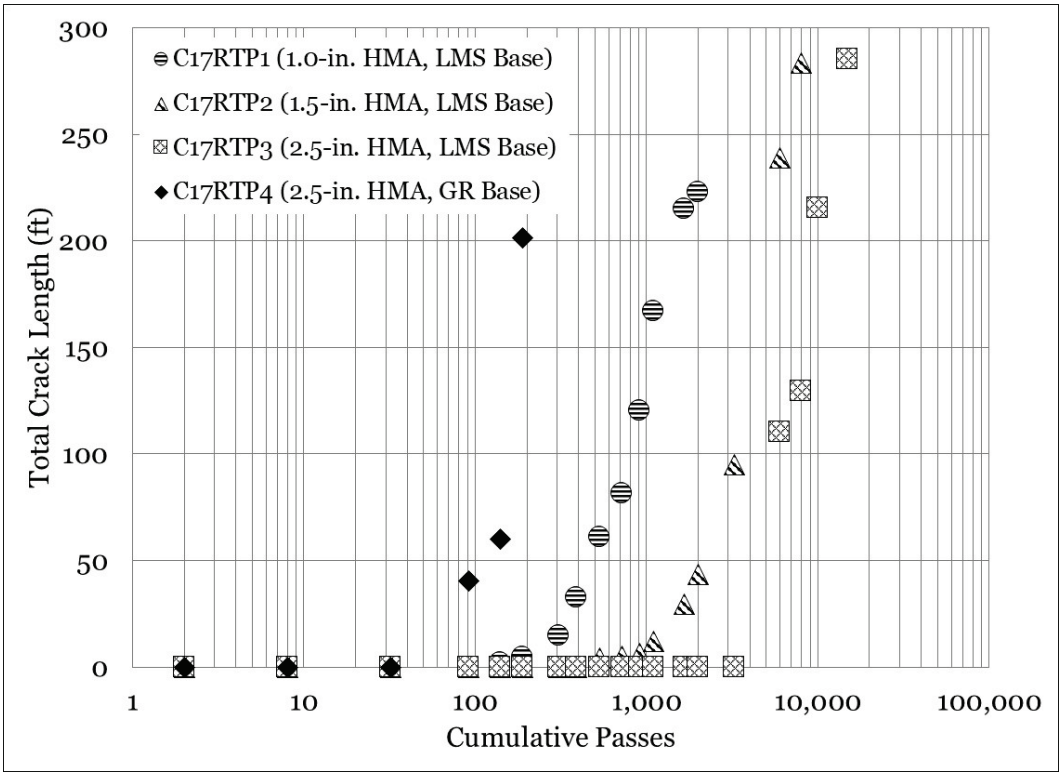

Figure 76. Equality plot – C-17 cracking (1.0-in. HMA, LMS base).

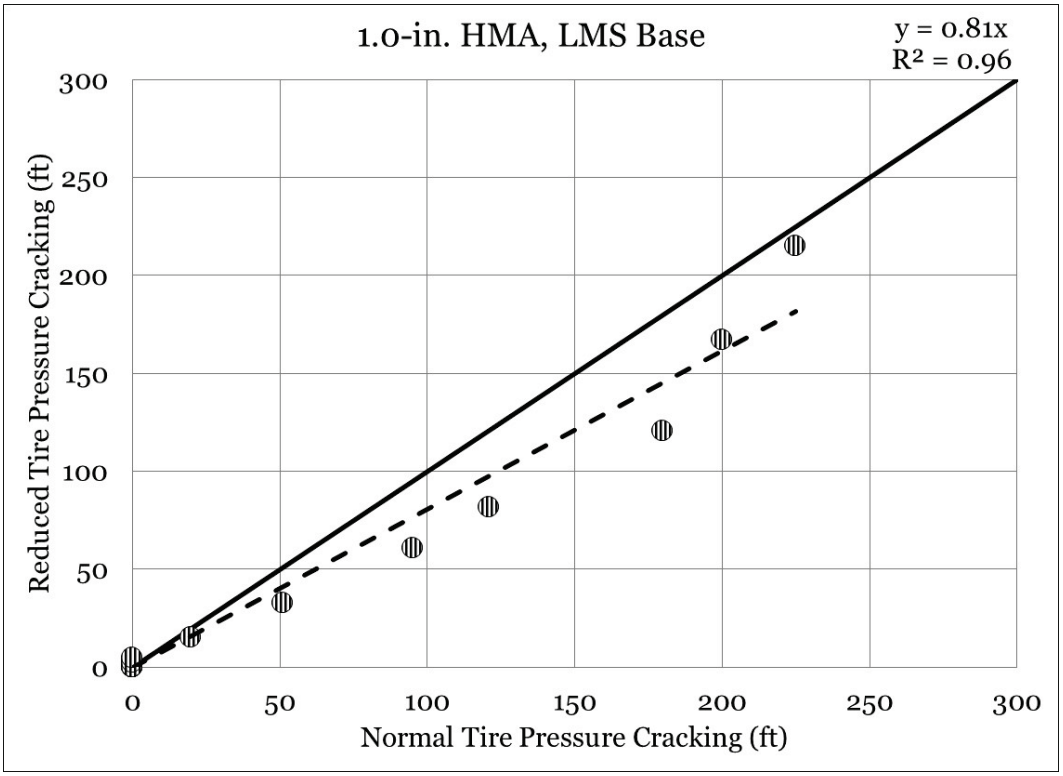

Figure 77. Equality plot – C-17 cracking (1.5-in. HMA, LMS base).

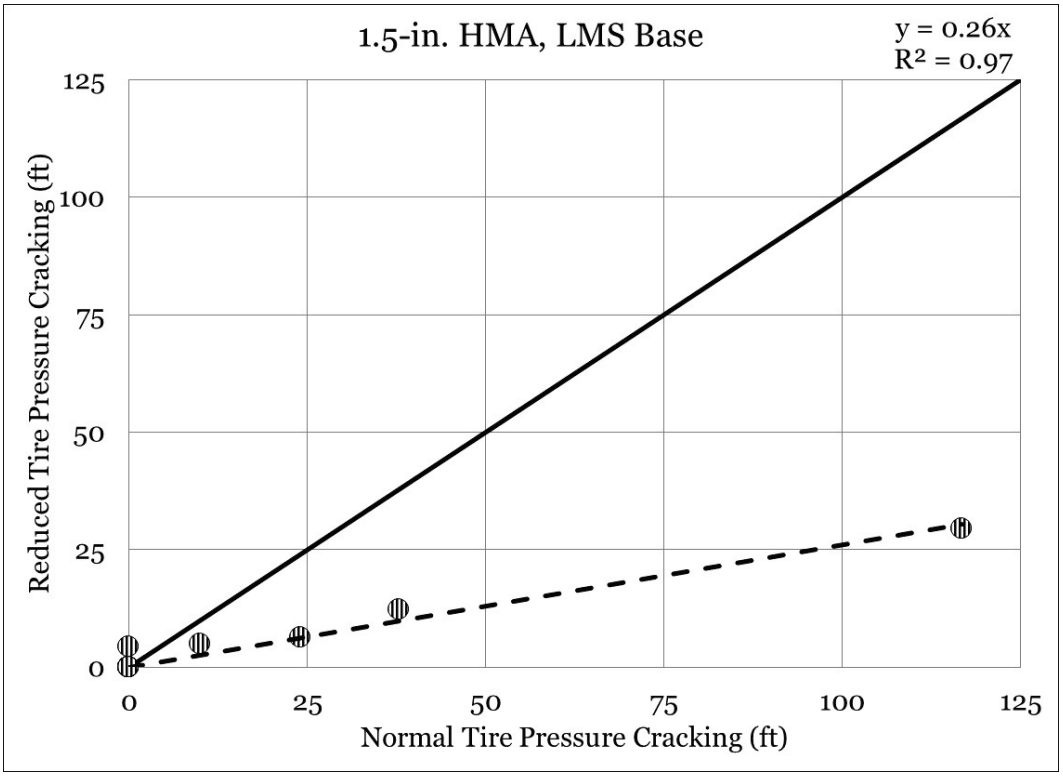

Figure 78. Photographs of cracking in C-17 test items.

(a) C17NTP1 overall cracking

(b) C17NTP1 cracking close-up

(c) C17RPT2 overall cracking

(d) C17RTP2 cracking close-up

(e) C17RPT3 overall cracking

(f) C17RTP3 cracking close-up

(g) C17NTP4 overall cracking

(h) C17NTP4 cracking close-up

C-17 passes to rut depth

A summary of C-17 passes to various rut depths of interest are shown in Figures 79 through 82. Rut depths were selected to match those currently defined as threshold values for varying levels of pavement condition determination: low (0.25 in. to 0.5 in.), medium (0.5 in. to 1.0 in.), and high (>1.0 in.). After 1.0 in. of rutting, data were selected in 0.5-in. intervals to monitor performance at excessive rutting levels.

A review of passes to specified rut depth for 1.0-in. HMA, LMS base (Figure 79) indicated that improvement with a reduction in tire pressure was observed at all rutting levels. Passes increased 1.8 times at low-level rutting (0.25 in.) up to over seven times the passes at the highest rutting level (3.0 in.) when compared to normal tire pressure. Similar improvements were observed in the 1.5-in. HMA, LMS base test item (Figure 80).

The 2.5-in. HMA, LMS base reduced tire pressure test item (Figure 81) performed better than the normal tire pressure counterpart, although the magnitude of comparative improvement was not as great as that observed in the thinner asphalt test items. At low-level rutting, the reduced tire pressure test item sustained approximately 1.3 times the passes of the normal tire pressure test item. More meaningful improvements were observed with increased rut depth, ranging from 2.6 times the passes at 1.0-in. rutting up to 3.5 times the passes at 2.5-in. rutting.

Little improvement attributed to a reduction in tire pressure was observed in the 2.5-in. HMA, GR base test item (Figure 82). Performance in the reduced tire pressure test item was found to be 70% of that observed in the normal tire pressure item at low (0.25 in.) and medium (0.50 in.) rutting levels. A slight (10%) improvement was observed at 1.0 in. of rutting, and improvement increased (up to 90% improvement) at 3.0 in. of rutting.

Figure 79. C-17 passes to various rut depths (1.0-in. HMA, LMS base).

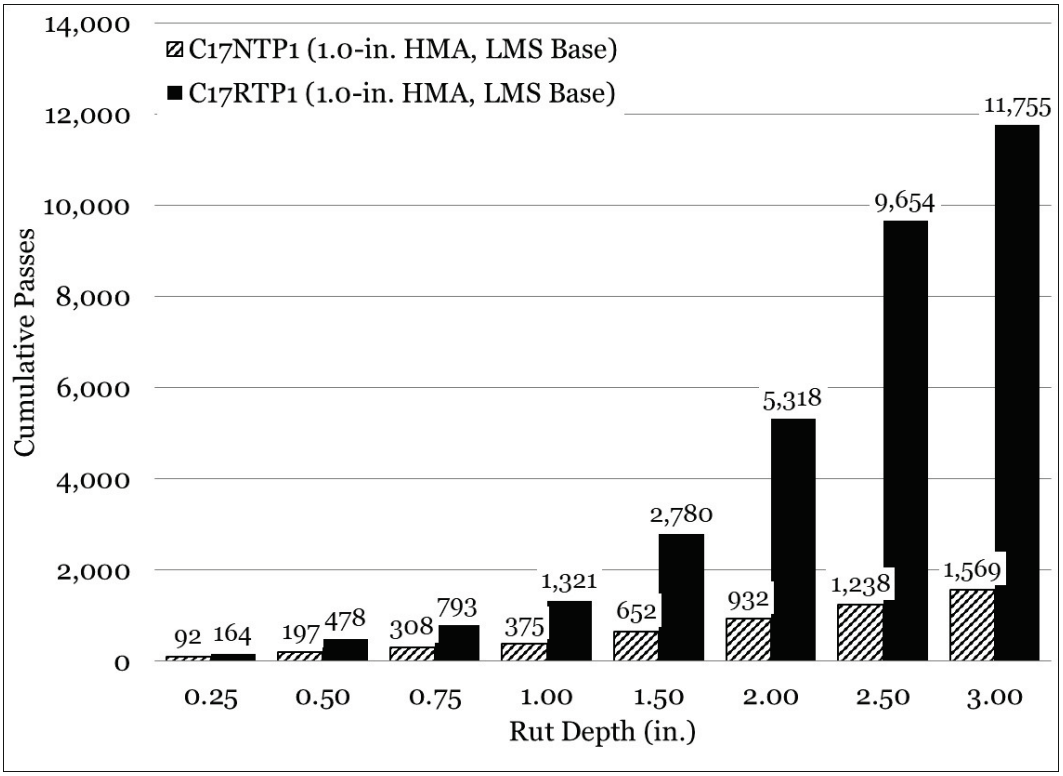

Figure 80. C-17 passes to various rut depths (1.5-in. HMS, LMS base).

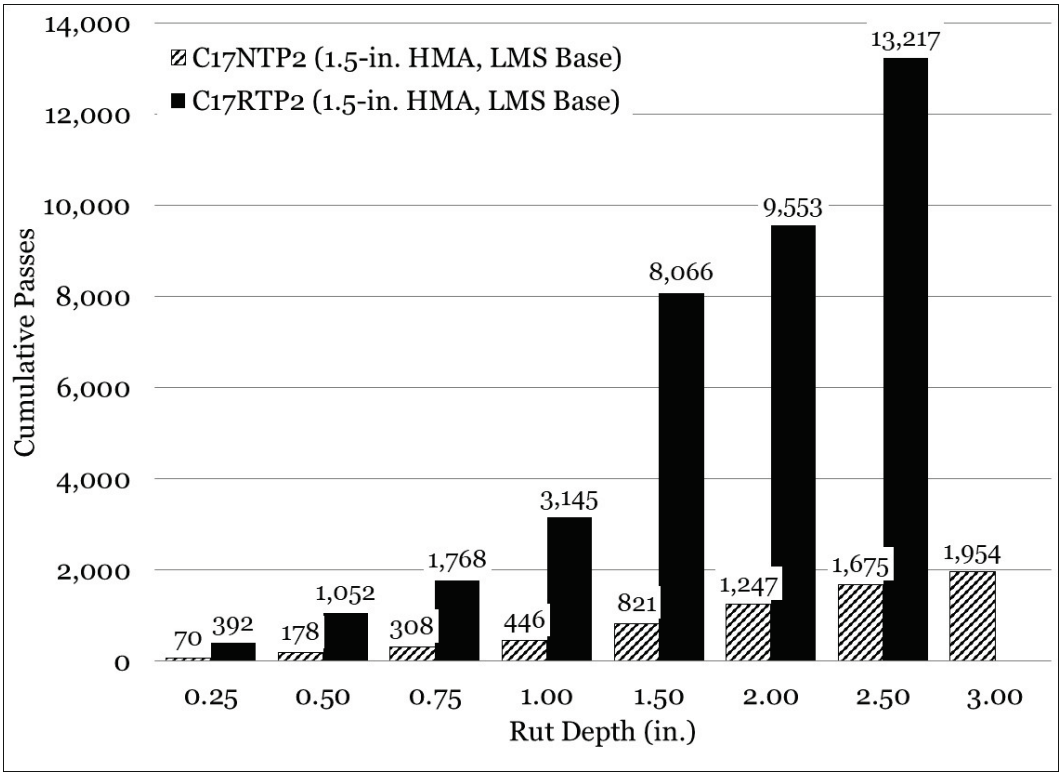

Figure 81. C-17 passes to various rut depths (2.5-in. HMA, LMS base).

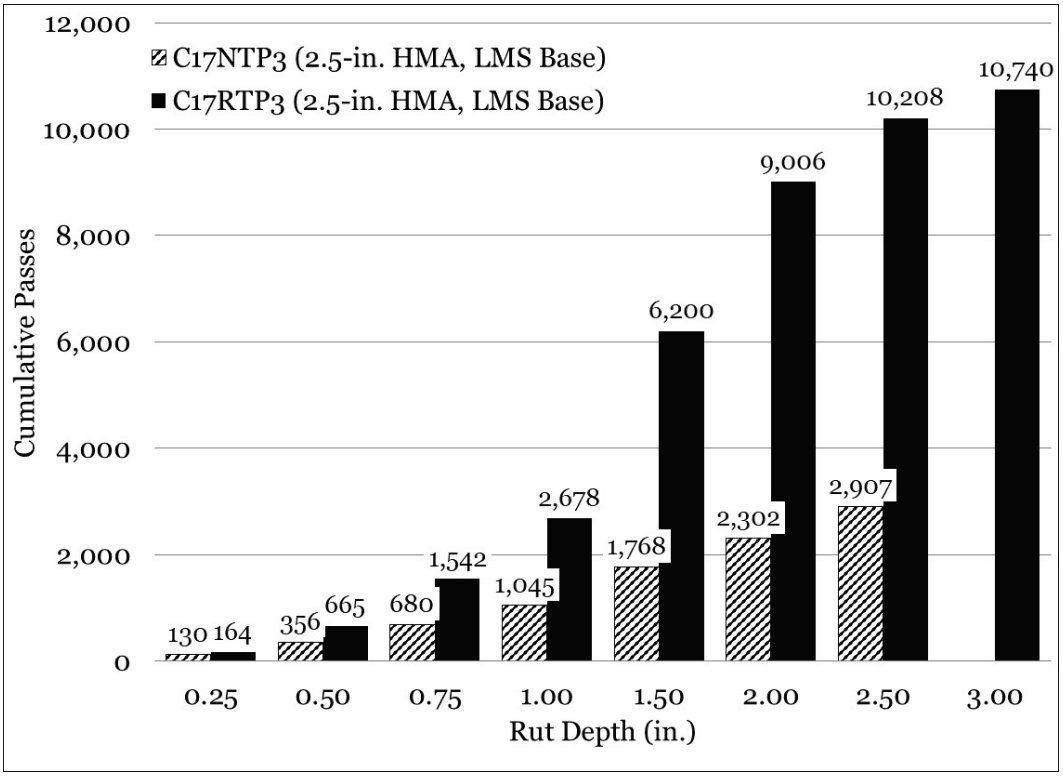

Figure 82. C-17 passes to various rut depths (2.5-in. HMA, GR base).

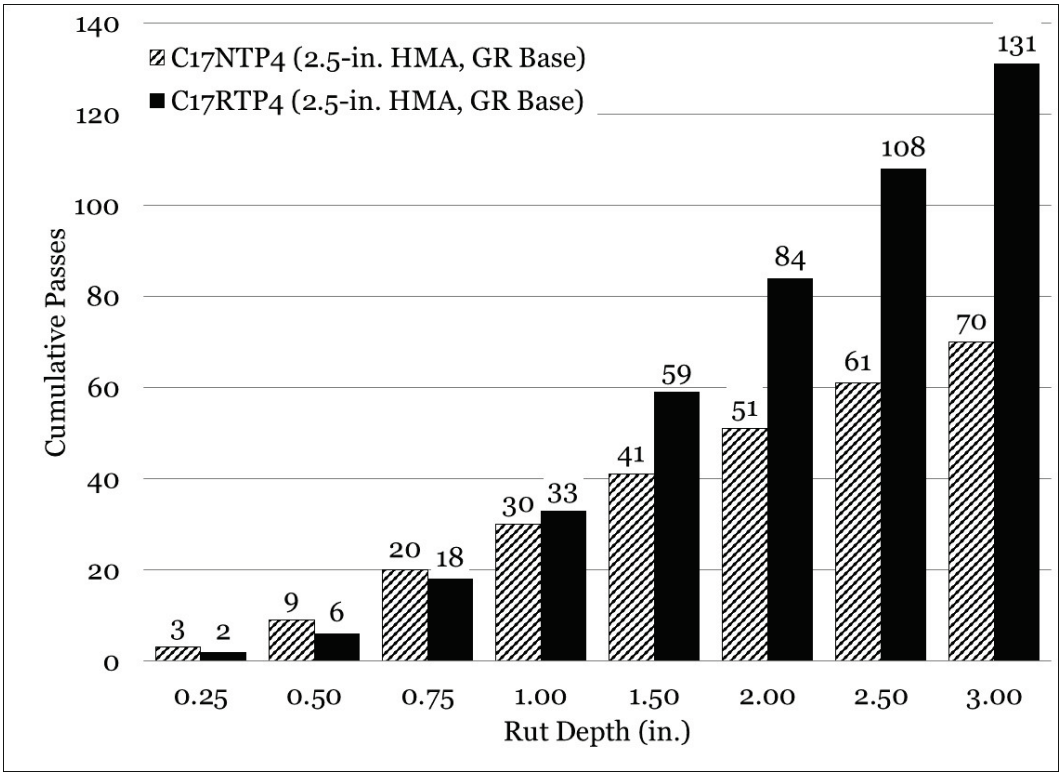

C-17 impulse stiffness

Average ISM values for the normal tire pressure test series are presented in Figure 83. Initial ISM values for the limestone base items were found to follow a logical order in terms of asphalt thickness. C17NPT3 had the highest initial ISM value and was approximately twice as stiff as the companion GR base test item. Differences in C17NTP2 and C17NTP1 were unremarkable, which agrees well with observations in the C-130 test series and supports the observation that the FWD was not capable of detecting the 0.5-in. asphalt thickness difference. Further, this is in general agreement with rut depth observations.

ISM values trended lower with increased traffic, indicating an increase in overall pavement deterioration. It was observed that deterioration trends were similar for all test items. A statistical analysis (Table 27) indicated that all comparisons between the test items were statistically significant.

Figure 83. C-17 normal tire pressure ISM.

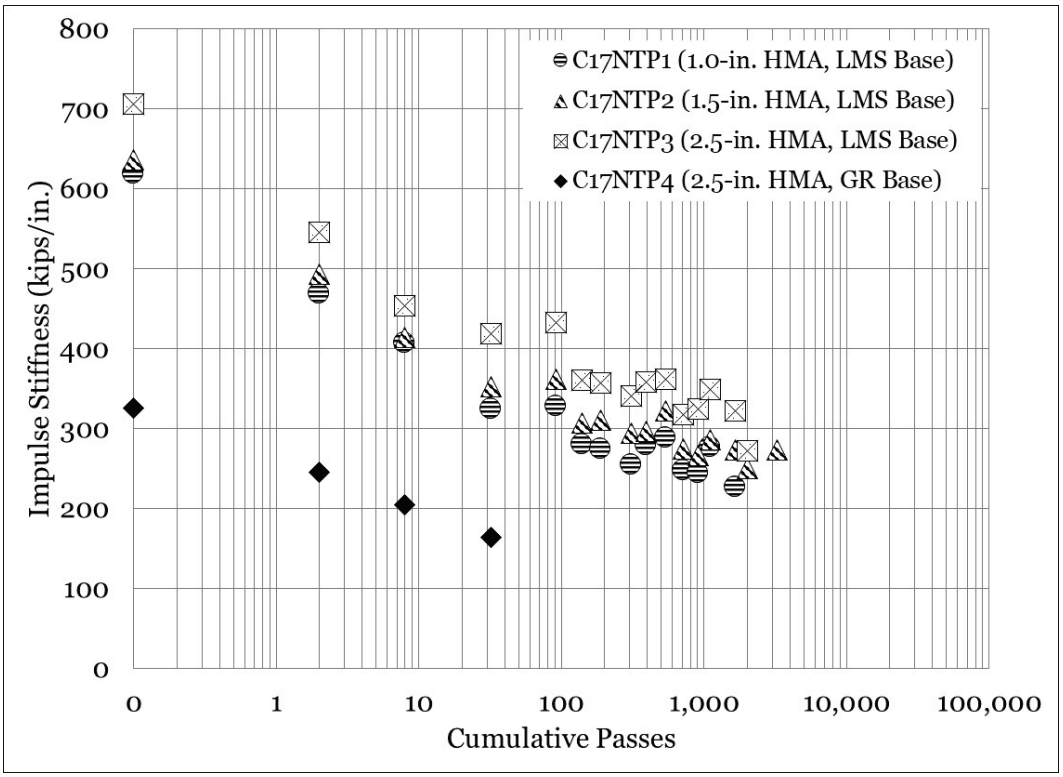

Table 27. Statistical analysis – C-17 normal tire pressure ISM.

Interaction	n	p-value	Significant	Better Performer
C17NTP1 vs. C17NTP2	14	<0.001	Yes	C17NTP2
C17NTP1 vs. C17NTP3	14	<0.001	Yes	C17NTP3
C17NTP1 vs. C17NTP4	4	0.004	Yes	C17NTP1
C17NTP2 vs. C17NTP3	15	<0.001	Yes	C17NTP3
C17NTP2 vs. C17NTP4	4	0.003	Yes	C17NTP2
C17NTP3 vs. C17NTP4	4	0.002	Yes	C17NTP3

Average ISM values for the reduced tire pressure test series are shown in Figure 84. Differences in initial ISM were relatively small for the LMS base test items, particularly when benchmarked against the strongest test item (C17RTP3); however, all were found to be statistically significant (Table 28). A 2% difference was observed in initial ISM for C17RTP3 and C17RTP2, which could explain the observed similar rut depth development. Similar to the normal tire pressure test series, a reduction in base course CBR resulted in a meaningful decrease in initial ISM. It was found that reducing base course CBR from 100 to 47 resulted in a 44% decrease in initial ISM.

Figure 84. C-17 reduced tire pressure ISM.

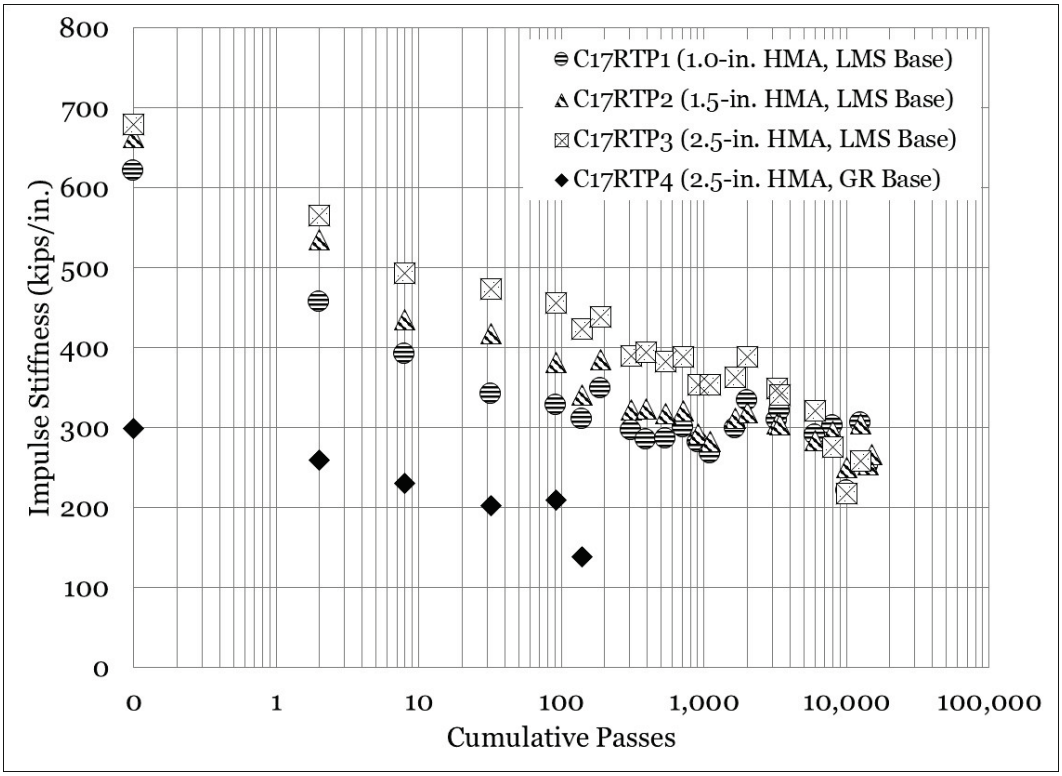

Table 28. Statistical analysis – C-17 reduced tire pressure ISM.

Interaction	n	p-value	Significant	Better Performer
C17RTP1 vs. C17RTP2	22	0.001	Yes	C17RTP2
C17RTP1 vs. C17RTP3	21	<0.001	Yes	C17RTP3
C17RTP1 vs. C17RTP4	6	0.001	Yes	C17RTP1
C17RTP2 vs. C17RTP3	21	<0.001	Yes	C17RTP3
C17RTP2 vs. C17RTP4	6	<0.001	Yes	C17RTP2
C17RTP3 vs. C17RTP4	6	<0.001	Yes	C17RTP3

Equality plots for C-17 ISM are shown in Figures 85 through 88. In most cases, the data were found to plot on or above the LOE. At lower ISM values, it was observed that data plotted nearly exclusively above the LOE, suggesting that reducing tire pressure reduced the rate of pavement structural deterioration. A statistical analysis (Table 29) found that all comparisons made for LMS base test items were statistically significant and that average ISM was higher in the reduced tire pressure test items. Comparison of the gravel test items was not statistically significant (p-value = 0.418), indicating ISM was statistically equivalent for all observed values.

Figure 85. Equality plot – C-17 ISM (1.0-in. HMA, LMS base).

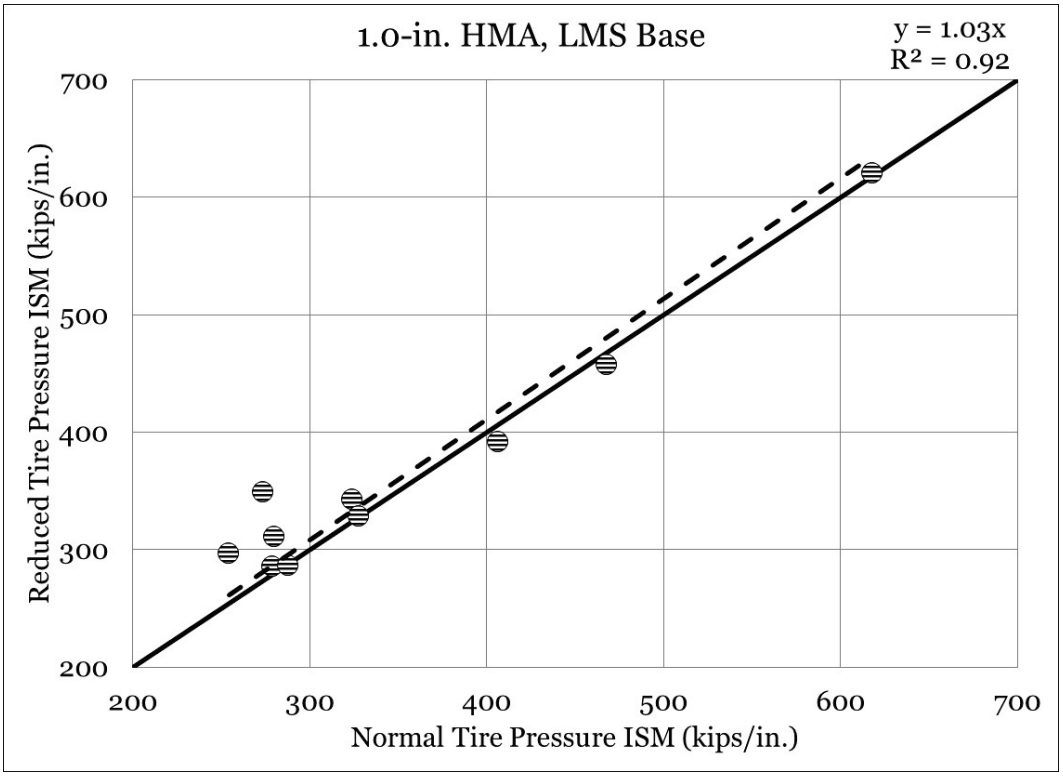

Figure 86. Equality plot – C-17 ISM (1.5-in. HMA, LMS base).

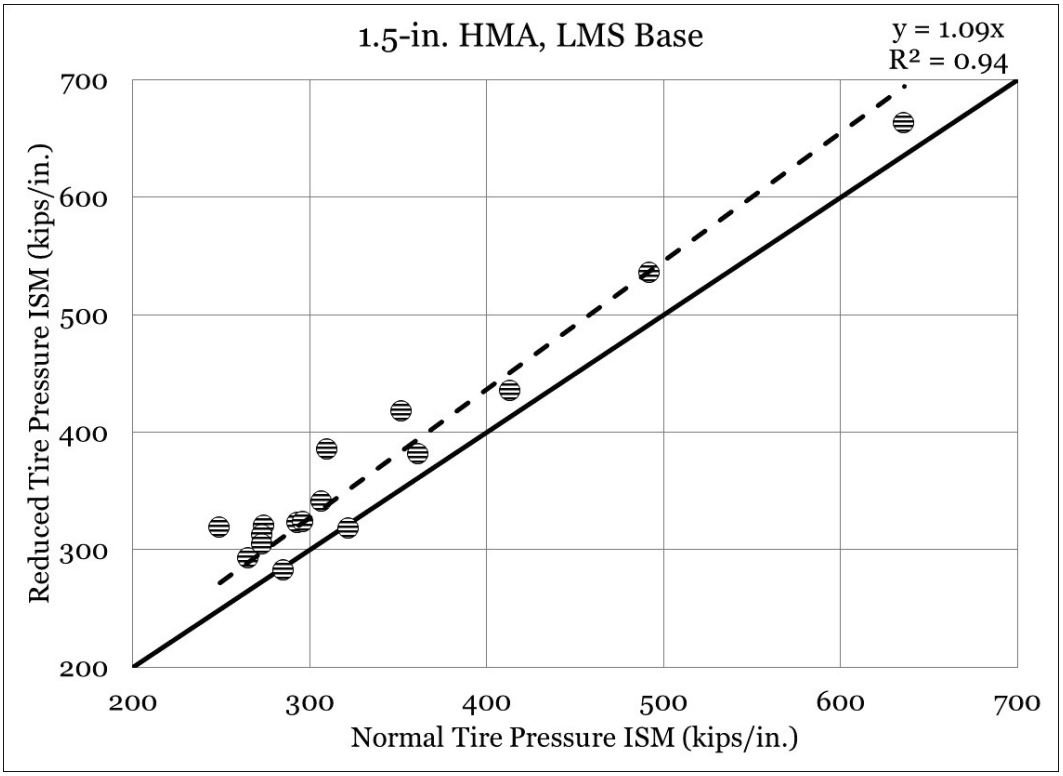

Figure 87. Equality plot – C-17 ISM (2.5-in. HMS, LMS base).

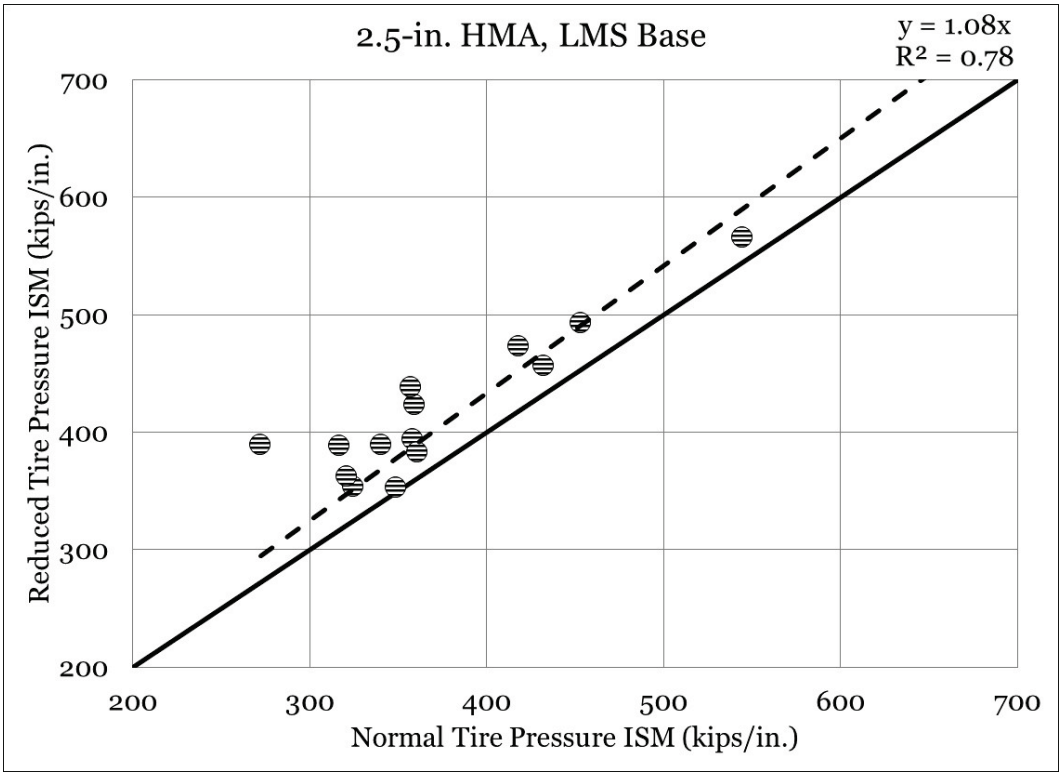

Figure 88. Equality plot – C-17 ISM (2.5-in. HMA, GR base).

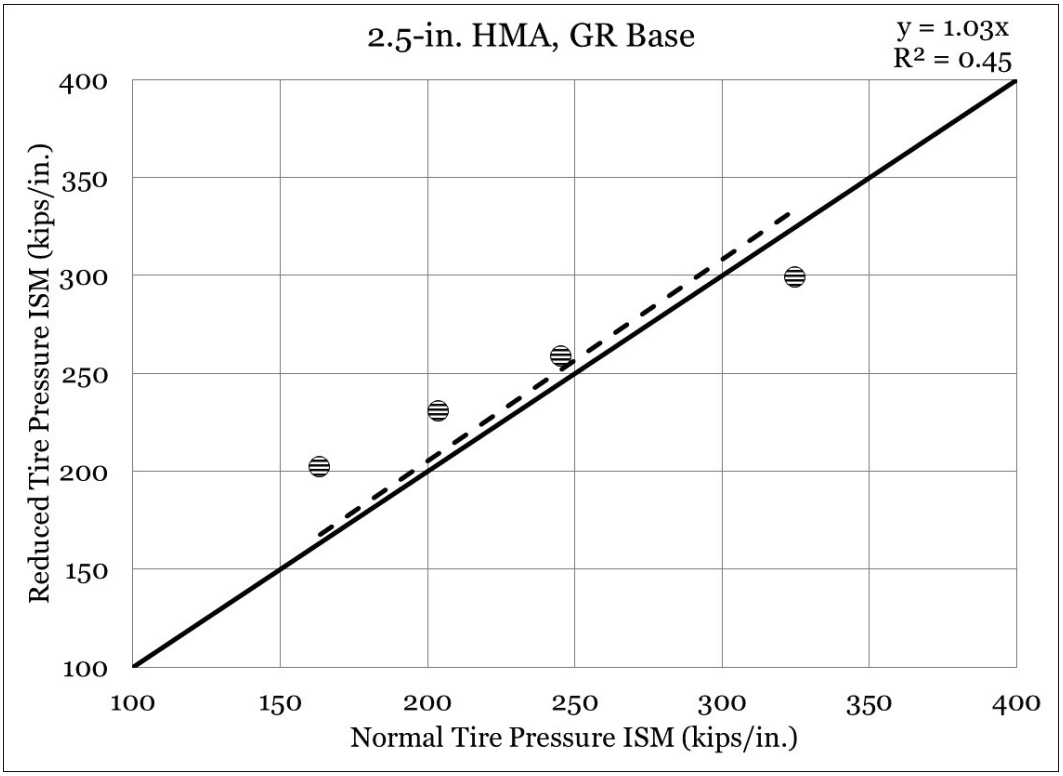

Table 29. Statistical analysis – C-17 ISM and tire pressure.

Interaction	n	p-value	Significant	Better Performer
C17NTP1 vs. C17RTP1	14	0.022	Yes	C17RTP1
C17NTP2 vs. C17RTP2	16	<0.001	Yes	C17RTP2
C17NTP3 vs. C17RTP3	15	<0.001	Yes	C17RTP3
C17NTP4 vs. C17RTP4	4	0.418	No	Same

C-17 subgrade pressure response

Subgrade vertical pressure response data for the C-17 normal tire pressure test series are presented in Figure 89. Subgrade vertical pressures were found to increase with increasing traffic, and subgrade vertical pressures were found to be consistently higher in C17NTP4 (2.5-in. HMA, GR base). Subgrade pressure in the LMS base test items was found to generally achieve steady-state after approximately 300 passes, which, when compared to approximately 200 passes for the C-130 test series, indicated that the increased load resulted in further densification or particle reorientation. Overall, subgrade pressures followed a logical order: thinner asphalt thickness resulted in higher pressures.

Figure 89. C-17 normal tire pressure subgrade pressure response.

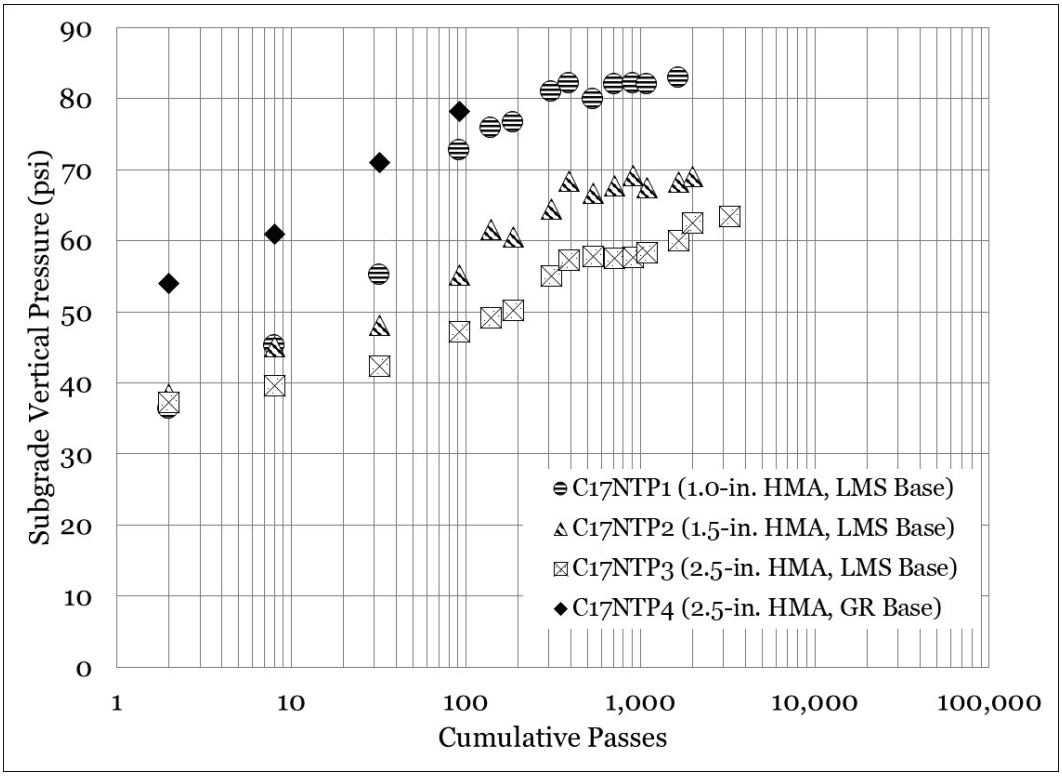

Statistical comparisons for subgrade pressure are summarized in Table 30. It was found that all comparisons were statistically significant and that average subgrade pressures in C17NTP4 were higher than those observed in all other test sections; thus, additional asphalt thickness was not capable of significantly reducing subgrade pressure when the pavement contained a much weaker base course. It was found that increased asphalt thickness (i.e., moving from thin to thicker pavement cross section) in the LMS base items resulted in statistically significant reductions in average subgrade pressure.

Table 30. Statistical analysis – C-17 normal tire pressure subgrade pressure.

Interaction	n	p-value	Significant	Better Performer
C17NTP1 vs. C17NTP2	13	<0.001	Yes	C17NTP2
C17NTP1 vs. C17NTP3	13	<0.001	Yes	C17NTP3
C17NTP1 vs. C17NTP4	4	0.016	Yes	C17NTP1
C17NTP2 vs. C17NTP3	14	<0.001	Yes	C17NTP3
C17NTP2 vs. C17NTP4	4	0.003	Yes	C17NTP2
C17NTP3 vs. C17NTP4	4	0.005	Yes	C17NTP3

Subgrade pressure response for the reduced tire pressure test series is presented in Figure 90. Similar to the normal tire pressure test series, the highest subgrade pressure was observed in C17RTP4 (2.5-in. HMA, GR base) until traffic was suspended. Unlike the normal tire pressure test series, a steady-state subgrade pressure condition was more difficult to define, although it appeared the pressure tended to level around 1,500 passes. This could suggest that reducing tire pressure effectively extends the period of initial densification or shakedown of the pavement structure. Comparatively, higher subgrade pressure was observed in C17RTP1 (1.0-in. HMA, LMS base) than in C17RTP2 and C17RTP3. Differences in C17RTP2 and C17RTP3 were not as noticeable as those observed in the normal tire pressure test series, which is consistent with both rutting and ISM observations.

A statistical analysis (Table 31) indicated that all comparisons were statistically significant. It should be noted C17RTP2 was found to be statistically different from C17RTP3, and that C17RTP2 had a lower average subgrade pressure than C17RTP3.

Figure 90. C-17 reduced tire pressure subgrade pressure response.

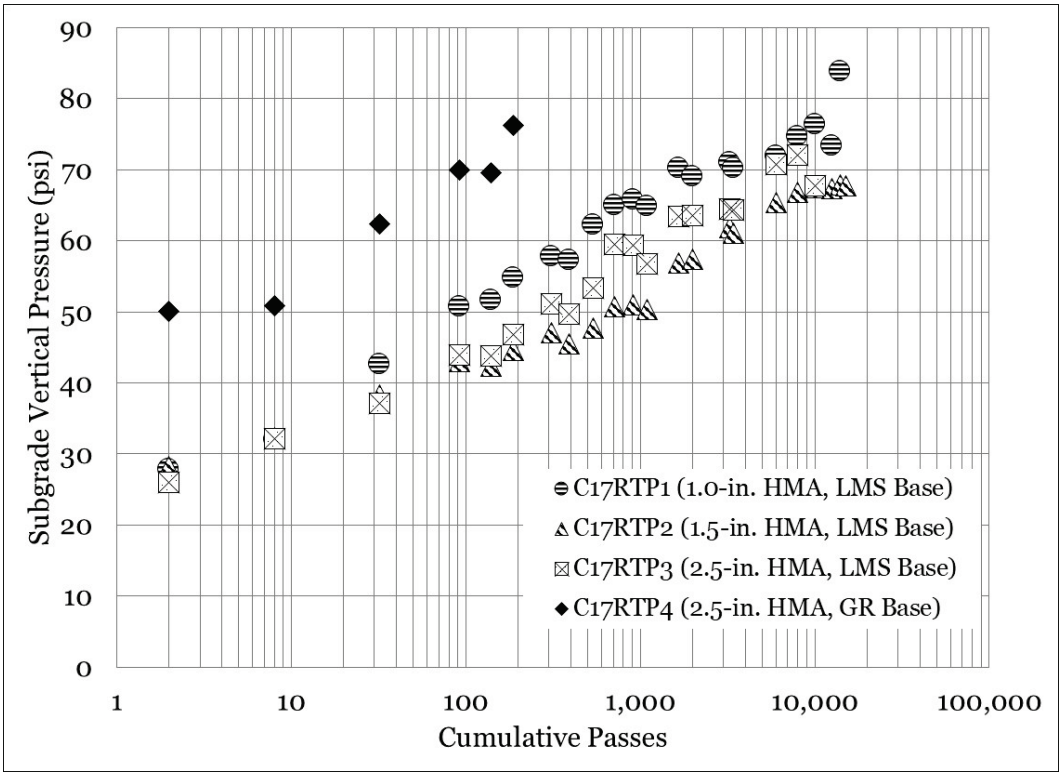

Table 31. Statistical analysis – C-17 reduced tire pressure subgrade pressure.

Interaction	n	p-value	Significant	Better Performer
C17RTP1 vs. C17RTP2	21	<0.001	Yes	C17RTP2
C17RTP1 vs. C17RTP3	19	<0.001	Yes	C17RTP3
C17RTP1 vs. C17RTP4	6	<0.001	Yes	C17RTP1
C17RTP2 vs. C17RTP3	19	<0.001	Yes	C17RTP2
C17RTP2 vs. C17RTP4	6	<0.001	Yes	C17RTP2
C17RTP3 vs. C17RTP4	6	<0.001	Yes	C17RTP3

Equality plots for reduced and normal tire pressure subgrade pressure response are presented in Figures 91 through 94. Subgrade pressure response for the reduced tire pressure test was plotted on the y-axis, and subgrade pressure response for the normal tire pressure was plotted on the x-axis. The LOE is represented by a solid line, and a best-fit linear trend (with y-intercept = 0) is represented by a dashed line. Data plotted below the LOE indicate better performance (i.e., comparatively lower subgrade pressures).

A review of the 1.0-in. HMA, LMS base plot (Figure 91) showed that the data plotted below the LOE, indicating that subgrade pressure was consistently lower in the reduced tire pressure test item. The fitted trend line suggested that subgrade pressure in the reduced tire pressure test item was approximately 25% lower than that in the normal tire pressure test item.

Similarly, in the 1.5-in. HMA, LMS base plot (Figure 92), an approximate 25% reduction in subgrade base pressure was observed in the reduced tire pressure test item. It was noted that all data plotted below the LOE, indicating that subgrade pressures were consistently lower in the reduced tire pressure test item.

The 2.5-in. HMA, LMS base equality plot (Figure 93) showed that the data plotted below the LOE in some cases and above in others. The fitted trend line indicated that the reduced tire pressure test item had a subgrade pressure approximately 5% lower than the normal tire pressure item, representing a smaller increase than that observed in other LMS base test items.

A review of the 2.5-in. HMA, GR base equality plot (Figure 94) indicated that reducing tire pressure resulted in an approximate 12% reduction in subgrade pressure.

Figure 91. Equality plot – C-17 subgrade pressure response (1.0-in. HMA, LMS base).

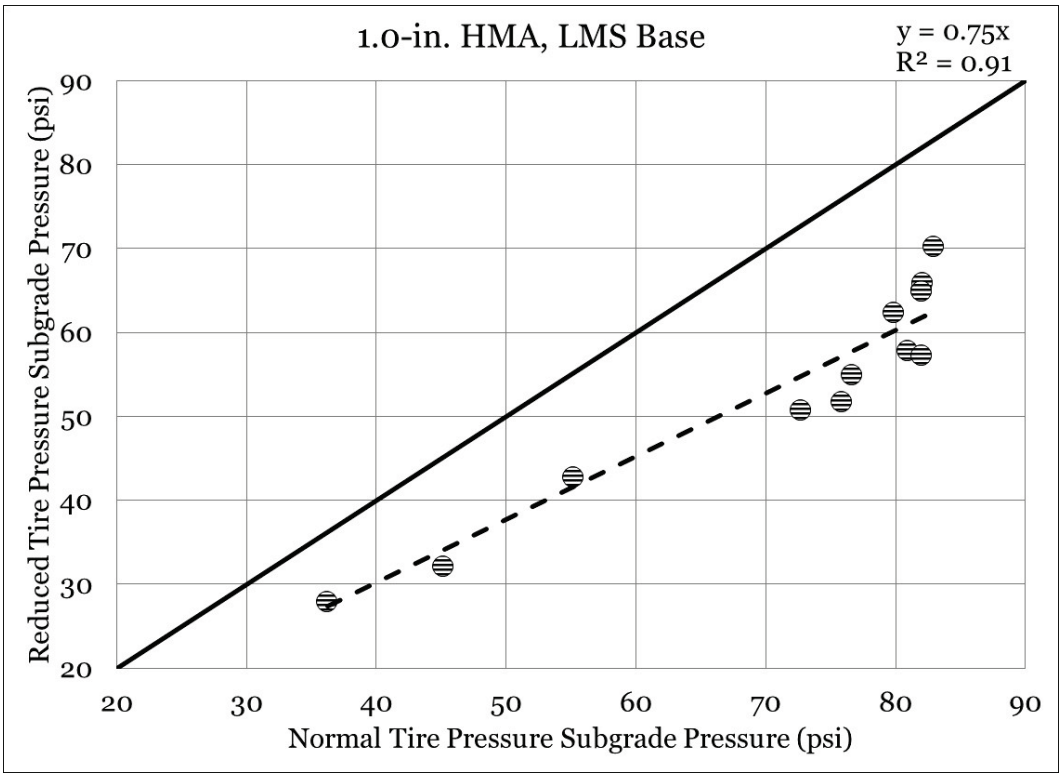

Figure 92. Equality plot – C-17 subgrade pressure response (1.5-in. HMA, LMS base).

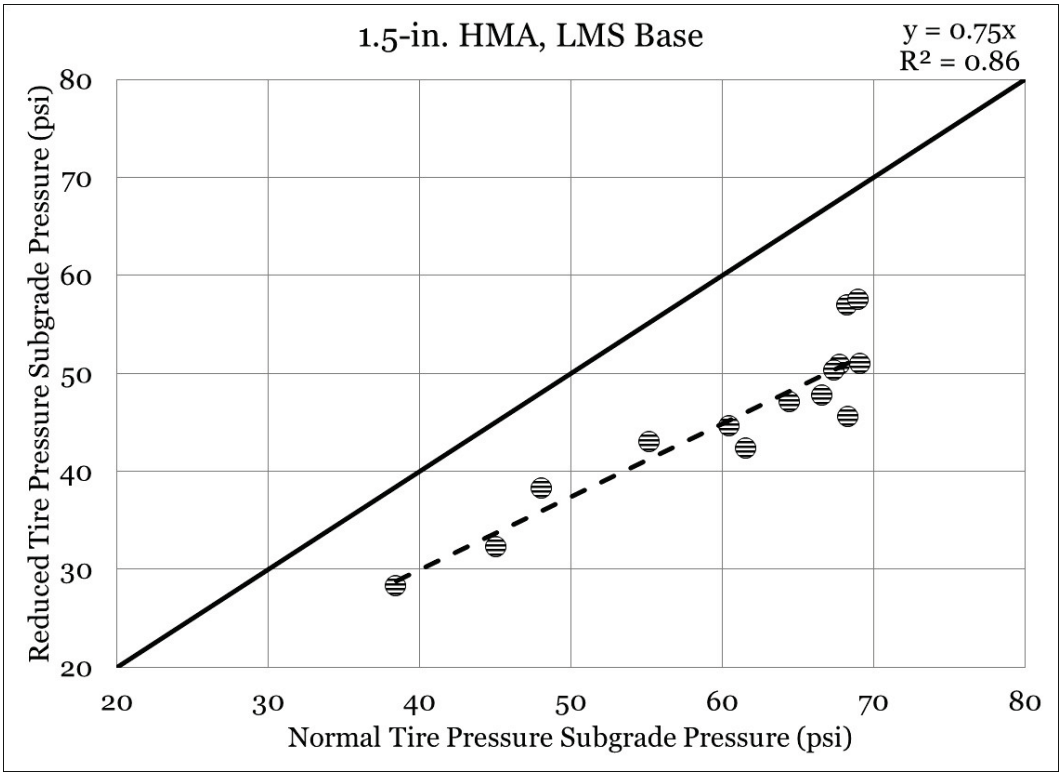

Figure 93. Equality plot – C-17 subgrade pressure response (2.5-in. HMA, LMS base).

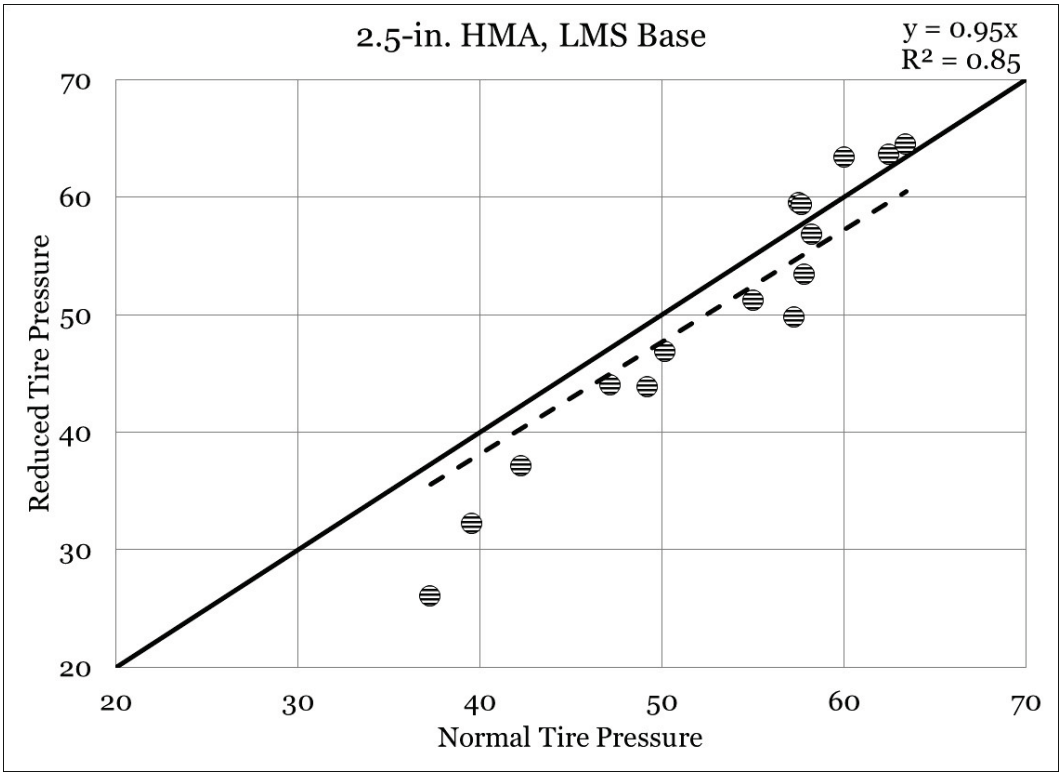

Figure 94. Equality plot – C-17 subgrade pressure response (2.5-in. HMA, GR base).

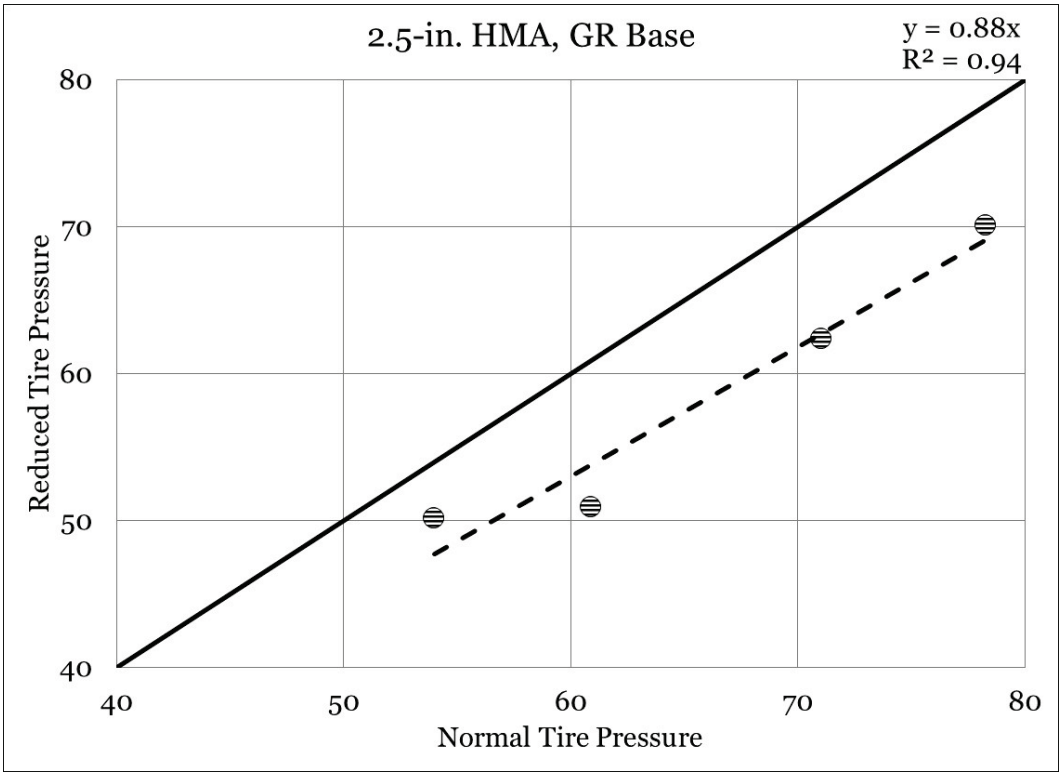

A statistical analysis (Table 32) found that all comparisons between companion normal and reduced tire pressure test items were statistically significant and that, in all cases, average measured subgrade response was lower in the reduced tire pressure test series.

Table 32. Statistical analysis – C-17 subgrade pressure and tire pressure.

Interaction	n	p-value	Significant	Better Performer
C17NTP1 vs. C17RTP1	13	<0.001	Yes	C17RTP1
C17NTP2 vs. C17RTP2	14	<0.001	Yes	C17RTP2
C17NTP3 vs. C17RTP3	15	0.016	Yes	C17RTP3
C17NTP4 vs. C17RTP4	4	0.010	Yes	C17RTP4

C-17 base pressure response

Base pressure response for the normal tire pressure test series is shown in Figure 95. Initial measured pressures in C17NTP4 (2.5-in. HMA, GR base) and C17NTP1 (1.0-in. HMA, LMS base) were observed to be similar (the weaker base was only slightly higher), suggesting that an additional 1.5 in. of asphalt could not overcome the weaker base course. Similarly, initial base pressures in C17NTP2 (1.5-in. HMA, LMS base) and C17NTP3 (2.5-in.

HMA, LMS base) were observed to be nearly equivalent. This suggested that at the C-17 load and tire pressure, the addition of 1.0-in. of asphalt did not have a meaningful effect on measured base pressure. It was observed that, unlike other observed response data, where performance diverged after a period of initial densification or shakedown, initial similarities in measured response remained consistent throughout traffic application.

A statistical analysis (Table 33) found that the observed difference between C17NTP2 (1.5-in. HMA, LMS base) and C17NTP3 (2.5-in. HMA, LMS base) was not statistically significant (p-value = 0.171), which was consistent with visual inspection. All other comparisons were found to be statistically significant, and it was noted that an increase in asphalt thickness resulted in a decrease in average measured base pressure. All LMS base test items were found to have statistically lower average base pressure than the GR base test item, as expected.

Figure 95. C-17 normal tire pressure base pressure response.

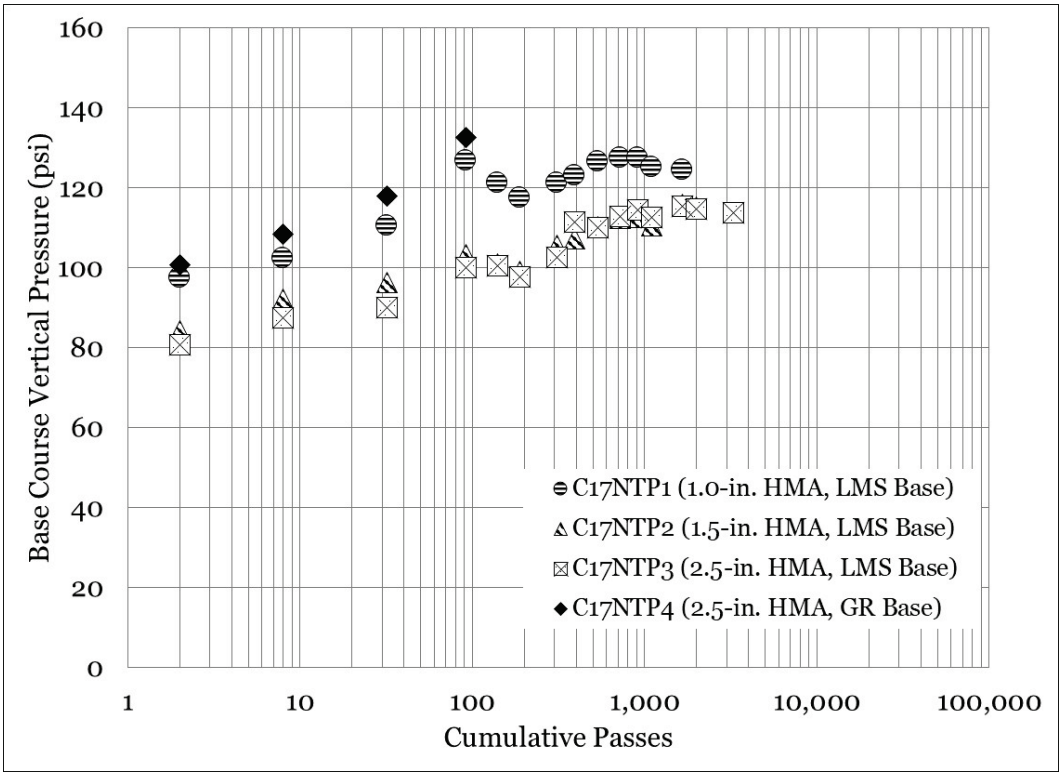

Table 33. Statistical analysis – C-17 normal tire pressure base pressure.

Interaction	n	p-value	Significant	Better Performer
C17NTP1 vs. C17NTP2	13	<0.001	Yes	C17NTP2
C17NTP1 vs. C17NTP3	13	<0.001	Yes	C17NTP3
C17NTP1 vs. C17NTP4	4	0.006	Yes	C17NTP1
C17NTP2 vs. C17NTP3	14	0.171	No	Same
C17NTP2 vs. C17NTP4	4	0.006	Yes	C17NTP2
C17NTP3 vs. C17NTP4	4	0.003	Yes	C17NTP3

Base pressure response for the reduced tire pressure test series is shown in Figure 96. Initial base pressure response was found to be highest in C17RTP4 (2.5-in. HMA, GR base) as expected. Similar to the normal tire pressure test series, initial base pressures in C17RTP2 and C17RTP3 were found to be practically equivalent. It was observed that similarities in base pressure began to diverge after initial traffic, suggesting that the reduction of tire pressure resulted in a meaningful difference in pressure response that was not observed in the normal tire pressure test series.

A statistical comparison summarized in Table 34 indicated that all comparisons were statistically significant. An increase in asphalt thickness generally resulted in a decrease in average base pressure; however, it was found that C17RTP2 had a lower average base pressure than C17RTP3.

Figure 96. C-17 reduced tire pressure base pressure response.

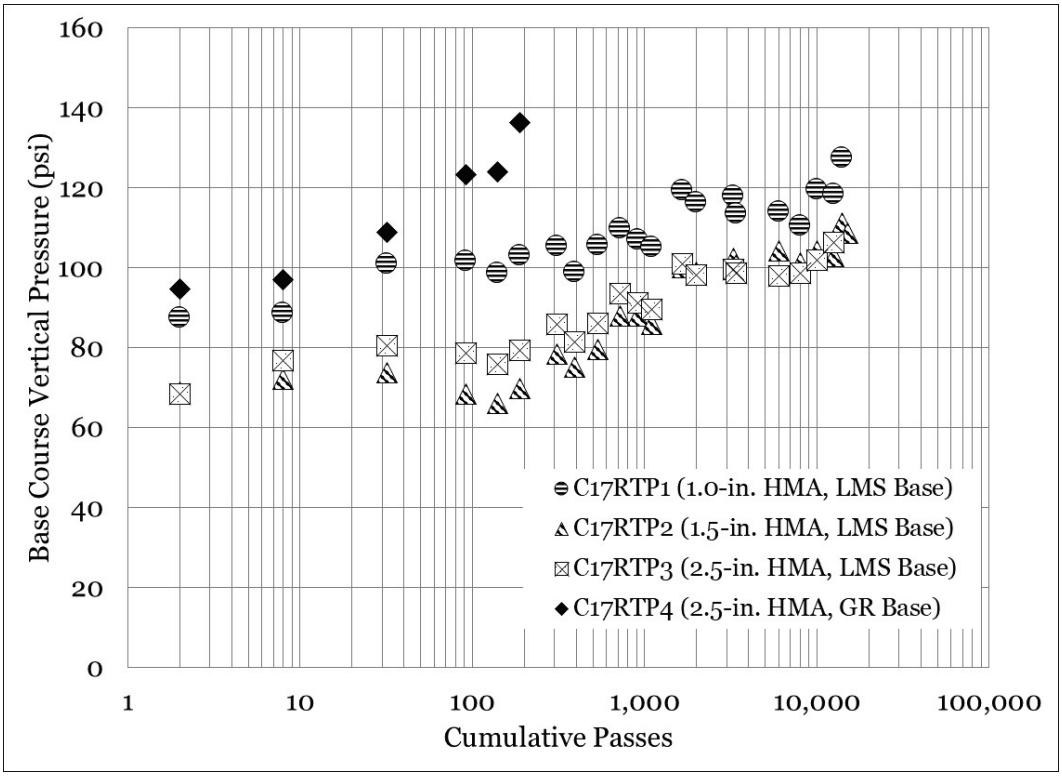

Table 34. Statistical analysis – C-17 reduced tire pressure base pressure.

Interaction	n	p-value	Significant	Better Performer
C17RTP1 vs. C17RTP2	21	<0.001	Yes	C17RTP2
C17RTP1 vs. C17RTP3	20	<0.001	Yes	C17RTP3
C17RTP1 vs. C17RTP4	6	0.012	Yes	C17TRP1
C17RTP2 vs. C17RTP3	20	0.012	Yes	C17RTP2
C17RTP2 vs. C17RTP4	6	0.002	Yes	C17RTP2
C17RTP3 vs. C17RTP4	6	0.001	Yes	C17RTP3

Equality plots for reduced and normal tire pressure base pressure response are presented in Figures 97 through 100. Base pressure response for the reduced tire pressure test was plotted on the y-axis, and base pressure response for the normal tire pressure was plotted on the x-axis. The LOE is represented by a solid line, and a best-fit linear trend (with y-intercept = 0) is represented by a dashed line. Data plotted below the LOE indicated better performance (i.e., comparatively lower base pressure).

A review of the 1.0-in. HMA, LMS plot (Figure 97) revealed that the data consistently plotted below the LOE, indicating that reducing tire pressure was successful in reducing measured base pressure. The fitted trend line

suggested that base pressure in the reduced tire pressure test item was approximately 85% of that observed in the normal tire pressure test item.

Similarly, data consistently plotted below the LOE for the 1.5-in. HMA, LMS base (Figure 98) and 2.5-in. HMA, LMS base (Figure 99) test item comparisons. The fitted trend line indicated that base pressure in the reduced tire pressure test item was approximately 75% of that observed in the normal tire pressure test series for the 1.5-in. HMA, LMS base test and 82% for the 2.5-in. HMA, LMS base test.

A lesser reduction was observed in the 2.5-in. HMA, GR base test item (Figure 100), and the fitted trend line indicated that the reduced tire pressure item experienced base pressure 92% of the normal tire pressure test item. While all data plotted below the LOE, the reduced pressure did not result in a meaningful difference in rutting performance.

A summary of the statistical analysis for C-17 base pressure as a function of tire pressure is shown in Table 35. All comparisons were found to be statistically significant, indicating that reducing tire pressure had a meaningful impact on measured base pressure. It was found that, in each case, the reduced tire pressure item had statistically lower base pressure than the normal tire pressure counterpart.

Figure 97. Equality plot – C-17 base pressure response (1.0-in. HMA, LMS base).

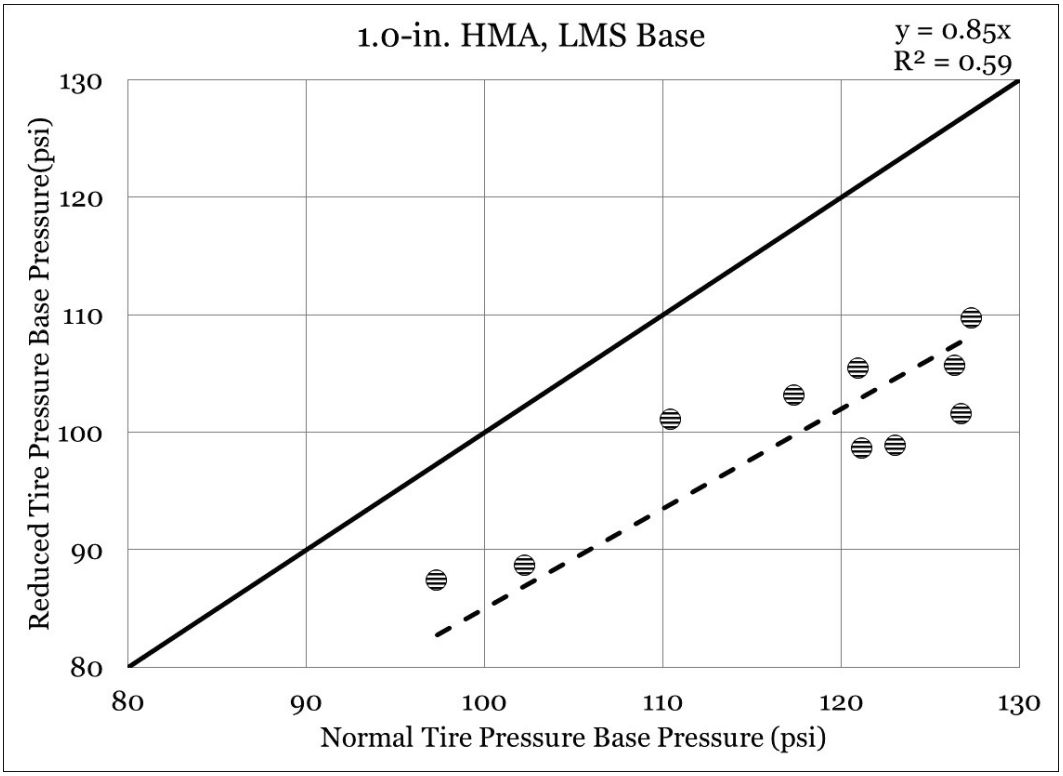

Figure 98. Equality plot – C-17 base pressure response (1.5-in. HMA, LMS base).

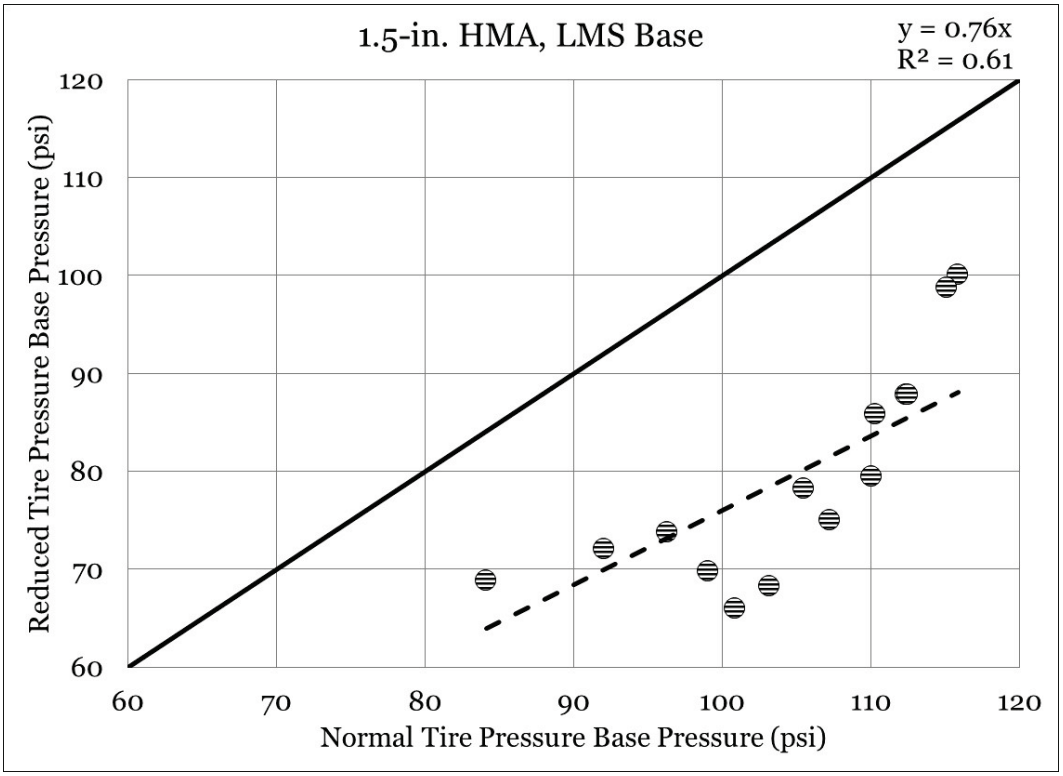

Figure 99. Equality plot – C-17 base pressure response (2.5-in. HMA, LMS base).

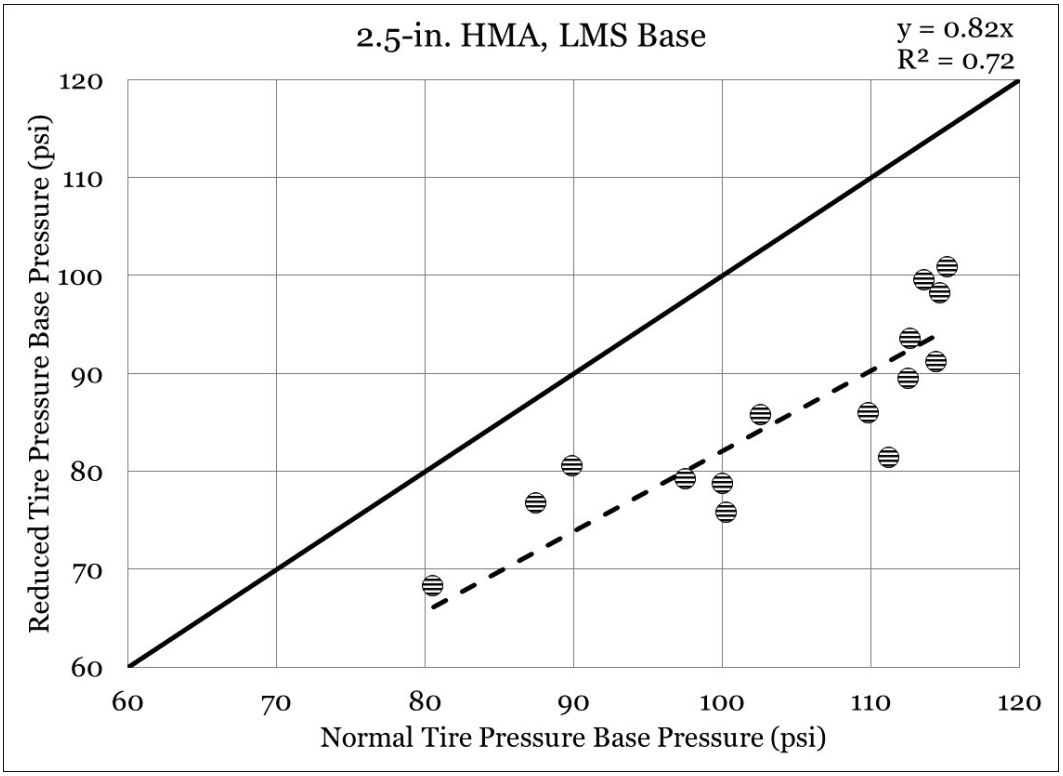

Figure 100. Equality plot – C-17 base pressure response (2.5-in. HMA, GR base).

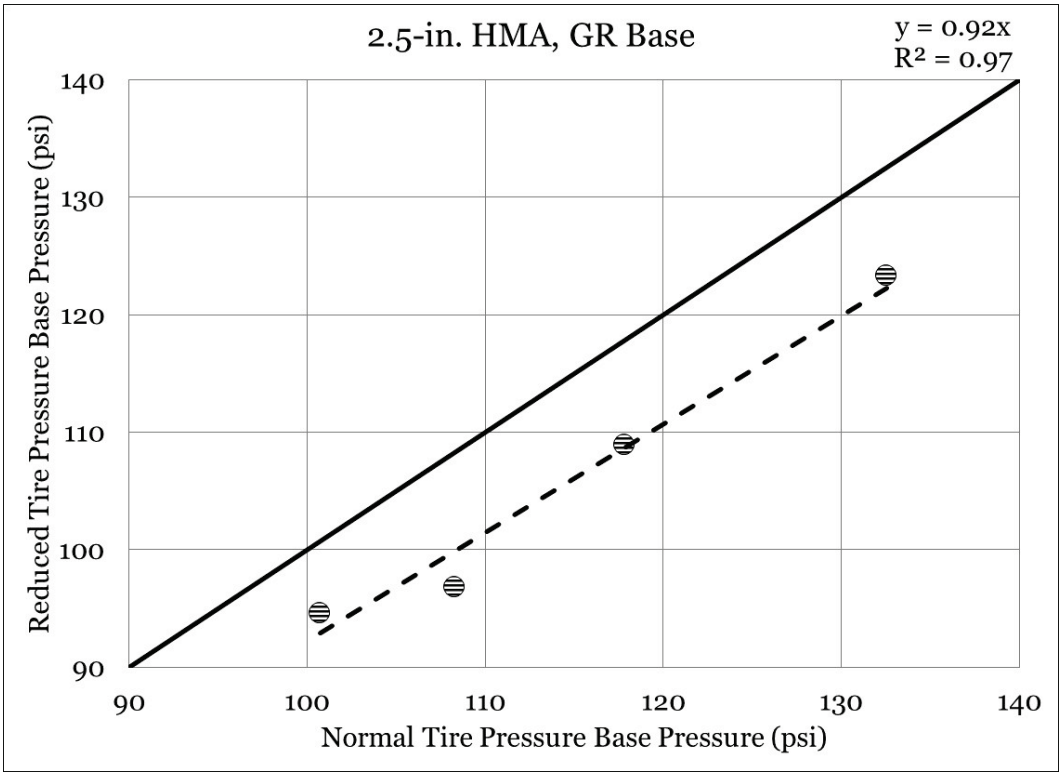

Table 35. Statistical analysis – C-17 base pressure and tire pressure.

Interaction	n	p-value	Significant	Better Performer
C17NTP1 vs. C17RTP1	13	<0.001	Yes	C17RTP1
C17NTP2 vs. C17RTP2	14	<0.001	Yes	C17RTP2
C17NTP3 vs. C17RTP3	15	<0.001	Yes	C17RTP3
C17NTP4 vs. C17RTP4	4	0.004	Yes	C17RTP4

C-17 single-depth deflectometer response

A summary of SDD response for the normal tire pressure test series is shown in Figure 101. It should be noted that the SDD installed in C17NTP4 (2.5-in. HMA, GR base) failed during construction; thus, no usable data were available and the test item was omitted from the summary plot. Minor differences were observed in C17NTP1 (1.0-in. HMA, LMS base) and C17NTP2 (1.5-in. HMA, LMS base), both initially and throughout traffic application, suggesting that the additional 0.5-in. HMA did not have a meaningful impact on subgrade deflection. However, C17NTP3 (2.5-in. HMA, LMS base) was found to be a clearly better performer, notable after approximately 30 traffic passes.

Figure 101. C-17 normal tire pressure total subgrade deflection.

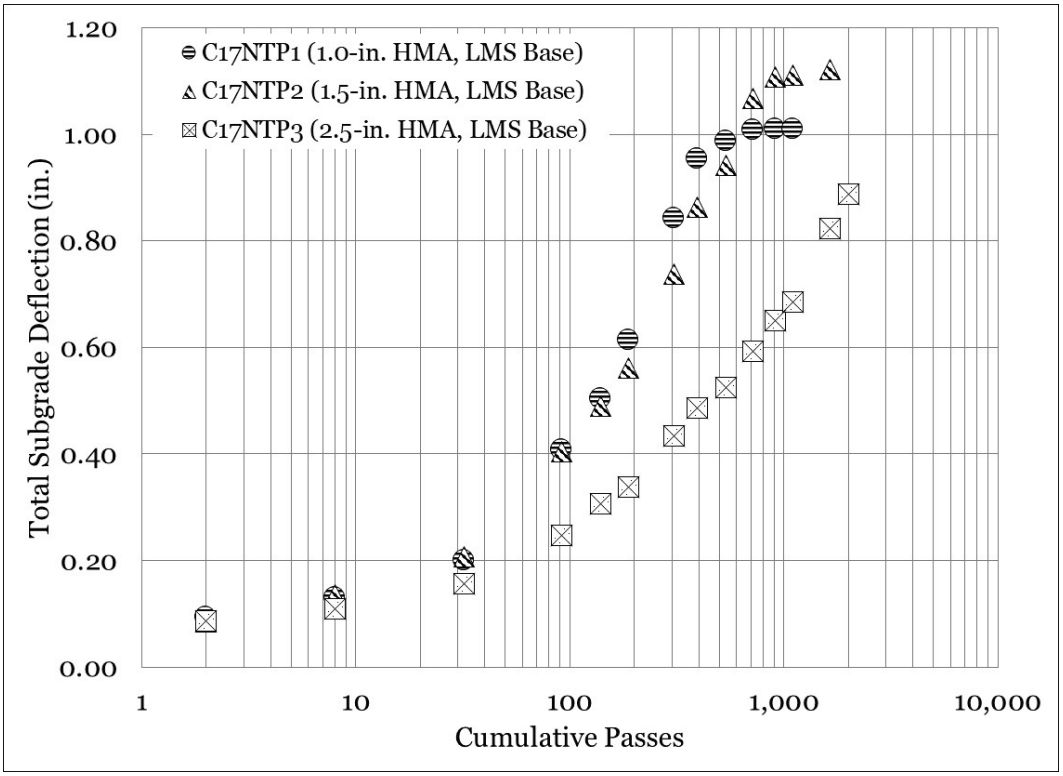

A statistical comparison (Table 36) confirmed that the differences in C17NTP1 and C17NTP2 were not statistically significant (p-value = 0.834). As expected, statistically significant differences were observed in comparisons to C17NTP3, in which C17NTP3 was found to have lower average subgrade deflection.

Table 36. Statistical analysis – C-17 normal tire pressure subgrade deflection.

Interaction	n	p-value	Significant	Better Performer
C17NTP1 vs. C17NTP2	12	0.834	No	Same
C17NTP1 vs. C17NTP3	12	<0.001	Yes	C17NTP3
C17NTP1 vs. C17NTP4	ND	ND	ND	ND
C17NTP2 vs. C17NTP3	13	<0.001	Yes	C17NTP3
C17NTP2 vs. C17NTP4	ND	ND	ND	ND
C17NTP3 vs. C17NTP4	ND	ND	ND	ND

Total subgrade deflection for the reduced tire pressure test series is shown in Figure 102. C17TRP4 (2.5-in. HMA, GR base) had the highest and most rapid increase in subgrade deflection, which was expected due to the weaker gravel base course. The LMS base items followed logical trends, and decreasing deflections were observed with increases in asphalt thickness.

The statistical comparison for subgrade deflection in the reduced tire pressure test series is summarized in Table 37. It was found that all comparisons were statistically significant and that C17RTP4 had the highest average subgrade deflection in all cases. Statistically, an increase in asphalt thickness resulted in a significant decrease in measured subgrade deflection. C17RTP3 was found to have the lowest average subgrade deflection.

Equality plots for subgrade deflection are shown in Figures 103 through 105. Total subgrade deflection for the reduced tire pressure item was plotted on the y-axis, and total subgrade deflection for the normal tire pressure item was plotted on the x-axis. The solid line represents the LOE, and the dashed line represents the best-fit linear trend line through the data, where the y-intercept was set equal to zero. Data plotted below the LOE indicated lower subgrade deflection (i.e., improved performance from reduced tire pressure).

Figure 102. C-17 reduced tire pressure total subgrade deflection.

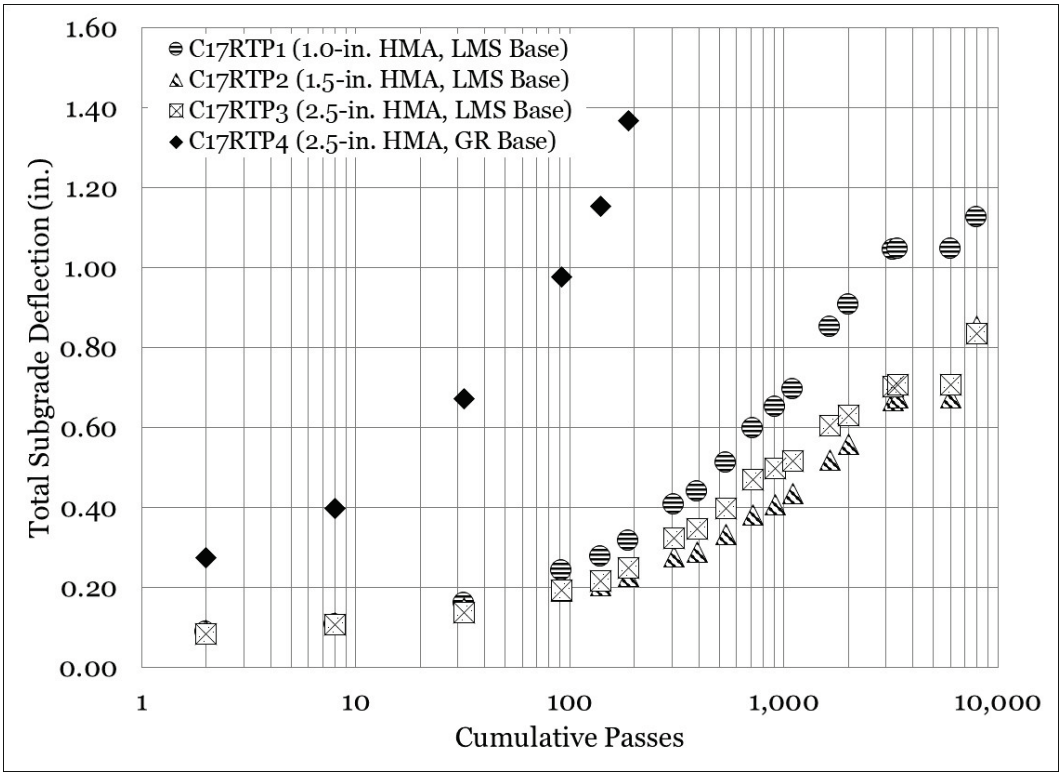

Table 37. Statistical analysis – C-17 reduced tire pressure subgrade deflection.

Interaction	n	p-value	Significant	Better Performer
C17RTP1 vs. C17RTP2	18	<0.001	Yes	C17RTP2
C17RTP1 vs. C17RTP3	18	<0.001	Yes	C17RTP3
C17RTP1 vs. C17RTP4	6	0.008	Yes	C17TRP4
C17RTP2 vs. C17RTP3	18	0.004	Yes	C17RTP2
C17RTP2 vs. C17RTP4	6	0.009	Yes	C17RTP2
C17RTP3 vs. C17RTP4	6	0.008	Yes	C17RTP3

The equality plots confirmed that a reduction in tire pressure resulted in a reduction in total subgrade deflection. Improvement based on the fitted trend line ranged from 50-60% in the thinner asphalt sections, down to 26% in the thickest asphalt test item. This suggested that, as asphalt thickness increased, the benefit on subgrade deflection from reduction in tire pressure became less evident. It is noted that due to the lack of data in C17NTP4, no equality plot is presented for the 2.5-in. HMA, GR base test items.

Figure 103. Equality plot – C-17 subgrade deflection (1.0-in. HMA, LMS base).

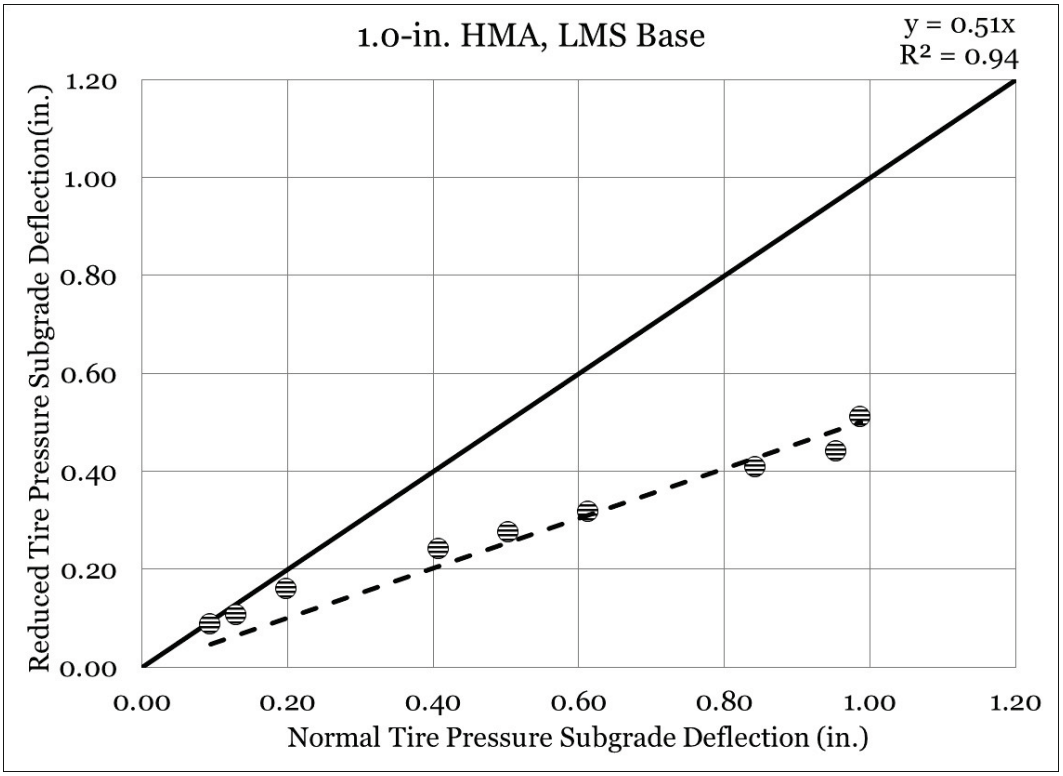

Figure 104. Equality plot – C-17 subgrade deflection (1.5-in. HMA, LMS base).

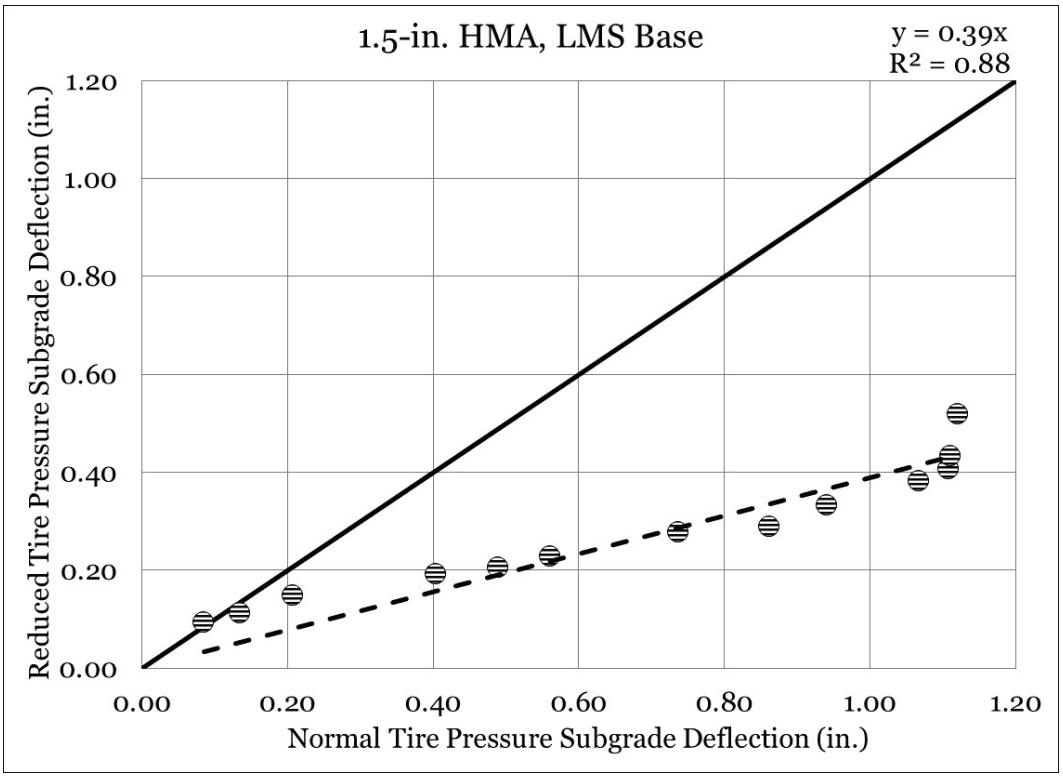

Figure 105. Equality plot – C-17 subgrade deflection (2.5-in. HMA, LMS base).

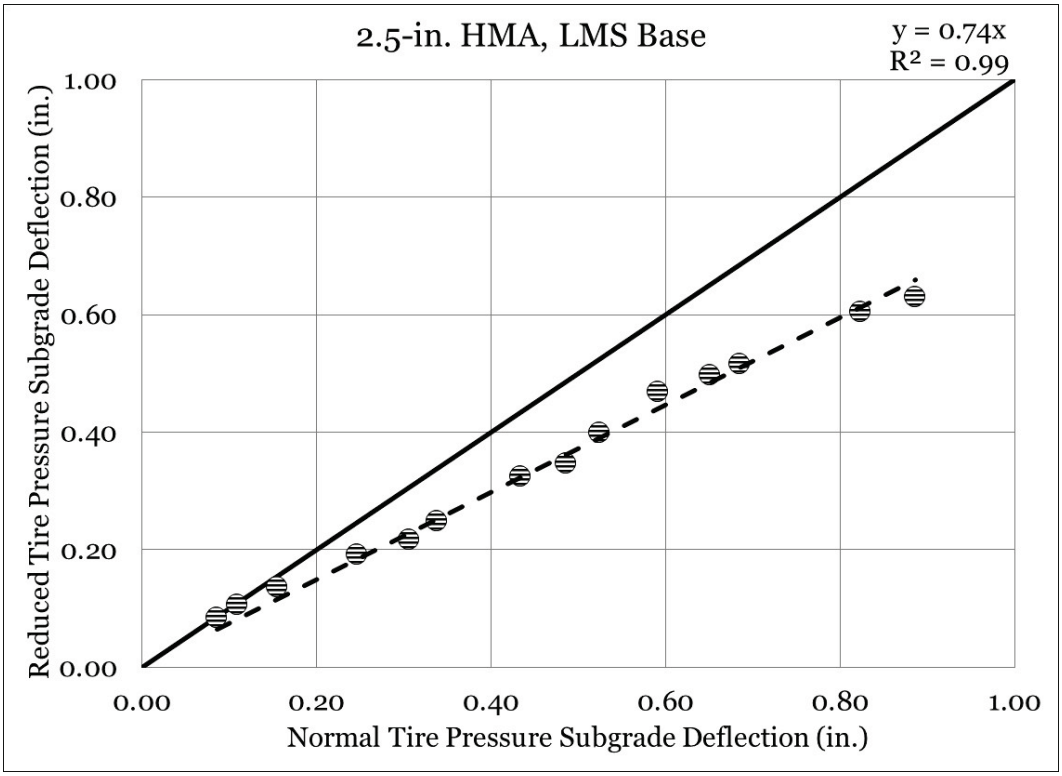

A statistical analysis of total subgrade deflection as a function of tire pressure (Table 38) indicated that all comparisons were statistically significant, confirming that a reduction in tire pressure resulted in a reduction in average subgrade deflection. Comparisons were not available for the 2.5-in. HMA, GR base test items, due to SDD failure in C17NTP4.

Table 38. Statistical analysis – C-17 subgrade deflection and tire pressure.

Interaction	n	p-value	Significant	Better Performer
C17NTP1 vs. C17RTP1	12	<0.001	Yes	C17RTP1
C17NTP2 vs. C17RTP2	13	<0.001	Yes	C17TRP2
C17NTP3 vs. C17RTP3	14	<0.001	Yes	C17RTP3
C17NTP4 vs. C17RTP4	ND	ND	ND	ND

C-17 asphalt strain gauge response

Asphalt strain gauge response for the normal tire pressure test series is shown in Figure 106. Asphalt strain gauge values represent total strain response, which consists of a compression component and a tension component. Thus, the response values shown are the difference of

minimum values and maximum values (i.e., peak to trough). This provided a simplified means for comparing total response between test items.

The highest total asphalt strain values were observed in C17NTP4, a logical finding considering the rapid deformation that occurred due to the weaker gravel base. Total strain values were lower in the LMS base test items, and it was observed that total strain increase was much slower than that of the GR base test item.

The results of a statistical comparison for total asphalt strain are shown in Table 39. It was found that C17NTP2 and C17NTP3 were statistically different from C17NTP1 (p-value <0.001), indicating that an increase in asphalt thickness resulted in a significant reduction in strain for the LMS base test items. Comparison of C17NTP2 and C17NTP3 was not found to be statistically significant (p-value = 0.059), although the comparison would be significant at a lower confidence level. It was noted that no comparisons to C17NTP4 were statistically significant, although practically the difference was meaningful. The lack of significance could be attributed to the rather small sample size (n =4) that was evaluated.

Figure 106. C-17 normal tire pressure total asphalt strain.

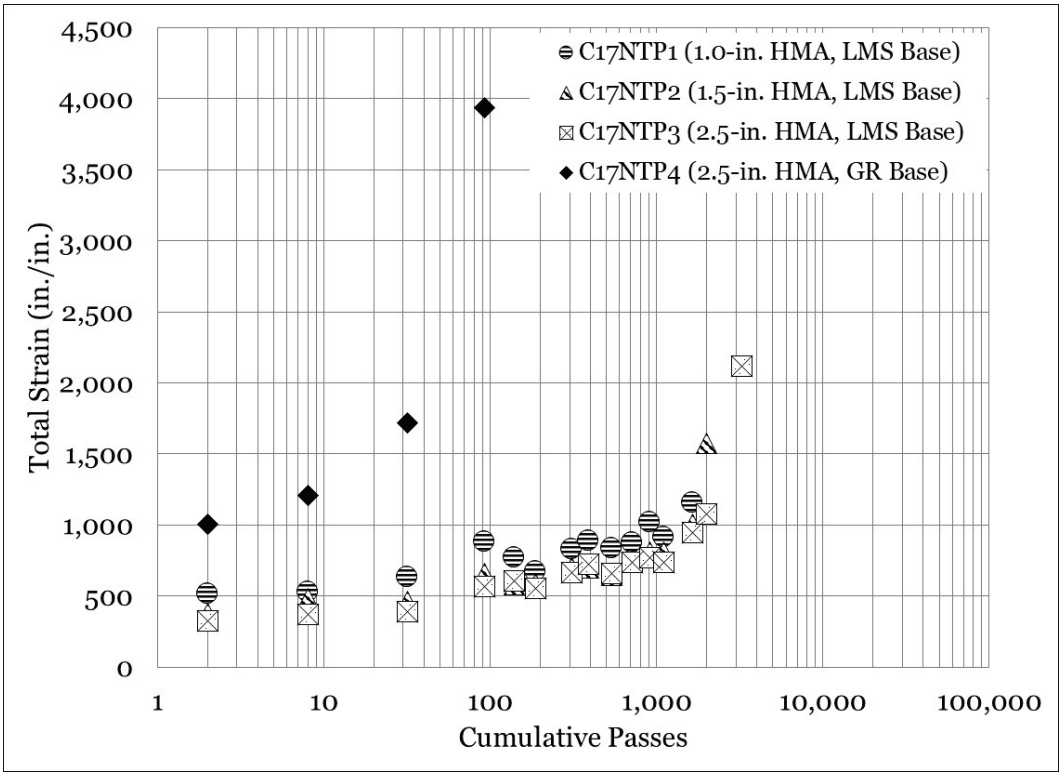

Table 39. Statistical analysis – C-17 normal tire pressure asphalt strain response.

Interaction	n	p-value	Significant	Better Performer
C17NTP1 vs. C17NTP2	13	<0.001	Yes	C17NTP2
C17NTP1 vs. C17NTP3	13	<0.001	Yes	C17NTP3
C17NTP1 vs. C17NTP4	4	0.109	No	Same
C17NTP2 vs. C17NTP3	14	0.059	No	Same
C17NTP2 vs. C17NTP4	4	0.097	No	Same
C17NTP3 vs. C17NTP4	4	0.088	No	Same

Total asphalt strain for the reduced tire pressure series is shown in Figure 107. Similar to the normal tire pressure series, C17RTP4 (2.5-in. HMA, GR base) experienced a rapid increase in strain. Differences in the LMS base test items were unremarkable and were consistent throughout a majority of traffic application.

Figure 107. C-17 reduced tire pressure total asphalt strain.

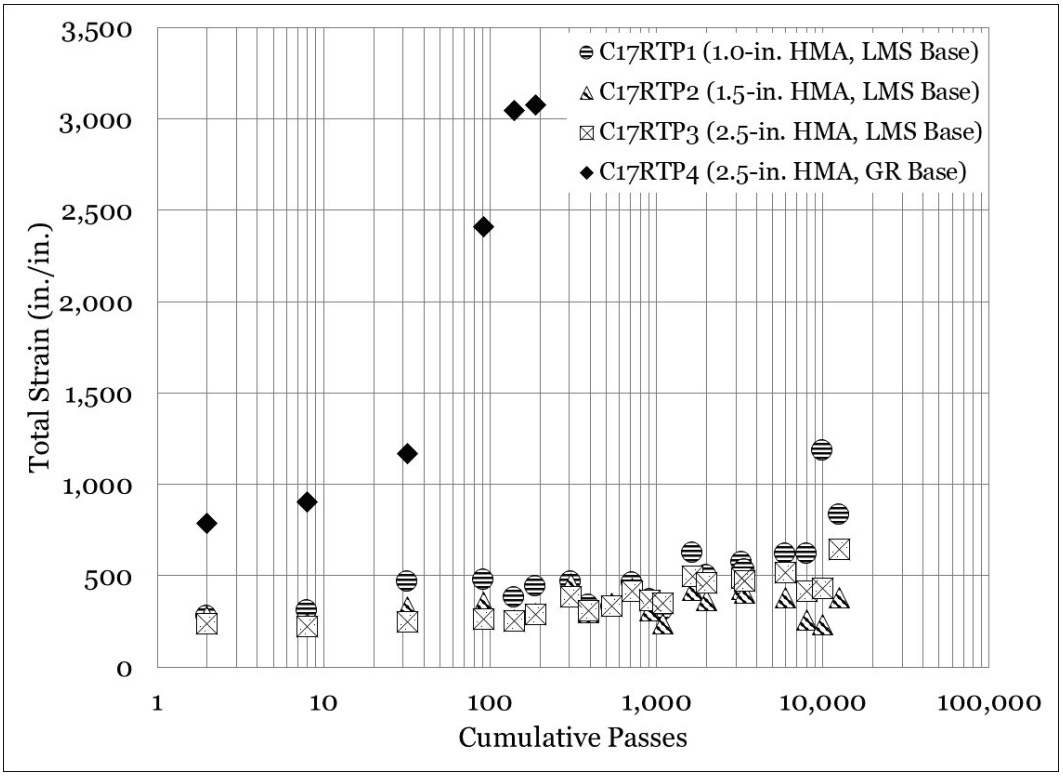

A statistical comparison of total asphalt strain is presented in Table 40. Most interactions were found to be statistically significant, except C17RTP2 and C17RTP3 (p-value = 0.050). C17RTP4 was found to have the highest average asphalt strain when compared to the other LMS base

items. It was observed that, in general, statistical comparisons were logical relative to asphalt thickness for the LMS base test items.

Table 40. Statistical analysis – C-17 reduced tire pressure asphalt strain response.

Interaction	n	p-value	Significant	Better Performer
C17RTP1 vs. C17RTP2	20	0.002	Yes	C17RTP2
C17RTP1 vs. C17RTP3	20	0.003	Yes	C17RTP3
C17RTP1 vs. C17RTP4	6	0.016	Yes	C17RTP1
C17RTP2 vs. C17RTP3	20	0.050	No	Same
C17RTP2 vs. C17RTP4	6	0.014	Yes	C17RTP2
C17RTP3 vs. C17RTP4	6	0.012	Yes	C17RTP3

Equality plots for total asphalt strain are presented in Figures 108 through 111. Total asphalt strain for the reduced tire pressure test item was plotted on the y-axis, and total asphalt strain for the normal tire pressure test item was plotted on the x-axis. The LOE is represented by a solid line, and the best-fit linear trend line is represented by a dashed line. Data plotted below the LOE indicated lower total asphalt strain.

A review of the 1.0-in. HMA, LMS base equality plot (Figure 108) indicated that measured total strain was lower (51%) in the reduced tire pressure item when compared to the normal tire pressure item. However, it was noted that the linear regression had a poor fit, with an $R^2 = 0.09$.

When other total strain equality plots were considered (Figure 109 and Figure 110), it was observed that all R^2 values were negative, indicating that the linear model was a worse fit than a horizontal line. Thus, it could be concluded that there was no correlation between total strain for the reduced tire pressure and normal tire pressure test series, when a linear model subject to the constraint y-intercept=0 was considered.

The 2.5-in. HMA, GR base equality plot (Figure 111) indicated that an improvement in asphalt strain of 36% was gained from a reduction in tire pressure. However, based on observations in other test items and the limited dataset (n = 4), correlations between strain response in this item were questionable.

Figure 108. Equality plot – C-17 asphalt strain (1.0-in. HMA, LMS base).

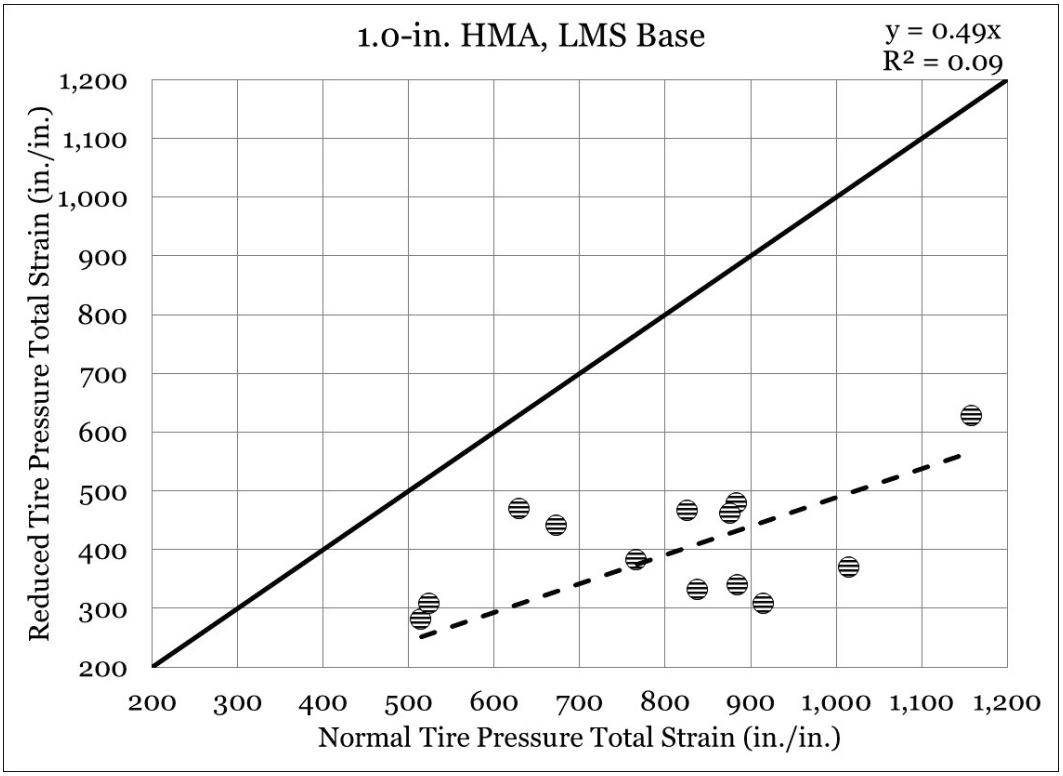

Figure 109. Equality plot – C-17 asphalt strain (1.5-in. HMA, LMS base).

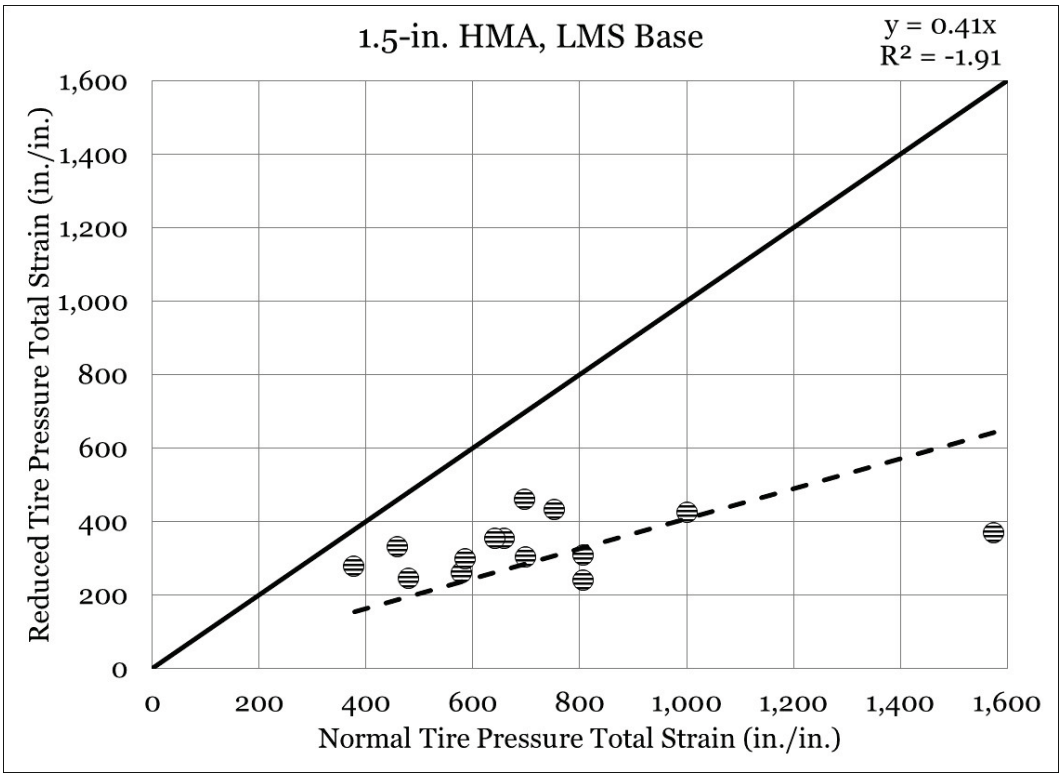

Figure 110. Equality plot – C-17 asphalt strain (2.5-in. HMA, LMS base).

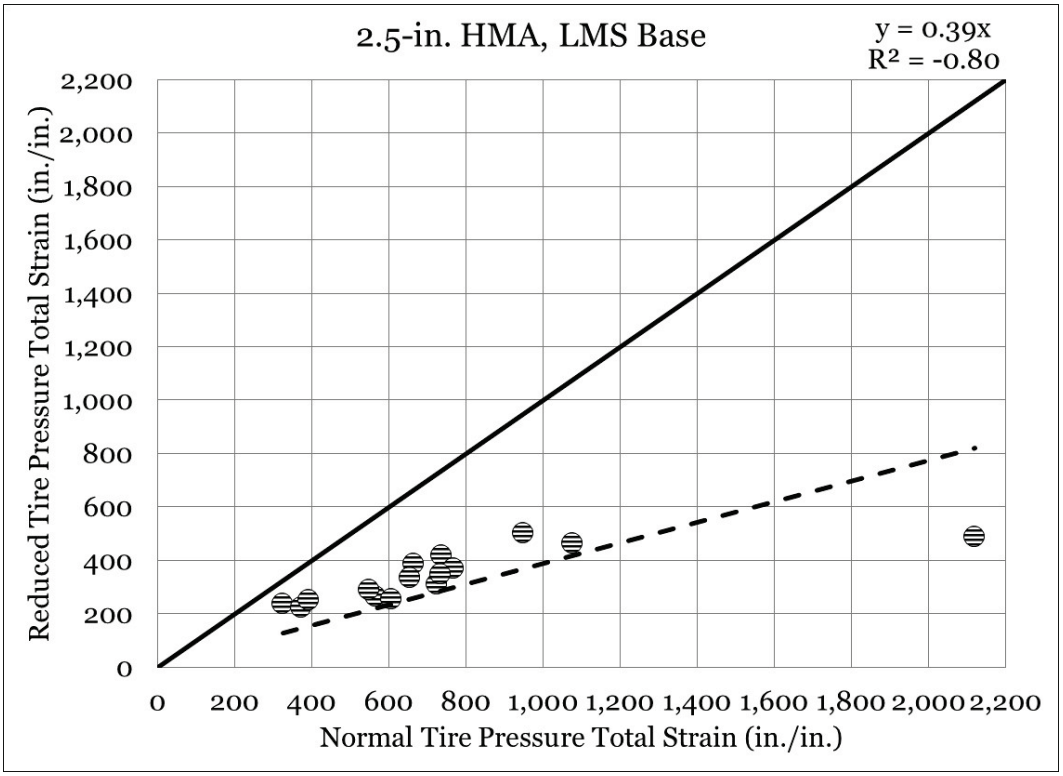

Figure 111. Equality plot – C-17 asphalt strain (2.5-in. HMA, GR base).

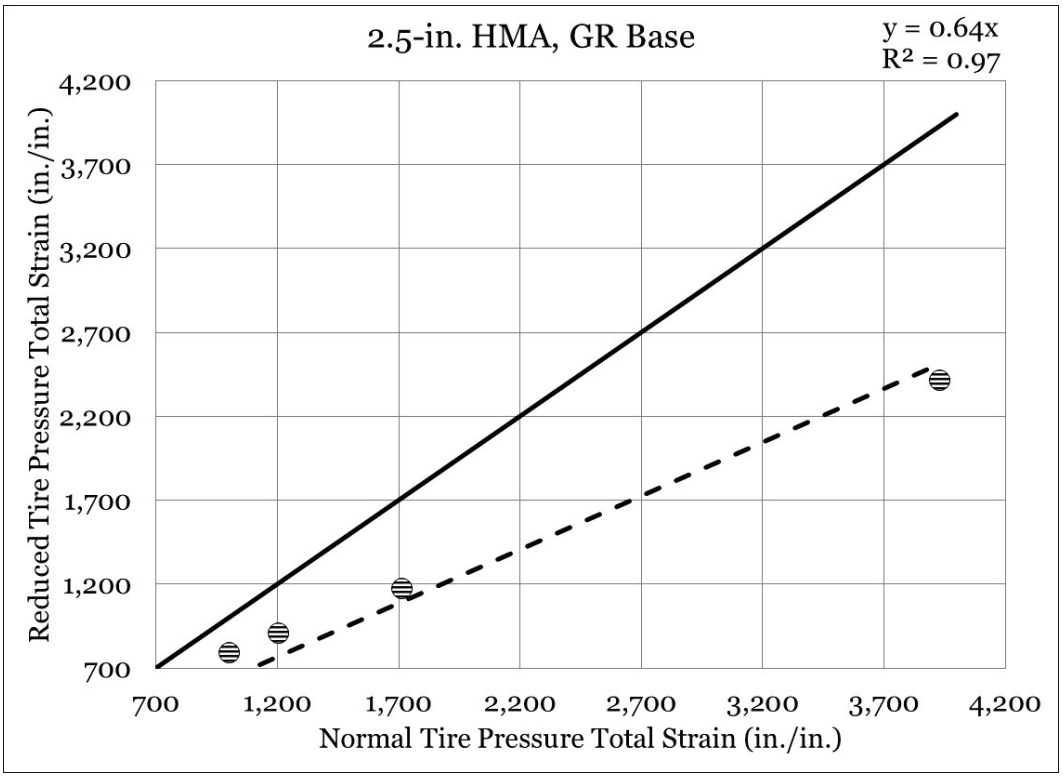

A statistical comparison (Table 41) of the LMS base test items found that a reduction in tire pressure resulted in a statistically significant reduction in average strain response. Comparison of the 2.5-in. HMA, GR base test item was not found to be statistically significant (p-value = 0.120), suggesting that a reduction in tire pressure did not result in a significant reduction in average asphalt strain.

Table 41. Statistical analysis – C-17 total asphalt strain and tire pressure.

Interaction	n	p-value	Significant	Better Performer
C17NTP1 vs. C17RTP1	13	<0.001	Yes	C17RTP1
C17NTP2 vs. C17RTP2	14	<0.001	Yes	C17RTP2
C17NTP3 vs. C17RTP3	15	0.001	Yes	C17RTP3
C17NTP4 vs. C17RTP4	4	0.120	No	Same

7.3 Comparison of C-130 and C-17 traffic results

Rut depth

Equality plots were generated to investigate the relationship between C-130 and C-17 rut depth development (Figures 112 through 115). Data were paired such that tire pressure condition (i.e., normal or reduced tire pressure) and item cross section were consistent. Rut depths for C-17 traffic were plotted on the x-axis, and rut depths for C-130 traffic were plotted on the y-axis. An LOE is represented by a solid dark line, and a best-fit linear trend line with a y-intercept = 0 was plotted through the data.

A review of the normal tire pressure equality plots indicated that the C-130 rutting performance was better than the C-17 rutting performance in all cases, as was expected due to the total load reduction and the reduced tire pressure. It was observed that the difference in C-130 and C-17 rutting performance was relatively consistent, and the C-130 items had rutting that was on the order of 70 to 80% less than the C-17 items. The largest difference was observed in the 2.5-in. HMA, LMS test item (Figure 113), where the C-130 rutting was 81% less than the C-17 rutting. The smallest improvement was observed in the 1.0-in. HMA, LMS test item (Figure 115), where the C-130 rutting was 74% less than the C-17 rutting. It was observed that all the best-fit trend lines were a reasonable fit to the plotted data and that all R^2 values exceeded 0.90.

Figure 112. Equality plot - normal tire pressure rut depth (2.5-in. HMA, GR base).

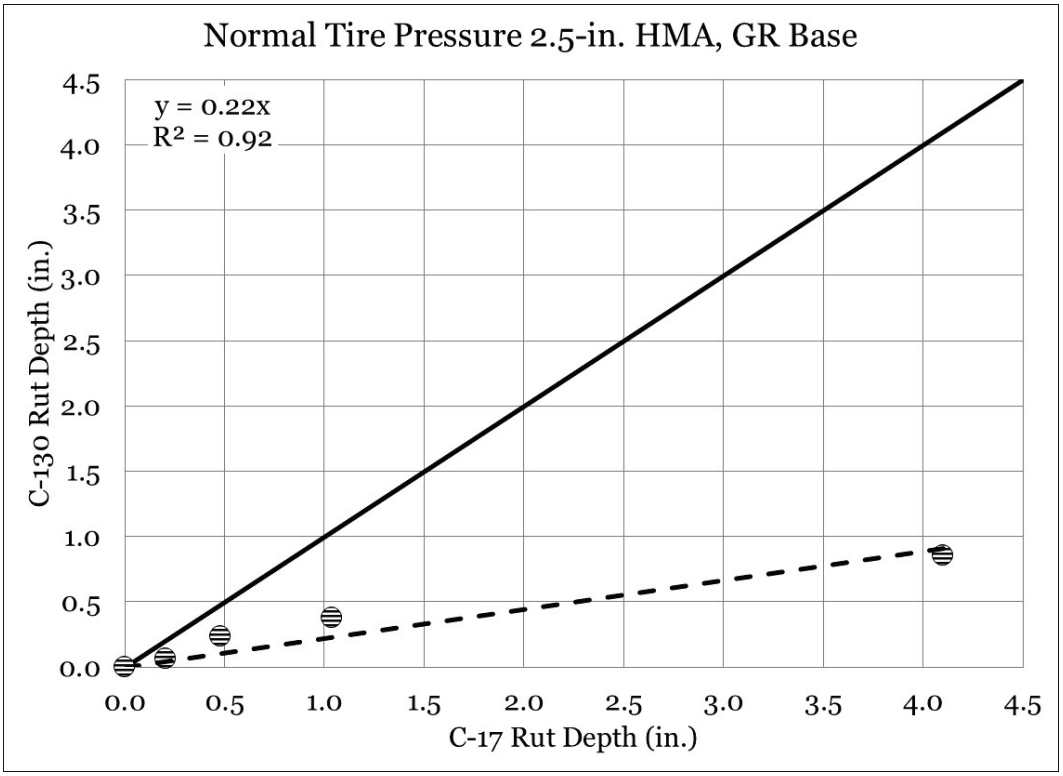

Figure 113. Equality plot - normal tire pressure rut depth (2.5-in. HMA, LMS base).

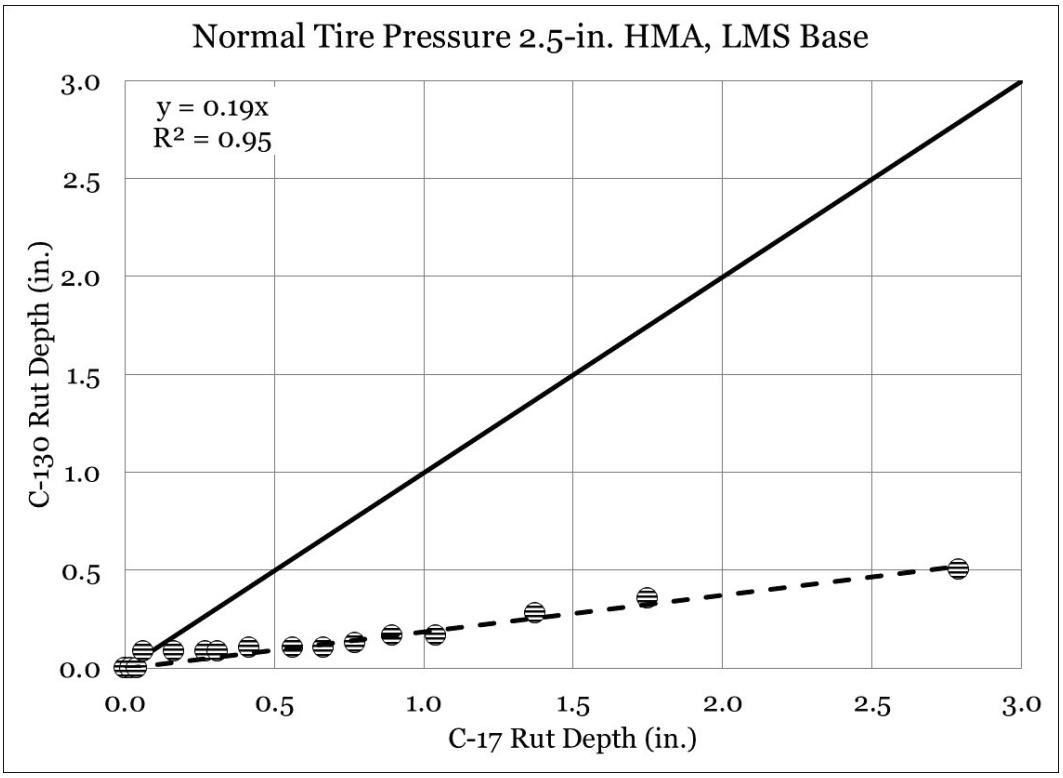

Figure 114. Equality plot - normal tire pressure rut depth (1.5-in. HMA, LMS base).

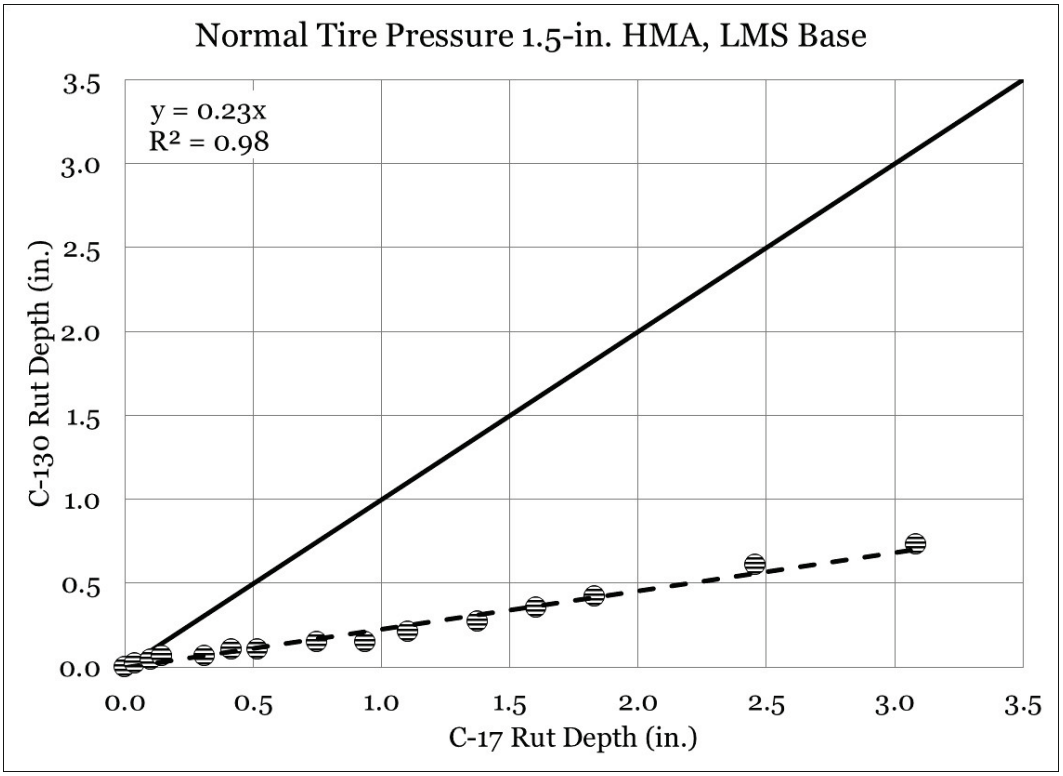

Figure 115. Equality plot - normal tire pressure rut depth (1.0-in. HMA, LMS base).

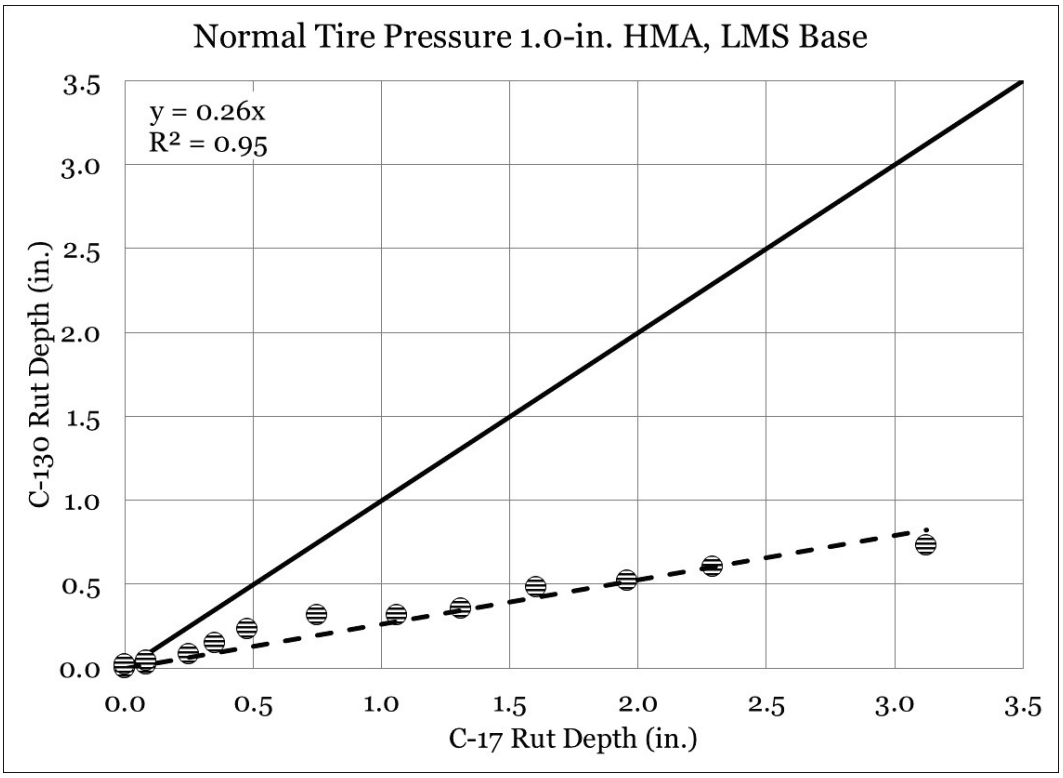

Equality plots for the relationship between C-130 rut depth and C-17 rut depth for reduced tire pressure are shown in Figures 116 to 119. Similar to the normal tire pressure comparisons, the C-130 rutting was consistently less than the C-17 rutting, as expected. It was observed that performance differences when comparing C-130 rutting to C-17 rutting were more variable in the reduced tire pressure than in the normal tire pressure. Rutting performance in the C-130 reduced tire pressure test series was found to be 50-83% less than rutting performance in the C-17 reduced tire pressure test series. Similar to the normal tire pressure comparison, the largest improvement (83%) was observed in the 2.5-in. HMA, LMS base test item (Figure 117). The smallest improvement (50%) was observed in the 1.5-in. HMA, LMS base (Figure 118) and 1.0-in. HMA, LMS base test items (Figure 119). A relatively good trend line fit was observed, with most relationships having R^2 values greater than 0.90, with the exception of the 2.5-in. HMA, LMS base, which had an R^2 of 0.86.

Figure 116. Equality plot - reduced tire pressure rut depth (2.5-in. HMA, GR base).

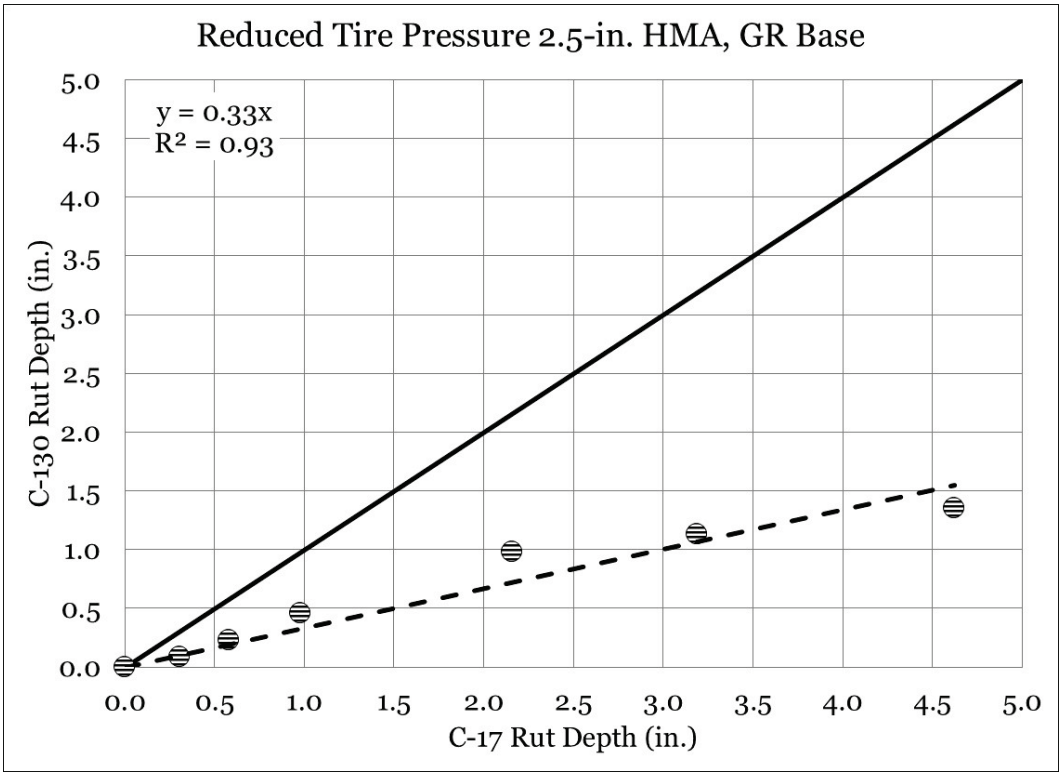

Figure 117. Equality plot - reduced tire pressure rut depth (2.5-in. HMA, LMS base).

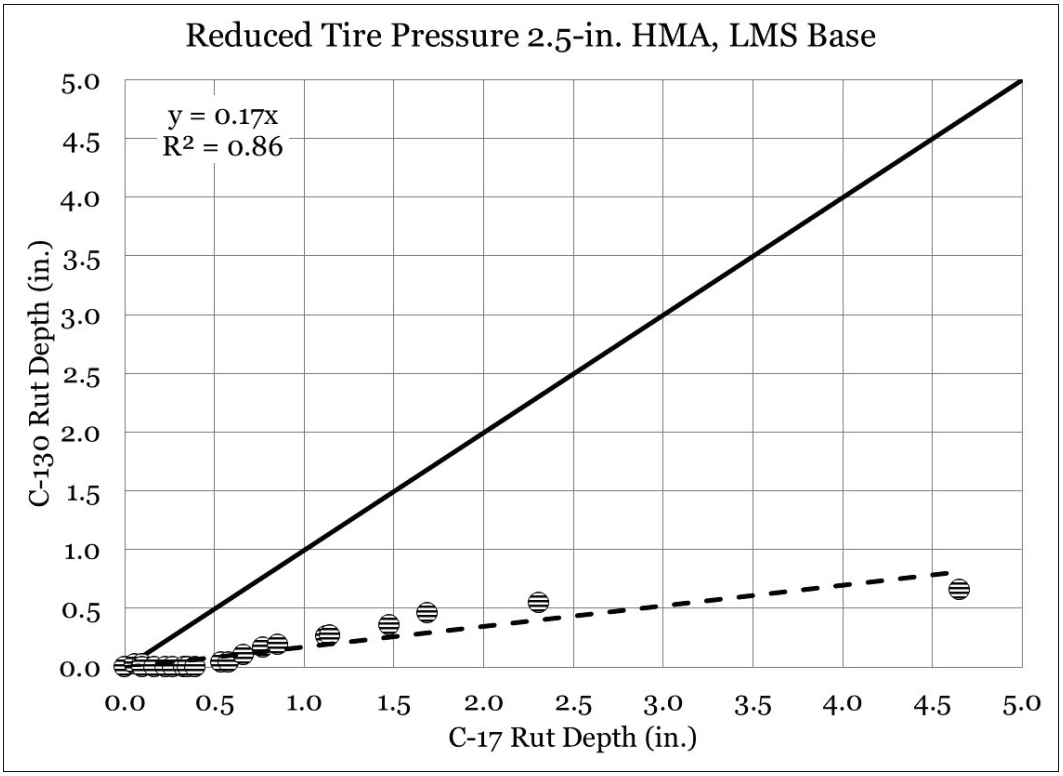

Figure 118. Equality plot - reduced tire pressure rut depth (1.5-in. HMA, LMS base).

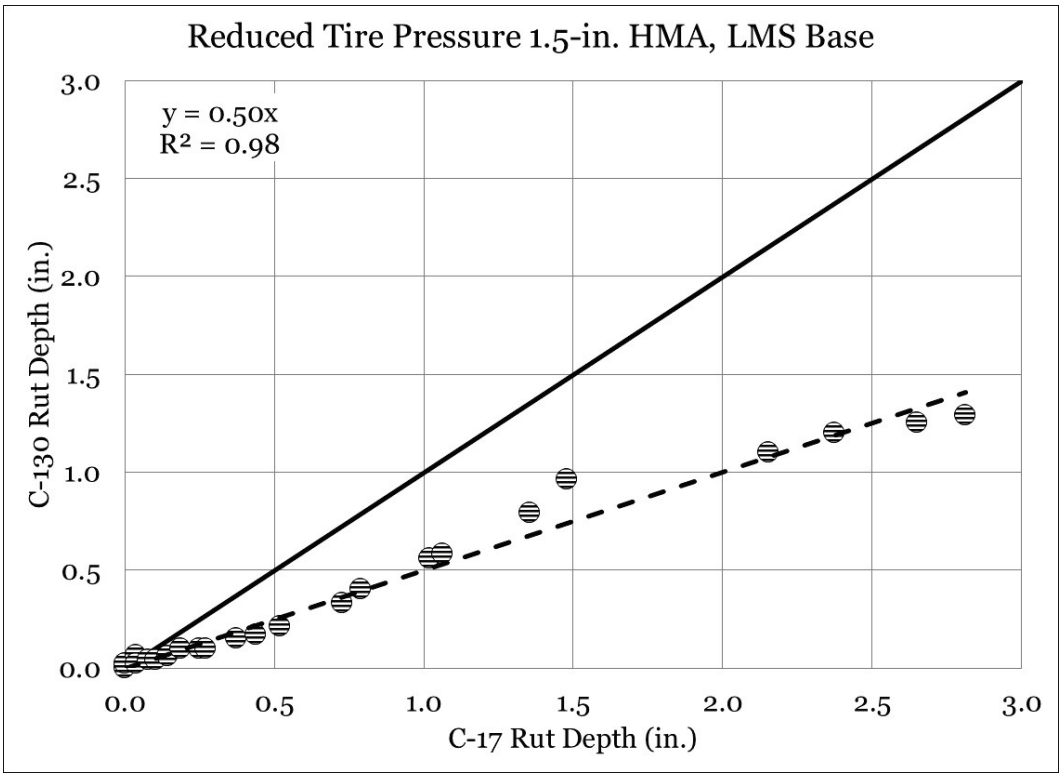

Figure 119. Equality plot - reduced tire pressure rut depth (1.0-in. HMA, LMS base).

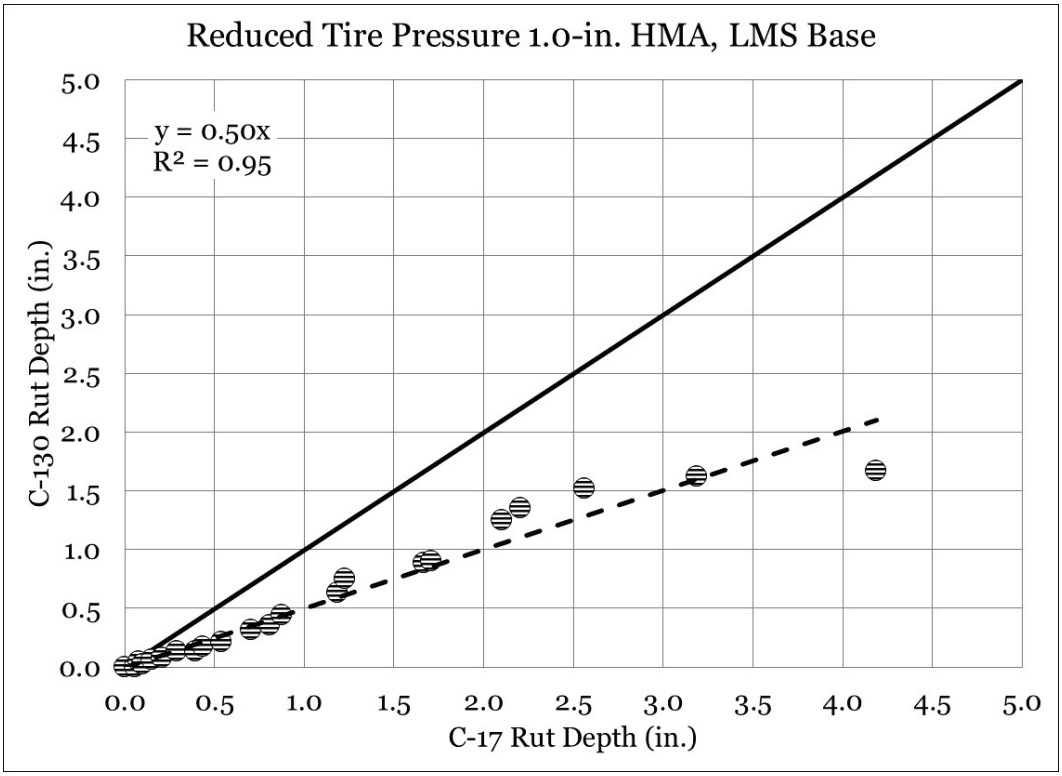

Cracking

Comparisons of total linear feet of cracking recorded at various rut depths are presented in Figures 120 through 127. A review of total cracking in the 2.5-in. HMA, GR base normal tire pressure test items (Figure 120) found that no cracking was observed in either loading condition until after 1.0 in. of rutting was achieved. Similarly, cracking was not observed in the 2.5-in. HMA, LMS base normal tire pressure test items (Figure 121) until nearly 2.0 in. of rutting, and no cracking was observed in the C-130 traffic test item, suggesting that the lower tire pressure (100 psi vs. 142 psi) reduced surface shear forces.

Total cracking in the 1.5-in. HMA, LMS base normal tire pressure test items (Figure 122) was nearly equivalent up to 1.5 in. of rutting. The C-17 test item displayed increased cracking beyond 1.5 in. of rutting, and it was noted that the C-130 item was not trafficked beyond 2.0 in. of rutting; thus, direct comparisons could not be made.

A review of cracking performance in the 1.0-in. HMA, LMS base normal tire pressure test items (Figure 123) indicated that more cracking was

observed in the C-130 test item up to 1.0 in. of rutting, but more cracking was observed in the C-17 test item after 1.0 in. of rutting.

The 2.5-in. HMA, GR base reduced tire pressure test items (Figure 124) did not display a meaningful amount of cracking up to 1.0 in. rutting. After 1.0 in. rutting, it was observed that a steep increase was observed in the C-130 test item, while a less steep increase was observed in the C-17 test item. Recall the C-17 item sustained fewer passes to failure than the C-130 item; thus, a lack of load repetitions (i.e., fatigue) could explain the unexpected cracking reduction in the C-17 item.

The 2.5-in. HMA, LMS base reduced tire pressure test items (Figure 125) did not have any measurable cracking up to 1.0 in. of rutting, and the C-130 test item did not have any measurable cracking for the duration of traffic application. This was expected, as the C-130 normal tire pressure displayed no cracking throughout traffic application. The C-17 test item displayed a rapid increase in cracking after 1.0 in. of rutting.

Total cracking in the 1.5-in. HMA, LMS base reduced tire pressure test items (Figure 126) was first observed at 0.5 in. of rutting in the C-17 test item, and cracking was observed in both test items thereafter. It was observed that cracking was greater in the C-17 test item at all rut depths, as expected.

Cracking was observed early, at 0.25 in. of rutting, in the 1.0-in. HMA, LMS base test items (Figure 127). Unlike the normal tire pressure test series, cracking was first observed in the C-17 test item, and it was found that more cracking was observed in the C-17 test item at all selected rut depths.

In general, it can be observed that a meaningful amount of cracking was not observed in most test items until near or after 1.0 in. of rutting. Thus, it can be concluded that, under the test conditions of this investigation, the primary mode of failure was pavement rutting rather than extensive fatigue cracking.

Figure 120. Total cracking comparison normal tire pressure (2.5-in. HMA, GR base).

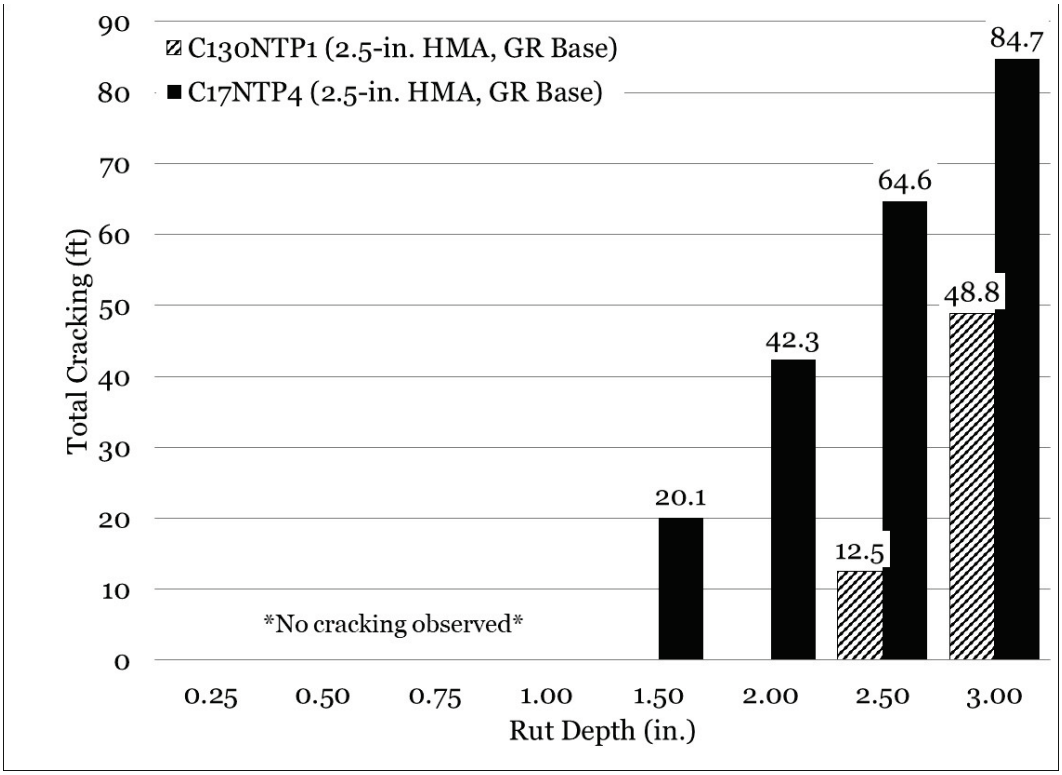

Figure 121. Total cracking comparison normal tire pressure (2.5-in. HMA, LMS base).

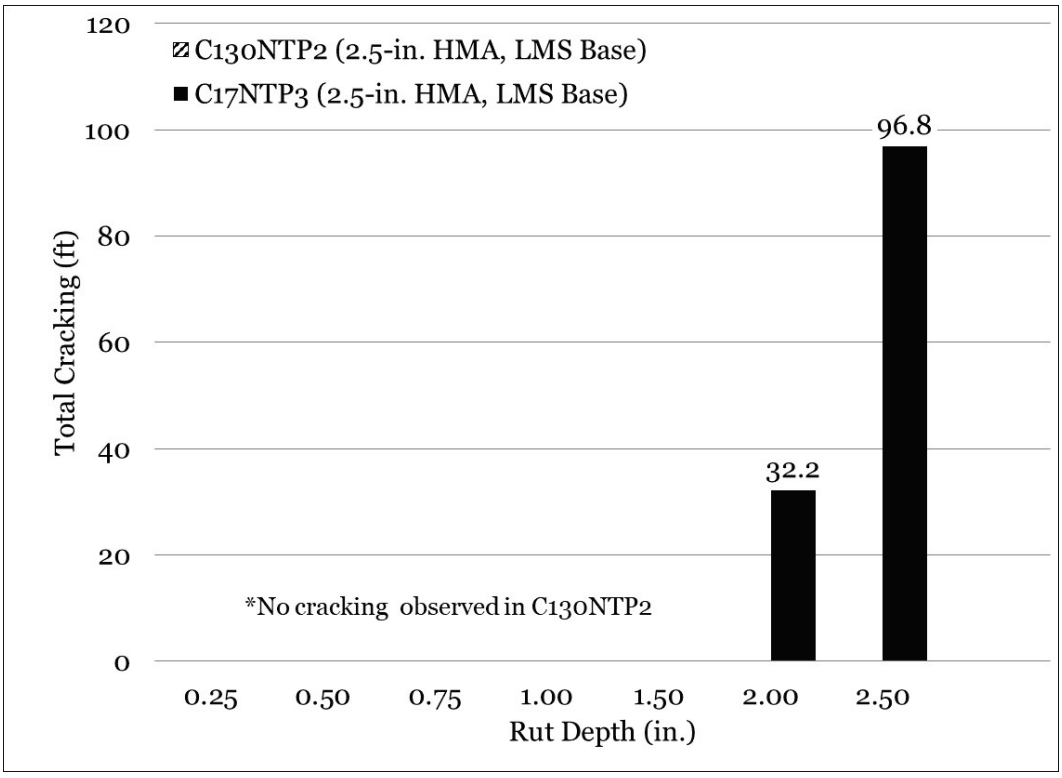

Figure 122. Total cracking comparison normal tire pressure (1.5-in. HMA, LMS base).

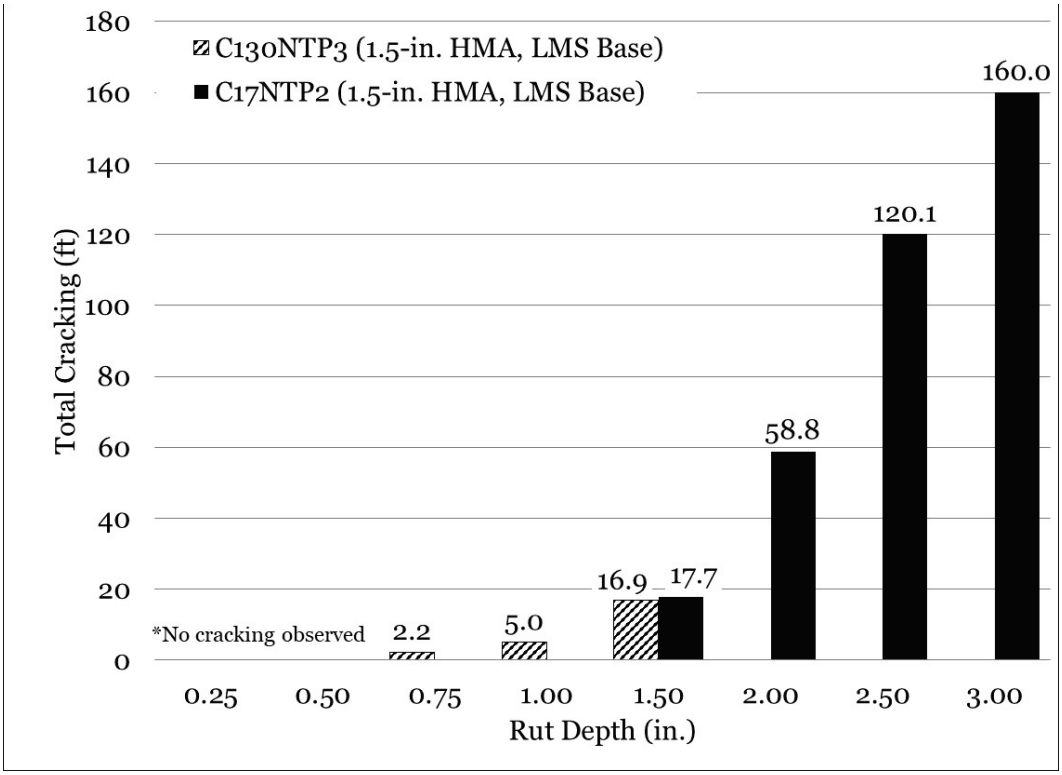

Figure 123. Total cracking comparison normal tire pressure (1.0-in. HMA, LMS base).

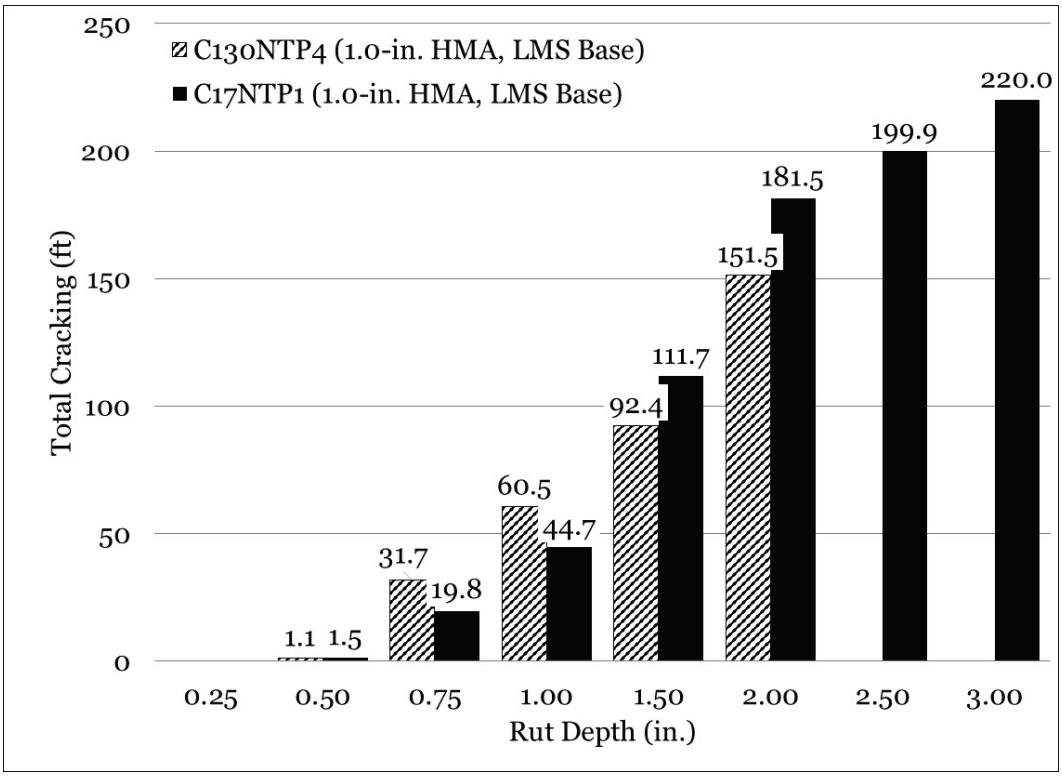

Figure 124. Total cracking comparison reduced tire pressure (2.5-in. HMA, GR base).

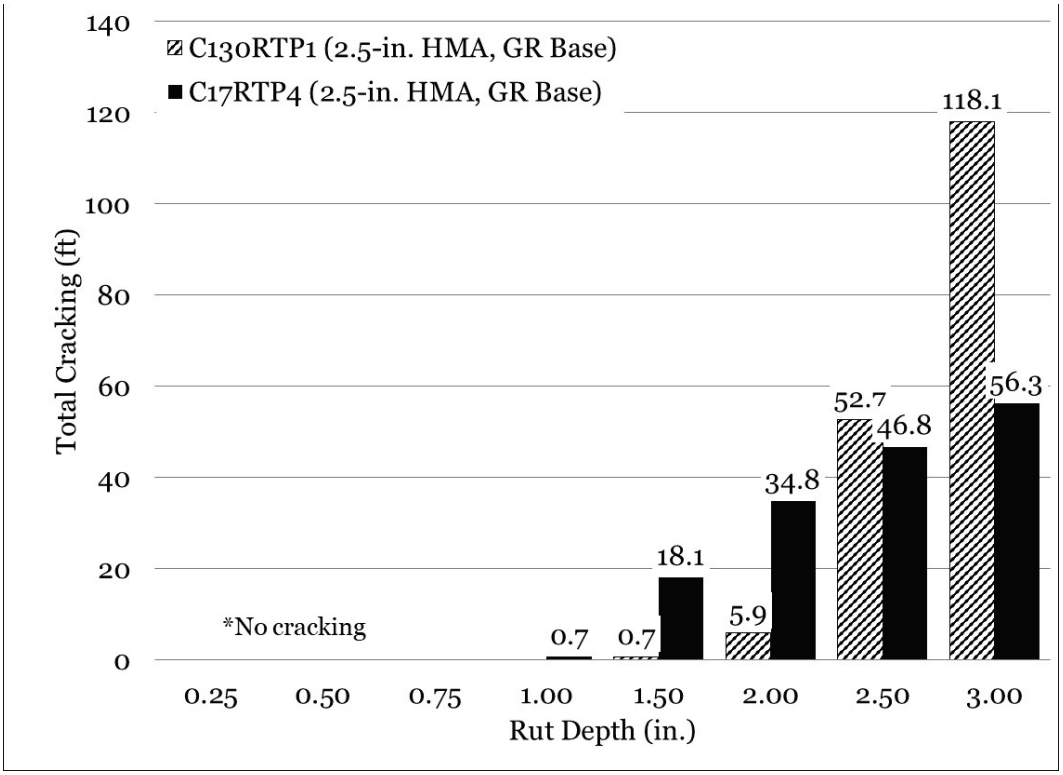

Figure 125. Total cracking comparison reduced tire pressure (2.5-in. HMA, LMS base).

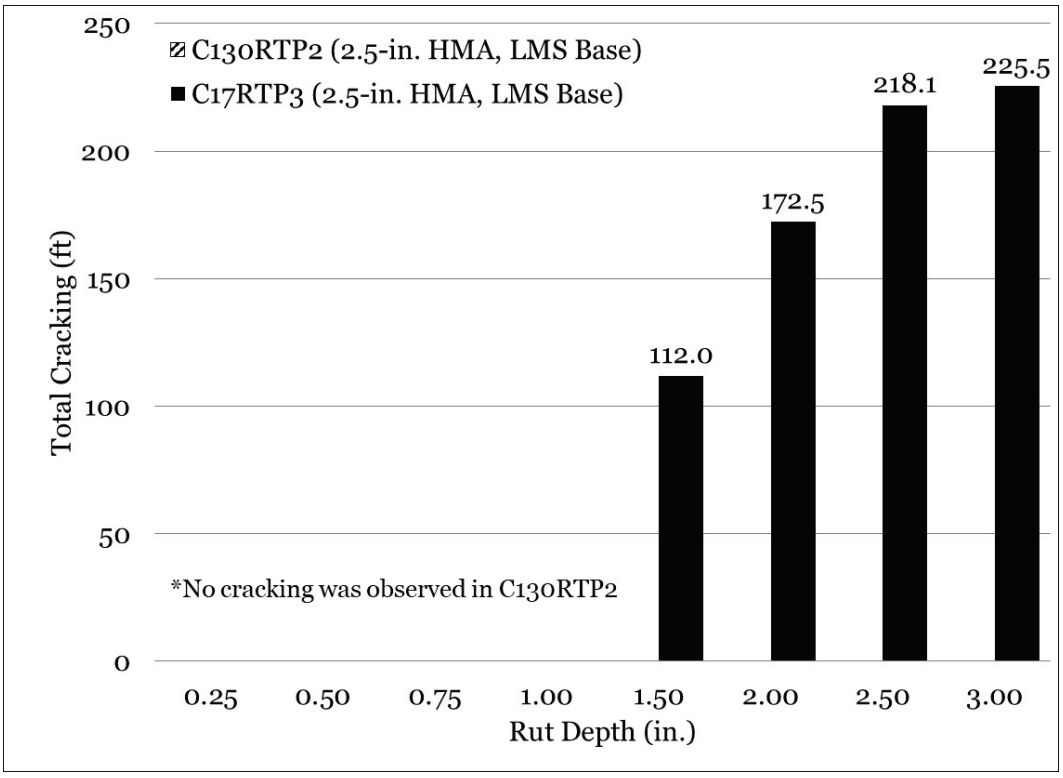

Figure 126. Total cracking comparison reduced tire pressure (1.5-in. HMA, LMS base).

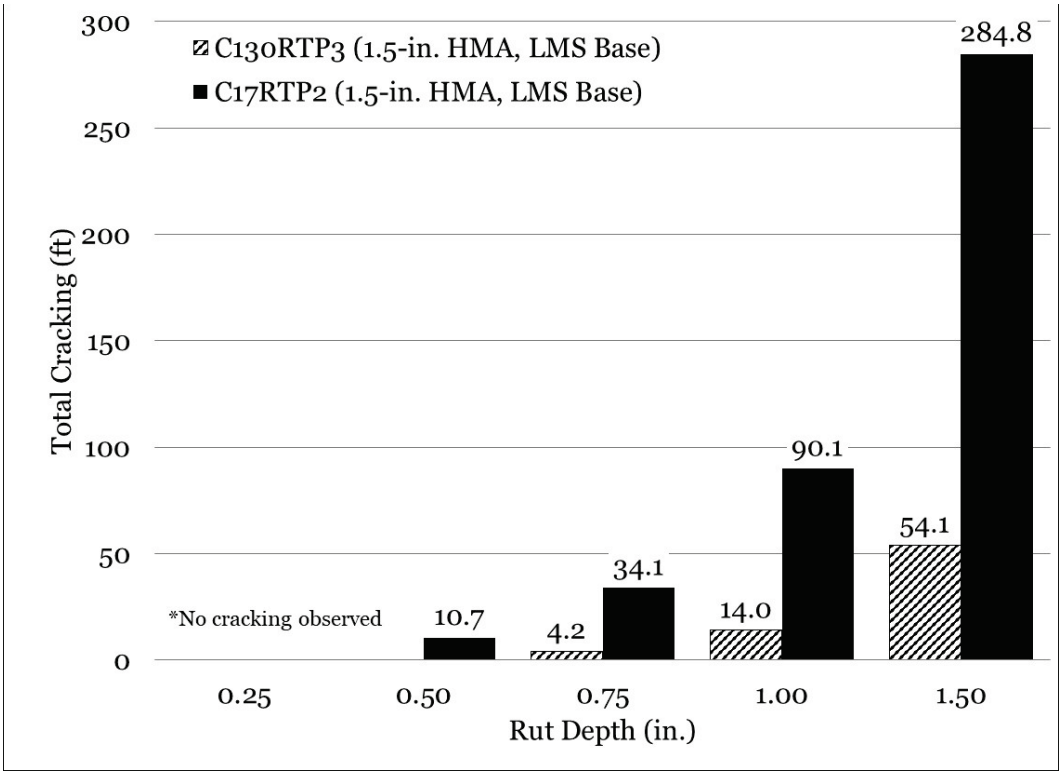

Figure 127. Total cracking comparison reduced tire pressure (1.0-in. HMA, LMS base).

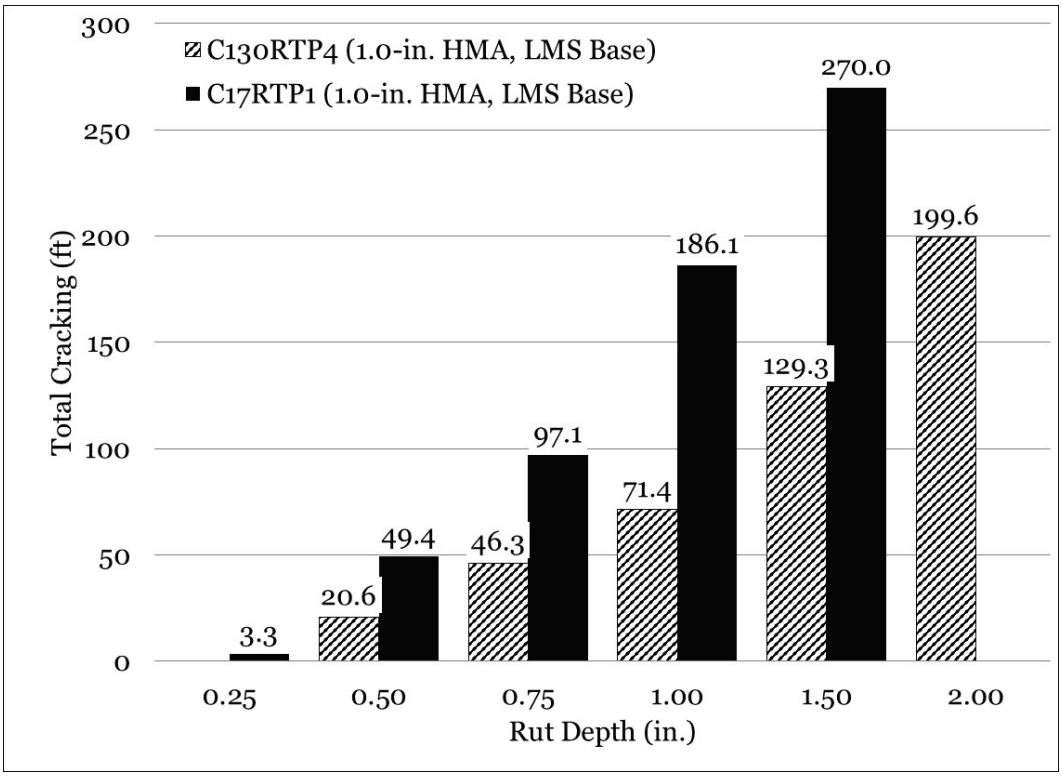

Passes to rut depth

Comparisons of passes to various rut depths of interest are presented in Figures 128 through 135. Rut depths were selected to match those currently defined as threshold values for varying levels of pavement condition determination: low (0.25 in. to 0.5 in.), medium (0.5 in. to 1.0 in.), and high (>1.0 in.). After 1.0 in. of rutting, data were selected in 0.5-in. intervals to monitor performance at excessive rutting levels.

A review of passes to rut depth for 2.5-in. HMA, GR base normal tire pressure (Figure 128) indicated that the C-130 test item performed substantially better than the C-17 test item. The C-130 test item sustained approximately four times the passes at 1.0-in. rutting and approximately 12 times the passes at 3.0-in. rutting. This suggested that the increased load and tire pressure severely overwhelmed the strength of the weak base course, resulting in a much more rapid rut development under C-17 loading conditions.

A review of pass to rut depth for 2.5-in. HMA, LMS base normal tire pressure (Figure 129) indicated that the C-130 test item sustained approximately 12 times the passes of the C-17 test item at 1.0-in. rutting. Further, it was observed that 1.5 in. of rutting could not be achieved in a reasonable number of passes in the C-130 test item, while 1.5-in. rutting was achieved at 1,786 passes in the C-17 test item.

Performance to 1.0-in. rutting of the C-130 trafficked 1.5-in. HMA, LMS base normal tire pressure test item (Figure 130) was approximately 7.5 times that of the C-17 test item. Similar performance differences were observed in the 1.0-in. HMA, LMS base normal tire pressure test items (7.6 times).

A review of passes to rut depth for 2.5-in. HMA, GR base reduced tire pressure test items (Figure 132) showed that the C-130 test item sustained approximately three times the passes of the C-17 at 1.0-in. of rutting and approximately four times the passes at 3.0-in. of rutting. Note that the performance differences are similar to the normal tire pressure test series at 1.0-in. of rutting, suggesting that total load rather than tire pressure was the primary performance influencer in the weak gravel base.

A review of passes to rut depth for 2.5-in. HMA, LMS base reduced tire pressure test items (Figure 133) indicated that performance in the C-130 test item was approximately eight times that of the C-17 test item at 1.0-in.

rutting. It was noted that the C-17 item achieved a 3.0-in. rut depth (10,740 passes) while the C-130 item did not achieve 1.5-in. rutting in a reasonable number of passes.

Performance to 1.0-in. rutting of the C-130 1.5-in. HMA, LMS base reduced tire pressure test item (Figure 134) was approximately 2.7 times that of the C-17 item, which was much less than that observed in the 2.5-in. HMA comparison, suggesting that the additional 1.0-in. HMA had a meaningful effect on the performance of the items. A similar improvement was observed in the 1.0-in. HMA, LMS base reduced tire pressure comparison (Figure 135), with the C-130 item having 3.2 times the passes of the C-17 item at 1.0-in. rutting. When comparisons are made to the respective normal tire pressure, it was observed that the magnitude of improvement was much smaller.

Figure 128. Rut depth comparison normal tire pressure (2.5-in. HMA, GR base).

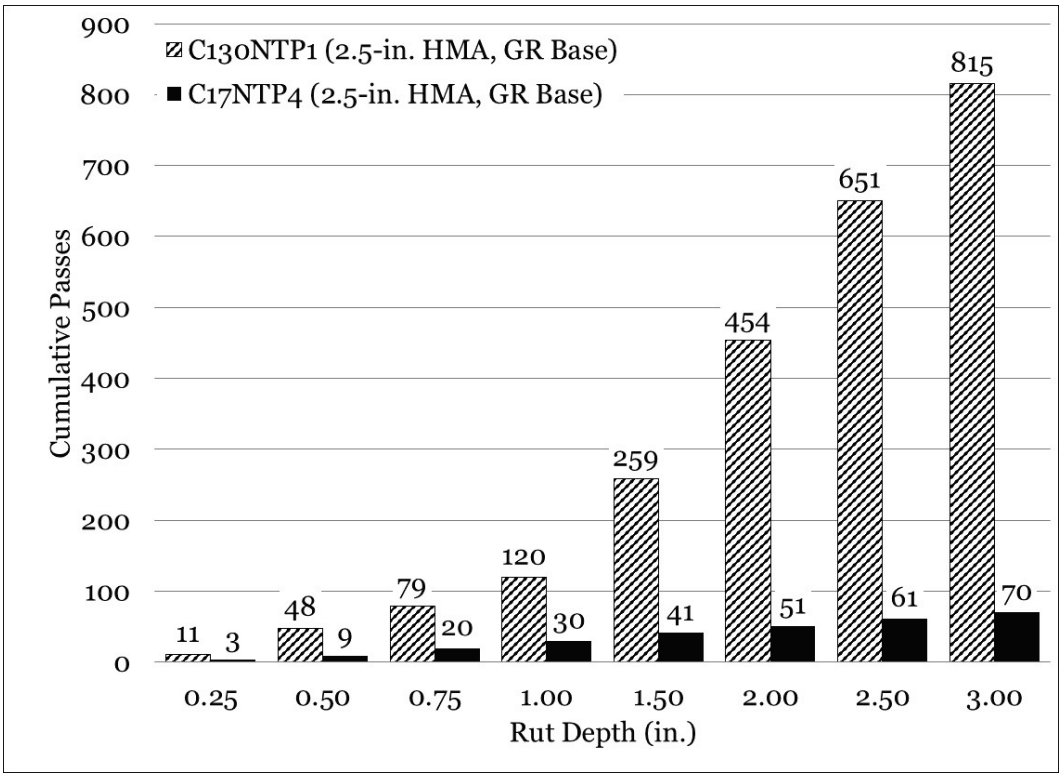

Figure 129. Rut depth comparison normal tire pressure (2.5-in. HMA, LMS base).

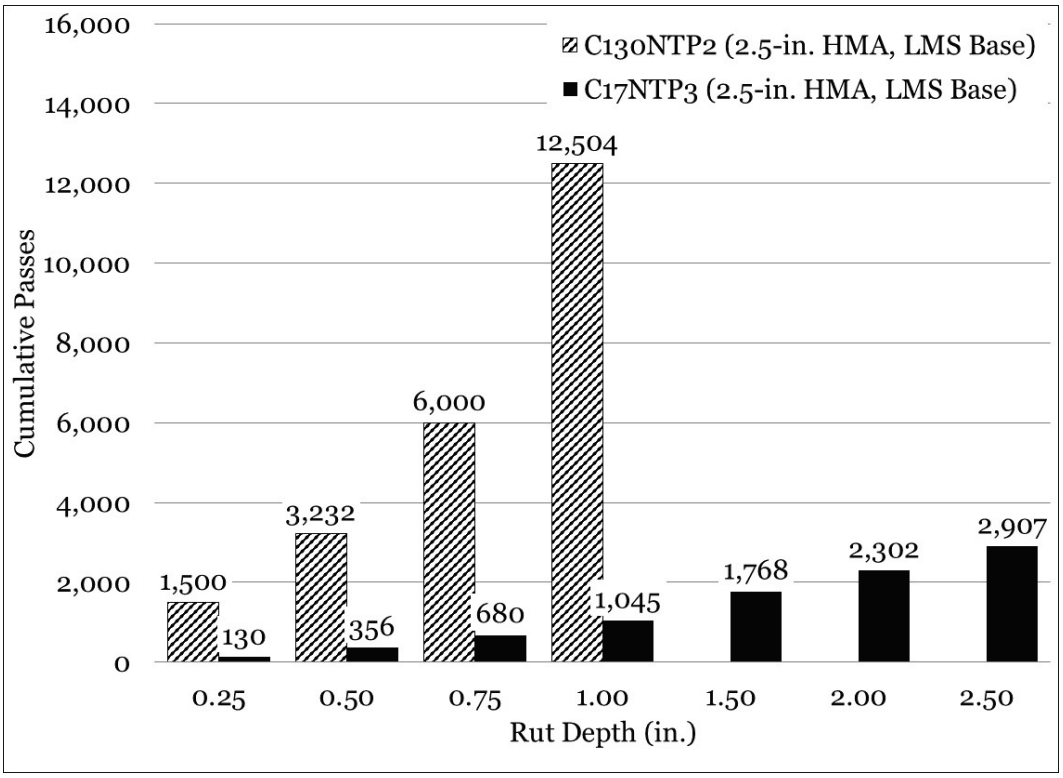

Figure 130. Rut depth comparison normal tire pressure (1.5-in. HMA, LMS base).

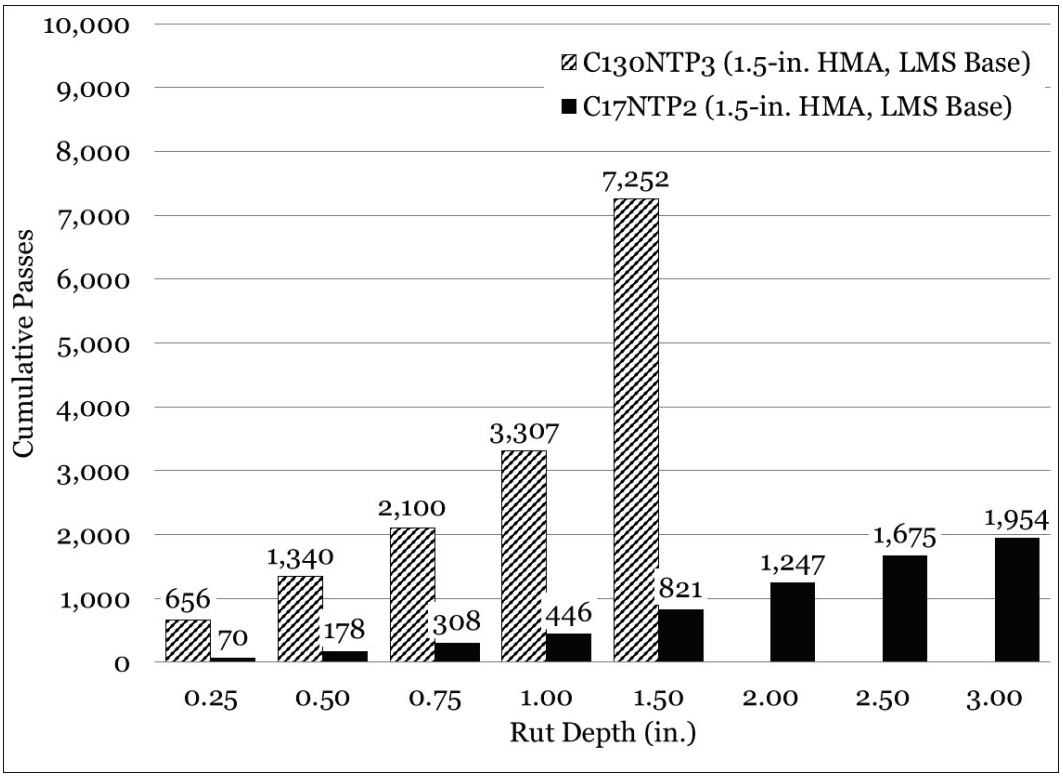

Figure 131. Rut depth comparison normal tire pressure (1.0-in. HMA, LMS base).

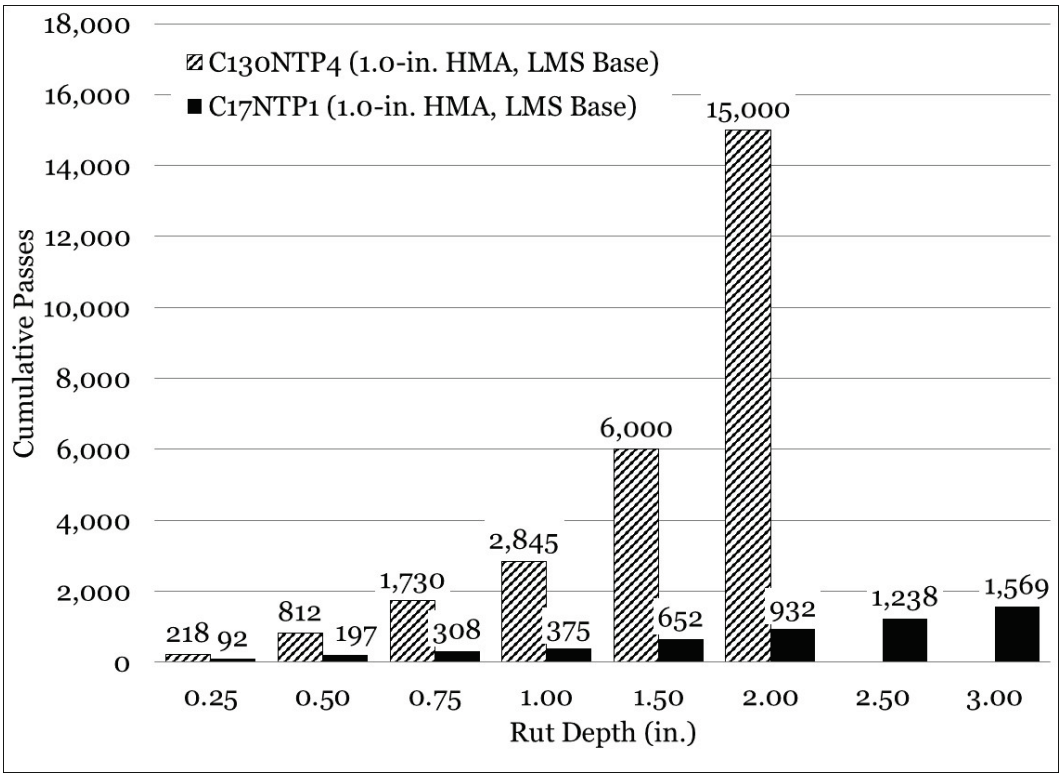

Figure 132. Rut depth comparison reduced tire pressure (2.5-in. HMA, GR base).

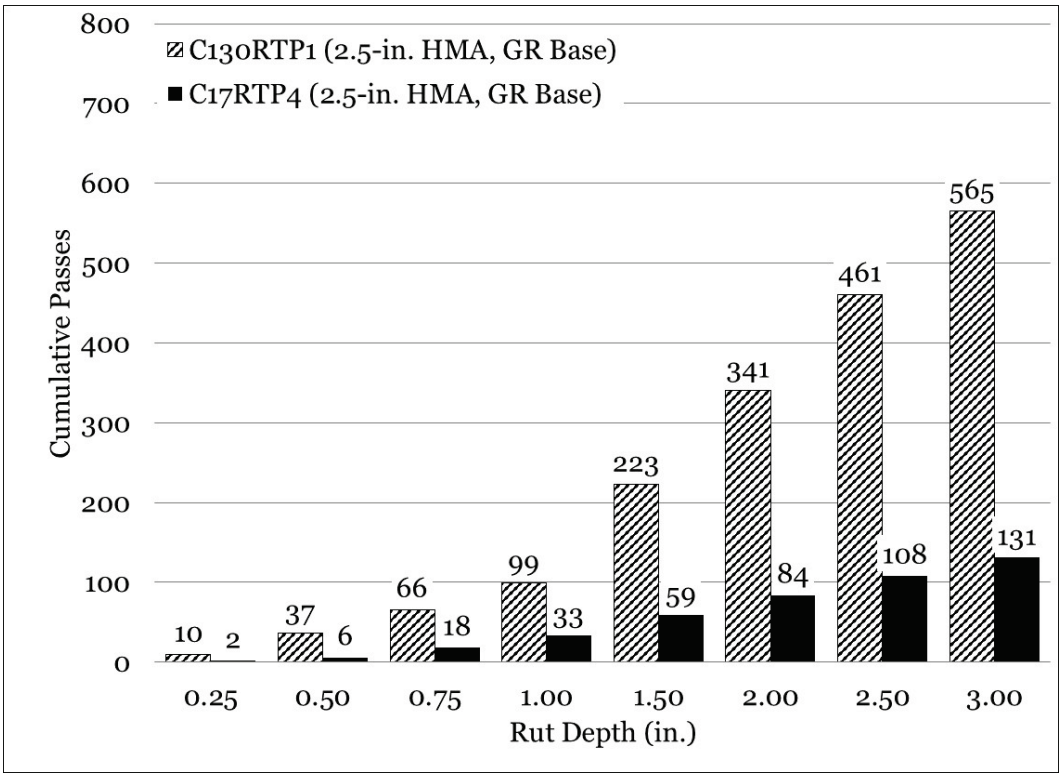

Figure 133. Rut depth comparison reduced tire pressure (2.5-in. HMA, LMS base).

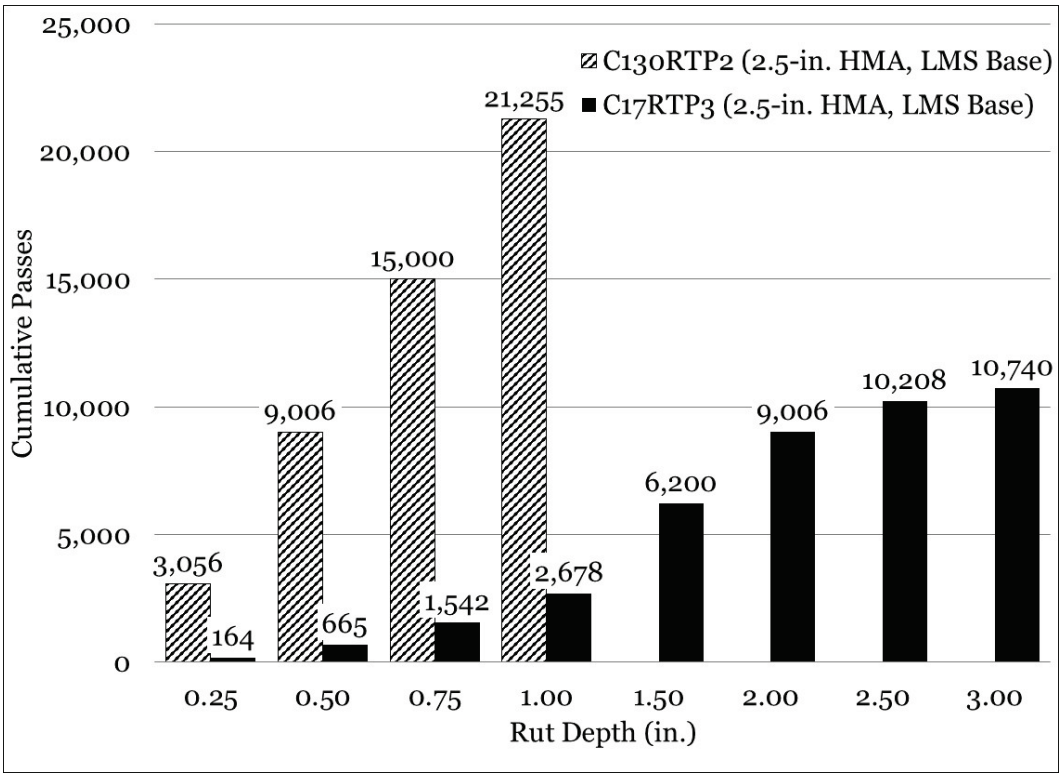

Figure 134. Rut depth comparison reduced tire pressure (1.5-in. HMA, LMS base).

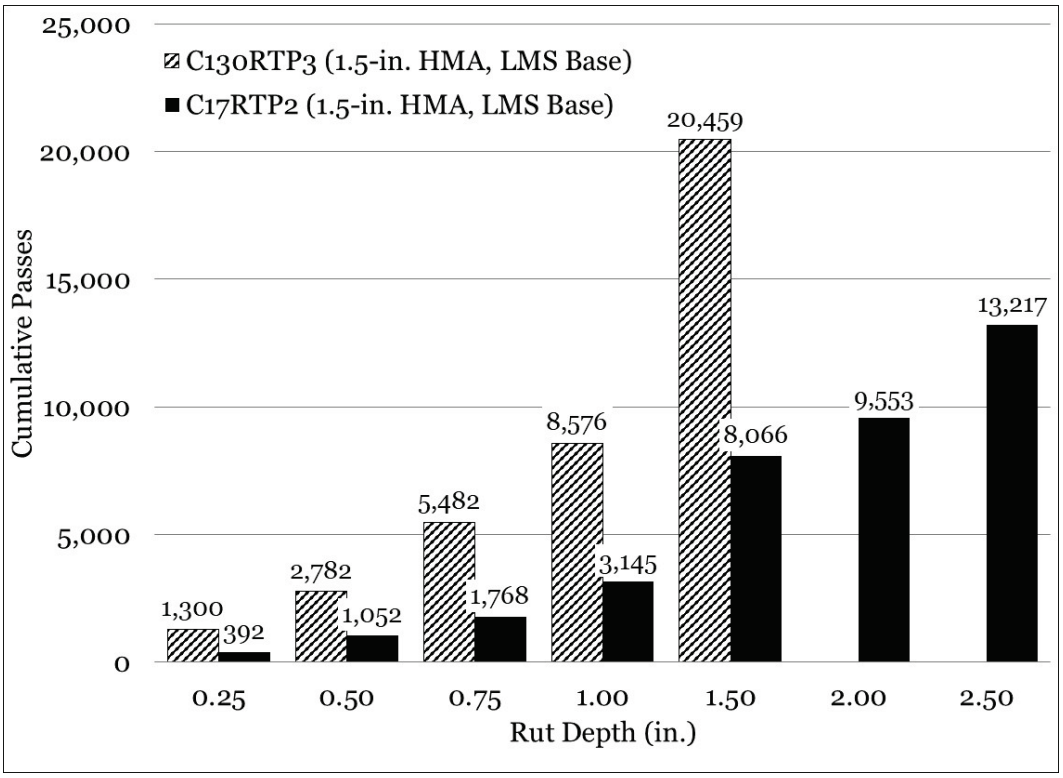

Figure 135. Rut depth comparison reduced tire pressure (1.0-in. HMA, LMS base).

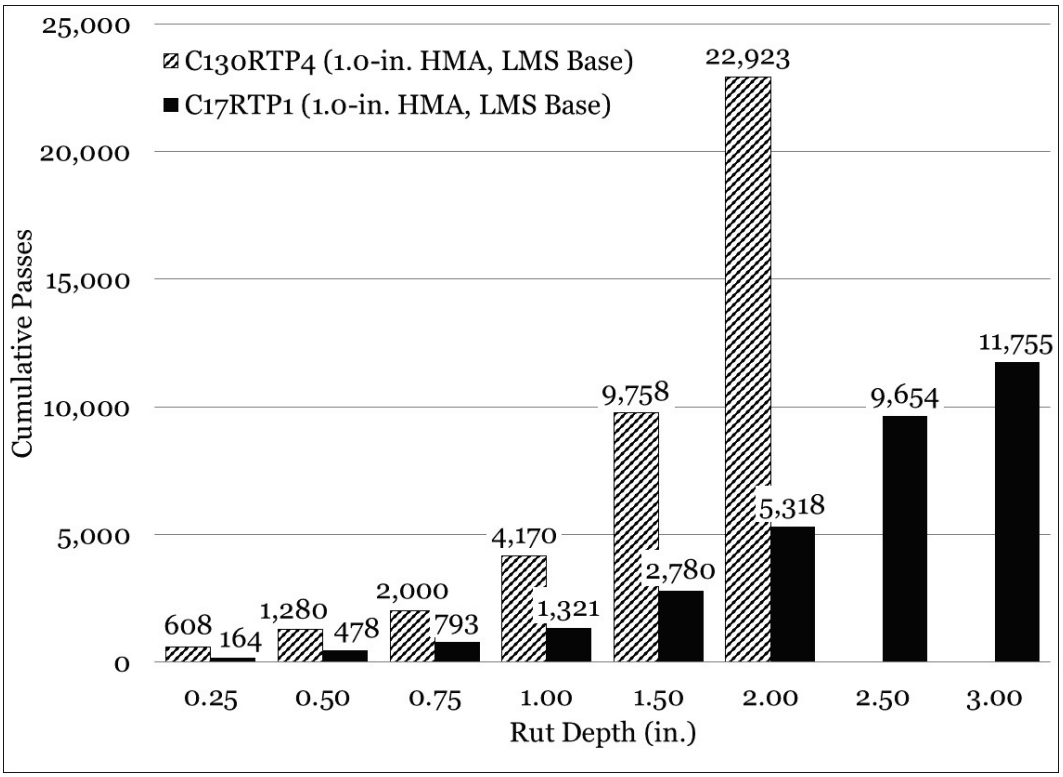

Impulse stiffness

Equality plots were generated to investigate the relationship between C-130 and C-17 impulse stiffness (Figures 136 through 143). Data were paired such that tire pressure condition (i.e., normal or reduced tire pressure) and item cross section were consistent. Impulse stiffness for C-17 traffic was plotted on the x-axis, and impulse stiffness for C-130 traffic was plotted on the y-axis. An LOE is represented by a solid dark line, and a best-fit linear trend line with a y-intercept = 0 was plotted through the data.

A review of the normal tire pressure comparison indicated a poor correlation between C-130 and C-17 ISM, evidenced by negative R^2 values. Negative R^2 values indicate that the linear model was a worse fit than a horizontal line. Thus, it could be concluded that there was no correlation between ISM for the C-130 and C-17 test series, when a linear model subject to the constraint y-intercept=0 was considered.

A better correlation was observed in the reduced tire pressure C-130/C-17 equality plots, and R^2 values ranged from 0.57 to 0.85. In general, the ISM linear trend line plotted below the LOE for the C-130 test series, which suggested that ISM was higher in the C-17 test series than in the C-130 test

series. However, a practical review of the data found that, in most cases, the data plotted above, below, and on the LOE. Thus, definitive conclusions regarding the relationship between C-130 and C-17 ISM for the reduced tire pressure series could not be drawn.

Figure 136. Equality plot - normal tire pressure ISM (2.5-in. HMA, GR base).

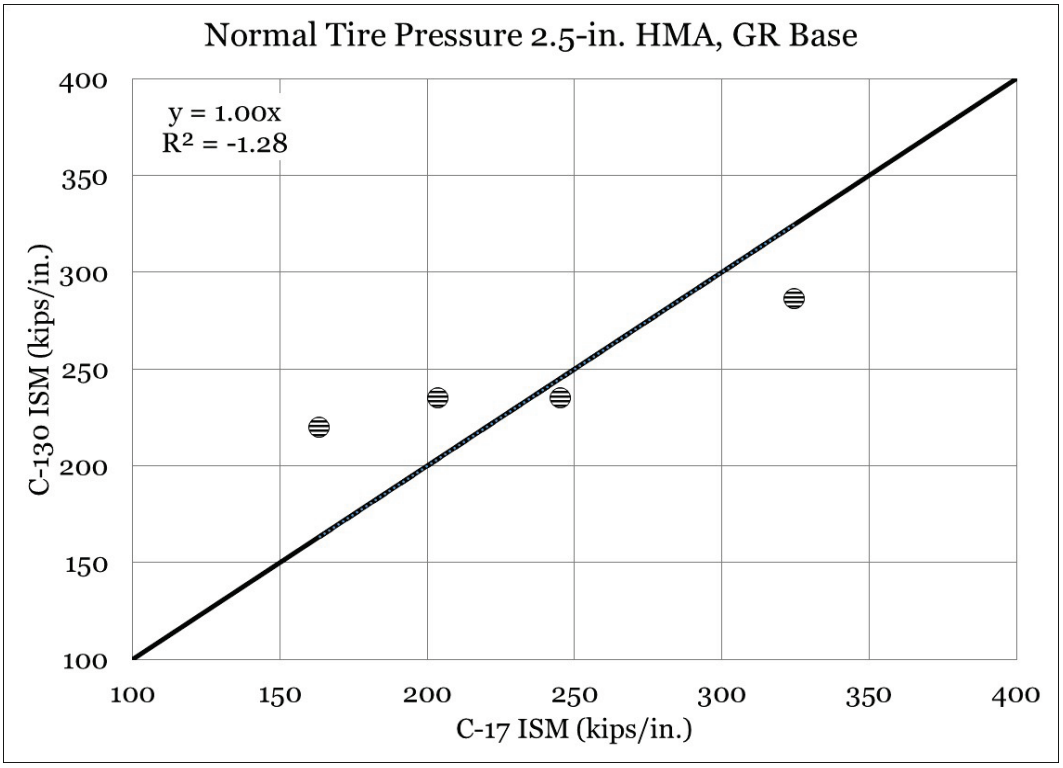

Figure 137. Equality plot - normal tire pressure ISM (2.5-in. HMA, LMS base).

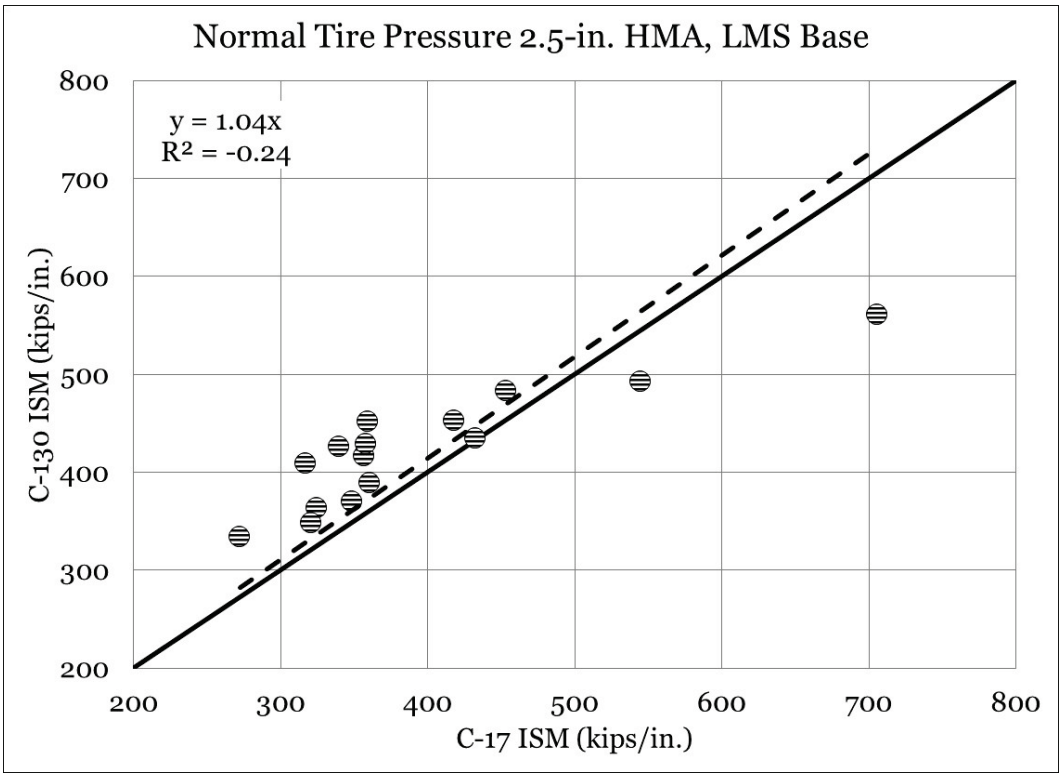

Figure 138. Equality plot - normal tire pressure ISM (1.5-in. HMA, LMS base).

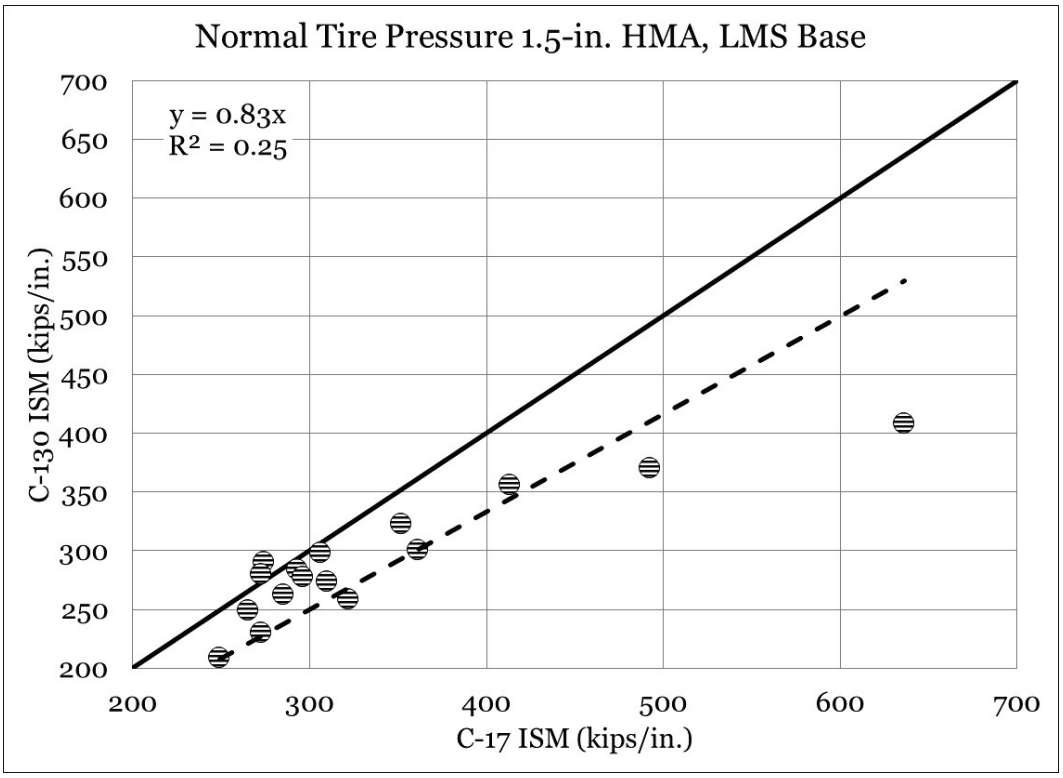

Figure 139. Equality plot - normal tire pressure ISM (1.0-in. HMA, LMS base).

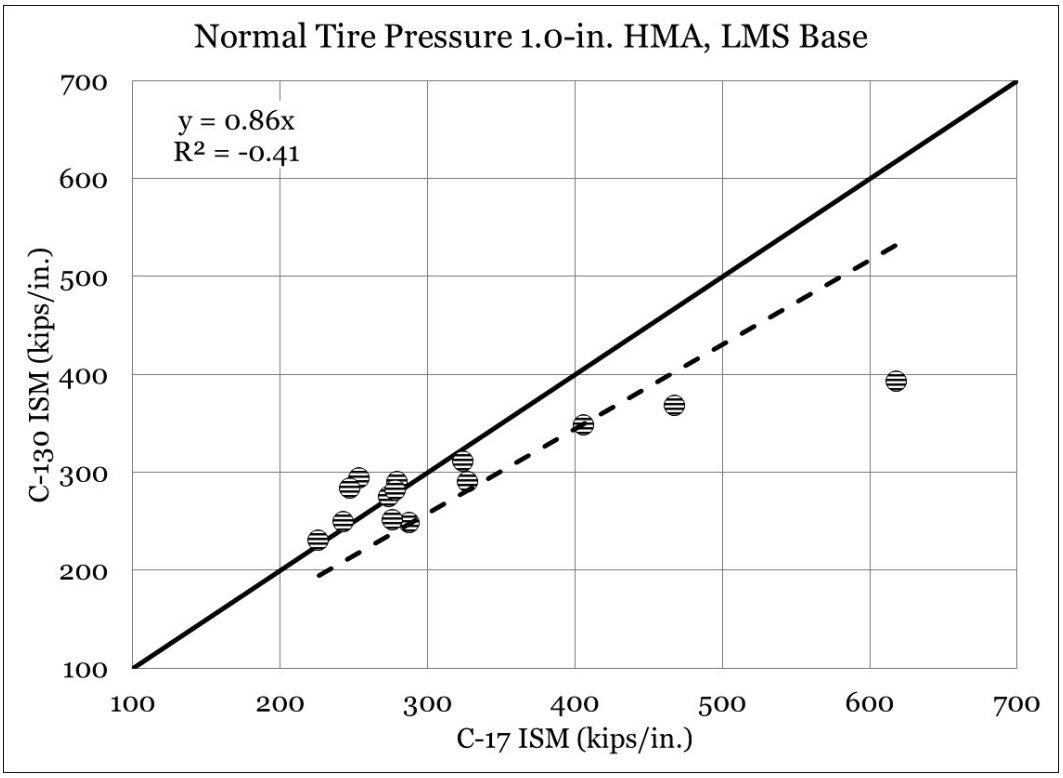

Figure 140. Equality plot - reduced tire pressure ISM (2.5-in. HMA, GR base).

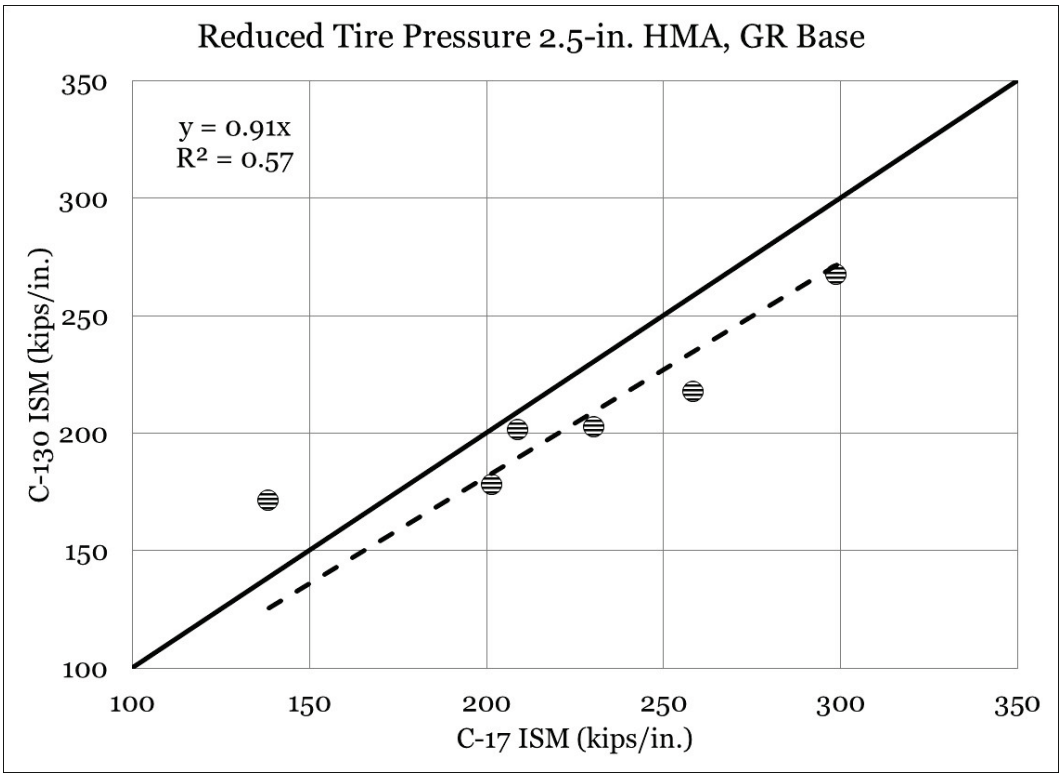

Figure 141. Equality plot - reduced tire pressure ISM (2.5-in. HMA, LMS base).

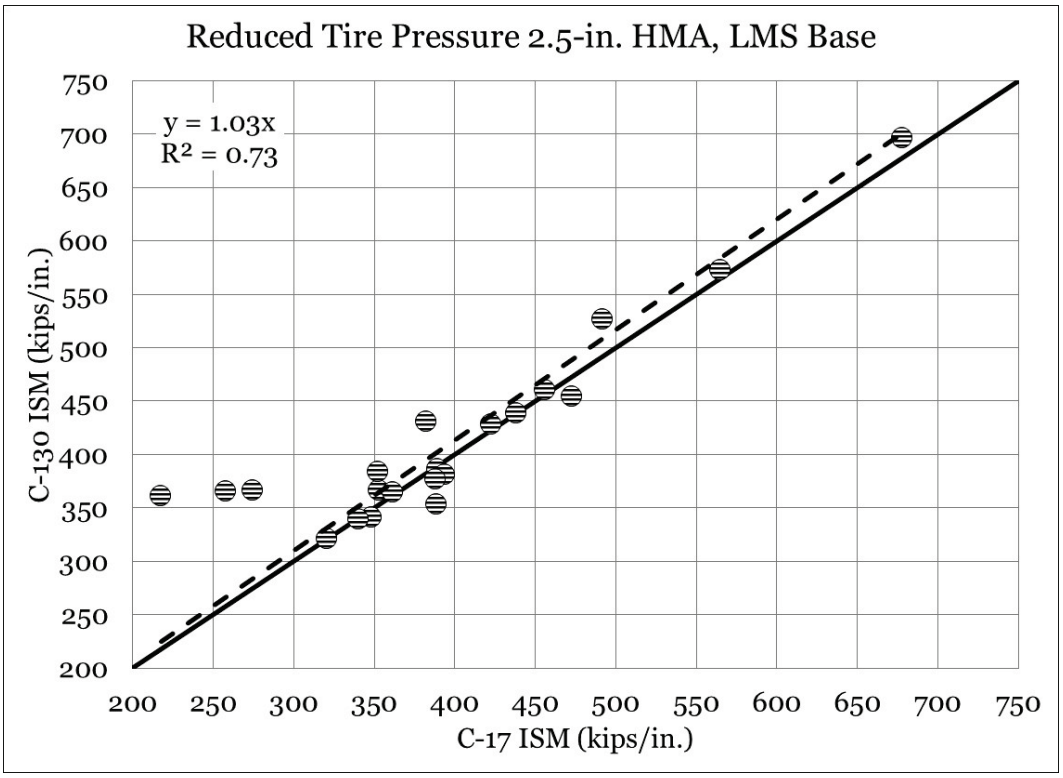

Figure 142. Equality plot - reduced tire pressure ISM (1.5-in. HMA, LMS base).

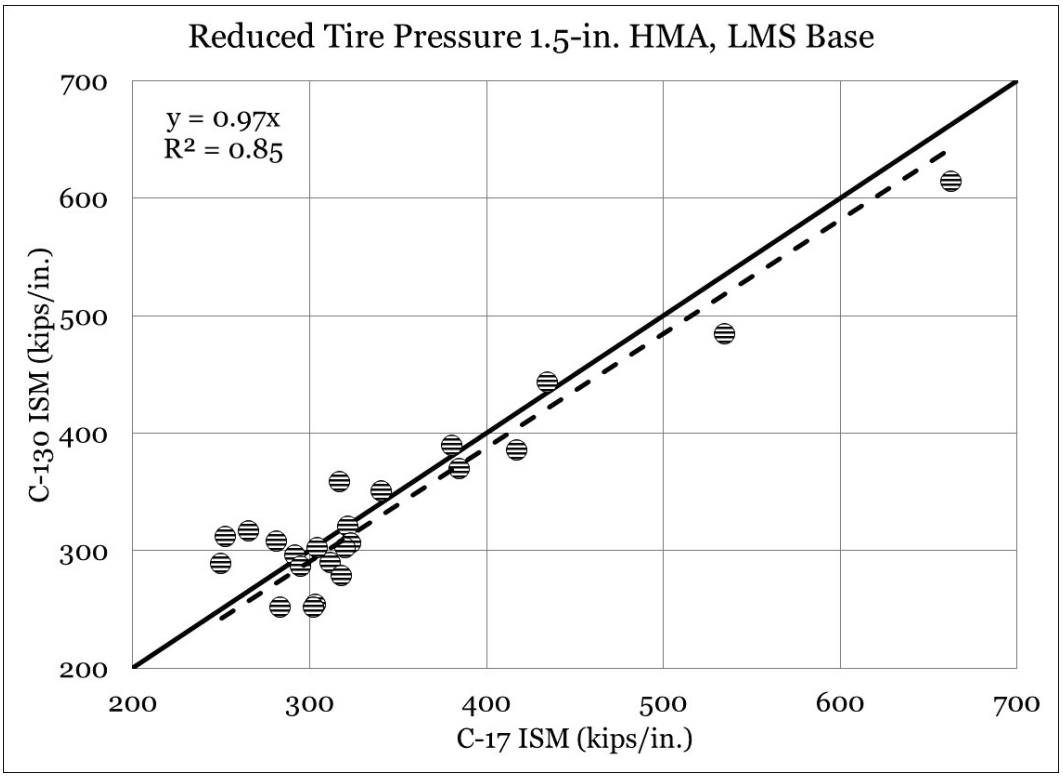

Figure 143. Equality plot - reduced tire pressure ISM (1.0-in. HMA, LMS base).

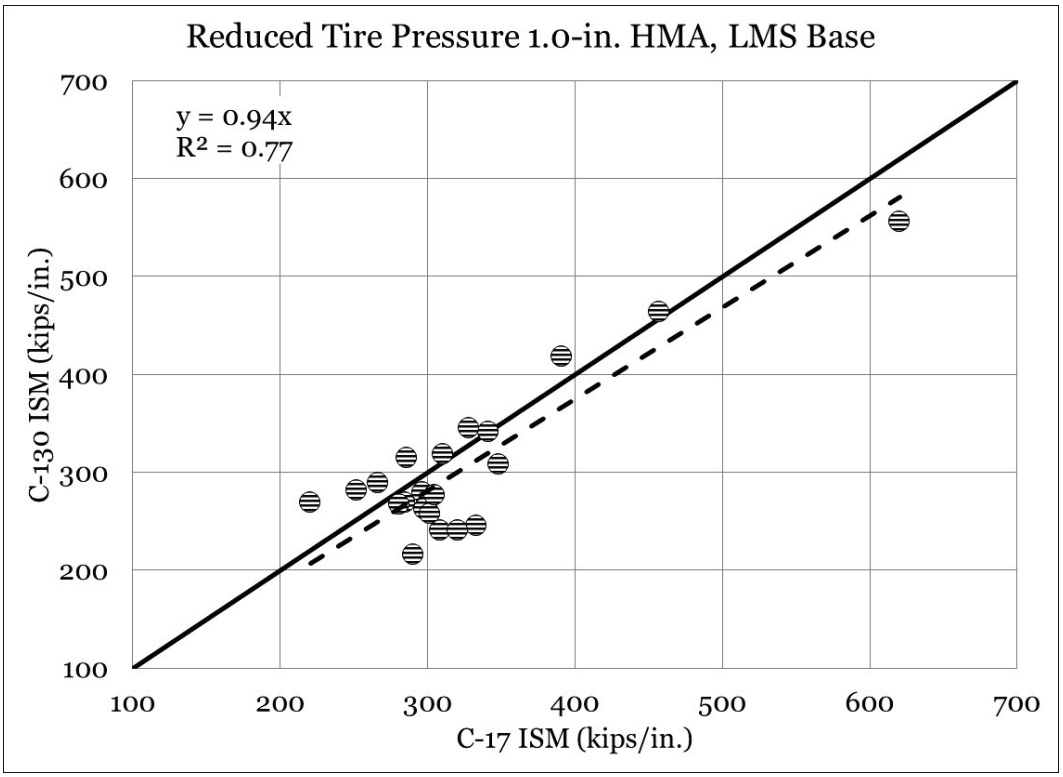

Subgrade pressure response

Equality plots to investigate the relationship between C-130 and C-17 subgrade pressure response are shown in Figures 144 through 151. Data were paired such that tire pressure condition (i.e., normal or reduced tire pressure) and item cross section were consistent. Subgrade pressure response for C-17 traffic was plotted on the x-axis, and subgrade pressure response for C-130 traffic was plotted on the y-axis. An LOE is represented by a solid dark line, and a best-fit linear trend line with a y-intercept = 0 was plotted through the data.

A review of the normal tire pressure equality plots indicated that the reduction in subgrade pressure in the C-130 test series ranged from 33-49% compared to the C-17 test series. All data plotted below the LOE in all cases, as was expected considering a 10,000-lb reduction in total load and a 42 psi reduction in tire pressure. It was noted that when the tire characteristics were considered, total load was reduced approximately 22% under C-130 conditions, and tire pressure was reduced approximately 30% under C-130 conditions.

Figure 144. Equality plot - normal tire pressure subgrade pressure (2.5-in. HMA, GR base).

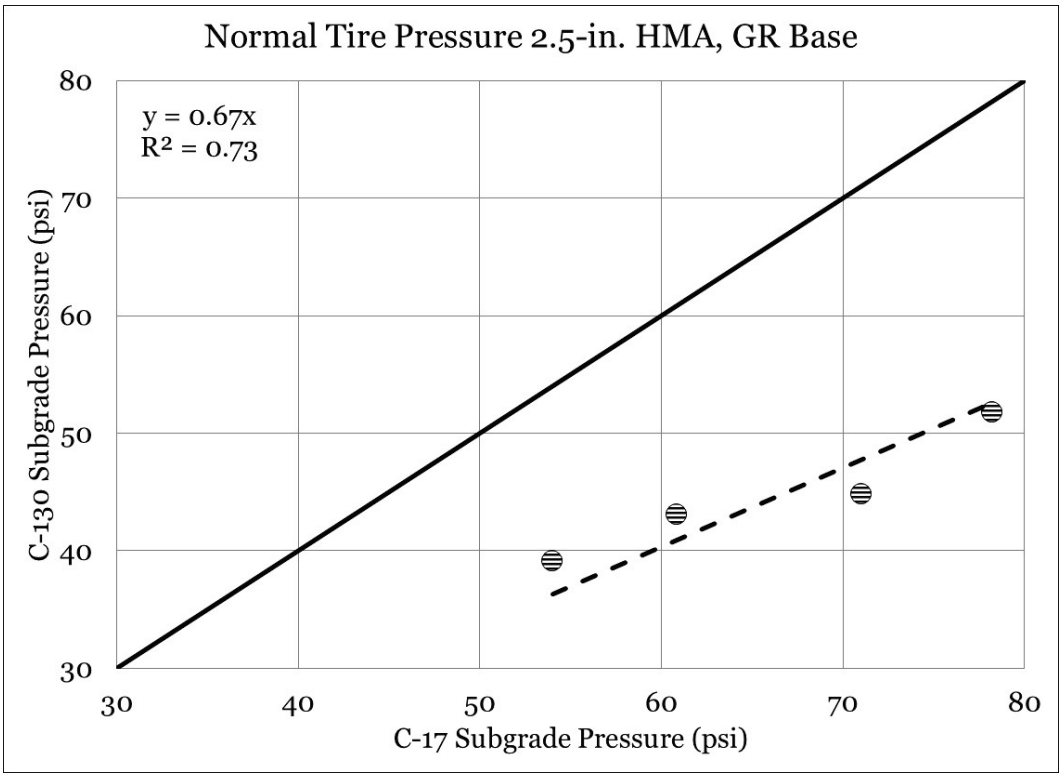

Figure 145. Equality plot - normal tire pressure subgrade pressure (2.5-in. HMA, LMS base).

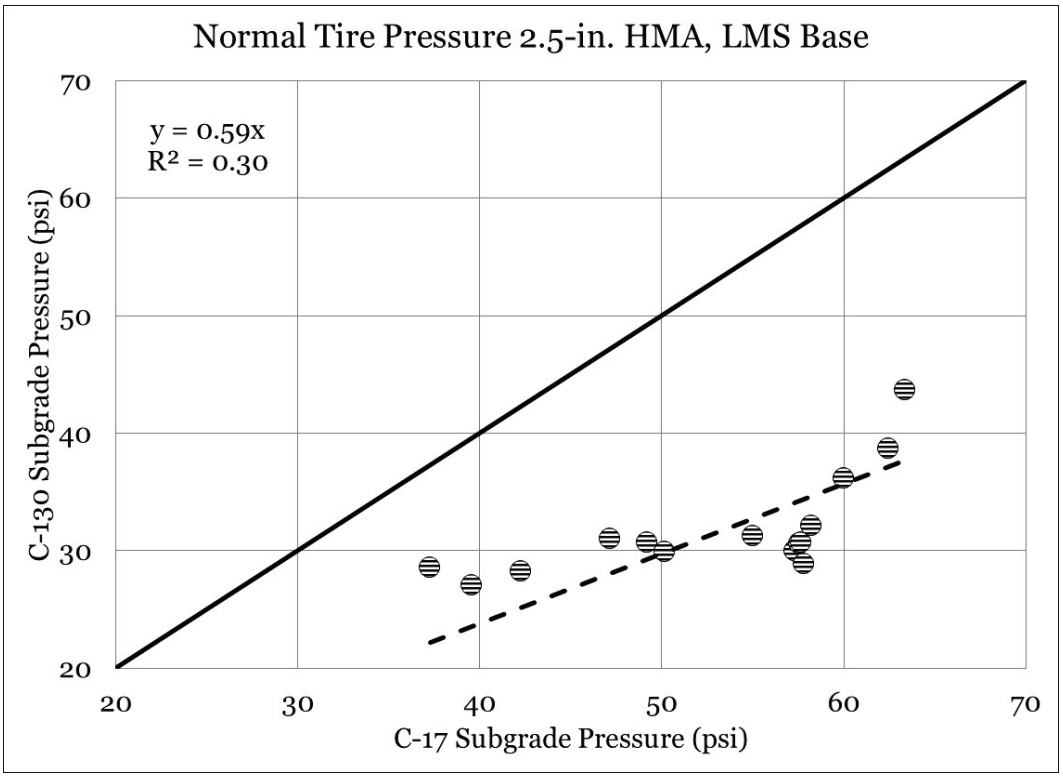

Figure 146. Equality plot - normal tire pressure subgrade pressure (1.5-in. HMA, LMS base).

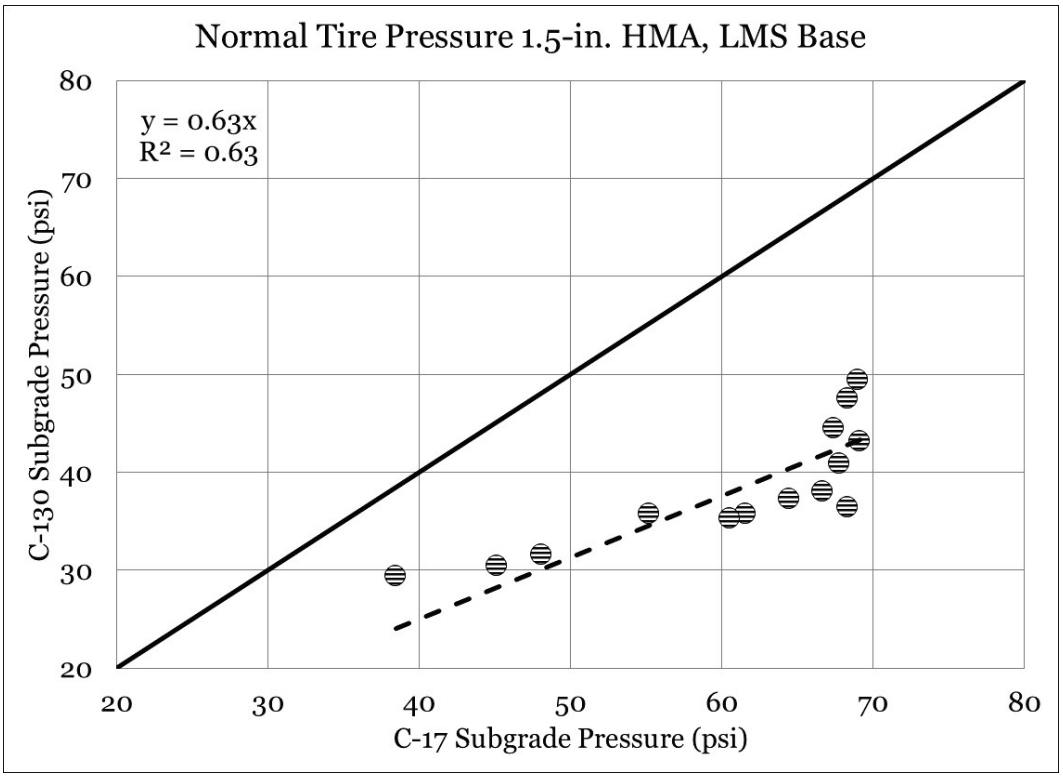

Figure 147. Equality plot - normal tire pressure subgrade pressure (1.0-in. HMA, LMS base).

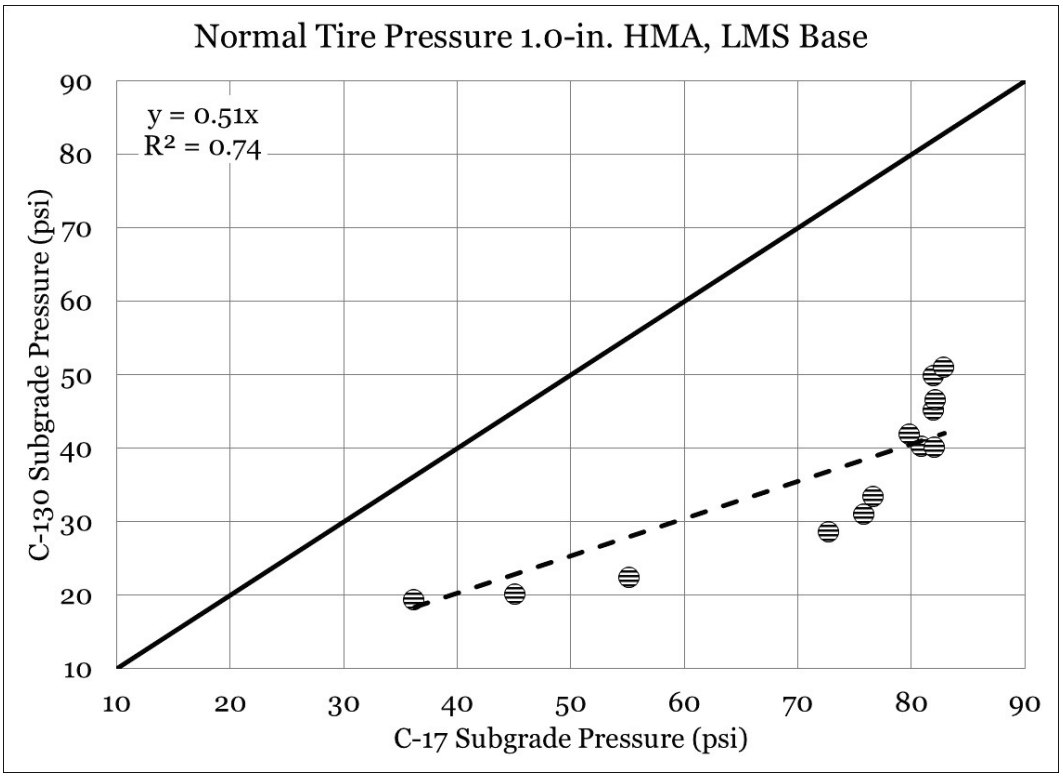

A review of the equality plots for subgrade pressure in the reduced tire pressure test series indicated that reductions in subgrade pressure attributed to C-130 loading ranged from 12% to 31%, which was somewhat lower than that observed in the normal tire pressure test comparisons. It was noted that reduction in total load was the same (22%) as the normal tire pressure test series and that percent reductions in tire pressure were the same (30%) as the normal tire pressure test series. However, the magnitude of change was different: the normal test series was a 42-psi reduction whereas the reduced test series was a 35-psi reduction, which could explain the observed reduced performance differences when compared to the normal tire pressure observations.

Figure 148. Equality plot - reduced tire pressure subgrade pressure (2.5-in. HMA, GR base).

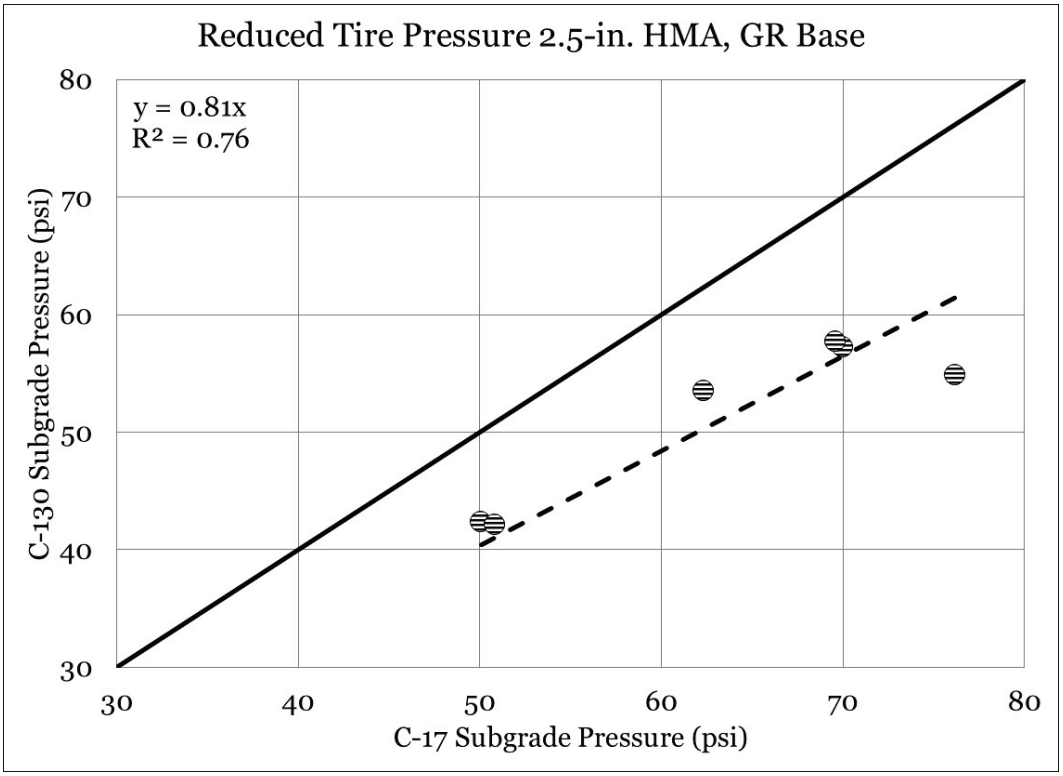

Figure 149. Equality plot - reduced tire pressure subgrade pressure (2.5-in. HMA, LMS base).

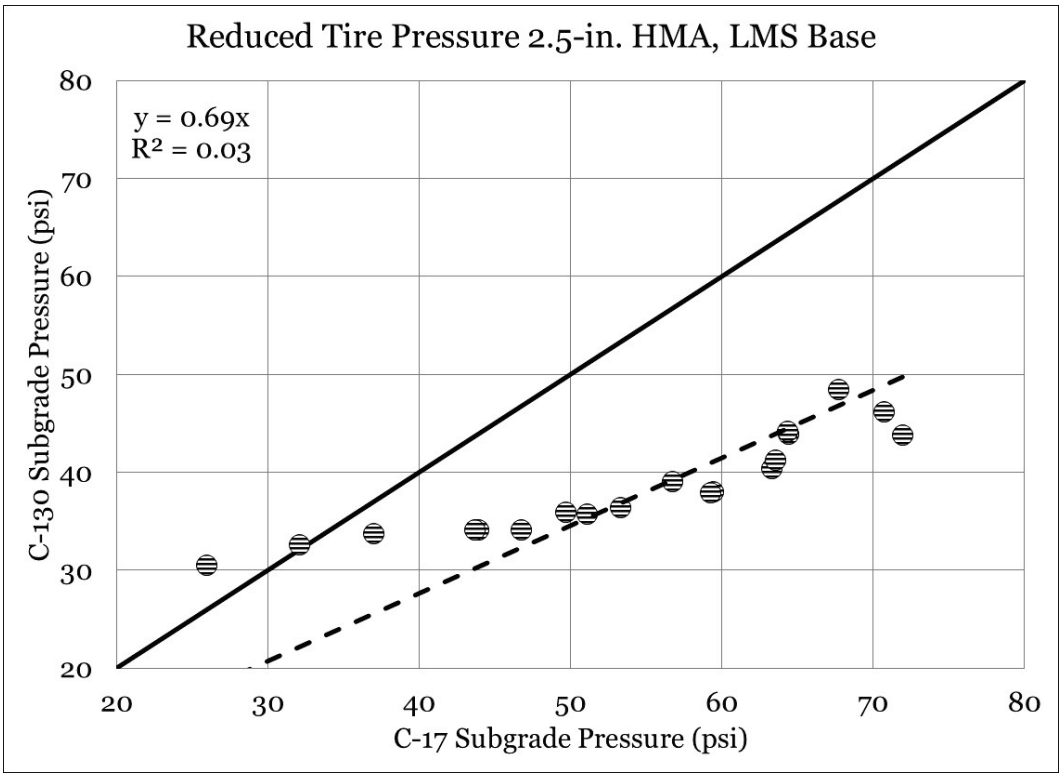

Figure 150. Equality plot - reduced tire pressure subgrade pressure (1.5-in. HMA, LMS base).

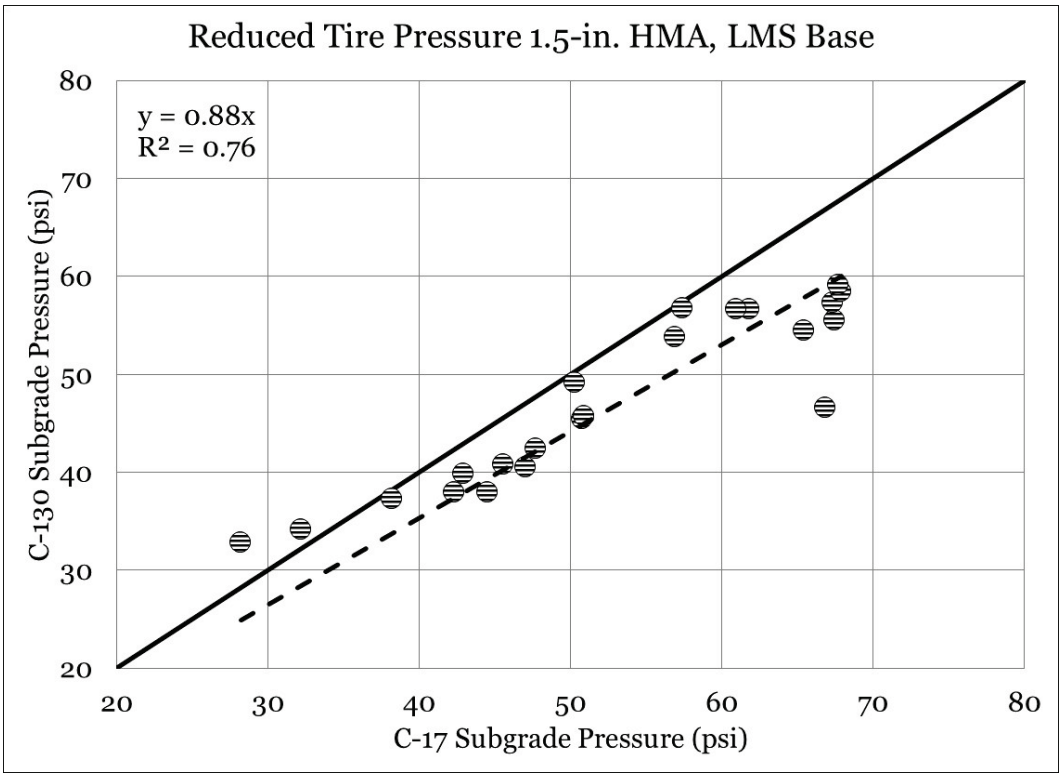

Figure 151. Equality plot - reduced tire pressure subgrade pressure (1.0-in. HMA, LMS base).

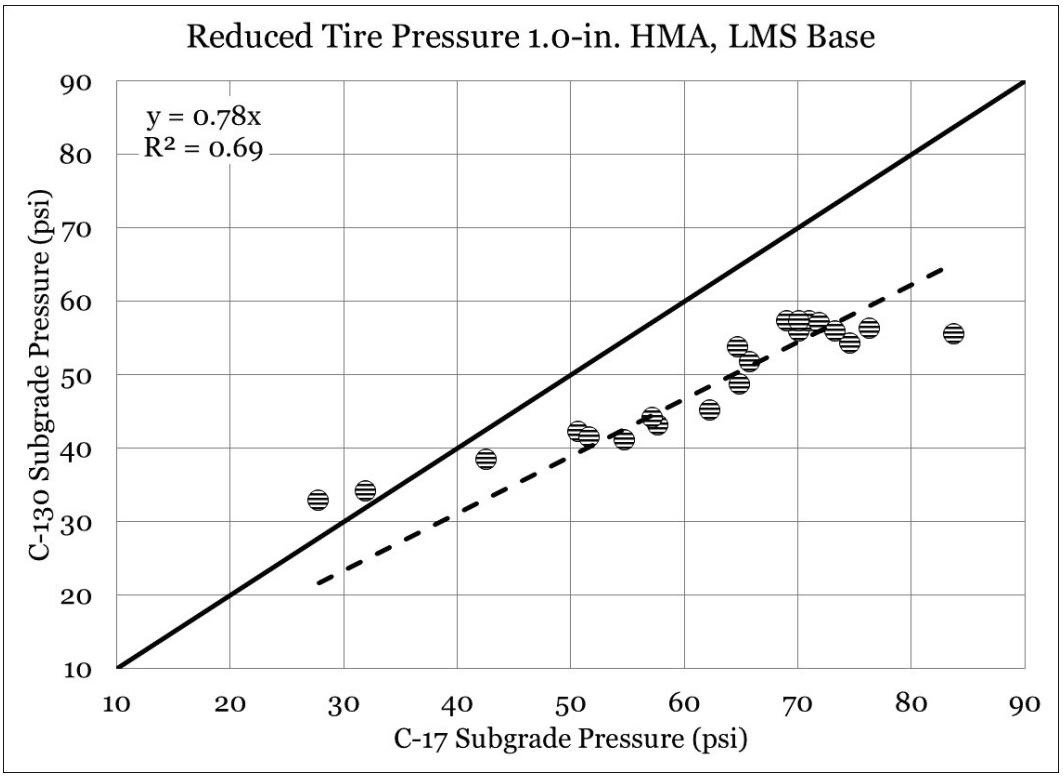

Base pressure response

Equality plots to investigate the relationship between C-130 and C-17 base pressure response are shown in Figures 152 through 159. Data were paired such that tire pressure condition (i.e., normal or reduced tire pressure) and item cross section were consistent. Base pressure response for C-17 traffic was plotted on the x-axis, and base pressure response for C-130 traffic was plotted on the y-axis. An LOE is represented by a solid dark line, and a best-fit linear trend line with a y-intercept = 0 was plotted through the data.

A review of equality plots for the normal tire pressure test series indicated that reductions in base pressure for the C-130 test series ranged from 24% to 38%; however, the fitted equation was very poor for the 1.5-in. HMA, LMS base (R^2 = -3.36; Figure 154) and 1.0-in. HMA, LMS base (R^2 = -0.34; Figure 155) test item comparisons. All data were found to plot below the LOE, indicating that base pressure was consistently less in the C-130 test items when compared to the C-17 test items, as expected.

Figure 152. Equality plot - normal tire pressure base pressure (2.5-in. HMA, GR base).

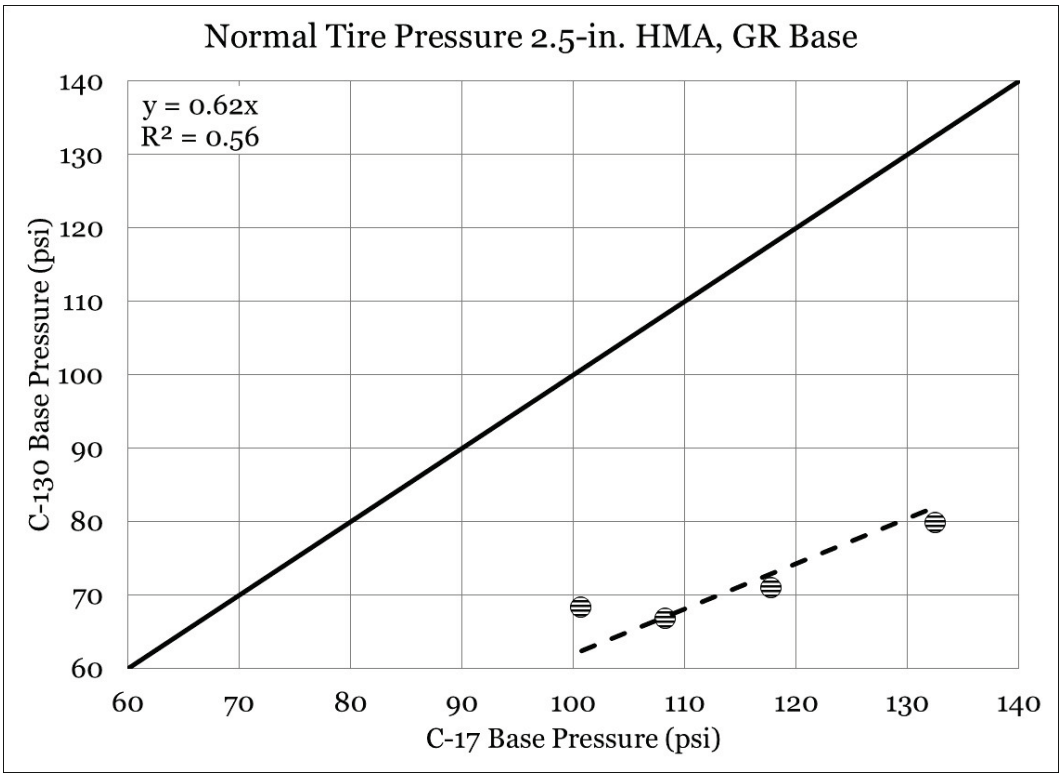

Figure 153. Equality plot - normal tire pressure base pressure (2.5-in. HMA, LMS base).

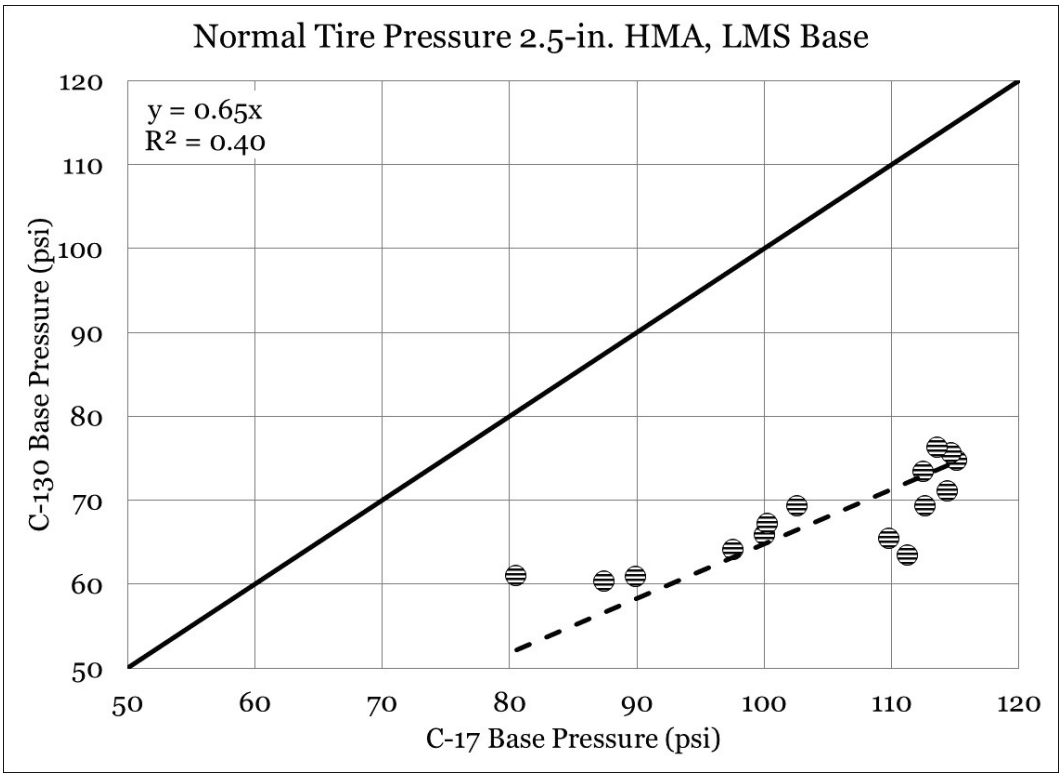

Figure 154. Equality plot - normal tire pressure base pressure (1.5-in. HMA, LMS base).

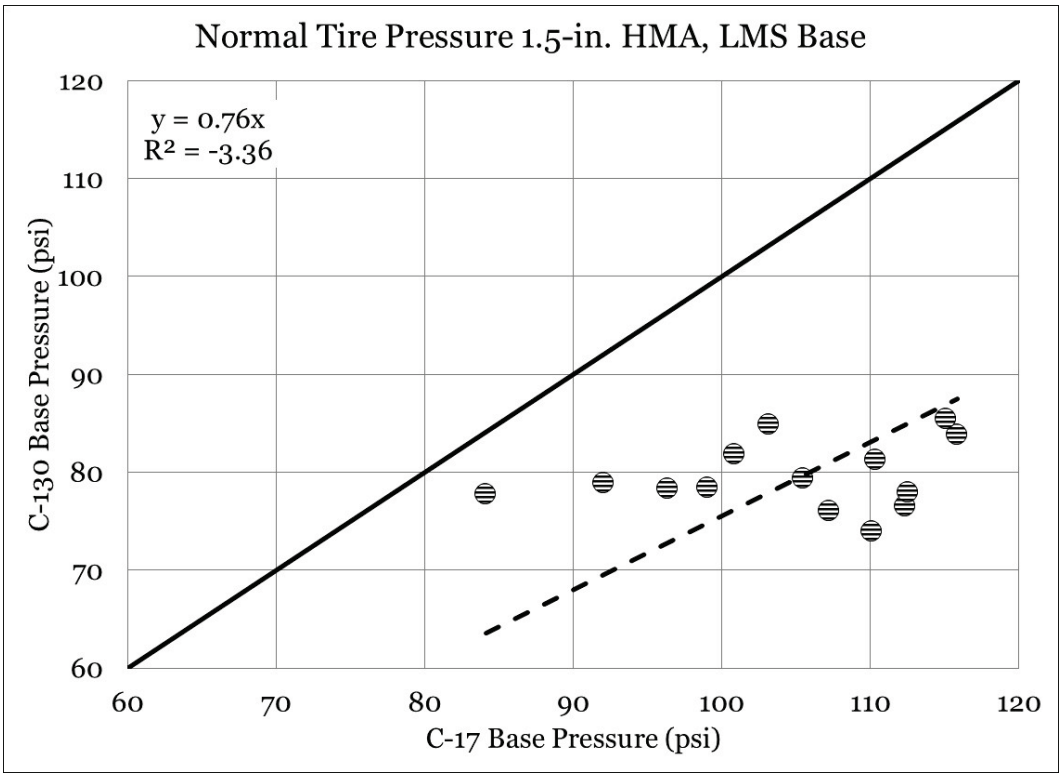

Figure 155. Equality plot - normal tire pressure base pressure (1.0-in. HMA, LMS base).

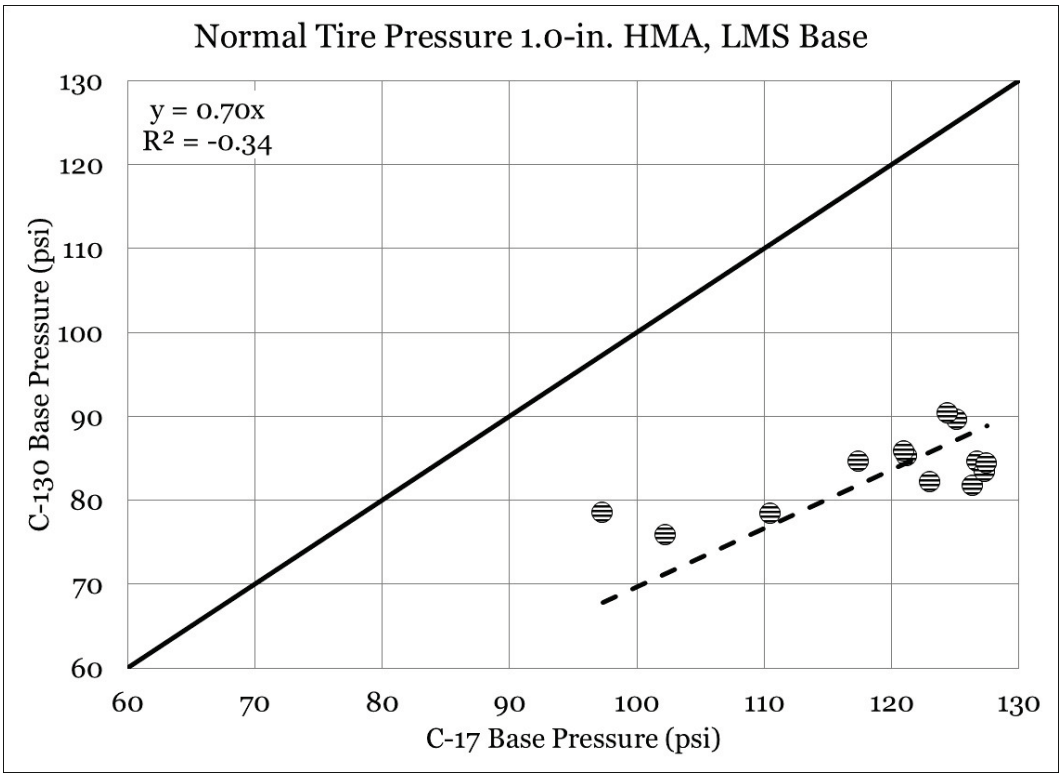

Reductions in base pressure for the reduced tire pressure comparisons were found to range from 10-31%, which was less than differences observed in the normal tire pressure comparisons. Similar observations were made in the subgrade pressure response comparisons, and it is suggested that a smaller magnitude reduction in tire pressure likely influenced the observed relationships. Similar to the normal tire pressure series, a poor fit of the linear trend line to the plotted data was observed. Data were observed to plot below the LOE, particularly at higher pressure (i.e., damaged pavement), whereas the data were found to plot above the LOE at lower pressure (i.e., start of traffic). These differences support the hypothesis that there was a period of shakedown or initial densification that occurred early in traffic, after which the comparisons tend to trend as expected (i.e., fall below the LOE).

Figure 156. Equality plot - reduced tire pressure base pressure (2.5-in. HMA, GR base).

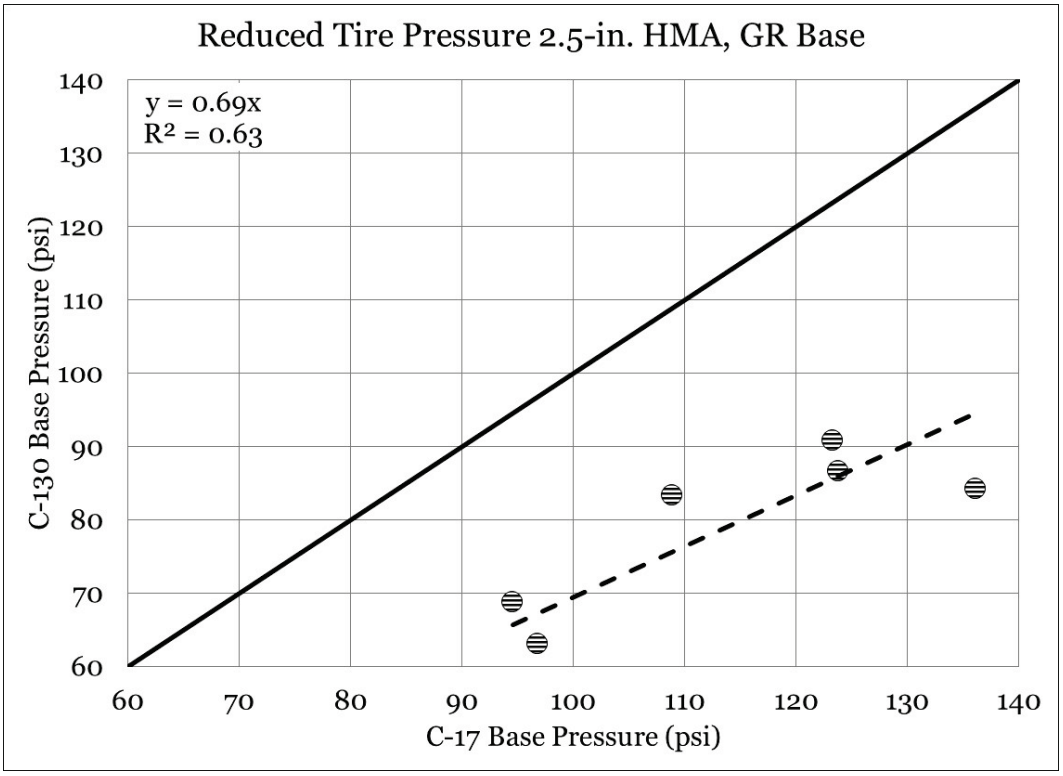

Figure 157. Equality plot - reduced tire pressure base pressure (2.5-in. HMA, LMS base).

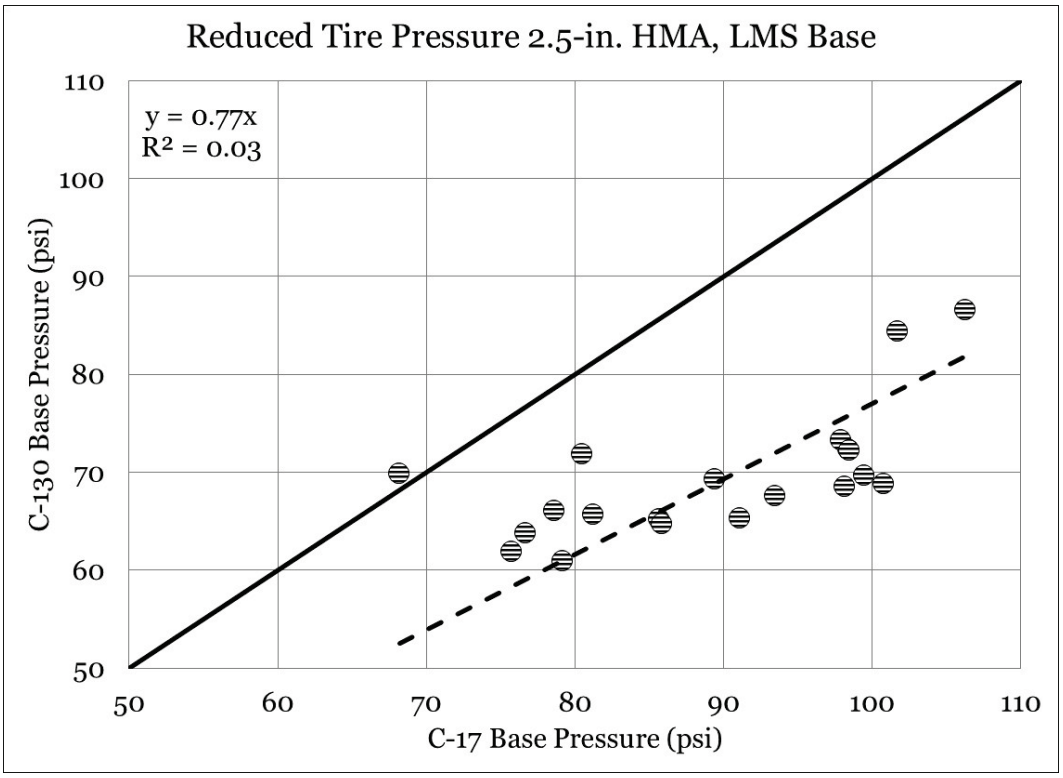

Figure 158. Equality plot - reduced tire pressure base pressure (1.5-in. HMA, LMS base).

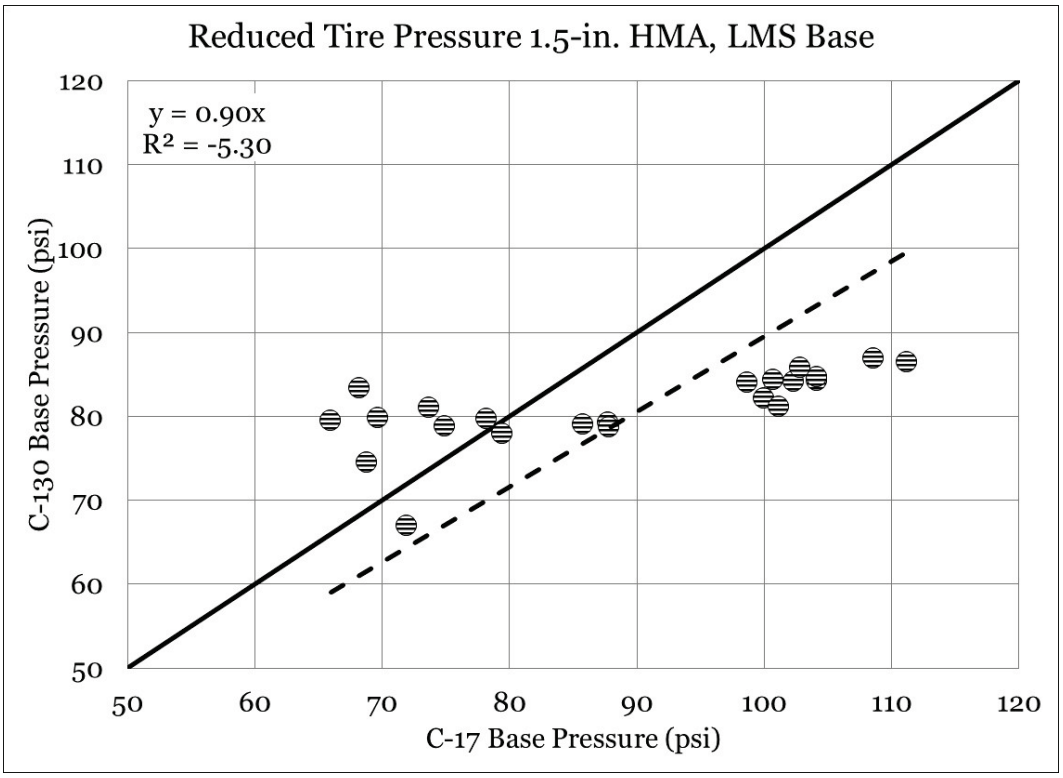

Figure 159. Equality plot - reduced tire pressure base pressure (1.0-in. HMA, LMS base).

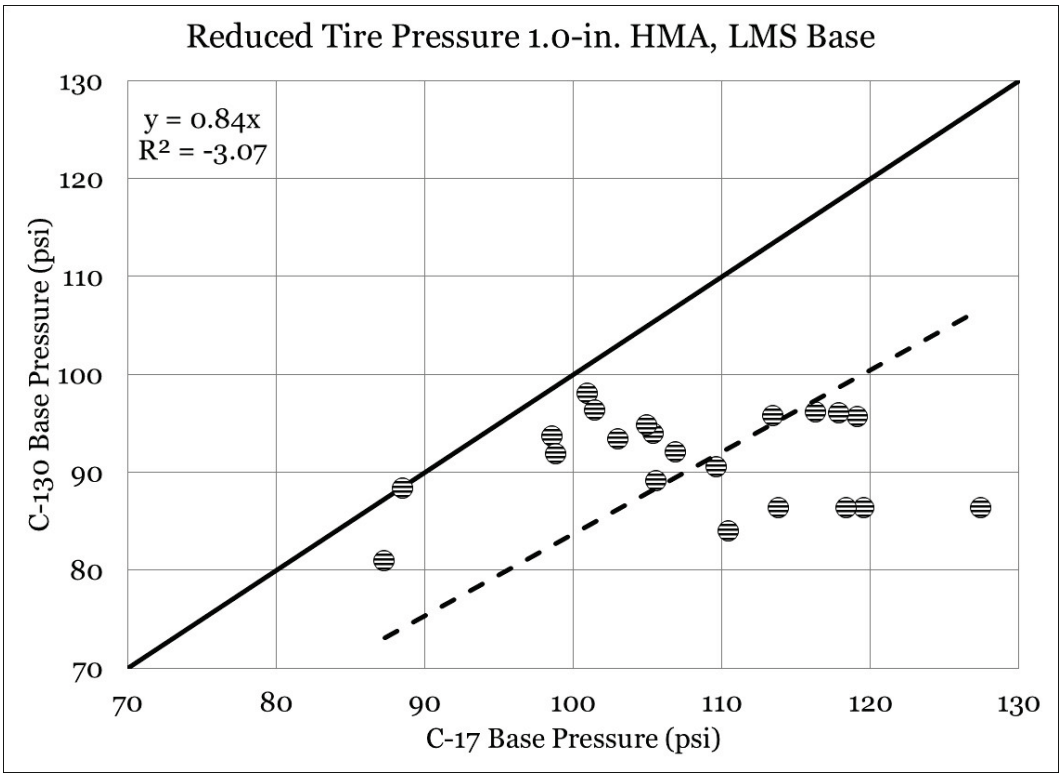

Single-depth deflectometer response

Equality plots to investigate the relationship between C-130 and C-17 subgrade deflection responses are shown in Figures 160 through 166. It is noted that data were not available for C17NTP4 (2.5-in. HMA, GR base, normal tire pressure); thus, no plots were generated for this test item. Data were paired such that tire pressure condition (i.e., normal or reduced tire pressure) and item cross section were consistent. Subgrade deflection response for C-17 traffic was plotted on the x-axis, and subgrade deflection response for C-130 traffic was plotted on the y-axis. An LOE is represented by a solid dark line, and a best-fit linear trend line with a y-intercept = 0 was plotted through the data.

A review of the normal tire pressure test comparisons found that a good correlation existed between the C-130 and C-17 subgrade deflections, and R^2 values ranged from 0.82 to 0.91. All data were found to plot below the LOE in each test case, which was expected from the reduced load and tire pressure of the C-130. Reductions in subgrade deflection were observed to range from 76% in the 2.5-in. HMA, LMS base section (Figure 160) to 53% in the 1.0-in. HMA, LMS base section (Figure 162). Further, it was found

that improvements in subgrade deflection decreased (generally on the order of 10%) with a decrease in asphalt thickness.

Similar trends in subgrade deflection comparisons were observed in the reduced tire pressure test series. Improvements in subgrade deflection attributed to C-130 traffic were found to range from 26% to 59%. All data were found to plot below the LOE, indicating that subgrade deflection was consistently lower in the C-130 test series. A good correlation between C-130 and C-17 subgrade deflections was observed, and R^2 values were found to range from 0.89 to 0.97. When compared to the normal tire pressure comparisons, it was observed that improvements in performance were less in the reduced tire pressure test series. These observations mimic those observed in both base and subgrade pressure response data, further suggesting that the overall magnitude of tire pressure played a consequential role in measured pavement response.

Figure 160. Equality plot - normal tire pressure subgrade deflection (2.5-in. HMA, LMS base).

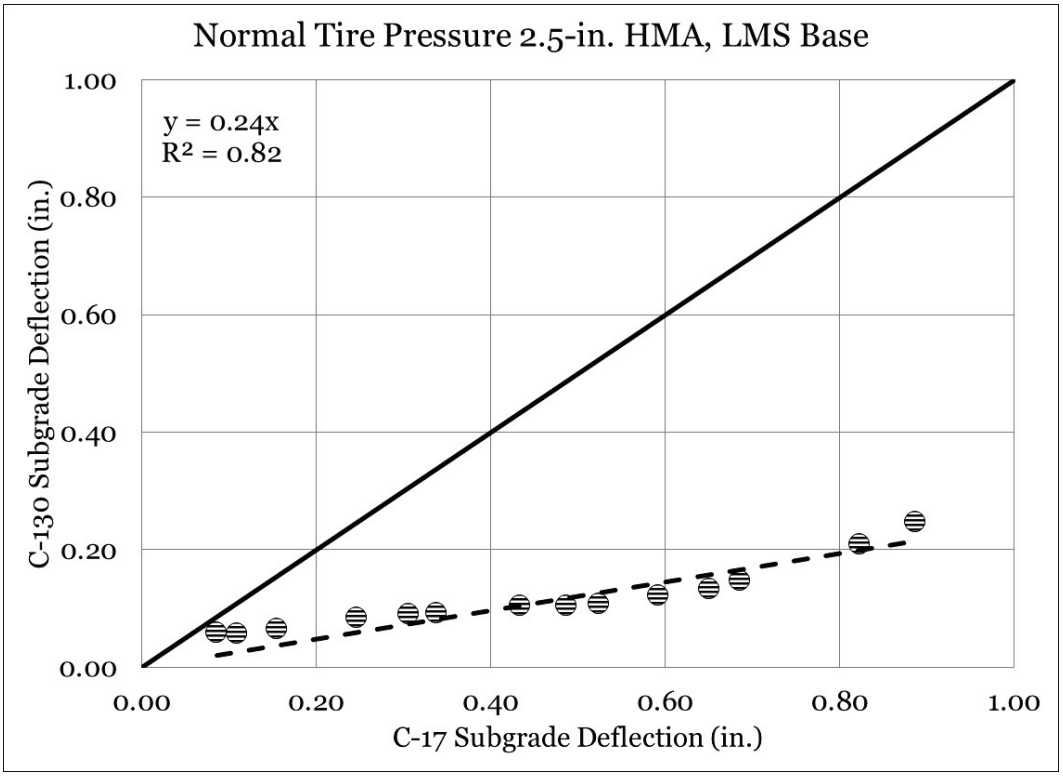

Figure 161. Equality plot - normal tire pressure subgrade deflection (1.5-in. HMA, LMS base).

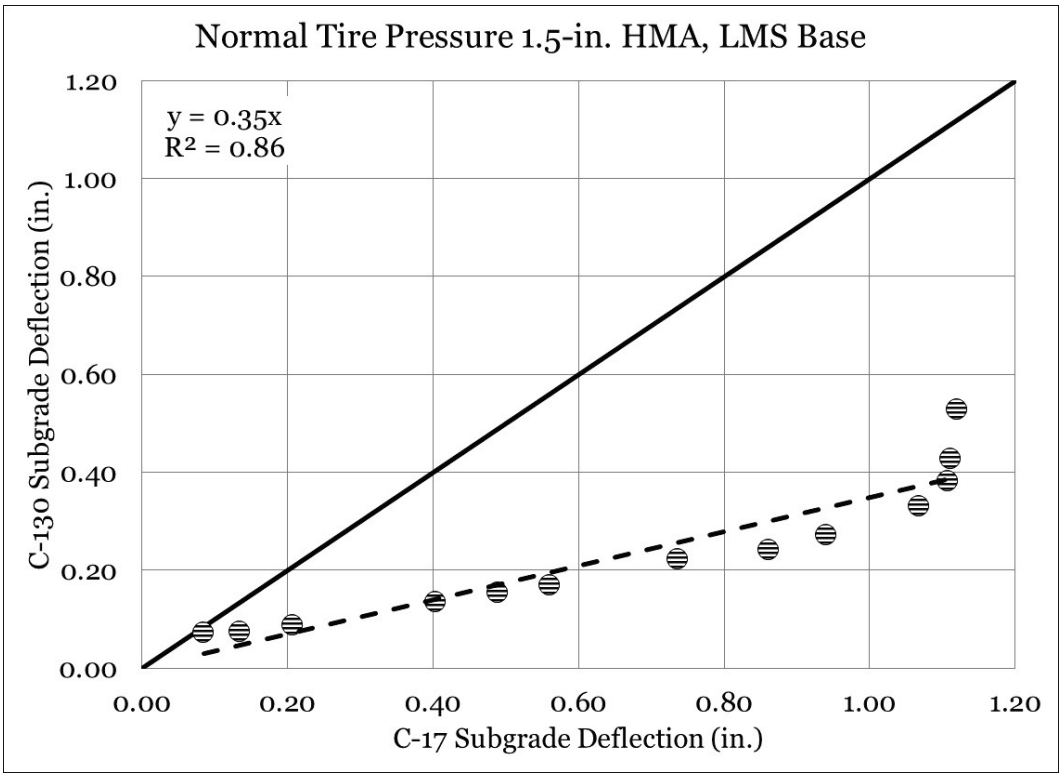

Figure 162. Equality plot - normal tire pressure subgrade deflection (1.0-in. HMA, LMS base).

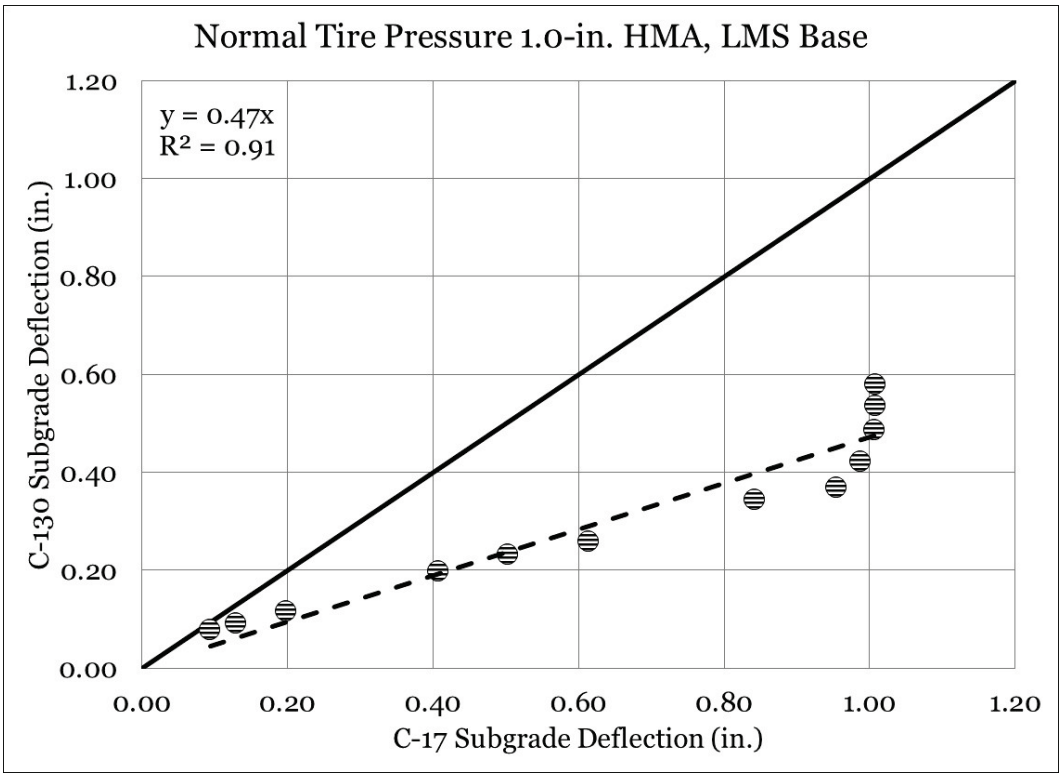

Figure 163. Equality plot - reduced tire pressure subgrade deflection (2.5-in. HMA, GR base).

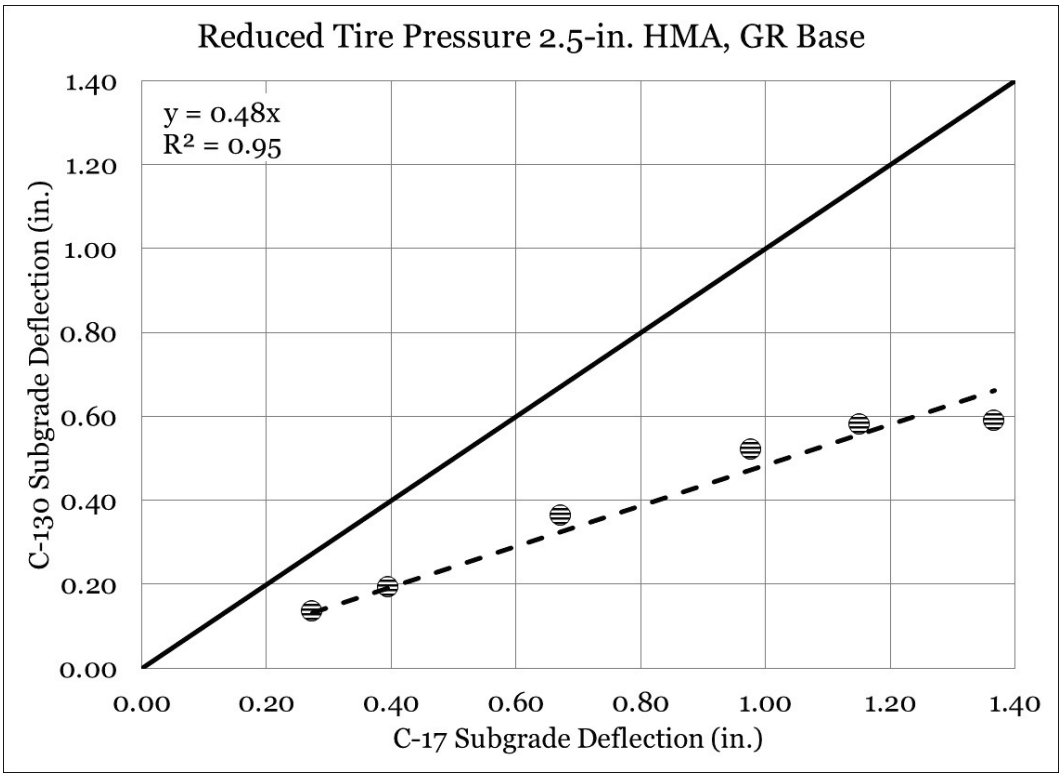

Figure 164. Equality plot - reduced tire pressure subgrade deflection (2.5-in. HMA, LMS base).

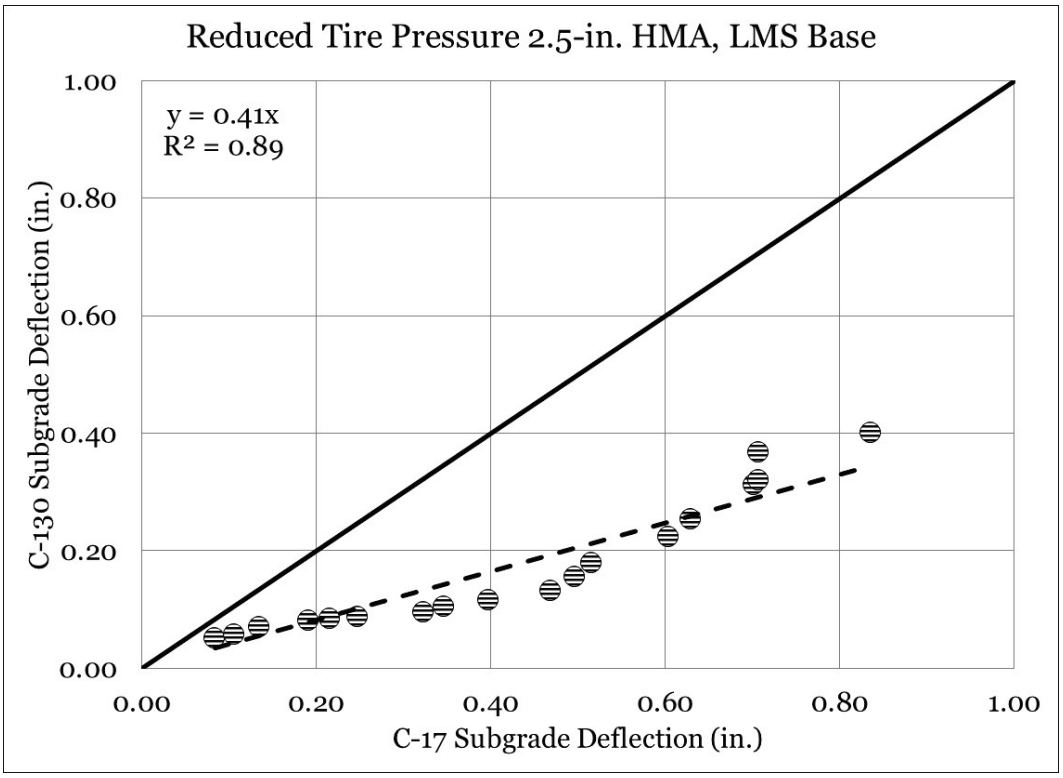

Figure 165. Equality plot - reduced tire pressure subgrade deflection (1.5-in. HMA, LMS base).

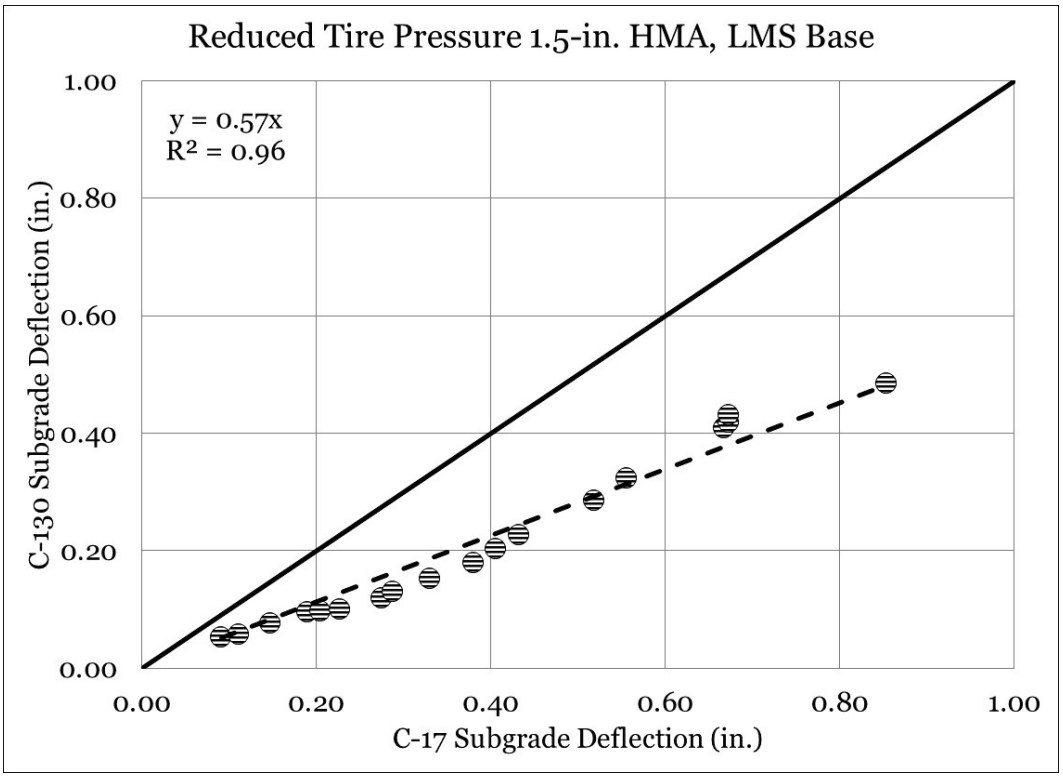

Figure 166. Equality plot - reduced tire pressure subgrade deflection (1.0-in. HMA, LMS base).

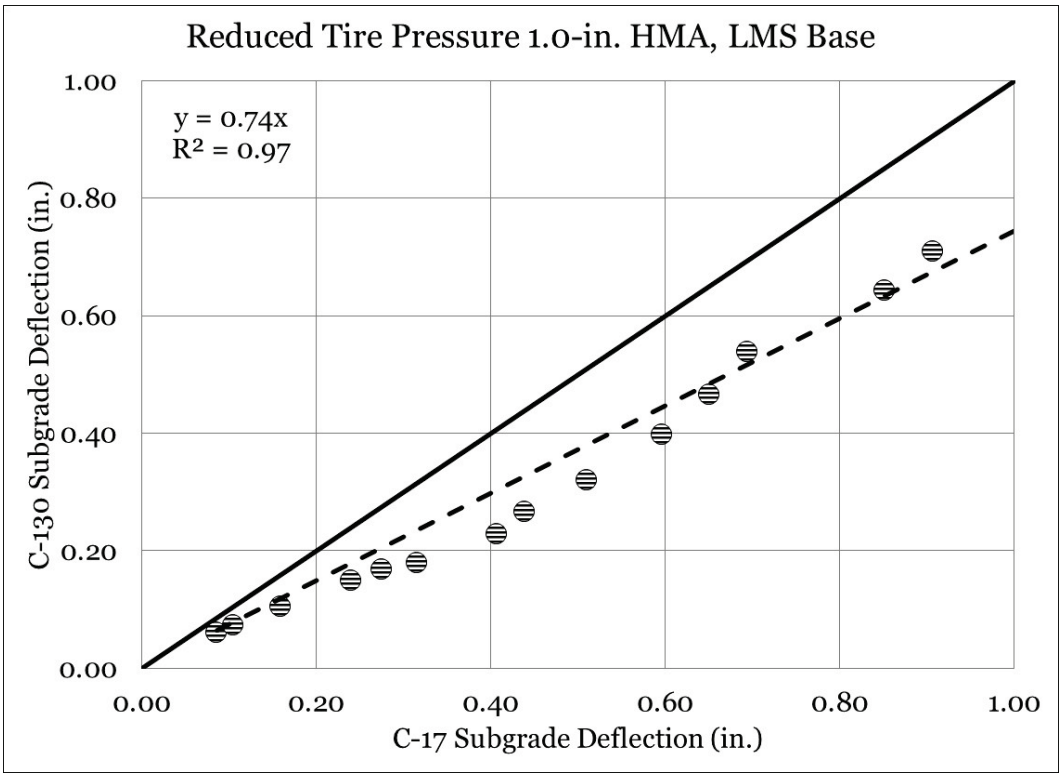

Asphalt strain gauge response

Equality plots to investigate the relationship between C-130 and C-17 total asphalt strain responses are shown in Figures 167 through 174. It is noted that data were not available for C17NTP4 (2.5-in. HMA, GR base, normal tire pressure); thus, no plots were generated for this test item. Data were paired such that tire pressure condition (i.e., normal or reduced tire pressure) and item cross section were consistent. Total asphalt strain response for C-17 traffic was plotted on the x-axis, and total strain response for C-130 traffic was plotted on the y-axis. An LOE is represented by a solid dark line, and a best-fit linear trend line with a y-intercept = 0 was plotted through the data.

A review of the equality plots for the total asphalt strain data indicated that little to no correlation existed between the total strain in the C-130 test series and that in the C-17 test series, evidenced by the low or negative R^2 values. Most data for each test comparison plotted below the LOE, indicating that measured total asphalt strain response in the C-130 test series was lower than that in the C-17 test series. The exception to this observation was in the 1.0-in. HMA, LMS base reduced tire pressure comparison (Figure 174), in which most of the data plotted above the LOE, indicating that total asphalt strain was higher in the C-130 test item than in the C-17 test item.

Figure 167. Equality plot - normal tire pressure ASG response (2.5-in. HMA, GR base).

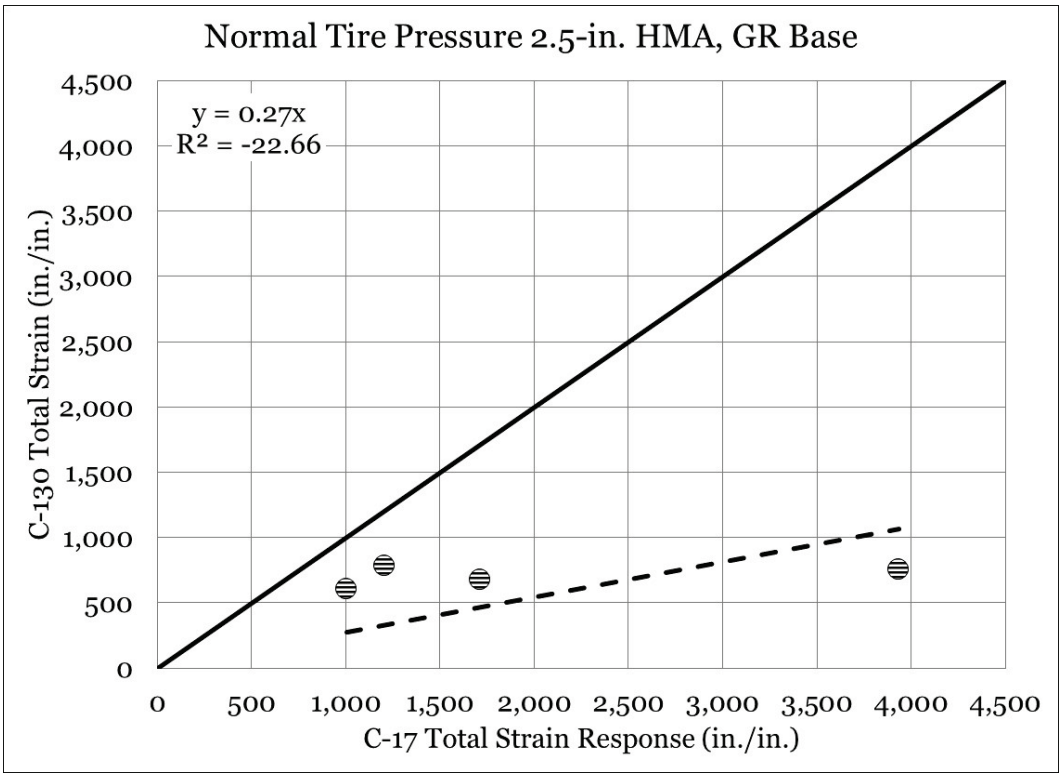

Figure 168. Equality plot - normal tire pressure ASG response (2.5-in. HMA, LMS base).

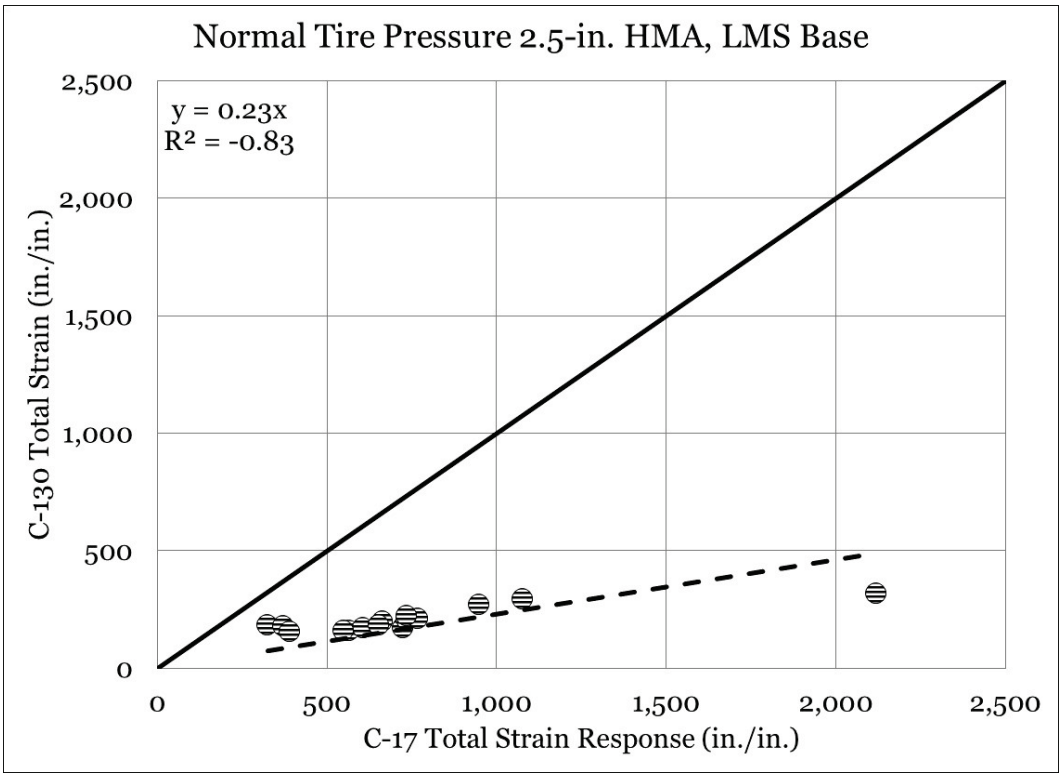

Figure 169. Equality plot - normal tire pressure ASG response (1.5-in. HMA, LMS base).

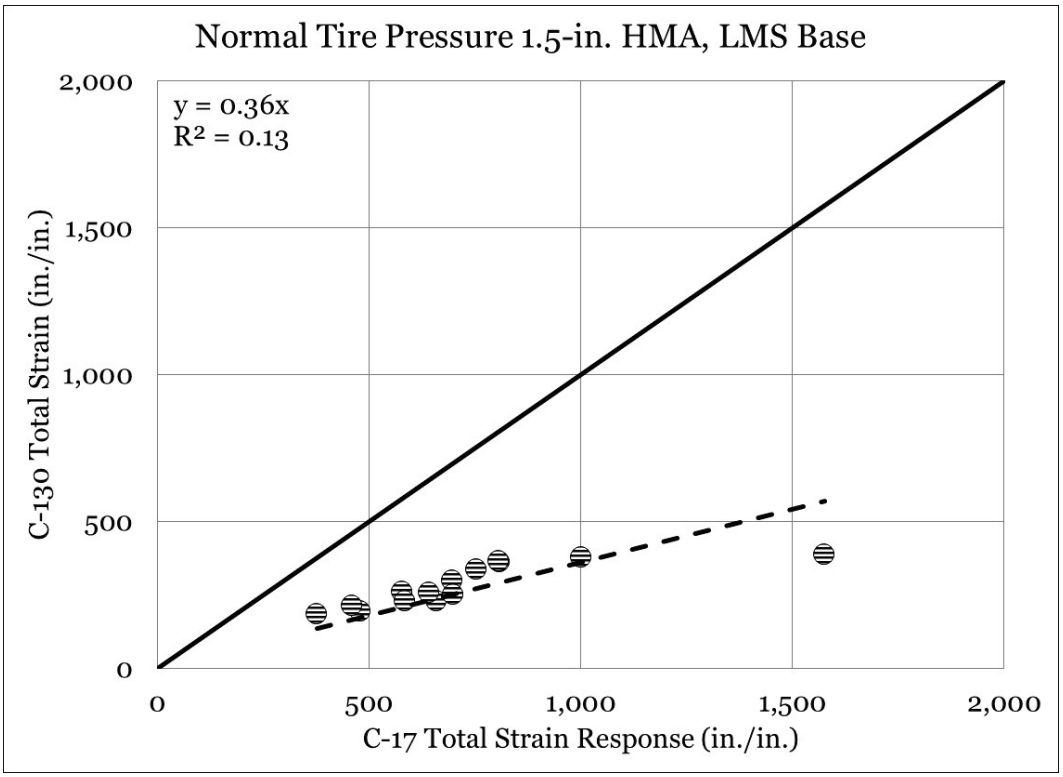

Figure 170. Equality plot - normal tire pressure ASG response (1.0-in. HMA, LMS base).

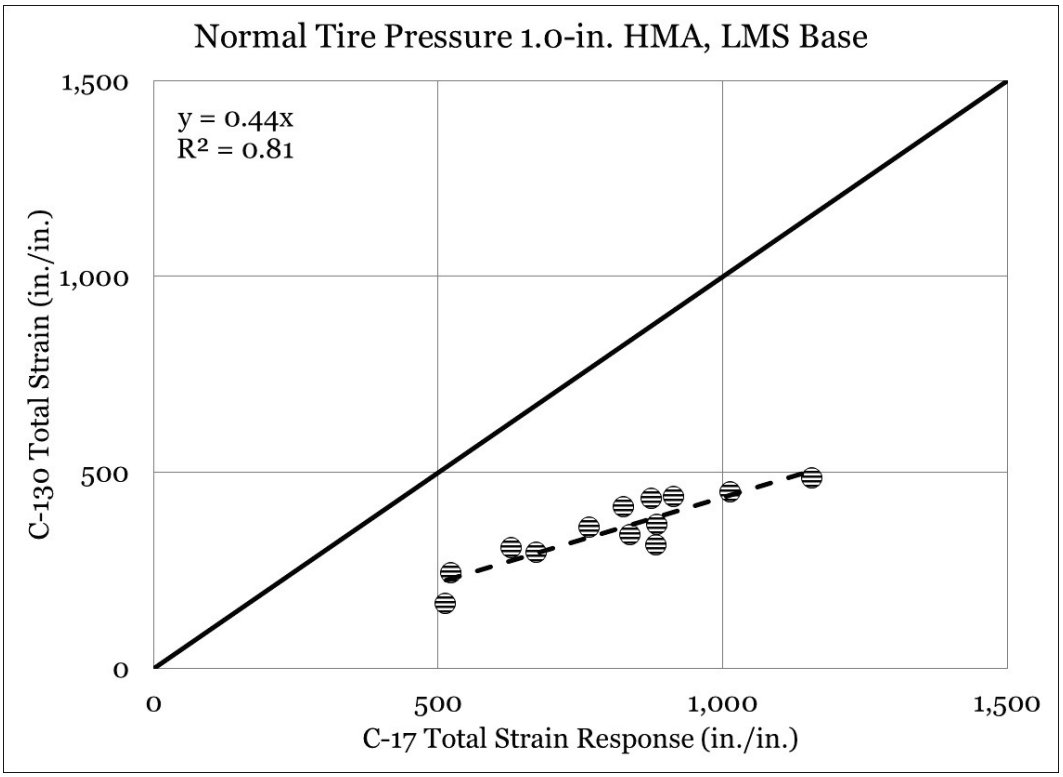

Figure 171. Equality plot - reduced tire pressure ASG response (2.5-in. HMA, GR base).

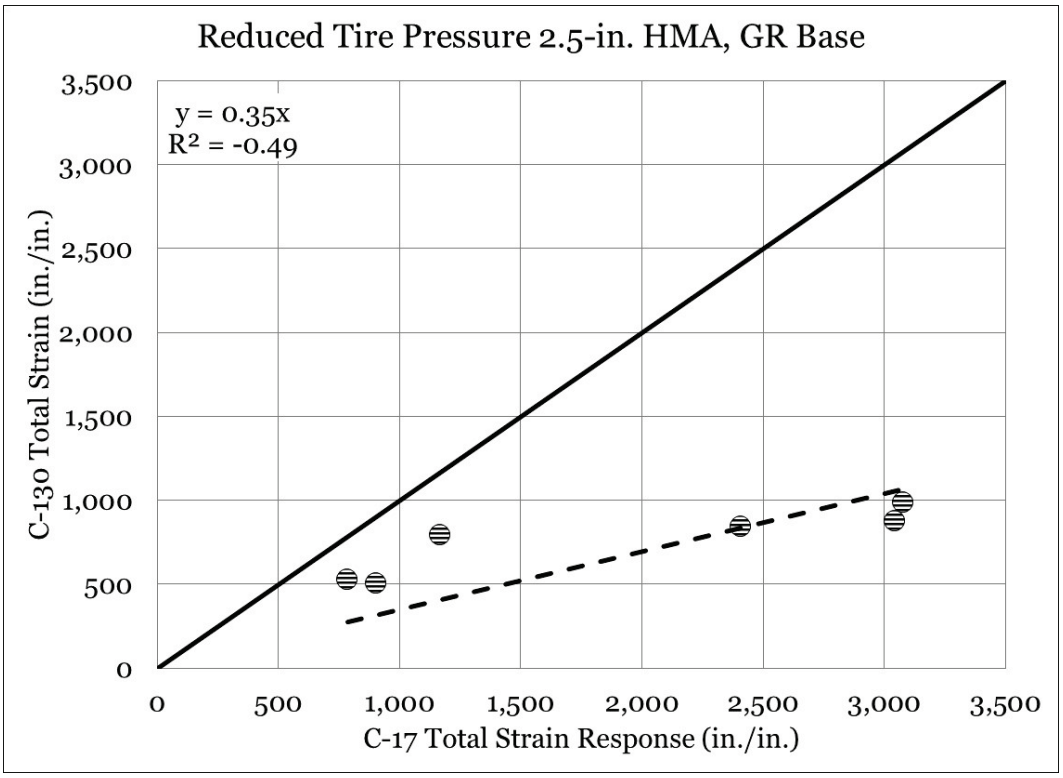

Figure 172. Equality plot - reduced tire pressure ASG response (2.5-in. HMA, LMS base).

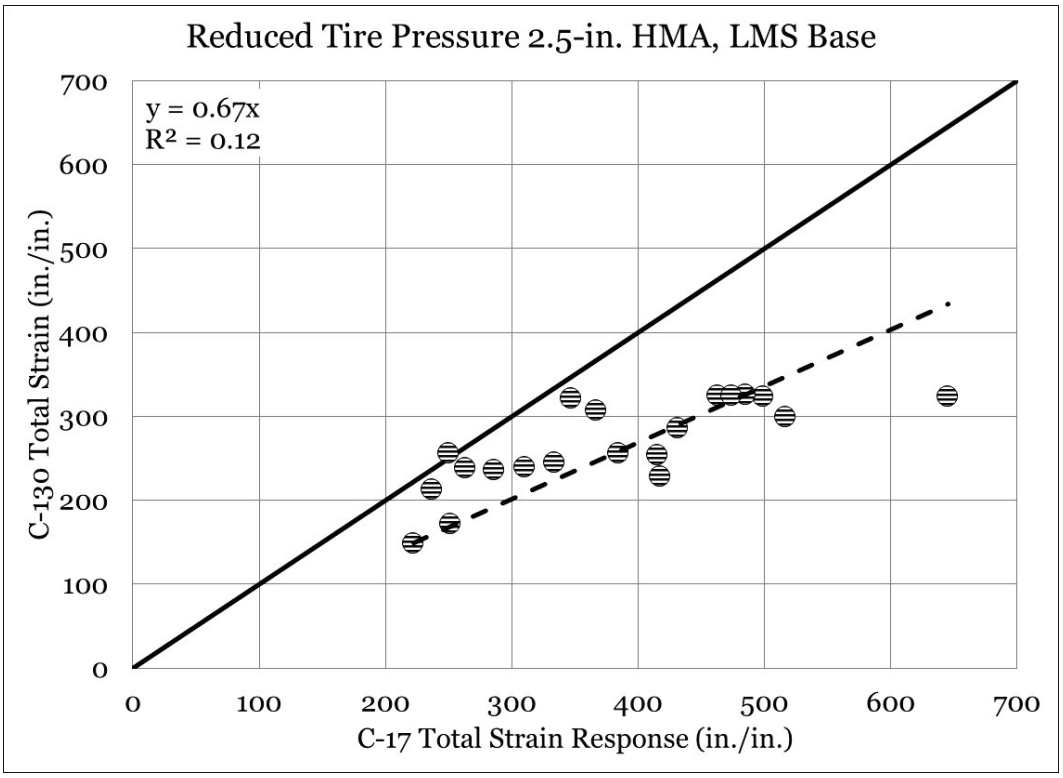

Figure 173. Equality plot - reduced tire pressure ASG response (1.5-in. HMA, LMS base).

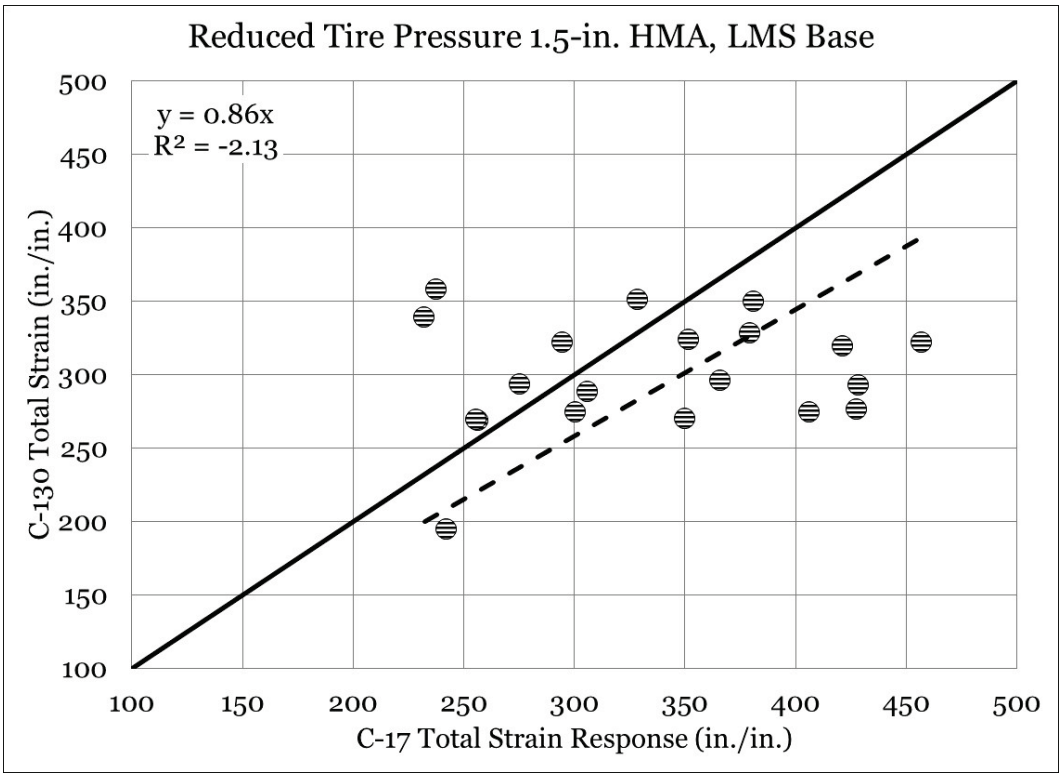

Figure 174. Equality plot - reduced tire pressure ASG response (1.0-in. HMA, LMS base).

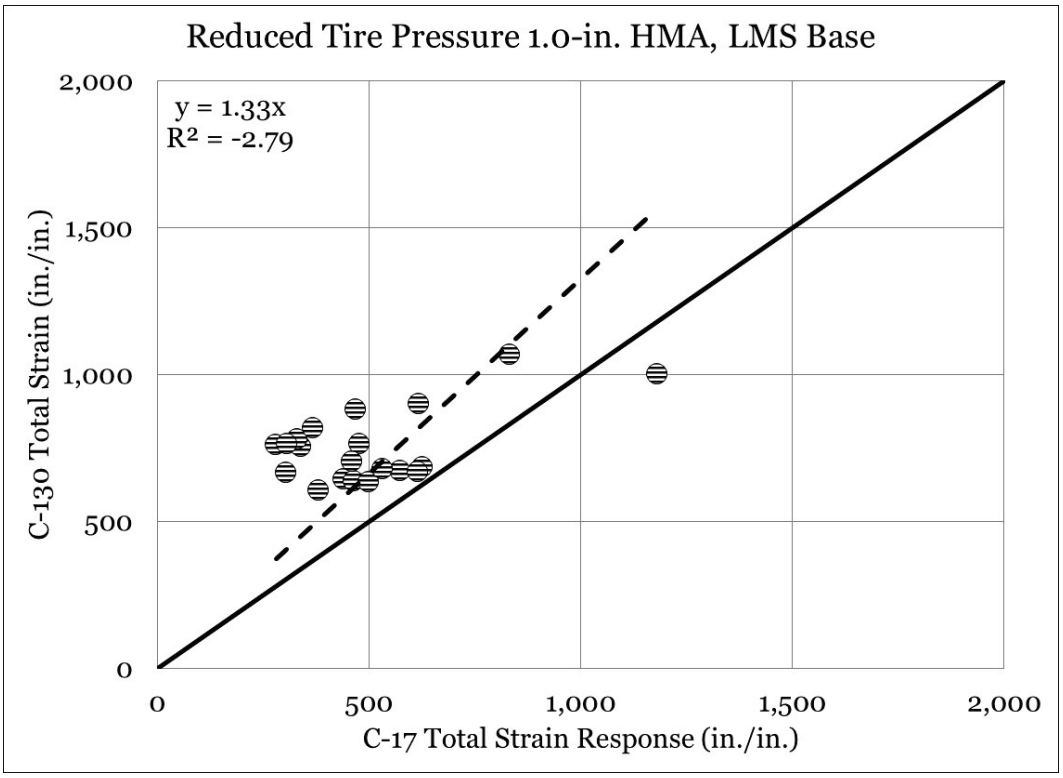

8 Forensic Investigation

A forensic investigation was performed to measure posttest material properties and to study the method of pavement failure. Trenches, approximately 10 ft wide, were excavated near the center cross section of each pavement test item. Excavation began by saw cutting the HMA surface and carefully removing it in an attempt to minimize disturbance to the underlying base course. Layer deformation measurements were made at each trench location, as well as field CBR tests, nuclear density tests, and moisture content tests.

8.1 C-130 posttest layer deformation

Elevation measurements were made at 6-in. intervals by using a robotic total station on the surface of each pavement layer to determine individual layer deformation. Rutting in each layer was calculated by averaging maximum elevation on each side of the wheel path (i.e., upheaval) and subtracting the minimum elevation within the wheel path (i.e., bottom of rut). Thus, calculated rut depth via total station measurement techniques may be slightly different from those measured with a straightedge. However, the measurements gave an indication of the magnitude of rutting in each layer relative to each other. Individual layer deformation is summarized in Table 42, and the results of elevation measurements made on the C-130 test items are shown in Figures 175 through 183.

Table 42. Summary of C-130 layer deformation.

Test Item	Asphalt (in.)	Base (in.)	Subgrade (in.)
C130NTP1 (2.5-in. HMA, GR Base)	4.4	4.0	0.9
C130RTP1 (2.5-in. HMA, GR Base)	4.2	4.2	1.4
C130NTP2 (2.5-in. HMA, LMS Base)	1.4	1.7	0.5
C130RTP2 (2.5-in. HMA, LMS Base)	1.2	1.0	1.0
C130NTP3 (1.5-in. HMA, LMS Base)	2.4	2.4	0.8
C130RTP3 (1.5-in. HMA, LMS Base)	2.0	2.4	0.9
C130NTP4 (1.0-in. HMA, LMS Base)	2.5	2.5	1.2
C130RTP4 (1.0-in. HMS, LMS Base)	2.3	2.6	1.1

It was observed that rutting primarily occurred within the upper pavement layers of most test items. Elevation measurements in

C130RTP2 (2.5-in. HMA, LMS base; Figure 178) indicated that rutting occurred nearly equally in all layers, suggesting that pavement deformation may have initiated in the subgrade layer. In general, reducing tire pressure improved rutting performance in the asphalt layer but provided little improvement in the base course layer (with the exception of the 2.5-in. HMA, LMS base test items). Notably, reducing tire pressure did not improve rutting performance in the subgrade layer, and it was observed that rutting in the reduced tire pressure items was greater than or equivalent to rutting in the normal tire pressure counterparts. However, as noted previously, the reduced tire pressure test items (particularly the LMS base items) sustained more overall passes than the normal tire pressure test items.

Photographs of each excavated trench are shown in Figure 183. Layer interfaces are denoted by yellow dashed lines in each photograph.

Figure 175. C-130 normal tire pressure layer deformation (2.5-in. HMA, GR base).

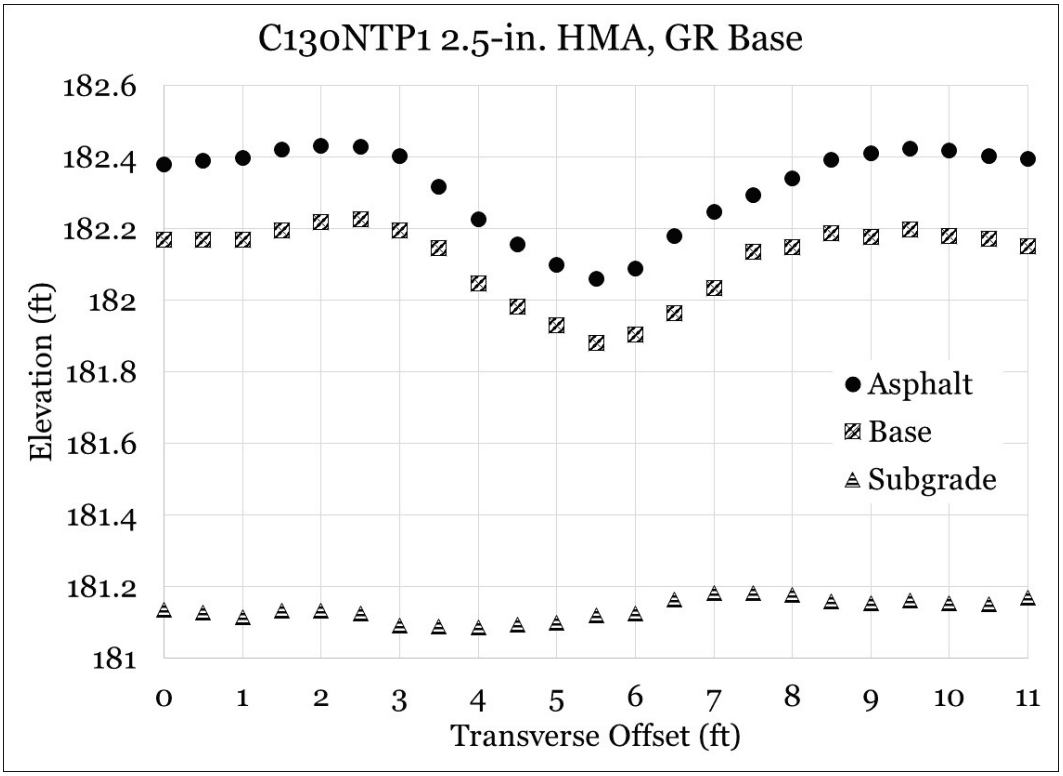

Figure 176. C-130 reduced tire pressure layer deformation (2.5-in. HMA, GR base).

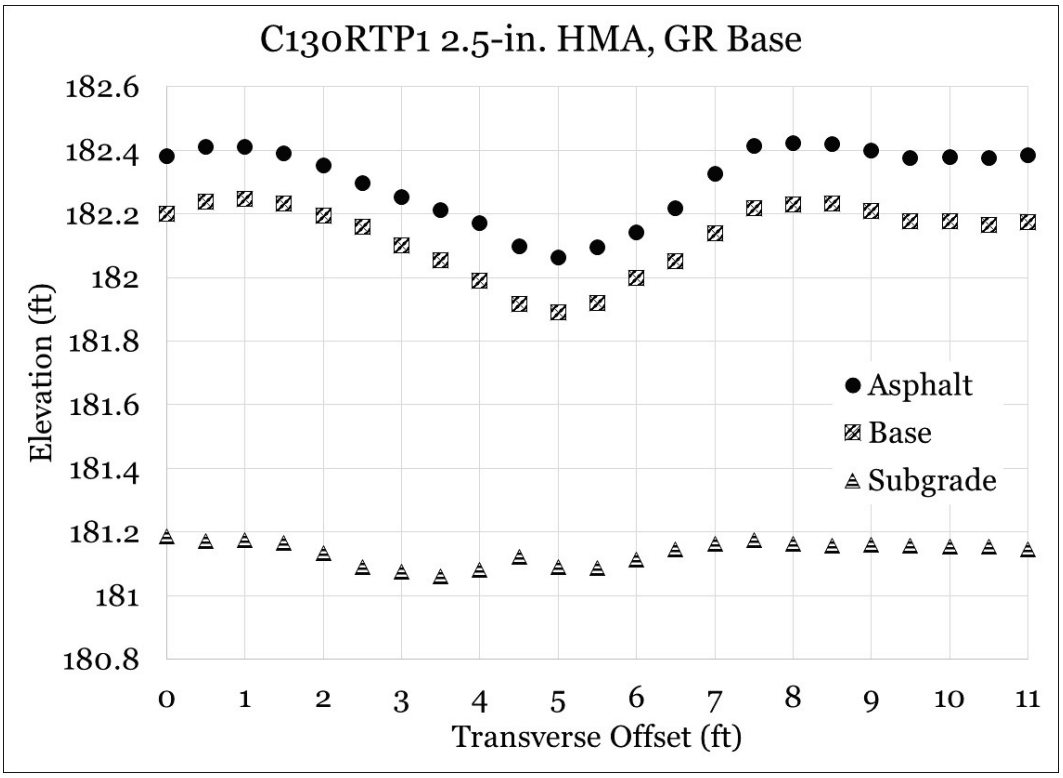

Figure 177. C-130 normal tire pressure layer deformation (2.5-in. HMA, LMS base).

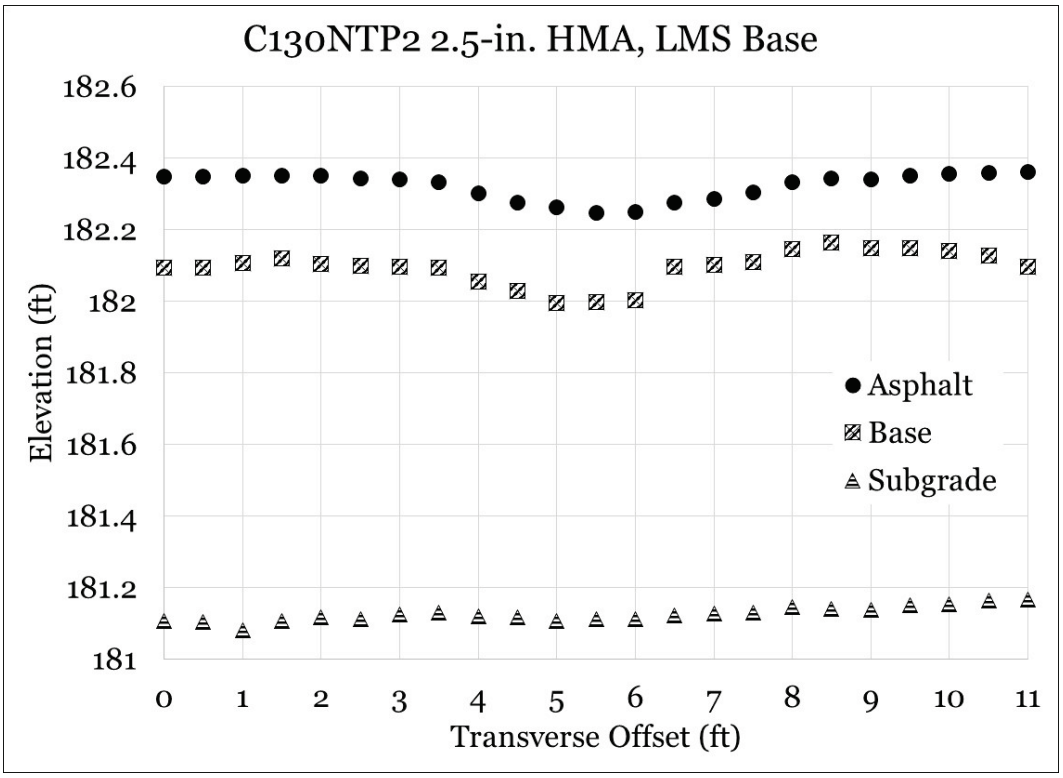

Figure 178. C-130 reduced tire pressure layer deformation (2.5-in. HMA, LMS base).

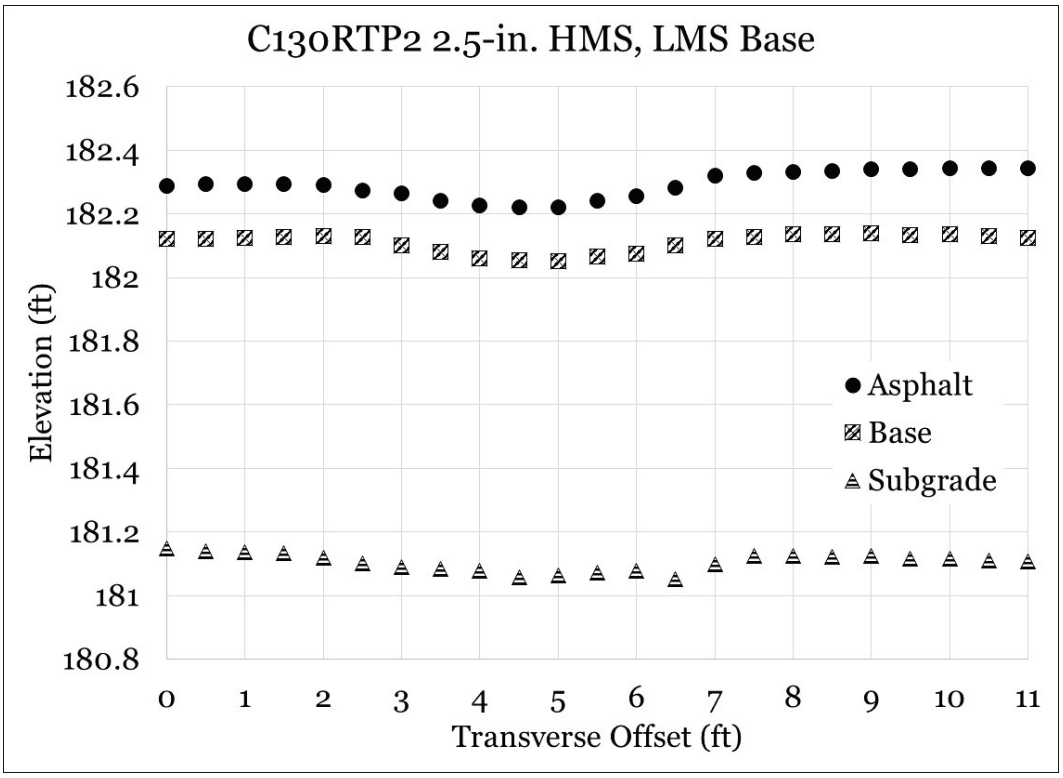

Figure 179. C-130 normal tire pressure layer deformation (1.5-in. HMA, LMS base).

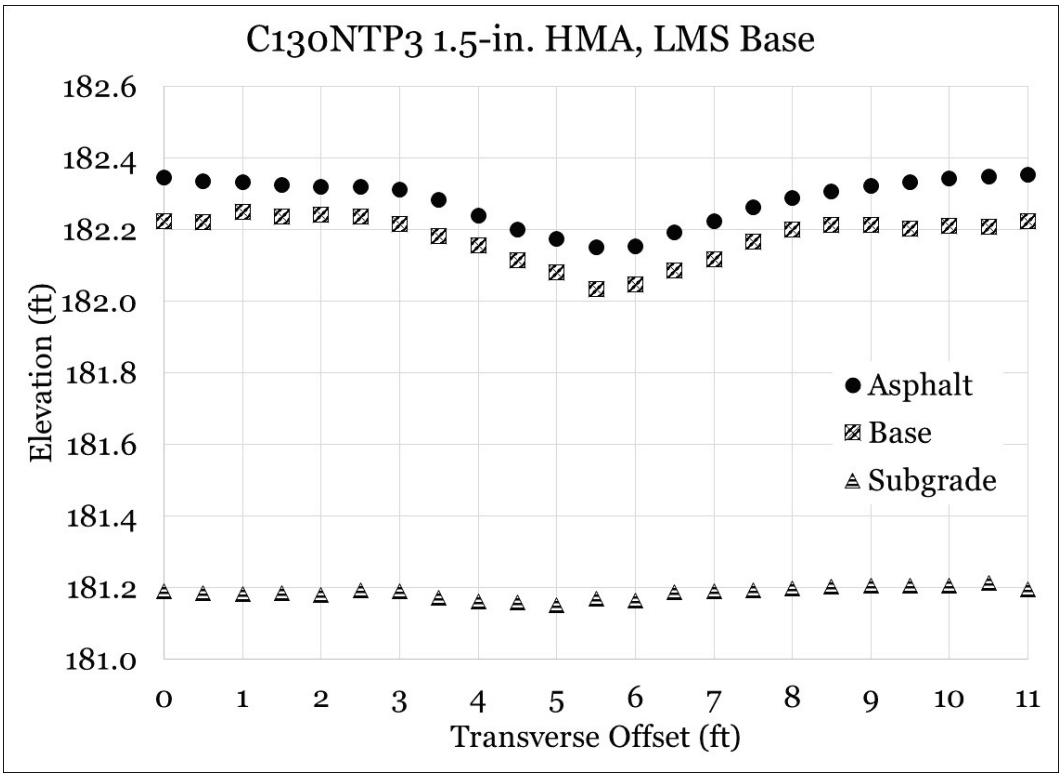

Figure 180. C-130 reduced tire pressure layer deformation (1.5-in. HMA, LMS base).

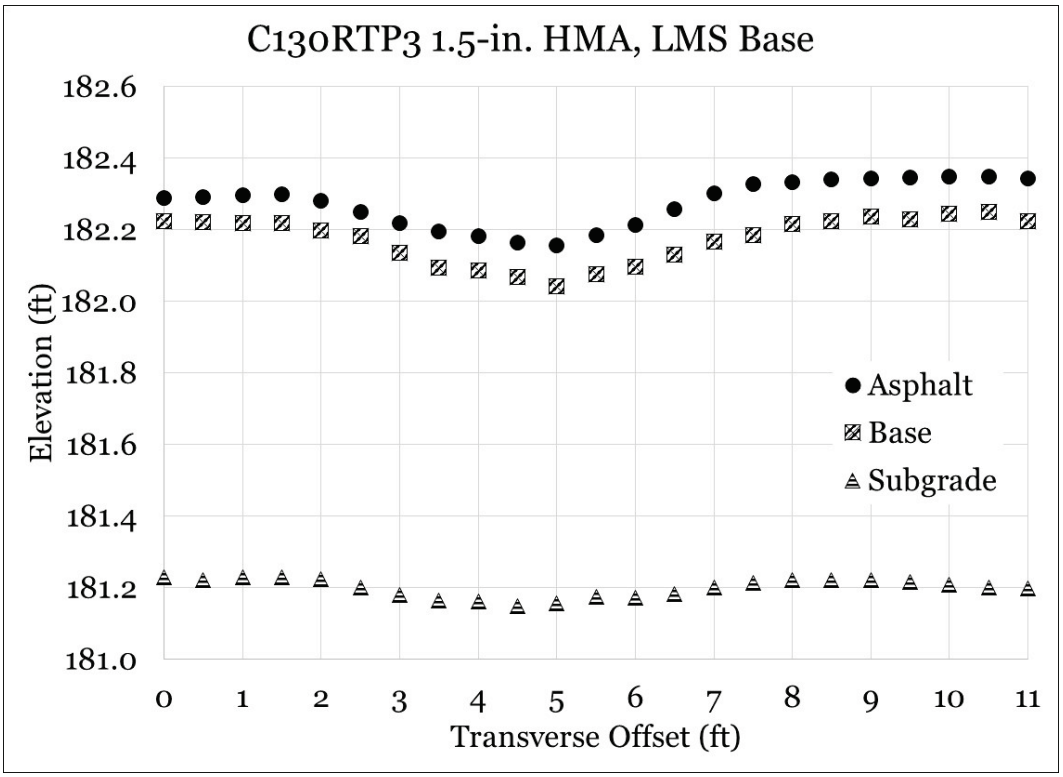

Figure 181. C-130 normal tire pressure layer deformation (1.0-in. HMA, LMS base).

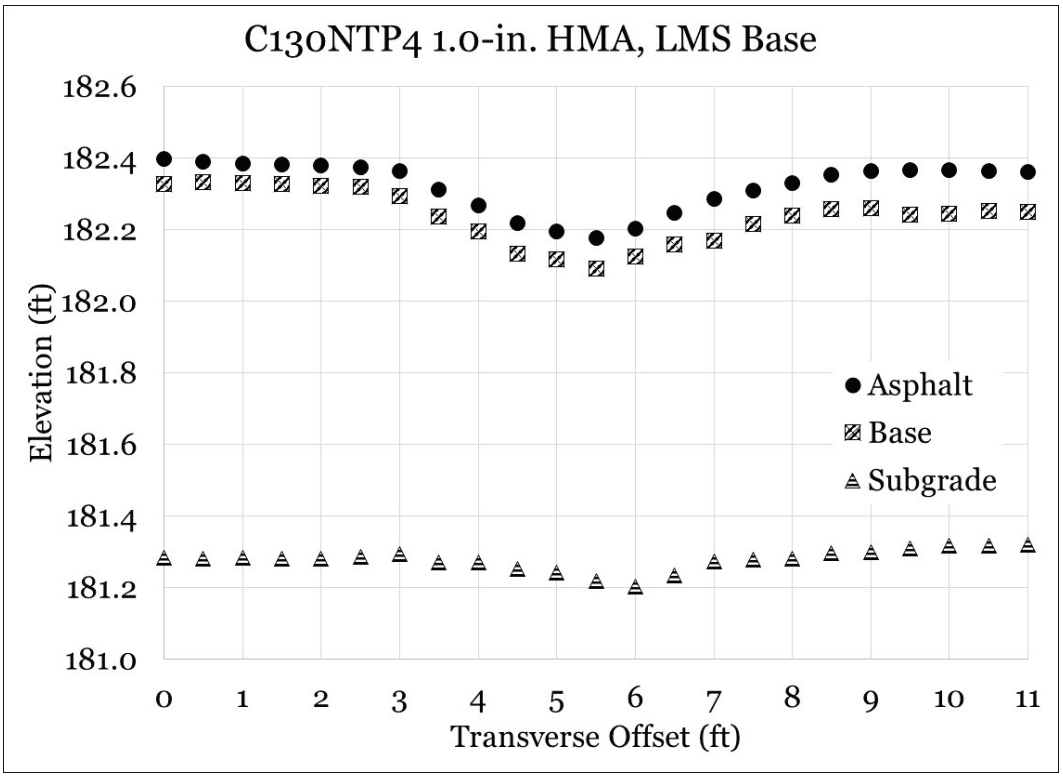

Figure 182. C-130 reduced tire pressure layer deformation (1.0-in. HMA, LMS base).

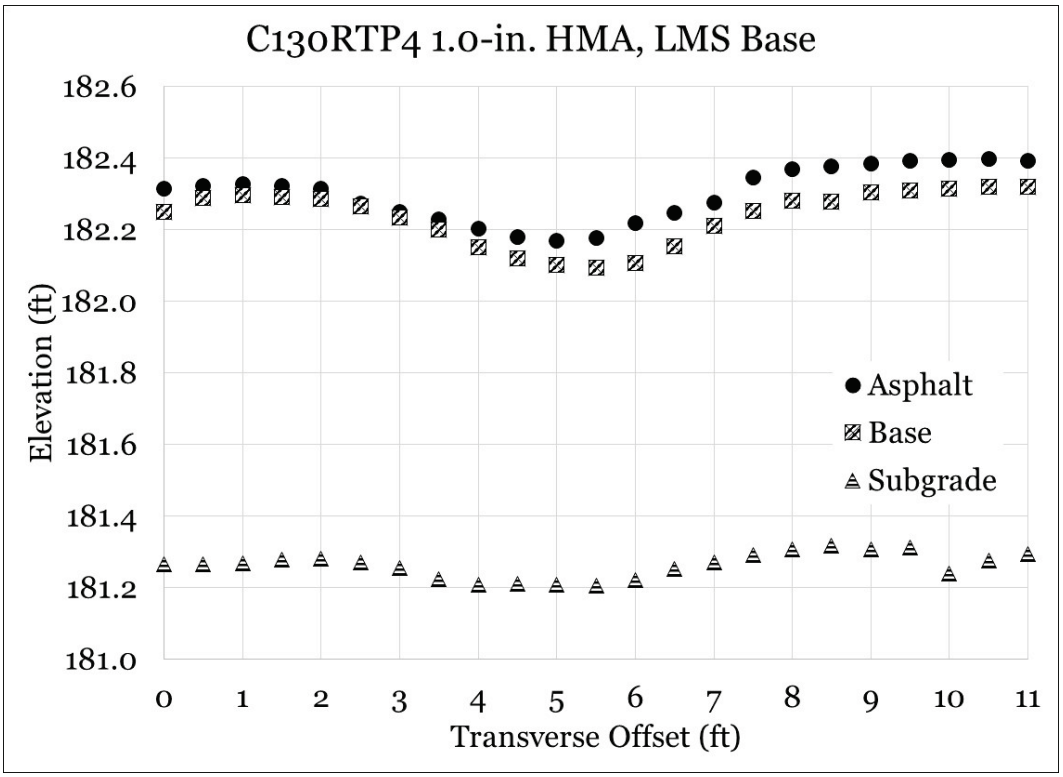

Figure 183. C-130 excavation photographs.

(a) C130NTP1 (2.5-in. HMA, LMS base)

(b) C130RTP1 (2.5-in. HMA, LMS base)

(c) C130NTP2 (2.5 in.-HMA, LMS base)

(d) C130RTP2 (2.5-in. HMS, LMS base)

(e) C130NTP3 (1.5-in. HMA, LMS base)

(f) C130RTP3 (1.5-in. HMA, LMS base)

(g) C130NTP4 (1.0-in. HMA, LMS base)

(h) C130RTP4 (1.0-in. HMA, LMS base)

8.2 C-17 posttest layer deformation

Posttest layer deformation results for the C-17 test series are summarized in Table 43. Rutting was primarily observed in the upper pavement layers. It was observed that reducing tire pressure generally improved rutting performance in the base course layer but did not improve rutting performance in the subgrade layer. A noted exception is the 2.5-in. HMA, GR base test item, where a reduction in tire pressure resulted in a rutting improvement in both the base and subgrade layers.

The results of individual layer elevation measurements are shown in Figures 184 through 191. It should be noted that the asphalt surface was deteriorated to the point of being completely absent in the wheel path of C17RTP1 (1.0-in. HMA, LMS base). Also, the subgrade surface of C17NTP2 was severely disturbed during excavation activities; thus, conclusions regarding subgrade deformation in this item could not be drawn.

Photographs of each excavated trench are shown in Figure 192. Layer interfaces are denoted by yellow dashed lines in each photograph.

Table 43. Summary of C-17 layer deformation.

Test Item	Asphalt (in.)	Base (in.)	Subgrade (in.)
C17NTP1 (1.0-in. HMA, LMS Base)	3.0	3.1	1.3
C17RTP1 (1.0-in. HMA, LMS Base)	3.7[1]	2.8	1.6
C17NTP2 (1.5-in. HMA, LMS Base)	3.4	4.1	--[2]
C17RTP2 (1.5-in. HMS, LMS Base)	2.6	2.6	2.2
C17NTP3 (2.5-in. HMA, LMS Base)	4.0	3.7	1.7
C17RTP3 (2.5-in. HMA, LMS Base)	5.0	5.3	2.0
C17NTP4 (2.5-in. HMA, GR Base)	4.4	4.2	3.5
C17RTP4 (2.5-in. HMA, GR Base)	4.4	3.8	1.2

[1]Asphalt was severely deteriorated and absent in some areas.

[2]Subgrade was damaged during excavation.

Figure 184. C-17 normal tire pressure layer deformation (1.0-in. HMA, LMS base).

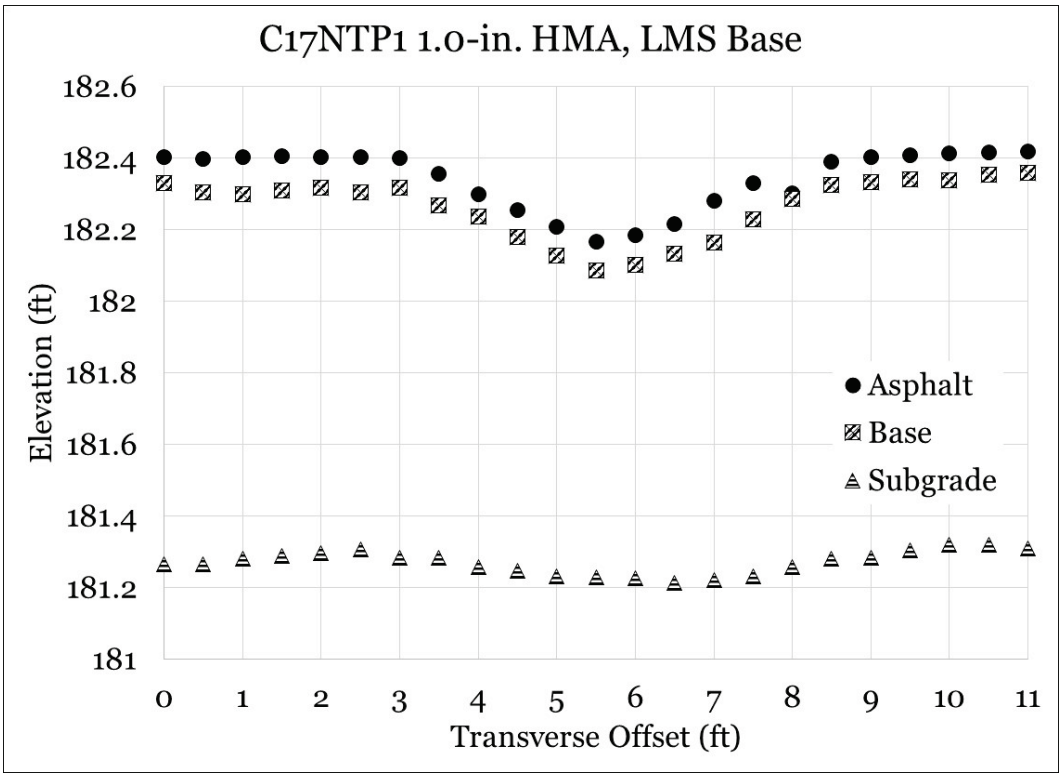

Figure 185. C-17 reduced tire pressure layer deformation (1.0-in. HMA, LMS base).

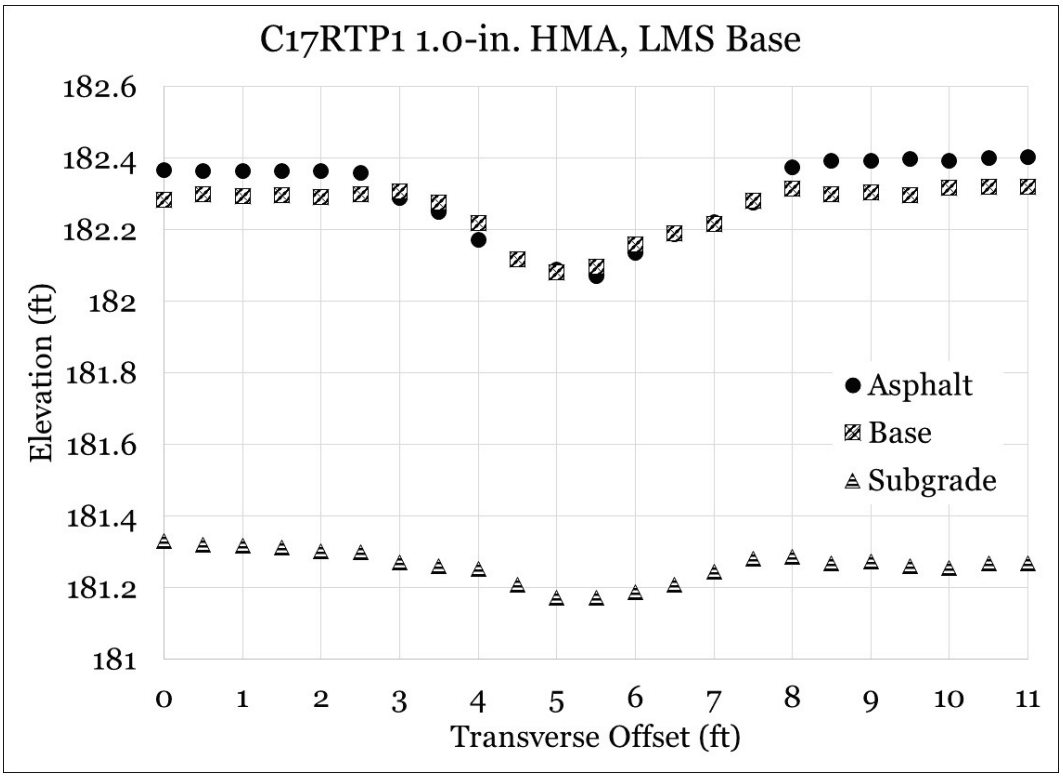

Figure 186. C-17 normal tire pressure layer deformation (1.5-in. HMA, LMS base).

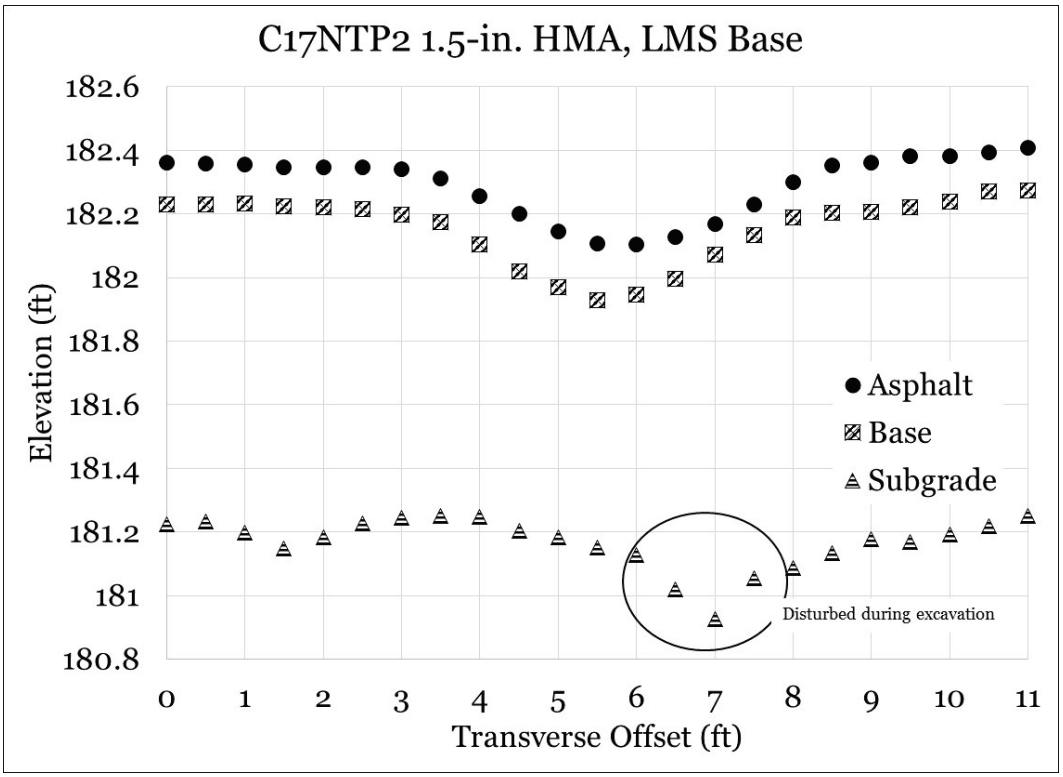

Figure 187. C-17 reduced tire pressure layer deformation (1.5-in. HMA, LMS base).

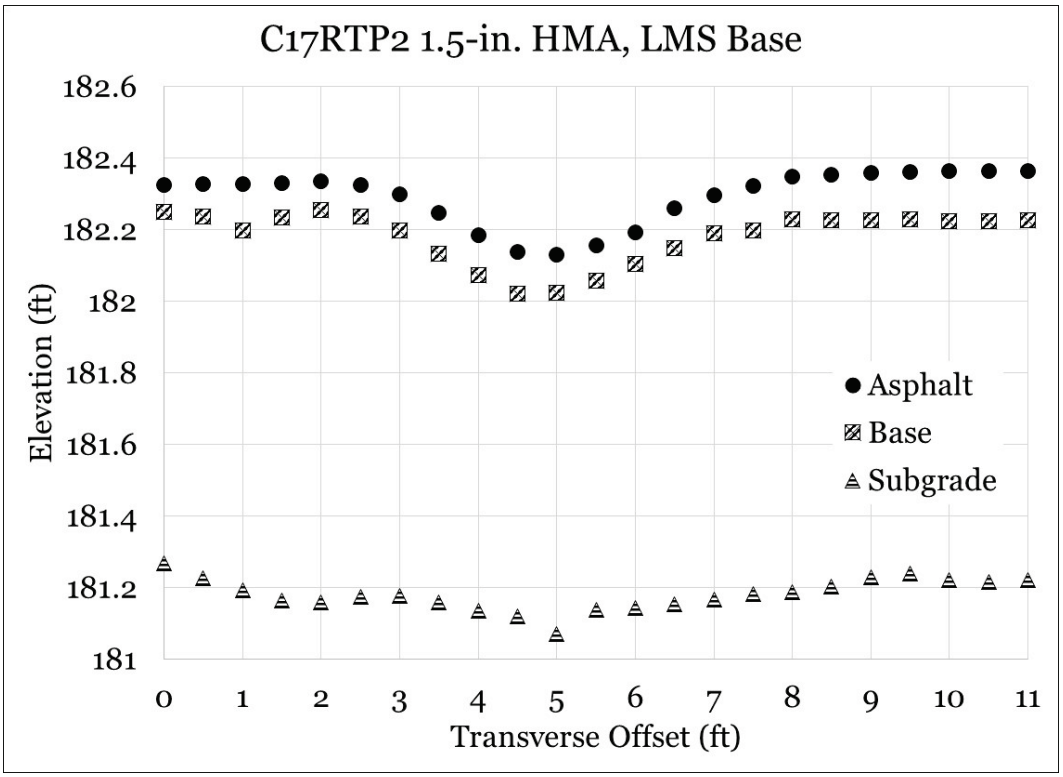

Figure 188. C-17 normal tire pressure layer deformation (2.5-in. HMA, LMS base).

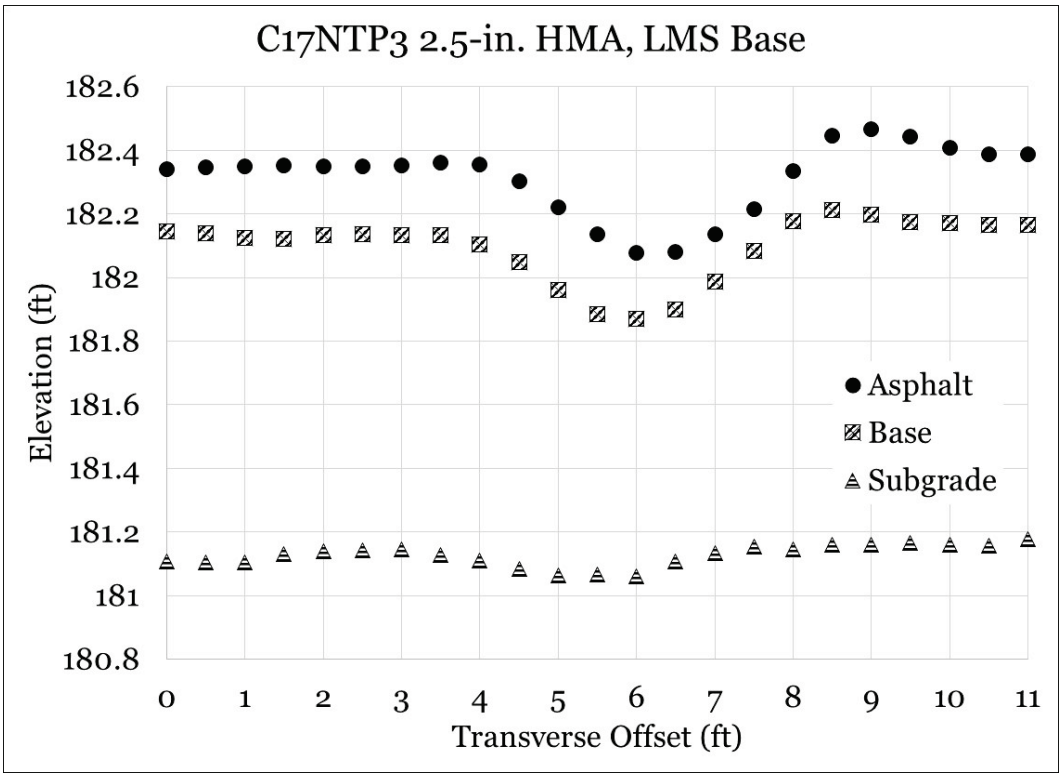

Figure 189. C-17 reduced tire pressure layer deformation (2.5-in. HMA, LMS base).

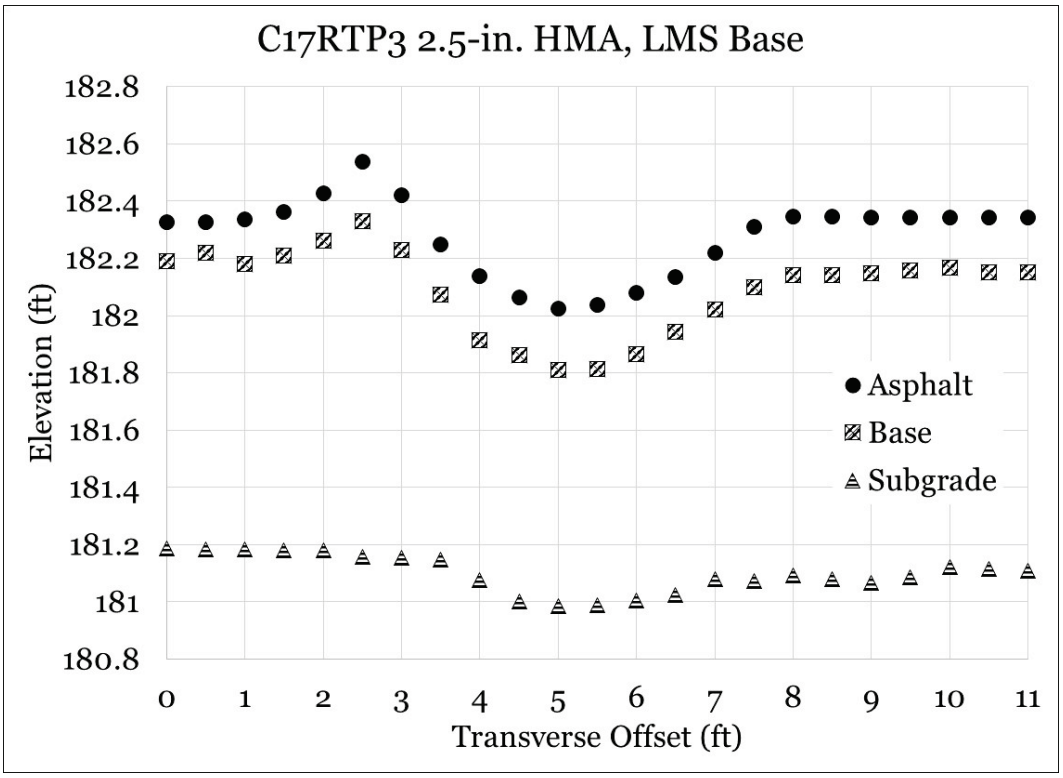

Figure 190. C-17 normal tire pressure layer deformation (2.5-in. HMA, GR base).

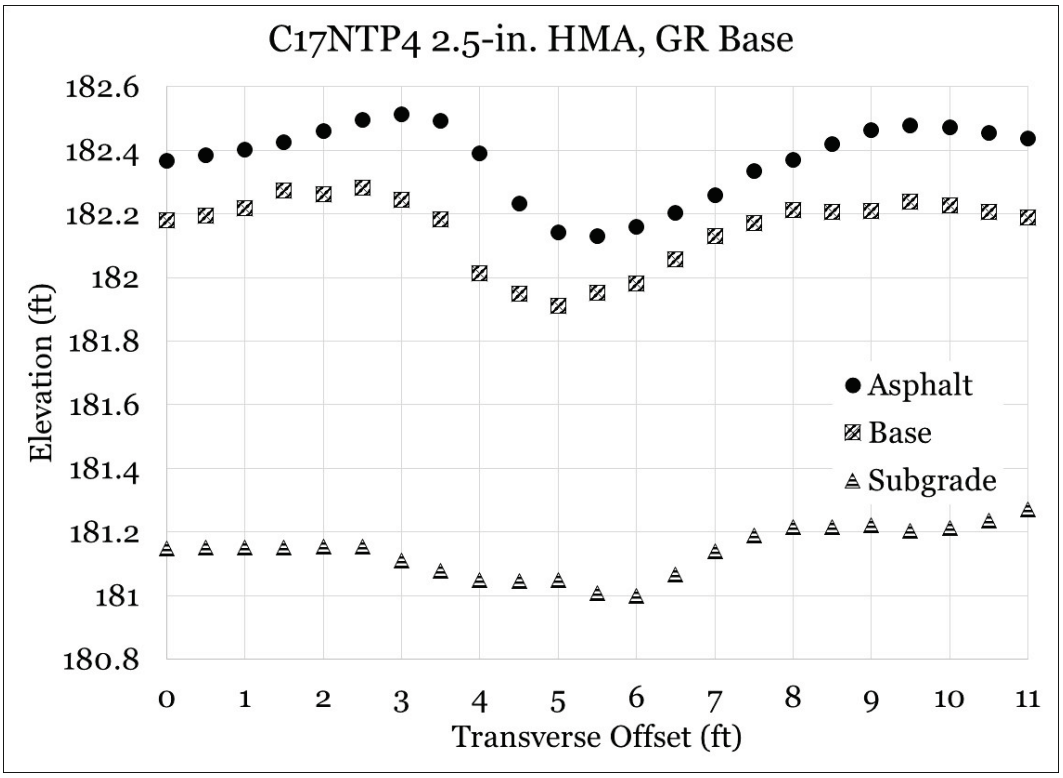

Figure 191. C-17 reduced tire pressure layer deformation (2.5-in. HMA, GR base).

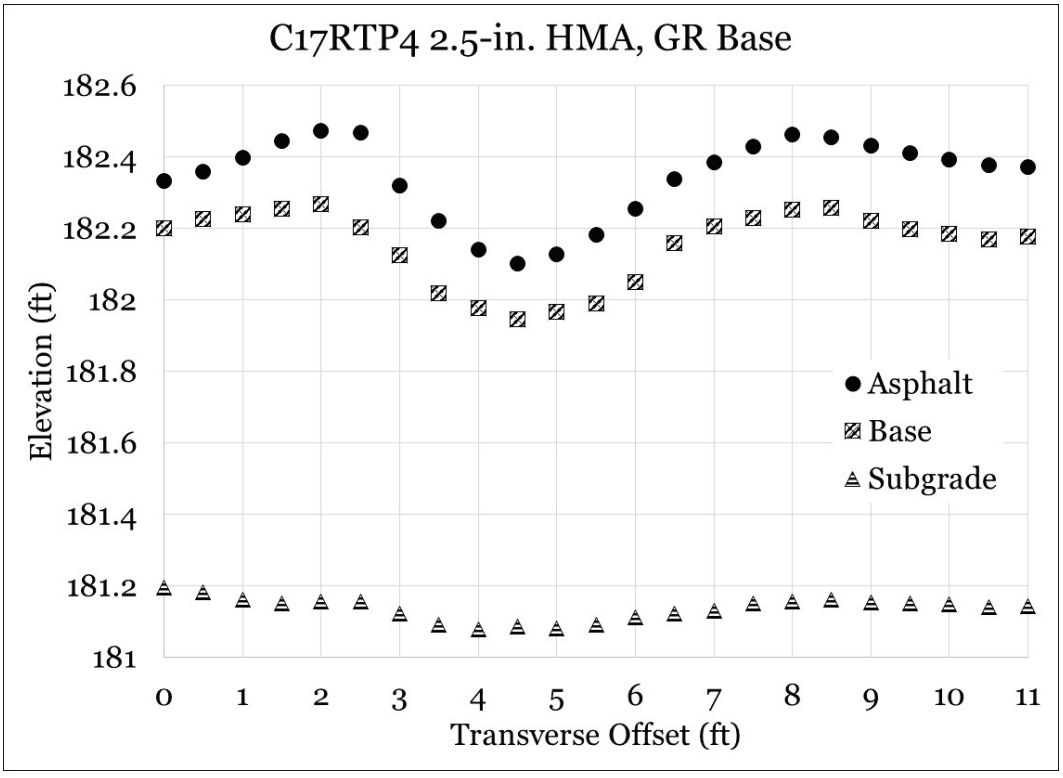

Figure 192. C-17 cross-section photographs.

(a) C17NTP1 (1.0-in. HMA, LMS base) (b) C17RTP1 (1.0-in. HMA, LMS base)

(c) C17NTP2 (1.5-in. HMA, LMS base) (d) C17RTP2 (1.5-in. HMA, LMS base)

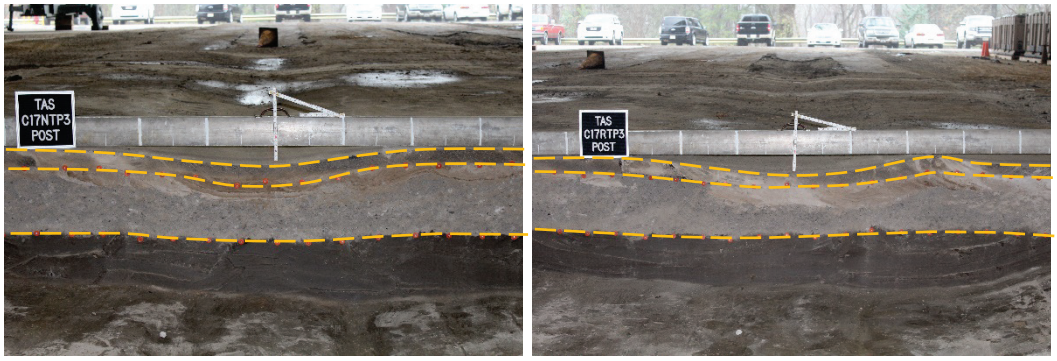

(e) C17NTP3 (2.5-in. HMA, LMS base) (f) C17RTP3 (2.5-in. HMA, LMS base)

(g) C17NTP4 (2.5-in. HMA, GR base) (h) C17RTP4 (2.5-in. HMA, GR base)

8.3 C-130 posttest material properties

Posttest measured material properties for the C-130 test series are shown in Table 44. Changes in material properties (as-built minus posttest properties) are summarized in Table 45.

A reduction in measured dry density was observed in the CH subgrade layer of all test items. The highest loss of density was observed in the 2.5-in. HMA, LMS base (both tire pressure conditions) and was found to be on the order of 11%. In the limestone base test items, reducing tire pressure generally reduced density loss in the CH subgrade, although permanent deformation was found to be greater. This suggested that reducing tire pressure may have influenced the failure mode near the CH surface from primarily shear failure (in the case of normal tire pressure) to partially shear/consolidation (in the case of reduced tire pressure). Increases in CH subgrade CBR were observed in most limestone base test items, and higher increases were observed in the reduced tire pressure test items. Equivalent decreases in CBR were observed in the gravel base test items, suggesting that the gravel base course was not effective in adequately protecting the CH subgrade.

A review of density measurements made on the limestone base course indicated that compaction increased in some cases and decreased in others. It was noted that there was no change in the field-measured CBR of the limestone base test items, while there was a decrease in measured CBR of the gravel base test items. Moisture content in the base course was found to be relatively equivalent to pre-test values.

Table 44. C-130 posttest measured material properties.

Property	C130RTP1	C130RTP2	C130RTP3	C130RTP4	C130NTP1	C130NTP2	C130NTP3	C130NTP4
CH Subgrade (104.2 pcf @ 19.7%)								
Wet Density (pcf)	112.4	106.9	114.7	109.4	111.9	105.1	113.9	108.3
Dry Density (pcf)	86.5	80.5	88.4	84.3	85.9	79.9	87.6	82.7
Nuclear Moisture Content (%)	30.2	32.8	30.5	29.6	30.4	31.5	29.9	30.9
Compaction (%)	83.0	77.3	84.8	80.9	82.4	76.7	84.1	79.4
Oven-Dried Moisture (%)	32.2	28.4	30.1	30.2	32.9	30.5	31.3	31.3
In-Place CBR (%)	8.1	13.2	11.9	12.0	8.1	11.9	10.4	9.5
Base Course (146.7 pcf @ 5.9%; 124.7 pcf @ 7.6%)								
Material Type	GR	LMS	LMS	LMS	GR	LMS	LMS	LMS
Wet Density (pcf)	105.2	147.9	147.5	141.6	117.2	133	148	144.8
Dry Density (pcf)	102.5	144.7	144.5	138.8	114.5	130.1	145.3	141.7
Nuclear Moisture Content (%)	2.7	1.8	2.0	2.0	2.4	2.2	1.9	2.2
Compaction (%)	82.2	98.7	98.6	94.7	91.9	88.8	99.1	96.7
Oven-Dried Moisture (%)	2.7	1.9	2.3	2.1	2.4	1.9	2.2	2.1
In-Place CBR (%)	33	100	100	100	43	100	100	100

Table 45. C-130 change in material properties (as-built minus posttest).

Property	C130RTP1	C130RTP2	C130RTP3	C130RTP4	C130NTP1	C130NTP2	C130NTP3	C130NTP4
CH Subgrade (104.2 pcf @ 19.7%)								
Wet Density (pcf)	-6.9	-10.8	-2.1	-8.7	-7.2	-13.3	-4.2	-9.5
Dry Density (pcf)	-6.7	-11.1	-1.9	-7.5	-6.5	-11.7	-4.4	-8.8
Nuclear Moisture Content (%)	2.7	5.1	2.3	1.9	1.7	3.3	2.3	3.2
Compaction (%)	-6.4	-10.6	-1.8	-7.2	-6.3	-11.2	-4.2	-8.4
Oven-Dried Moisture (%)	2.3	-1.4	0.0	0.8	3.2	0.0	1.8	1.5
In-Place CBR (%)	-1.7	3.6	2.5	2.1	-1.7	2.1	0.3	0.0
Base Course (146.7 pcf @ 5.9%; 124.7 pcf @ 7.6%)								
Material Type	GR	LMS	LMS	LMS	GR	LMS	LMS	LMS
Wet Density (pcf)	-18.8	-0.6	-0.2	-4.1	-6.6	-17.0	0.8	-1.2
Dry Density (pcf)	-15.5	1.8	2.5	-1.5	-3.6	-13.1	3.8	0.9
Nuclear Moisture Content (%)	-2.5	-2.2	-1.9	-1.8	-2.3	-2.6	-2.2	-1.9
Compaction (%)	-12.4	1.2	1.7	-1.1	-2.8	-8.9	2.5	0.7
Oven-Dried Moisture (%)	1.3	-0.3	-0.2	-0.9	1.0	-0.3	-0.3	-0.9
In-Place CBR (%)	-9.0	0.0	0.0	0.0	-4.0	0.0	0.0	0.0

8.4 C-17 posttest material properties

Posttest material properties for the C-17 test series are shown in Table 46. Changes in material properties (as-built minus posttest properties) are summarized in Table 47.

A reduction in measured dry density was observed in the CH subgrade layer for all test items. Reductions in tire pressure generally reduced density loss in all test items, except C17RTP2, where compaction decreased 10.4% in the reduced tire pressure item compared to 9.6% in the normal tire pressure item. In-place measured CBR increased in all items, except C17NTP4, where an almost 2% decrease was observed. Higher increases in subgrade CBR were observed in the thinner asphalt test sections; and it was observed that as the asphalt thickness increased, the increase in subgrade CBR decreased.

Base course density decreased in all test items, and it was observed that density decreases were generally greater than those observed in the C-130 test items. This was expected due to the increased loading conditions and more material shear movement under the C-17 test tire. Measured CBR values in the LMS base test items remained unchanged from the as-built measurements (i.e., 100+); however, meaningful CBR decreases were observed in the gravel base test items.

Table 46. C-17 posttest measured material properties.

Property	C17RTP1	C17RTP2	C17RTP3	C17RTP4	C17NTP1	C17NTP2	C17NTP3	C17NTP4
CH Subgrade (104.2 pcf @ 19.7%)								
Wet Density (pcf)	108.7	106.8	114.1	111.9	108.4	109.7	108.1	108.9
Dry Density (pcf)	83.8	81.4	90.1	85.2	83.0	83.6	82.3	83.7
Nuclear Moisture Content (%)	29.7	31.3	26.8	31.3	30.6	31.1	32.5	30.1
Compaction (%)	80.4	78.1	86.4	81.8	79.6	80.3	79.0	80.3
Oven-Dried Moisture (%)	28.8	27.0	30.7	31.8	28.8	26.3	31.5	31.9
In-Place CBR (%)	16.2	12.4	13.8	10.9	17.0	12.7	11.0	7.7
Base Course (146.7 pcf @ 5.9%; 124.7 pcf @ 7.6%)								
Material Type	LMS	LMS	LMS	GR	LMS	LMS	LMS	GR
Wet Density (pcf)	122.9	136.2	122.5	110.8	136.7	127.8	126.0	116.5
Dry Density (pcf)	119.3	132.9	119.1	108.4	133.5	124.6	122.8	113.3
Nuclear Moisture Content (%)	3.0	2.6	3.0	2.2	2.4	2.6	2.6	2.9
Compaction (%)	81.4	90.7	81.2	87.0	91.1	85.0	83.8	90.9
Oven-Dried Moisture (%)	1.4	2.3	1.8	2.2	1.9	2.3	2.4	2.9
In-Place CBR (%)	100	100	100	26	100	100	100	21

Table 47. C-17 change in material properties (as-built minus post-test).

Property	C17RTP1	C17RTP2	C17RTP3	C17RTP4	C17NTP1	C17NTP2	C17NTP3	C17NTP4
CH Subgrade (104.2 pcf @ 19.7%)								
Wet Density (pcf)	-9.6	-11.4	-2.3	-4.6	-10.7	-8.6	-9.1	-9.0
Dry Density (pcf)	-9.3	-10.8	-0.4	-5.2	-10.0	-7.9	-8.9	-7.3
Nuclear Moisture Content (%)	2.4	3.8	-1.1	3.6	2.7	2.7	5.0	2.4
Compaction (%)	-8.9	-10.4	-0.5	-5.0	-9.6	-7.5	-8.5	-7.0
Oven-Dried Moisture (%)	-0.6	-1.9	0.2	2.8	-0.4	-3.4	1.9	1.5
In-Place CBR (%)	6.5	2.4	4.2	1.0	7.5	3.1	1.5	-1.7
Base Course (146.7 pcf @ 5.9%; 124.7 pcf @ 7.6%)								
Material Type	LMS	LMS	LMS	GR	LMS	LMS	LMS	GR
Wet Density (pcf)	-26.3	-15.8	-28.6	-14.2	-14.3	-22.1	-20.8	-9.0
Dry Density (pcf)	-23.1	-12.3	-25.3	-11.6	-10.5	-18.5	-17.1	-7.2
Nuclear Moisture Content (%)	-1.9	-2.2	-1.9	-1.9	-2.6	-2.1	-2.3	-1.3
Compaction (%)	-15.7	-8.3	-17.2	-9.2	-7.1	-12.6	-11.6	-5.7
Oven-Dried Moisture (%)	-1.4	-0.3	-0.8	0.8	-0.9	-0.3	-0.2	1.5
In-Place CBR (%)	0.0	0.0	0.0	-21.0	0.0	0.0	0.0	-25.0

9 Implementation of Test Results into Existing Design and Evaluation Methodology

This chapter investigates current military pavement design methodology and uses the data generated from this study to suggest improvements to the methodology.

9.1 Existing design methodology

Current DoD design methodology is based on the concept of limiting stress on top of the subgrade, whereby there is sufficient pavement thickness to reduce the risk of subgrade shear failure. Development of this procedure began in the 1940s as an extrapolation of the California design procedure for highway pavements. Over the years, adjustments were made to account for single-wheel loading, multiple-wheel loading, aircraft wheel wander, and equivalent single-wheel loading conditions. The procedure was used for over 40 years as the primary means for military pavement thickness design.

Most important was the development of an adjustment factor termed "α" that was based on a collaborative research program in the 1970s between the FAA and the USACE. The α-factor was a load adjustment factor that was a function of traffic volume and tire count in a heavily loaded multiple-wheel aircraft gear and resulted in the CBR design equation (Equation 1) having the form

$$t\ \alpha\sqrt{\frac{ESWL}{8.1CBR}-\frac{A}{\pi}} \tag{1}$$

where,

t = design thickness
α = load adjustment factor
ESWL = equivalent single-wheel load
CBR = California Bearing Ratio
A = tire contact area

The α-factor (Equation 2) is calculated by using the following equation.

$$\alpha = 0.15 + 0.23 \log_{10} (\text{coverages}) \quad (2)$$

Recognizing that the design thickness was a function of the ratio of applied stress to subgrade strength, Gonzalez (2015) set to improve the design methodology by eliminating the conversion of multi-gear traffic to an ESWL and removing the load adjustment factor, α. The improvement resulted in a new term, β, that related calculated vertical stress on the subgrade to strength of the subgrade. A relationship between the β term and the results of full-scale accelerated pavement test data was developed, resulting in a mechanistic-empirical pavement design model.

The stress-based design procedure in its current form was well characterized by Gonzalez (2015) and is described by the following equation (Equation 3).

$$\log \beta = \frac{a + c \log(coverages)}{1 + b \log(coverages)} \quad (3)$$

where,

β = Beta-parameter
a = 1.5441
b = 0.2354
c = 0.0730
coverages = number of aircraft passes in terms of lateral wander.

The Beta-parameter is calculated from the equation (Equation 4).

$$\beta = \frac{\sigma\pi}{CBR} \quad (4)$$

where,

σ = stress at the top of the subgrade
CBR = California Bearing Ratio.

This procedure works well in providing adequate structural designs to protect the subgrade by distributing the applied stress from the surface through a series of sufficiently strong but progressively lower-quality layers. The design procedure includes minimum requirements for asphalt concrete surface layer thickness and aggregate base quality. The minimum asphalt concrete surface layer requirements and associated asphalt concrete material specifications provide a competent wearing surface with

sufficient strength and thickness to withstand the near-surface applied stresses while distributing those stresses at a reduced level to the top of the aggregate base layer. The requirement for a high-quality aggregate base material and the related stringent material specifications ensure that selected base materials will possess high strength and durability characteristics to resist and further distribute the applied stresses. The combination of the minimum asphalt concrete surface layer thickness and the high-quality aggregate base material properties ensures that the stress applied to the surface of the aggregate base is within the capacity of the aggregate base strength.

It is important to understand the limitations of an existing model based on the constraints of the test data that were originally used to select the model. In examining the original test studies used to formulate the CBR-Beta design procedure, it was found that the data were gathered from work completed by the FAA (Hayhoe 2004) and ERDC (Gonzalez 2015; Ahlvin et al. 1971; Porter 1949; WES 1947; WES 1950; Cooksey and Ladd 1971). The data consisted of numerous loading condition (both multi-wheel and single-wheel) configurations, as well as varying overall pavement thicknesses. A review of the data found that overall pavement thickness (i.e., total thickness above the subgrade; Figure 193a) ranged from 5.0 in. to 57.1 in. and that approximately 75% of the data exceeded 15.0 in. overall pavement thickness. A closer inspection of the data found that asphalt thickness (Figure 193b) ranged from 1.0 in. to 7.0 in. and only five of the 45 data points had an asphalt thickness less than 3.0 in. Thus, few data points comprising the original dataset were intended to investigate thin asphalt pavement layers. Further, it is noted that most studies were intended to force failure to occur primarily in the subgrade layer. This can be observed in the original CBR formulation that was noted to have a linear relationship up to a CBR of about 12. Gonzalez (2015) plotted vertical stress on the subgrade as a function of subgrade CBR (later identified as the β-parameter) by mathematically rearranging Equation 1 and solving for vertical stress based on a constant contact pressure. These data were plotted at various traffic levels, and it was found that a linear relationship existed between calculated stress and subgrade CBR up to about 12 CBR. If this relationship is expanded beyond a CBR of 12 (as shown in Figure 194), it can be observed that the relationship rapidly becomes nonlinear, indicating the subgrade becomes sufficiently strong to resist failure. In addition, it was observed that at higher CBRs the design curves begin to converge, indicating the methodology is insensitive to

traffic volume at high subgrade CBRs. Thus, the beta design methodology based on the assumption of failure in the subgrade is valid for subgrade CBR values less than 12 and is founded on the results of pavement thicknesses greater than those evaluated in this study.

Figure 193. Summary of pavement thickness from historical data.

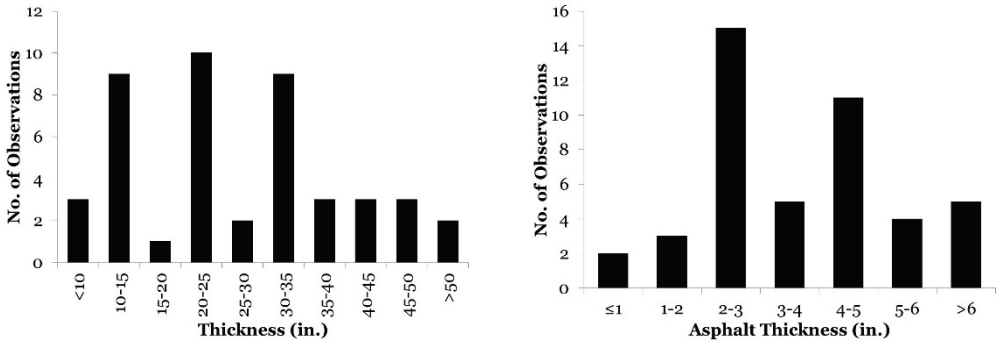

(a) Overall thickness (b) Asphalt thickness

Figure 194. Failure vertical stress with increasing CBR.

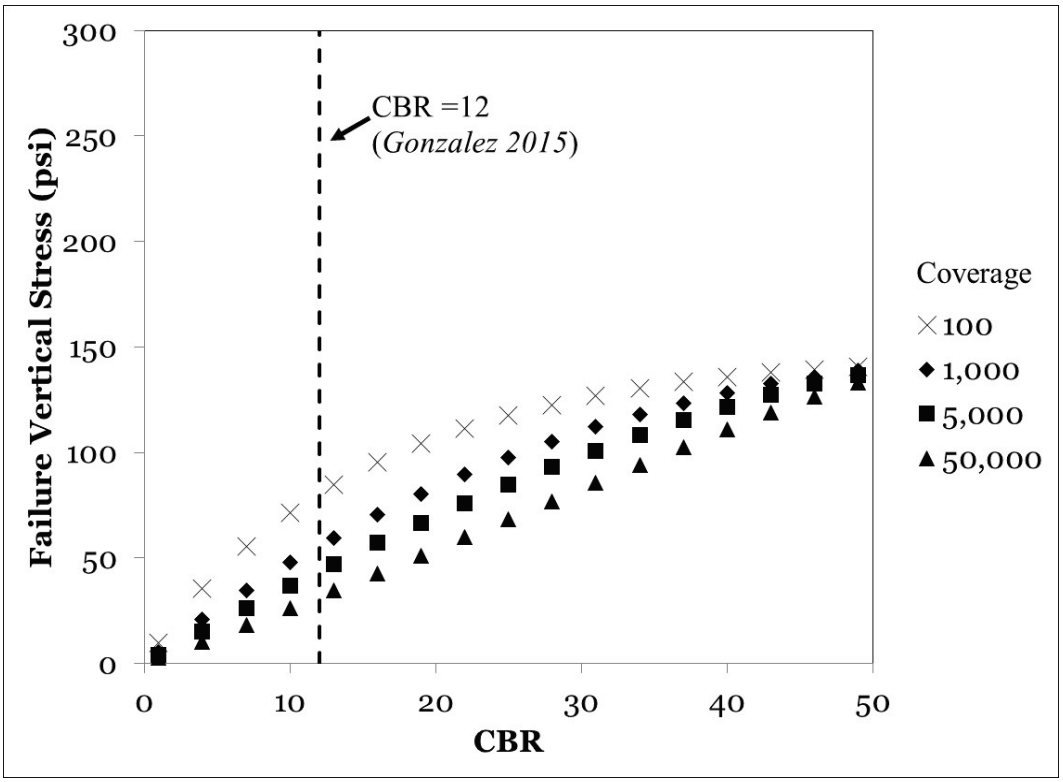

Using the current design methodology (i.e., assuming failure in the subgrade), researchers computed coverages to failure based on the as-built subgrade CBR and as-built thickness. Calculations were made using PCASE, an in-house developed software tool. Calculated coverages from

the subgrade are shown in Table 48. It was observed that the existing criterion poorly predicted the coverages to failure and that the existing model overpredicted coverages to failure for the gravel base test items, as was expected (recall the specification assumes a high-quality base). The test items containing limestone base were under-predicted by the current design methodology.

Table 48. Calculated coverages using existing model.

Item	Base Type	Design HMA (in)	Total Thickness (in.)	Calculated Coverages	Actual Coverages	Difference
C130NTP1	GR	2.5	14.8	1,200	60	-1,140
C130NTP2	LMS	2.5	14.6	941	6,252	5,312
C130NTP3	LMS	1.5	13.4	466	1,654	1,188
C130NTP4	LMS	1.0	12.9	229	1,423	1,194
C130RTP1	GR	2.5	14.6	2,171	50	-2,121
C130RTP2	LMS	2.5	14.7	1,964	10,628	8,664
C130RTP3	LMS	1.5	13.7	760	4,288	3,528
C130RTP4	LMS	1.0	13.0	683	2,085	1,402
C17NTP1	LMS	1.0	13.0	37	188	151
C17NTP2	LMS	1.5	13.3	46	223	178
C17NTP3	LMS	2.5	14.6	91	523	432
C17NTP4	GR	2.5	14.6	86	15	-71
C17RTP1	LMS	1.0	12.9	60	661	601
C17RTP2	LMS	1.5	13.6	106	1,573	1,467
C17RTP3	LMS	2.5	14.3	125	1,339	1,215
C17RTP4	GR	2.5	14.7	193	17	-177

9.2 Development of criteria for nonstandard pavement

A similar approach was used to investigate data obtained from this study in terms of base failure. Initial measured vertical pressure at mid-depth of the base course and as-constructed CBR for each test item were used to calculate an index of performance indicated by the Beta parameter, as summarized in Table 49. The associated Beta parameters were plotted against the corresponding number of passes to failure of each test item, as shown in Figure 195 (expressed in terms of coverages to account for traffic lateral wander). A preliminary proposed criterion was drawn through those points for the gravel base test items and the limestone base test

items with approximately the same shape as the current criterion (i.e., Equation 3); the derived coefficients are summarized in Table 50. The data plotted show good agreement for the test points generated from this study. Since the current Beta performance criterion was derived for subgrade failures with CBR values typically less than about 12, the inclusion of the proposed criterion for aggregate bases will significantly improve and expand the CBR-Beta design and evaluation procedure for substandard bases where failure may occur. Additional full-scale test data are needed to further validate and refine the proposed base criterion; however, the data presented herein suggest that adjustments to current design or evaluation procedures to account for nonstandard base materials or thin asphalt pavements are reasonable.

Table 49. Calculated Beta-value assuming base failure.

Item	Thickness (in.)	Pressure (psi)	CBR	Beta	Coverages to Failure
C130NTP1	14.8	68.2	9.8	4.6	60
C130NTP2	14.6	60.9	9.8	1.9	6,252
C130NTP3	13.4	77.7	10.1	2.4	1,654
C130NTP4	12.9	78.5	9.5	2.5	1,423
C130RTP1	14.6	68.7	9.8	5.1	50
C130RTP2	14.7	69.8	9.6	2.2	10,628
C130RTP3	13.7	74.5	9.4	2.3	4,288
C130RTP4	13.0	80.9	9.9	2.5	2,085
C17NTP1	13.0	97.4	9.5	3.1	188
C17NTP2	13.3	84.2	9.6	2.6	223
C17NTP3	14.6	80.6	9.5	2.5	523
C17NTP4	14.6	100.8	9.4	6.9	15
C17RTP1	12.9	87.3	9.7	2.7	661
C17RTP2	13.6	68.8	10	2.2	1,573
C17RTP3	14.3	68.2	9.6	2.1	1,339
C17RTP4	14.7	94.6	9.9	6.3	17

Figure 195. Proposed aggregate base Beta criteria.

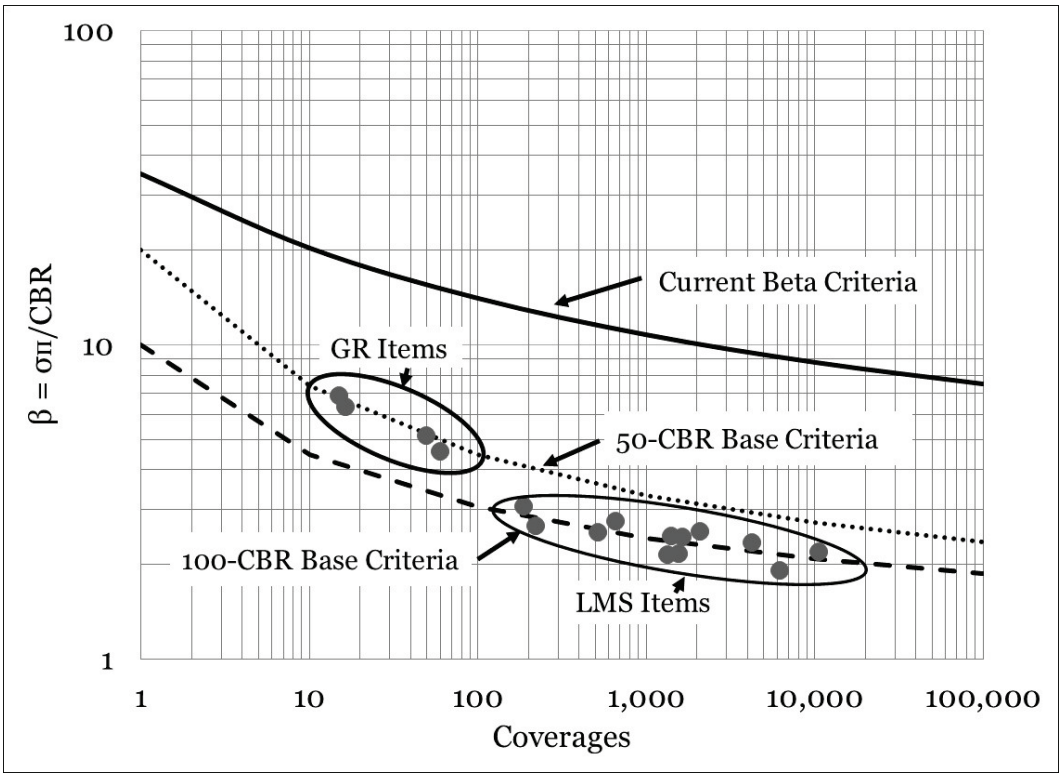

Table 50. Coefficients for proposed base failure models.

Criteria	a	b	c
Current	1.5441	0.2354	0.073
50-CBR Base	1.3010	0.4984	0.000
100-CBR Base	0.9999	0.5333	0.000

10 Conclusions and Recommendations

Sixteen full-scale nonstandard airfield pavement test items were constructed and trafficked with the primary goal of developing improved performance models to describe behavior in thin asphalt pavements. Analysis of the test results yielded the following conclusions.

C-130 test item conclusions:

1. The lack of a competent aggregate base (i.e., ~50 CBR) resulted in poor rutting performance.
2. On a competent aggregate base (i.e., 100 CBR) an increase in asphalt thickness resulted in a statistically significant rutting improvement.
3. Reducing tire pressure did not improve rutting performance on weak base materials, suggesting that total load rather than tire pressure controlled pavement performance.
4. Reducing tire pressure on limestone base test items provided an improvement in rutting performance ranging from ~15 to 36%.
5. A statistical analysis indicated that average measured subgrade pressure was lower in the normal tire pressure test items, suggesting that a reduction in tire pressure did not have a significant effect on subgrade pressure response.
6. A tire pressure reduction did not have a meaningful effect on base pressure response in some cases but did have an effect in others.
7. An increase in asphalt thickness resulted in a meaningful reduction in subgrade deflection.
8. Reducing tire pressure did not result in a meaningful reduction in subgrade deflection in the gravel base test item.
9. Lower asphalt strain values were observed in the limestone base test items, regardless of asphalt thickness, than in the gravel base test items.

C-17 test item conclusions:

1. Reducing tire pressure did not improve rutting performance in the weak base course test item, but did result in statistically significant rutting improvements in the limestone base course test items.
2. Increasing asphalt thickness did not significantly reduce measured subgrade pressure when the pavement contained a weak base course.
3. Reducing tire pressure resulted in a significant reduction in measured subgrade pressure response.

4. An increase in asphalt thickness resulted in a meaningful reduction in measured base pressure.
5. A reduction in tire pressure resulted in a meaningful reduction in measured base pressure.
6. The addition of 0.5-in. HMA did not result in a significant difference in measured subgrade deflection.
7. Improvements in subgrade deflection, attributed to a reduction in tire pressure, appeared to diminish with an increase in asphalt thickness.

Overall conclusions:

1. The inclusion of a high-quality aggregate base course had a significant effect on rutting performance, and a reduction in base course CBR of approximately 50% yielded a much higher change in rutting performance.
2. In both loading cases, a reduction in tire pressure had little effect on rutting performance in the gravel base test items; thus, it can be concluded that total load dominated performance in the weaker base course test items.
3. An increase in asphalt thickness had a more meaningful effect on measured subgrade deflection than a reduction in tire pressure.
4. Reducing tire pressure increased passes to failure in the limestone base test items but had little effect in the gravel base test items.

A review of the existing design and evaluation model indicated that it was a poor predictor of performance in nonstandard pavement cross sections. The data collected in this experiment were used to propose a series of models that provide a means to estimate passes to failure in both a competent aggregate base as well as a reduced-strength aggregate base. While the data suggest that adjustments to the current design criteria are reasonable, the following recommendations to further expand and/or verify the proposed models are made.

1. It is recommended that pavement test items, including a base course CBR of approximately 30 and 80, be investigated to further develop a family of curves describing base course failure.
2. A series of test items containing a 100-CBR base course and targeting failure coverages of 20-100 should be investigated to validate the shape of the proposed failure curve at low coverage levels.

3. A series of test items containing a 50-CBR base course and targeting failure coverages ranging from 100 to 10,000 should be investigated to understand performance at higher coverage levels.
4. The HMA investigated in this study was considered an airfield quality asphalt mixture. It is recommended that lower quality or non-standard asphalt mixtures -- such as sand-asphalt, macadam, or high rap mixtures -- be investigated to understand the performance implications of nonstandard asphalt mixtures.

References

Ahlvin, R. G., H. H. Ulery, R. L. Hutchinson, and J. L. Rice. 1971. *Multiple-wheel heavy gear load pavement tests, volume I*. Technical Report AFWL-TR-70-113. Vicksburg, MS: U.S. Army Engineer Waterways Experiment Station.

ASTM (American Society for Testing and Materials). 2009. *Standard test method for CBR (California Bearing Ratio) of soils in place*. Designation: D 4429-09a. West Conshohocken, PA: ASTM International.

_____. 2012. *Standard test methods for laboratory compaction characteristics of soil using modified effort (56,000 ftblf/ft3 [2,700 kN-m/m3])*. Designation: D 1557-12e1. West Conshohocken, PA: ASTM International.

_____. 2016. *Standard test method for California Bearing Ratio (CBR) of laboratory-compacted soils*. Designation: D 1883-16. West Conshohocken, PA: ASTM International.

_____. 2017a. *Standard practice for classification of soils for engineering purposes (Unified Soil Classification System)*. Designation: D 2487-17. West Conshohocken, PA: ASTM International.

_____. 2017b. *Standard test methods for in-place density and water content of soil and soil-aggregate by nuclear methods (shallow depth)*. Designation: D 6938-17a. West Conshohocken, PA: ASTM International.

_____. 2017c. *Standard test methods for liquid limit, plastic limit, and plasticity index of soils*. Designation: D4318-17c1. West Conshohocken, PA: ASTM International.

_____. 2018. *Standard test method for use of the dynamic cone penetrometer in shallow pavement applications*. Designation: D 6951/6951M-18. West Conshohocken, PA: ASTM International.

AASHTO (Association of American Highway and Transportation Officials). 2012. *Standard specification for classification of soils and soil-aggregate mixtures for highway construction purposes*. AASHTO M 145. Washington, DC: AASHTO.

_____. 2016. *Standard method of test for bulk specific gravity (Gmb) of compacted hot mix asphalt (HMA) using saturated surface-dry specimens*. AASHTO T 166. Washington, DC: AASHTO.

Bell, H. P., and L. W. Mason. 2008. *Evaluation of minimum asphalt concrete thickness criteria*. ERDC/GSL-TR-08-26. Vicksburg, MS: U.S. Army Engineer Research and Development Center.

Bianchini, A., and C. R. Gonzalez. 2015. Reformulation of the design procedure for aggregate-surface airfield pavement. *Journal of Transportation Engineering* 141(3). DOI: 10.1061/(ASCE)TE.1943-5436.0000752.

Burns, C. D., and J. L. McCall. 1968. *Evaluation of load-distributing capability of T17 membrane in road construction*. Miscellaneous Paper S-68-10. Vicksburg, MS: U.S. Army Engineer Waterways Experiment Station.

Cooksey, D. L., and D. M. Ladd. 1971. *Pavement design for various levels of traffic volume*. Technical Report AFWL-TR-70-133. Kirtland AFB, NM: Air Force Systems Command.

Gonzalez, C. R. 2015. Development and validation of a stress-based procedure for the design of military flexible pavements. PhD diss., University of Illinois.

Hammitt, G. M. 1970. *Thickness requirements for unsurfaced roads and airfields*. Technical Report S-70-5. Vicksburg, MS: U.S. Army Engineer Waterways Experiment Station.

Hayhoe, G. F. 2004. Testing results from the FAA's national airport pavement testing facility. In *Proceedings of the 2nd International Conference on Accelerated Pavement Testing*. University of Minnesota.

Ladd, D. M. 1970. *Soil strength criteria for operation of fighter aircraft on unsurfaced airfields, bare base support project 3782-65.* Miscellaneous Paper S-70-24. Vicksburg, MS: U.S. Army Engineer Waterways Experiment Station.

Ladd, D. M., and H. Ulery. 1967. *Aircraft ground-flotation investigation, part I-basic report*. Technical Report 3-737. Vicksburg, MS: U.S. Army Engineer Waterways Experiment Station.

Porter, O. J. 1949. *Accelerated traffic tests at Stockton Airfield, Stockton California (Stockton test no. 2).* Sacremento, CA: Corps of Engineers Sacramento District.

Thompson, A. B., and C. D. Burns. 1960. *Criteria for designing runways to be surfaced with landing mat and membrane-type materials*. Technical Report 3-539. Vicksburg, MS: U.S. Army Engineer Waterways Experiment Station.

WES (Waterways Experiment Station). 1947. *Flexible pavement behavior studies*. Interim Report No. 2. Vicksburg, MS: U.S. Army Engineer Waterways Experiment Station.

_____. 1950. *Investigation of effects of traffic with high-pressure tire on asphalt pavements*. Technical Memorandum No. 3-312. Vicksburg, MS: U.S. Army Engineer Waterways Experiment Station.

Webster, S. L. 1993. *Geogrid reinforced base courses for flexible Ppvements for light airtraffic, laboratory tests, and design criteria*. Technical Report WES-TR-GL-93-6. Vicksburg, MS: U.S. Army Engineer Waterways Experiment Station.

Webster, S. L., R. W. Brown, and J. R. Porter. 1994. *Force projection site evaluation using the electrical cone penetrometer (ECPO) and the dynamic cone penetrometer (DCP)*. Technical Report GL-94-17. Vicksburg, MS: U.S. Army Engineer Waterways Experiment Station.

Webster, S. L., R. H. Grau, and T. P. Williams. 1992. *Description and application of dual-mass dynamic cone penetrometer*. Instruction Report GL 92-3. Vicksburg, MS: U.S. Army Engineer Waterways Experiment Station..

Appendix A: As-Built DCP Data

DCP TEST DATA

Project: *Thin Asphalt Section* Date: 3-May-19
Location: C130NTP1 Soil Type(s): High plasticity Clay

Hammer: ○ 10.1 lbs. ● 17.6 lbs. ○ Both hammers used

Soil Type: ● CH ○ CL ○ All other soils

No. of Blows	Accumulative Penetration (mm)	Type of Hammer
0	100	1
3	120	1
3	150	1
3	170	1
3	185	1
5	225	1
5	260	1
5	290	1
5	320	1
2	335	1
2	350	1
2	375	1
2	440	1
1	470	1
1	500	1
1	520	1
1	545	1
1	565	1
1	585	1
1	605	1
1	620	1
2	645	1
2	670	1
2	695	1
2	715	1
2	735	1
2	755	1
2	775	1
2	795	1
2	810	1
		1
		1
		1
		1
		1
		1
		1
		1
		1
		1
		1
		1
		1
		1
		1

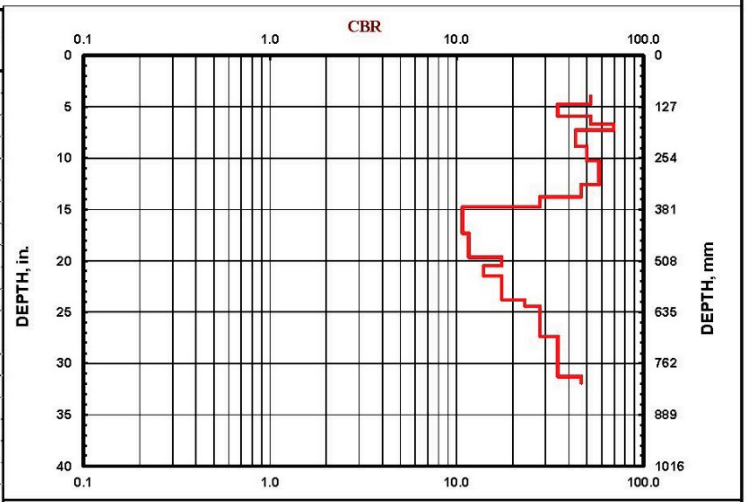

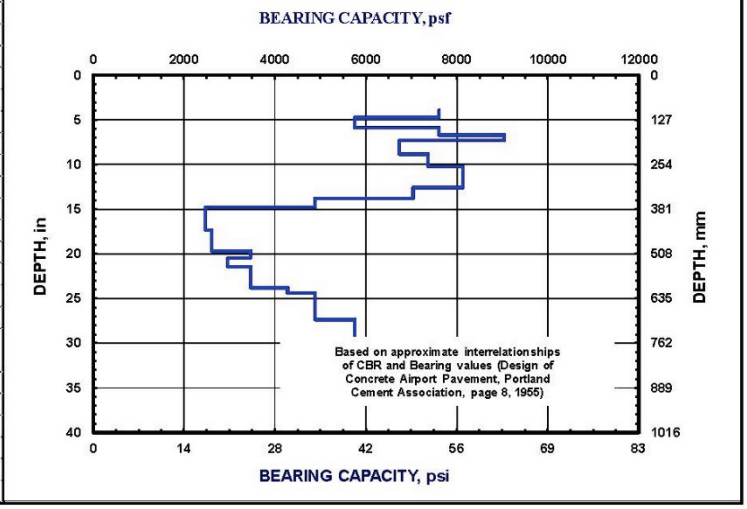

DCP TEST DATA

Project: *Thin Asphalt Section*
Location: C130RTP1
Date: 3-May-19
Soil Type(s): High plasticity Clay

Hammer
- ○ 10.1 lbs.
- ● 17.6 lbs.
- ○ Both hammers used

Soil Type
- ● CH
- ○ CL
- ○ All other soils

No. of Blows	Accumulative Penetration (mm)	Type of Hammer
0	110	1
3	130	1
4	160	1
4	195	1
2	220	1
2	240	1
4	270	1
4	295	1
4	325	1
4	355	1
2	385	1
1	420	1
1	455	1
1	485	1
1	515	1
1	540	1
1	570	1
1	595	1
1	630	1
1	660	1
1	685	1
1	705	1
1	730	1
1	750	1
1	765	1
2	800	1
		1
		1
		1
		1
		1
		1
		1
		1
		1
		1
		1
		1
		1
		1
		1
		1

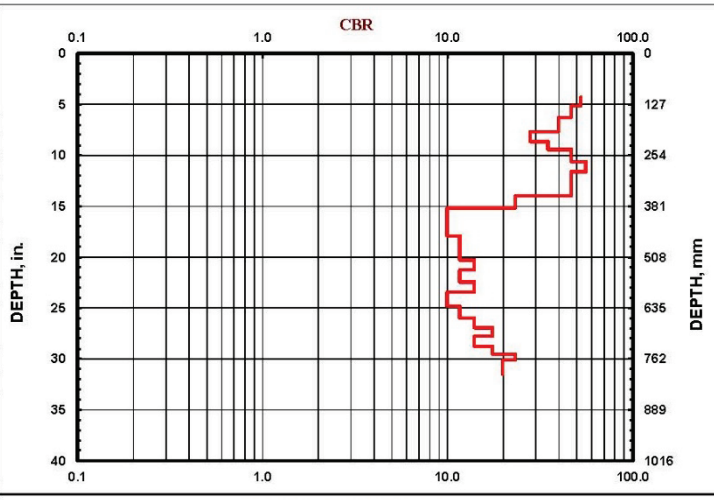

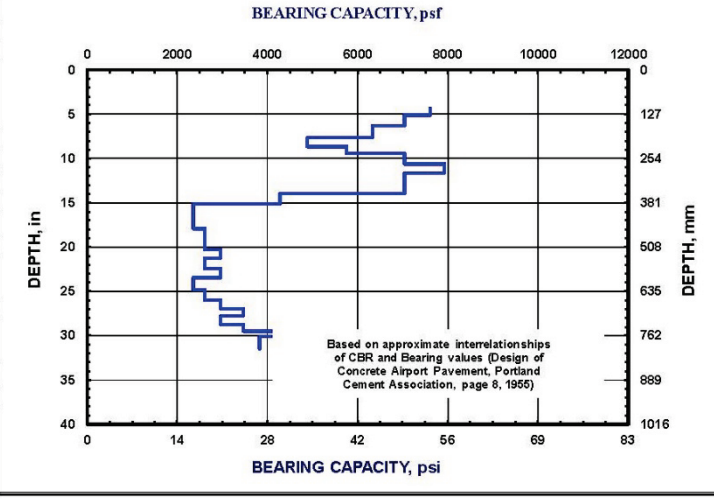

DCP TEST DATA

Project: *Thin Asphalt Section* Date: 3-May-19
Location: C17NTP4 Soil Type(s): High plasticity Clay

Hammer: ○ 10.1 lbs. ● 17.6 lbs. ○ Both hammers used

Soil Type: ● CH ○ CL ○ All other soils

No. of Blows	Accumulative Penetration (mm)	Type of Hammer
0	100	1
5	130	1
5	165	1
5	200	1
5	235	1
5	270	1
5	300	1
5	340	1
3	365	1
2	400	1
1	430	1
1	460	1
1	490	1
1	510	1
1	530	1
1	550	1
1	570	1
2	600	1
2	635	1
2	665	1
2	695	1
2	725	1
2	750	1
2	780	1
2	805	1
		1
		1
		1
		1
		1
		1
		1
		1
		1
		1
		1
		1
		1
		1
		1
		1
		1
		1
		1
		1
		1
		1

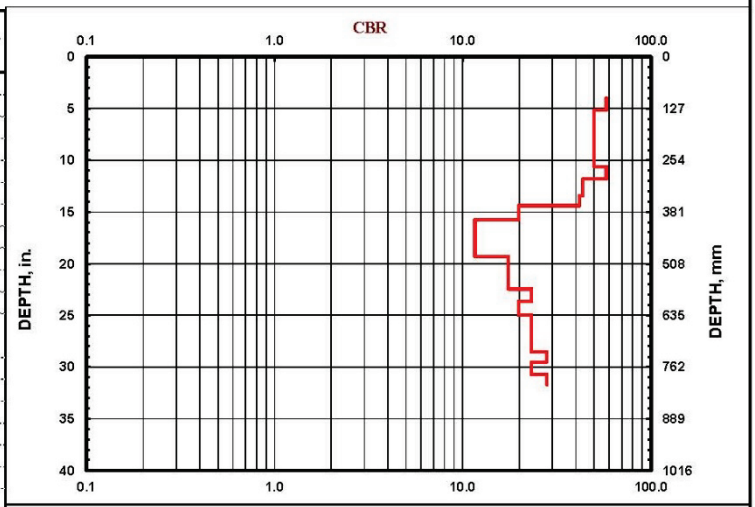

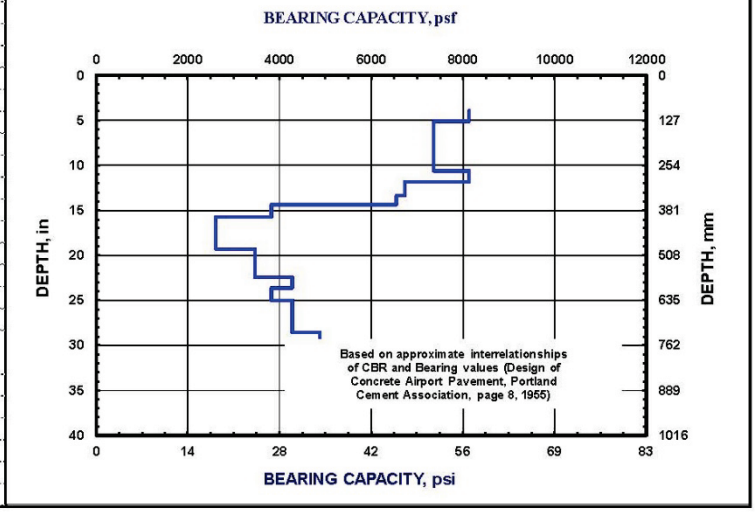

DCP TEST DATA

Project: *Thin Asphalt Section* Date: 3-May-19
Location: C17RTP4 Soil Type(s): High plasticity Clay

Hammer: ○ 10.1 lbs. ● 17.6 lbs. ○ Both hammers used
Soil Type: ● CH ○ CL ○ All other soils

No. of Blows	Accumulative Penetration (mm)	Type of Hammer
0	80	1
5	110	1
5	150	1
5	185	1
5	225	1
5	265	1
3	290	1
3	310	1
3	330	1
3	355	1
3	390	1
1	425	1
1	460	1
1	495	1
1	520	1
1	545	1
1	570	1
1	590	1
1	615	1
1	630	1
1	650	1
1	670	1
1	680	1
2	710	1
2	740	1
2	760	1
2	785	1
2	805	1
		1
		1
		1
		1
		1
		1
		1
		1
		1
		1
		1
		1
		1
		1
		1

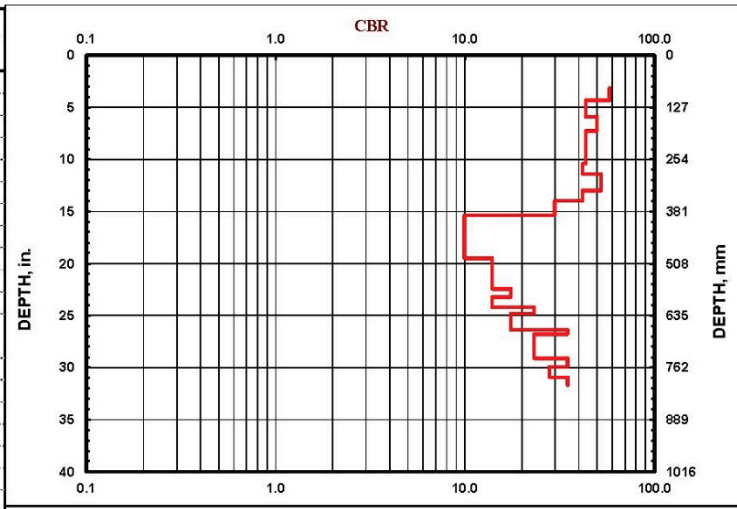

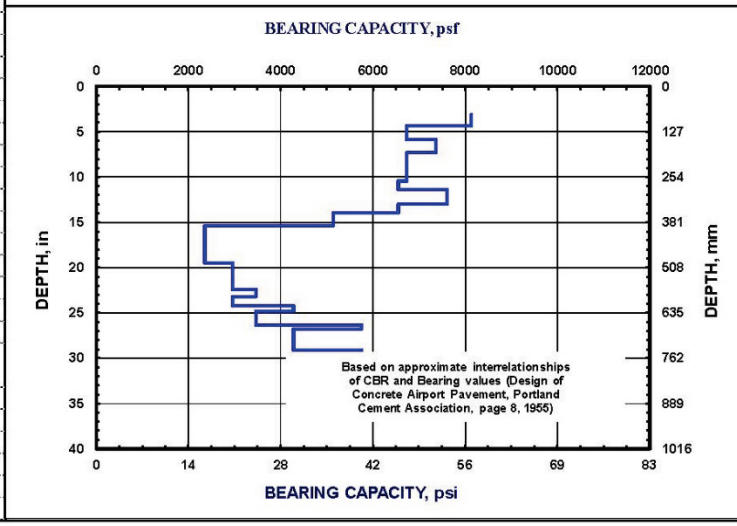

Appendix B: Rut Depth Data

Test Item	C130 NTP1	C130 NTP2	C130 NTP3	C130 NTP4	C130 RTP1	C130 RTP2	C130 RTP3	C130 RTP4
HMA (in.)	2.5	2.5	1.5	1.0	2.5	2.5	1.5	1.0
Base	GR	LMS	LMS	LMS	GR	LMS	LMS	LMS
Tire Pr.	Normal	Normal	Normal	Normal	Reduced	Reduced	Reduced	Reduced
Pass	Rut Depth (in.)							
0	0.00	0.00	0.00	0.00	0.00	0.00	0.00	0.00
2	0.06	0.00	0.02	0.02	0.08	0.02	0.02	0.00
8	0.23	0.00	0.04	0.02	0.23	0.02	0.06	0.04
32	0.38	0.08	0.06	0.04	0.46	0.00	0.02	0.02
92	0.85	0.08	0.06	0.08	0.98	0.00	0.04	0.06
140	1.10	0.08	0.10	0.15	1.13	0.00	0.04	0.08
188	1.23	0.08	0.10	0.23	1.35	0.00	0.06	0.13
308	1.69	0.10	0.15	0.31	1.85	0.00	0.10	0.13
392	1.88	0.10	0.15	0.31	2.23	0.00	0.10	0.17
536	2.17	0.10	0.21	0.35	2.79	0.00	0.10	0.21
716	2.69	0.13	0.27	0.48	4.10	0.04	0.15	0.31
908	3.29	0.17	0.35	0.52	–	0.04	0.17	0.35
1100	4.08	0.17	0.42	0.60	–	0.10	0.21	0.44
1652	–	0.28	0.61	0.73	–	0.16	0.33	0.63
2000	–	0.35	0.73	0.81	–	0.19	0.40	0.75
3260	–	0.50	0.99	1.09	–	0.26	0.56	0.88
3408	–	0.52	1.02	1.13	–	0.27	0.58	0.90
6000	–	0.75	1.40	1.50	–	0.35	0.79	1.25
8004	–	0.88	1.56	1.65	–	0.46	0.96	1.35
10008	–	0.94	1.65	1.73	–	0.54	1.10	1.52
12504	–	1.00	1.75	1.87	–	0.65	1.20	1.62
14052	–	1.04	1.81	1.95	–	0.71	1.25	1.67
15000	–	1.06	1.85	2.00	–	0.75	1.29	1.71
20004	–	1.15	1.94	2.02	–	0.96	1.48	1.85
25008	–	–	–	–	–	1.13	1.71	2.10

Note: Underlined data are interpolated.

Test Item	C17 NTP1	C17 NTP2	C17 NTP3	C17 NTP4	C17 RTP1	C17 RTP2	C17 RTP3	C17 RTP4
HMA (in.)	1.0	1.5	2.5	2.5	1.0	1.5	2.5	2.5
Base	LMS	LMS	LMS	GR	LMS	LMS	LMS	GR
Tire Pr.	Normal	Normal	Normal	Normal	Reduced	Reduced	Reduced	Reduced
Pass	Rut Depth (in.)							
0	0.00	0.00	0.00	0.00	0.00	0.00	0.00	0.00
2	0.00	0.04	0.02	0.21	0.06	0.00	0.06	0.31
8	0.08	0.10	0.04	0.48	0.08	0.04	0.10	0.58
32	0.08	0.15	0.06	1.04	0.10	0.04	0.10	0.98
92	0.25	0.31	0.17	4.10	0.15	0.08	0.17	2.16
140	0.35	0.42	0.27	–	0.21	0.10	0.23	3.19
188	0.48	0.52	0.31	–	0.29	0.15	0.27	4.63
308	0.75	0.75	0.42	–	0.40	0.19	0.33	–
392	1.06	0.94	0.56	–	0.44	0.25	0.35	–
536	1.31	1.10	0.67	–	0.54	0.27	0.40	–
716	1.60	1.38	0.77	–	0.71	0.38	0.54	–
908	1.96	1.60	0.90	–	0.81	0.44	0.58	–
1100	2.29	1.83	1.04	–	0.88	0.52	0.67	–
1652	3.13	2.46	1.38	–	1.19	0.73	0.77	–
2000	–	3.08	1.75	–	1.23	0.79	0.85	–
3260	–	–	2.79	–	1.67	1.02	1.13	–
3408	–	–	–	–	1.71	1.06	1.15	–
6000	–	–	–	–	2.10	1.35	1.48	–
8004	–	–	–	–	2.21	1.48	1.69	–
10008	–	–	–	–	2.56	2.15	2.31	–
12504	–	–	–	–	3.19	2.38	4.66	–
14052	–	–	–	–	4.19	2.65	–	–
15000	–	–	–	–	–	2.81	–	–
20004	–	–	–	–	–	–	–	–
25008	–	–	–	–	–	–	–	–

Appendix C: Visual Cracking Data

Test Item	C130 NTP1	C130 NTP2	C130 NTP3	C130 NTP4	C130 RTP1	C130 RTP2	C130 RTP3	C130 RTP4
HMA (in.)	2.5	2.5	1.5	1.0	2.5	2.5	1.5	1.0
Base	GR	LMS	LMS	LMS	GR	LMS	LMS	LMS
Tire Pr.	Normal	Normal	Normal	Normal	Reduced	Reduced	Reduced	Reduced
Pass	Total Cracking (linear ft.)							
0	0.0	0.0	0.0	0.0	0.0	0.0	0.0	0.0
2	0.0	0.0	0.0	0.0	0.0	0.0	0.0	0.0
8	0.0	0.0	0.0	0.0	0.0	0.0	0.0	0.0
32	0.0	0.0	0.0	0.0	0.0	0.0	0.0	0.0
92	0.0	0.0	0.0	0.0	0.0	0.0	0.0	0.0
140	0.0	0.0	0.0	0.0	0.0	0.0	0.0	0.0
188	0.0	0.0	0.0	0.0	0.0	0.0	0.0	0.0
308	0.0	0.0	0.0	0.0	2.3	0.0	0.0	0.0
392	0.0	0.0	0.0	0.0	11.4	0.0	0.0	0.0
536	0.0	0.0	0.0	0.0	97.6	0.0	0.0	0.0
716	19.5	0.0	0.0	0.0	225.0	0.0	0.0	0.0
908	76.3	0.0	0.0	2.2	–	0.0	0.0	4.1
1100	153.0	0.0	0.0	7.8	–	0.0	0.0	14.2
1652	–	0.0	0.0	28.7	–	0.0	0.0	33.9
2000	–	0.0	2.0	41.9	–	0.0	0.0	46.3
3260	–	0.0	4.9	69.6	–	0.0	0.0	91.1
3408	–	0.0	5.2	72.8	–	0.0	0.0	96.4
6000	–	0.0	12.8	92.4	–	0.0	5.3	111.4
8004	–	0.0	19.4	108.2	–	0.0	12.7	120.1
10008	–	0.0	31.0	134.2	–	0.0	17.3	130.6
12504	–	0.0	38.3	142.9	–	0.0	26.9	147.2
15000	–	0.0	45.5	151.5	–	0.0	36.4	163.7
20004	–	0.0	72.4	183.7	–	0.0	54.1	199.6
25008	–	–	–	–	–	–	–	–

Note: Underlined data are interpolated.

Test Item	C17 NTP1	C17 NTP2	C17 NTP3	C17 NTP4	C17 RTP1	C17 RTP2	C17 RTP3	C17 RTP4
HMA (in.)	1.0	1.5	2.5	2.5	1.0	1.5	2.5	2.5
Base	LMS	LMS	LMS	GR	LMS	LMS	LMS	GR
Tire Pr.	Normal	Normal	Normal	Normal	Reduced	Reduced	Reduced	Reduced
Pass	Total Cracking (linear ft)							
0	0.0	0.0	0.0	0.0	0.0	0.0	0.0	0.0
2	0.0	0.0	0.0	0.0	0.0	0.0	0.0	0.0
8	0.0	0.0	0.0	0.0	0.0	0.0	0.0	0.0
32	0.0	0.0	0.0	0.0	0.0	0.0	0.0	0.0
92	0.0	0.0	0.0	133.7	0.0	0.0	0.0	40.2
140	0.0	0.0	0.0	–	2.0	0.0	0.0	60.0
188	0.0	0.0	0.0	–	4.7	0.0	0.0	201.3
308	19.8	0.0	0.0	–	14.8	0.0	0.0	–
392	51.0	0.0	0.0	–	32.4	0.0	0.0	–
536	95.1	0.0	0.0	–	60.8	4.2	0.0	–
716	120.9	10.0	0.0	–	81.6	4.9	0.0	–
908	180.0	24.0	0.0	–	120.2	6.3	0.0	–
1,100	191.6	37.8	0.0	–	166.8	12.1	0.0	–
1,652	225.0	116.8	0.0	–	215.0	29.4	0.0	–
2,000	–	WS	0.0	–	222.9	43.6	0.0	–
3,260	–	–	134.5	–	WS	94.8	0.0	–
3,408	–	–	–	–	–	102.6	6.0	–
6,000	–	–	–	–	–	238.9	110.4	–
8,004	–	–	–	–	–	283.4	129.6	–
10,008	–	–	–	–	–	WS	215.3	–
12,504	–	–	–	–	–	–	250.2	–
15,000	–	–	–	–	–	–	285.1	–
20,004	–	–	–	–	–	–	–	–
25,008	–	–	–	–	–	–	–	–

Appendix D: Impulse Stiffness Data

Test Item	C130 NTP1	C130 NTP2	C130 NTP3	C130 NTP4	C130 RTP1	C130 RTP2	C130 RTP3	C130 RTP4
HMA (in.)	2.5	2.5	1.5	1.0	2.5	2.5	1.5	1.0
Base	GR	LMS	LMS	LMS	GR	LMS	LMS	LMS
Tire Pr.	Normal	Normal	Normal	Normal	Reduced	Reduced	Reduced	Reduced
Pass	Impulse Stiffness (kips/in.)							
0.1	286	560	408	392	267	696	614	556
2	235	492	370	368	217	572	484	463
8	235	483	355	348	202	526	442	418
32	220	453	322	311	178	454	385	341
92	206	435	301	290	201	460	389	345
140	202	451	298	290	171	428	350	318
188	184	416	273	274	173	438	369	308
308	174	426	284	293	143	386	320	279
392	176	429	277	281	129	381	306	269
536	168	388	258	248	126	430	358	314
716	158	409	290	283	–	376	302	267
908	131	363	249	248	–	366	295	267
1,100	–	370	262	251	–	383	307	289
1,652	–	348	229	230	–	365	289	262
2,000	–	334	209	217	–	353	278	245
3,260	–	412	280	274	–	340	254	241
3,408	–	421	288	281	–	339	251	240
6,000	–	404	278	256	–	321	251	216
8,004	–	311	233	244	–	366	286	257
10,008	–	322	237	238	–	361	288	269
12,504	–	335	243	246	–	365	302	277
14,052	–	342	247	251	–	367	311	281
15,000	–	347	249	254	–	369	316	284
20,004	–	354	259	265	–	342	297	248
25,008	–	–	–	–	–	359	308	275

Note: Underlined data are interpolated.

Test Item	C17 NTP1	C17 NTP2	C17 NTP3	C17 NTP4	C17 RTP1	C17 RTP2	C17 RTP3	C17 RTP4
HMA (in.)	1.0	1.5	2.5	2.5	1.0	1.5	2.5	2.5
Base	LMS	LMS	LMS	GR	LMS	LMS	LMS	GR
Tire Pr.	Normal	Normal	Normal	Normal	Reduced	Reduced	Reduced	Reduced
Pass	Impulse Stiffness (kips/in.)							
0.1	618	636	706	325	620	663	678	299
2	468	492	545	245	457	535	565	259
8	406	414	453	204	391	435	492	230
32	324	352	418	163	342	418	473	202
92	328	362	432	–	328	381	456	209
140	280	307	360	–	310	341	423	138
188	274	310	357	–	348	385	438	–
308	254	293	340	–	297	322	389	–
392	279	296	358	–	285	323	394	–
536	288	322	361	–	286	317	383	–
716	247	274	317	–	300	320	388	–
908	243	265	325	–	281	292	353	–
1,100	277	285	349	–	267	282	353	–
1,652	226	273	321	–	298	312	362	–
2,000	–	249	272	–	333	319	389	–
3,260	–	273	–	–	309	304	349	–
3,408	–	–	–	–	320	303	340	–
6,000	–	–	–	–	290	284	321	–
8,004	–	–	–	–	302	295	275	–
10,008	–	–	–	–	221	250	218	–
12,504	–	–	–	–	305	305	258	–
14,052	–	–	–	–	252	253	–	–
15,000	–	–	–	–	–	266	–	–
20,004	–	–	–	–	–	–	–	–
25,008	–	–	–	–	–	–	–	–

Appendix E: Subgrade Pressure Response Data

Test Item	C130 NTP1	C130 NTP2	C130 NTP3	C130 NTP4	C130 RTP1	C130 RTP2	C130 RTP3	C130 RTP4
HMA (in.)	2.5	2.5	1.5	1.0	2.5	2.5	1.5	1.0
Base	GR	LMS	LMS	LMS	GR	LMS	LMS	LMS
Tire Pr.	Normal	Normal	Normal	Normal	Reduced	Reduced	Reduced	Reduced
Pass	Subgrade Pressure (psi)							
2	39.1	28.5	29.4	19.3	42.3	30.4	32.8	32.80
8	43.0	27.0	30.4	19.9	42.1	32.5	34.1	34.07
32	44.7	28.2	31.6	22.2	53.5	33.6	37.2	38.32
92	51.7	30.9	35.7	28.4	57.2	34.0	39.8	42.1
140	52.7	30.7	35.7	30.8	57.7	34.0	37.9	41.4
188	51.6	29.9	35.3	33.3	54.8	34.0	37.9	41.0
308	56.6	31.2	37.2	40.1	58.5	35.6	40.5	43.0
392	52.4	29.9	36.4	40.0	62.8	35.8	40.8	44.0
536	51.7	28.9	38.0	41.7	65.2	36.3	42.4	45.0
716	58.4	30.6	40.9	45.1	72.2	37.9	45.4	48.6
908	62.1	30.7	43.2	46.5	–	37.8	45.7	51.6
1,100	68.4	32.1	44.5	49.8	–	39.0	49.1	53.7
1,652	–	36.1	47.5	50.9	–	40.3	53.8	55.9
2,000	–	38.6	49.4	51.6	–	41.1	56.7	57.2
3,260	–	43.6	50.7	51.5	–	43.8	56.6	57.2
3,408	–	44.2	50.8	51.5	–	44.1	56.6	57.2
6,000	–	48.5	53.2	52.6	–	46.1	54.4	56.9
8,004	–	48.6	54.1	50.6	–	43.7	46.6	54.1
10,008	–	49.0	53.6	50.4	–	48.4	55.5	56.2
12,504	–	49.0	52.9	50.0	–	50.5	57.3	55.8
14,052	–	49.0	52.4	49.7	–	51.8	58.4	55.5
15,000	–	49.0	52.1	49.5	–	52.6	59.1	55.3
20,004	–	47.9	51.1	48.4	–	52.1	59.4	53.2
25,008	–	–	–	–	–	51.0	58.0	52.4

Note: Underlined data are interpolated.

Test Item	C17 NTP1	C17 NTP2	C17 NTP3	C17 NTP4	C17 RTP1	C17 RTP2	C17 RTP3	C17 RTP4
HMA (in.)	1.0	1.5	2.5	2.5	1.0	1.5	2.5	2.5
Base Type	LMS	LMS	LMS	GR	LMS	LMS	LMS	GR
Tire Pr.	Normal	Normal	Normal	Normal	Reduced	Reduced	Reduced	Reduced
Pass	Subgrade Pressure (psi)							
2	36.3	38.5	37.3	54.0	27.8	28.2	26.0	50.1
8	45.2	45.1	39.6	60.9	32.0	32.2	32.1	50.9
32	55.2	48.1	42.3	71.1	42.7	38.2	37.1	62.3
92	72.7	55.2	47.2	78.3	50.7	43.0	44.0	70.0
140	75.9	61.6	49.2	–	51.7	42.3	43.8	69.6
188	76.7	60.5	50.2	–	54.8	44.5	46.8	76.2
308	81.0	64.5	55.0	–	57.8	47.1	51.1	–
392	82.1	68.4	57.3	–	57.2	45.6	49.7	–
536	79.9	66.7	57.8	–	62.3	47.7	53.4	–
716	82.1	67.8	57.6	–	65.0	50.8	59.5	–
908	82.1	69.1	57.7	–	65.8	50.9	59.3	–
1,100	82.0	67.4	58.3	–	64.8	50.3	56.8	–
1,652	82.9	68.3	60.0	–	70.2	56.9	63.4	–
2,000	–	69.0	62.5	–	69.1	57.4	63.6	–
3,260	–	–	63.4	–	71.0	61.9	64.5	–
3,408	–	–	–	–	70.2	61.0	64.4	–
6,000	–	–	–	–	71.9	65.4	70.8	–
8,004	–	–	–	–	74.6	66.9	72.0	–
10,008	–	–	–	–	76.4	67.5	67.8	–
12,504	–	–	–	–	73.4	67.3	–	–
14,052	–	–	–	–	83.8	67.9	–	–
15,000	–	–	–	–	–	67.7	–	–
20,004	–	–	–	–	–	–	–	–
25,008	–	–	–	–	–	–	–	–

Appendix F: Base Pressure Response Data

Test Item	C130 NTP1	C130 NTP2	C130 NTP3	C130 NTP4	C130 RTP1	C130 RTP2	C130 RTP3	C130 RTP4
HMA (in.)	2.5	2.5	1.5	1.0	2.5	2.5	1.5	1.0
Base	GR	LMS	LMS	LMS	GR	LMS	LMS	LMS
Tire Pr.	Normal	Normal	Normal	Normal	Reduced	Reduced	Reduced	Reduced
Pass	Base Pressure (psi)							
2	68.2	60.9	77.7	78.5	68.7	69.8	74.5	80.9
8	66.7	60.3	78.9	75.8	63.0	63.7	67.0	88.3
32	70.9	60.8	78.3	78.3	83.3	71.8	81.0	98.0
92	79.7	65.8	84.9	84.5	90.7	66.0	83.3	96.3
140	82.4	67.1	81.8	85.2	86.5	61.8	79.4	93.6
188	80.1	64.0	78.4	84.6	84.1	60.9	79.8	93.3
308	84.7	69.2	79.3	85.7	96.5	65.2	79.6	93.9
392	79.3	63.4	76.1	82.1	96.9	65.6	78.8	91.8
536	81.4	65.4	73.9	81.7	101.0	64.7	77.9	89.1
716	85.0	69.3	76.5	83.4	104.3	67.5	79.2	90.5
908	87.5	71.0	77.9	84.3	–	65.3	78.7	92.0
1,100	92.0	73.4	81.3	89.6	–	69.2	79.0	94.8
1,652	–	74.7	83.8	90.3	–	68.8	82.1	95.6
2,000	–	75.5	85.4	90.8	–	68.5	84.0	96.1
3,260	–	76.2	85.1	91.1	–	69.6	84.1	96.0
3,408	–	77.9	84.3	92.0	–	72.3	84.3	95.7
6,000	–	86.5	87.6	97.6	–	73.2	84.2	86.3
8,004	–	83.2	86.0	90.3	–	72.2	81.1	83.9
10,008	–	83.1	81.2	91.4	–	84.3	84.6	86.3
12,504	–	83.0	81.4	88.7	–	86.6	85.7	86.3
14,052	–	82.9	81.5	86.9	–	88.0	86.4	86.3
15,000	–	82.9	81.6	85.9	–	88.8	86.8	86.3
20,004	–	81.2	79.0	78.7	–	88.4	82.5	84.9
25,008	–	–	–	–	–	87.6	79.0	83.4

Note: Underlined data are interpolated.

Test Item	C17 NTP1	C17 NTP2	C17 NTP3	C17 NTP4	C17 RTP1	C17 RTP2	C17 RTP3	C17 RTP4
HMA (in.)	1.0	1.5	2.5	2.5	1.0	1.5	2.5	2.5
Base Type	LMS	LMS	LMS	GR	LMS	LMS	LMS	GR
Tire Pr.	Normal	Normal	Normal	Normal	Reduced	Reduced	Reduced	Reduced
Pass	Base Pressure (psi)							
2	97.4	84.2	80.6	100.8	87.3	68.8	68.2	94.6
8	102.3	92.1	87.5	108.3	88.6	72.0	76.7	96.8
32	110.5	96.3	89.9	117.9	101.0	73.7	80.5	108.9
92	126.8	103.2	100.1	132.5	101.5	68.2	78.7	123.3
140	121.2	100.9	100.3	–	98.6	66.0	75.8	123.8
188	117.4	99.1	97.6	–	103.1	69.7	79.2	136.2
308	121.0	105.5	102.6	–	105.4	78.2	85.7	–
392	123.1	107.2	111.3	–	98.8	75.0	81.3	–
536	126.4	110.1	109.9	–	105.6	79.5	85.9	–
716	127.4	112.4	112.7	–	109.7	87.8	93.5	–
908	127.5	112.5	114.4	–	106.9	87.8	91.1	–
1,100	125.2	110.3	112.6	–	105.0	85.8	89.4	–
1,652	124.4	115.9	115.2	–	119.2	100.0	100.8	–
2,000	–	115.1	114.7	–	116.4	98.7	98.2	–
3,260	–	–	113.6	–	117.9	102.4	99.5	–
3,408	–	–	–	–	113.5	100.7	98.5	–
6,000	–	–	–	–	113.9	104.2	97.9	–
8,004	–	–	–	–	110.5	101.2	98.5	–
10,008	–	–	–	–	119.6	104.2	101.8	–
12,504	–	–	–	–	118.4	102.8	106.3	–
14,052	–	–	–	–	127.5	111.2	–	–
15,000	–	–	–	–	–	108.6	–	–
20,004	–	–	–	–	–	–	–	–
25,008	–	–	–	–	–	–	–	–

Appendix G: SDD Response Data

Test Item	C130 NTP1	C130 NTP2	C130 NTP3	C130 NTP4	C130 RTP1	C130 RTP2	C130 RTP3	C130 RTP4
HMA (in.)	2.5	2.5	1.5	1.0	2.5	2.5	1.5	1.0
Base	GR	LMS	LMS	LMS	GR	LMS	LMS	LMS
Tire Pr.	Normal	Normal	Normal	Normal	Reduced	Reduced	Reduced	Reduced
Pass	Total Subgrade Deflection (in.)							
2	0.157	0.058	0.072	0.077	0.135	0.050	0.051	0.060
8	0.240	0.057	0.074	0.090	0.192	0.056	0.057	0.072
32	0.304	0.065	0.087	0.116	0.363	0.070	0.075	0.104
92	0.481	0.083	0.134	0.196	0.521	0.081	0.094	0.148
140	0.548	0.090	0.153	0.231	0.579	0.083	0.096	0.168
188	0.572	0.091	0.169	0.258	0.588	0.087	0.100	0.179
308	0.673	0.104	0.221	0.343	0.600	0.095	0.118	0.227
392	0.674	0.104	0.240	0.367	0.676	0.104	0.130	0.266
536	0.737	0.107	0.271	0.421	0.685	0.115	0.151	0.319
716	0.817	0.122	0.330	0.486	–	0.131	0.179	0.397
908	0.835	0.133	0.382	0.535	–	0.155	0.202	0.465
1,100	0.801	0.147	0.427	0.579	–	0.178	0.226	0.538
1,652	–	0.208	0.528	0.673	–	0.223	0.285	0.642
2,000	–	0.247	0.591	0.732	–	0.252	0.322	0.708
3,260	–	0.379	0.687	0.830	–	0.312	0.408	0.786
3,408	–	0.395	0.698	0.841	–	0.319	0.418	0.795
6,000	–	0.515	0.789	–	–	0.366	0.430	0.868
8,004	–	0.558	0.818	–	–	0.400	0.484	–
10,008	–	0.575	0.836	–	–	0.449	0.517	–
12,504	–	0.586	0.850	–	–	0.502	–	–
14,052	–	0.593	0.859	–	–	0.534	–	–
15,000	–	0.597	0.864	–	–	0.554	–	–
20,004	–	0.624	0.880	–	–	0.618	–	–
25,008	–	–	–	–	–	0.666	–	–

Note: Underlined data are interpolated.

Test Item	C17 NTP1	C17 NTP2	C17 NTP3	C17 NTP4	C17 RTP1	C17 RTP2	C17 RTP3	C17 RTP4
HMA (in.)	1.0	1.5	2.5	2.5	1.0	1.5	2.5	2.5
Base	LMS	LMS	LMS	GR	LMS	LMS	LMS	GR
Tire Pr.	Normal	Normal	Normal	Normal	Reduced	Reduced	Reduced	Reduced
Pass	Total Subgrade Deflection (in.)							
2	0.094	0.085	0.086	–	0.087	0.092	0.084	0.274
8	0.131	0.135	0.110	–	0.105	0.112	0.106	0.396
32	0.200	0.207	0.156	–	0.160	0.148	0.136	0.673
92	0.408	0.404	0.247	–	0.240	0.191	0.192	0.977
140	0.503	0.490	0.306	–	0.275	0.205	0.216	1.152
188	0.614	0.561	0.339	–	0.316	0.227	0.248	1.367
308	0.843	0.737	0.434	–	0.407	0.276	0.324	–
392	0.954	0.862	0.487	–	0.439	0.288	0.346	–
536	0.988	0.941	0.524	–	0.511	0.331	0.398	–
716	1.007	1.068	0.592	–	0.597	0.381	0.469	–
908	1.009	1.108	0.651	–	0.650	0.406	0.497	–
1,100	1.009	1.111	0.686	–	0.695	0.433	0.516	–
1,652	–	1.121	0.823	–	0.852	0.519	0.604	–
2,000	–	–	0.887	–	0.907	0.556	0.629	–
3,260	–	–	–	–	1.044	0.668	0.701	–
3,,408	–	–	–	–	1.045	0.673	0.707	–
6,000	–	–	–	–	1.045	0.673	0.707	–
8,004	–	–	–	–	1.126	0.854	0.835	–
10,008	–	–	–	–	–	–	–	–
12,504	–	–	–	–	–	–	–	–
14,052	–	–	–	–	–	–	–	–
15,000	–	–	–	–	–	–	–	–
20,004	–	–	–	–	–	–	–	–
25,008	–	–	–	–	–	–	–	–

Appendix H: ASG Response Data

Test Item	C130 NTP1	C130 NTP2	C130 NTP3	C130 NTP4	C130 RTP1	C130 RTP2	C130 RTP3	C130 RTP4
HMA (in.)	2.5	2.5	1.5	1.0	2.5	2.5	1.5	1.0
Base	GR	LMS	LMS	LMS	GR	LMS	LMS	LMS
Tire Pr.	Normal	Normal	Normal	Normal	Reduced	Reduced	Reduced	Reduced
Pass	Total Asphalt Strain (in./in.)							
2	604	180	182	164	526	212	293	757
8	780	175	193	241	500	148	194	664
32	673	152	210	305	790	255	350	880
92	755	158	226	313	839	238	323	763
140	815	167	259	358	873	172	268	602
188	768	155	226	293	984	236	322	641
308	1073	196	297	410	1382	255	321	636
392	897	169	250	364	1487	239	274	752
536	1024	180	255	338	1844	245	270	777
716	1350	206	335	432	3336	253	292	700
908	1749	208	361	447	–	307	288	814
1,100	2049	222	364	437	–	321	358	761
1,652	–	266	376	484	–	323	319	682
2,000	–	293	384	514	–	324	295	632
3,260	–	316	403	680	–	325	276	671
3,408	–	319	405	700	–	325	274	676
6,000	–	396	384	–	–	299	328	898
8,004	–	368	378	–	–	228	269	667
10,008	–	367	364	–	–	286	339	1000
12,504	–	367	344	–	–	323	349	1067
14,052	–	367	332	–	–	346	354	1108
15,000	–	367	324	–	–	360	358	1133
20,004	–	–	–	–	–	301	353	928
25,008	–	–	–	–	–	347	374	1098

Note: Underlined data are interpolated.

Test Item	C17 NTP1	C17 NTP2	C17 NTP3	C17 NTP4	C17 RTP1	C17 RTP2	C17 RTP3	C17 RTP4
HMA (in.)	1.0	1.5	2.5	2.5	1.0	1.5	2.5	2.5
Base	LMS	LMS	LMS	GR	LMS	LMS	LMS	GR
Tire Pr.	Normal	Normal	Normal	Normal	Reduced	Reduced	Reduced	Reduced
Pass	Total Asphalt Strain (in./in.)							
2	514	378	326	1006	280	276	237	787
8	524	481	373	1208	306	242	222	905
32	630	461	392	1717	469	329	250	1171
92	884	661	568	3935	479	352	264	2408
140	766	580	608	–	382	257	251	3047
188	674	587	551	–	441	295	286	3079
308	827	699	667	–	465	457	384	–
392	886	700	727	–	339	301	310	–
536	838	643	656	–	331	350	334	–
716	876	754	738	–	460	429	415	–
908	1015	808	769	–	368	306	367	–
1,100	916	808	736	–	307	238	347	–
1,652	1159	1003	949	–	626	422	499	–
2,000	–	1576	1078	–	500	366	463	–
3,260	–	–	2121	–	575	428	485	–
3,408	–	–	–	–	534	406	474	–
6,000	–	–	–	–	619	380	517	–
8,004	–	–	–	–	617	256	418	–
10,008	–	–	–	–	1181	232	432	–
12,504	–	–	–	–	833	381	645	–
14,052	–	–	–	–	–	–	–	–
15,000	–	–	–	–	–	–	–	–
20,004	–	–	–	–	–	–	–	–
25,008	–	–	–	–	–	–	–	–

Unit Conversion Factors

Multiply	By	To Obtain
cubic feet	0.02831685	cubic meters
cubic inches	1.6387064 E-05	cubic meters
cubic yards	0.7645549	cubic meters
degrees Fahrenheit	(F-32)/1.8	degrees Celsius
feet	0.3048	meters
inches	0.0254	meters
microinches	0.0254	micrometers
microns	1.0 E-06	meters
mils	0.0254	millimeters
pounds (force)	4.448222	newtons
pounds (force) per foot	14.59390	newtons per meter
pounds (force) per inch	175.1268	newtons per meter
pounds (force) per square foot	47.88026	pascals
pounds (force) per square inch	6.894757	kilopascals
pounds (mass)	0.45359237	kilograms
pounds (mass) per cubic foot	16.01846	kilograms per cubic meter
pounds (mass) per cubic inch	2.757990 E+04	kilograms per cubic meter
pounds (mass) per square foot	4.882428	kilograms per square meter
pounds (mass) per square yard	0.542492	kilograms per square meter
square feet	0.09290304	square meters
square inches	6.4516 E-04	square meters
tons (force)	8,896.443	newtons
tons (force) per square foot	95.76052	kilopascals
tons (2,000 pounds, mass)	907.1847	kilograms
tons (2,000 pounds, mass) per square foot	9,764.856	kilograms per square meter

Acronyms

Term	Definition
AASHTO	American Association of State and Highway Transportation Officials
AFCEC	Air Force Civil Engineer Center
APE	Airfield Pavement Evaluation
ASTM	American Society for Testing and Materials
CBR	California Bearing Ration
Cc	Coefficient of Curvature
CH	High-Plasticity Clay
Cu	Coefficient of Uniformity
DCP	Dynamic Cone Penetrometer
DGAC	Dense Grade Asphalt Concrete
DoD	Department of Defense
EPC	Earth Pressure Cell
ERDC	Engineer Research and Development Center
ESWL	Equivalent Single-Wheel Load
FAA	Federal Aviation Administration
FOD	Foreign Object Debris
FWD	Falling Weight Deflectometer
GR	Crushed Gravel
HMA	Hot-Mix Asphalt
HVS	Heavy Vehicle Simulator
ISM	Impulse Stiffness Modulus
LL	Liquid Limit
LMS	Crushed Limestone
LOE	Line of Equality
LVDT	Linear Velocity Displacement Transducer
MC	Moisture Content
NMAS	Nominal Maximum Aggregate Size
NTP	Normal Tire Pressure
pcf	Per Cubic Foot
PI	Plasticity Index
PL	Plastic Limit
PP	Pore Pressure
psi	Per Square Inch
RAP	Recycled Asphalt Pavement
RTP	Reduced Tire Pressure
SDD	Single-Depth Deflectometer
TMP	Temperature
USACE	United States Army Corps of Engineers
USAF	United States Air Force
USCS	United Soil Classification System

REPORT DOCUMENTATION PAGE

Form Approved
OMB No. 0704-0188

1. REPORT DATE *(DD-MM-YYYY)*	2. REPORT TYPE	3. DATES COVERED *(From - To)*
December 2020	Final	

4. TITLE AND SUBTITLE

Evaluation of Thin Flexible Pavements under Simulated Aircraft Traffic

5a. CONTRACT NUMBER

5b. GRANT NUMBER

5c. PROGRAM ELEMENT NUMBER

6. AUTHOR(S)

W. Jeremy Robinson

5d. PROJECT NUMBER

5e. TASK NUMBER

5f. WORK UNIT NUMBER
473719

7. PERFORMING ORGANIZATION NAME(S) AND ADDRESS(ES)

Geotechnical and Structures Laboratory
U.S. Army Engineer Research and Development Center
3909 Halls Ferry Road
Vicksburg, MS 39180-6199

8. PERFORMING ORGANIZATION REPORT NUMBER

ERDC/GSL TR-20-38

9. SPONSORING / MONITORING AGENCY NAME(S) AND ADDRESS(ES)

Headquarters, Air Force Civil Engineer Center
Tyndall Air Force Base, FL 32403-5319

10. SPONSOR/MONITOR'S ACRONYM(S)

11. SPONSOR/MONITOR'S REPORT NUMBER(S)

12. DISTRIBUTION / AVAILABILITY STATEMENT
Approved for public release; distribution is unlimited.

13. SUPPLEMENTARY NOTES

14. ABSTRACT

A full-scale airfield pavement test section was constructed and trafficked by the U.S. Army Engineer Research and Development Center (ERDC) to evaluate the performance of relatively thin airfield pavement structures. The test section consisted of 16 test items that included three asphalt pavement thicknesses and two different aggregate base courses. The test items were subjected to simulated aircraft traffic to evaluate their response and performance to realistic aircraft loads and to evaluate the effect of reductions in tire pressure on thin asphalt pavement. Rutting behavior, pavement cracking, instrumentation response, and falling weight deflectometer response were monitored at selected traffic intervals. The results of this study were used to extend existing Department of Defense pavement design and evaluation techniques to include the evaluation of airfield pavement sections that do not meet the current criteria for aggregate base quality and minimum asphalt concrete surface thickness. These performance data were used to develop new aggregate base failure design curves using existing stress-based design methodology.

15. SUBJECT TERMS
Thin asphalt pavements
Airfield pavement design
Accelerated pavement testing
Reduced tire pressure
Beta design methodology

16. SECURITY CLASSIFICATION OF:			17. LIMITATION OF ABSTRACT	18. NUMBER OF PAGES	19a. NAME OF RESPONSIBLE PERSON
a. REPORT	b. ABSTRACT	c. THIS PAGE			19b. TELEPHONE NUMBER *(include area code)*
Unclassified	Unclassified	Unclassified	SAR	222	